

Model-based Predictive Control for Improving  
Stability and Transparency in Time-delay  
Teleoperation

MODEL-BASED PREDICTIVE CONTROL FOR IMPROVING  
STABILITY AND TRANSPARENCY IN TIME-DELAY  
TELEOPERATION

BY

ALI SHAHDI, M.A.Sc., (Electrical Engineering)  
McMaster University, Hamilton, Canada

A THESIS

SUBMITTED TO THE DEPARTMENT OF ELECTRICAL & COMPUTER ENGINEERING  
AND THE SCHOOL OF GRADUATE STUDIES  
OF MCMASTER UNIVERSITY  
IN PARTIAL FULFILMENT OF THE REQUIREMENTS  
FOR THE DEGREE OF  
DOCTOR OF PHILOSOPHY

© Copyright by Ali Shahdi, April 2010

All Rights Reserved

Doctor of Philosophy (2010)  
(Electrical & Computer Engineering)

McMaster University  
Hamilton, Ontario, Canada

TITLE: Model-based Predictive Control for Improving Stability and Transparency in Time-delay Teleoperation

AUTHOR: Ali Shahdi  
M.A.Sc., (Electrical Engineering)  
McMaster University, Hamilton, Canada  
B.Sc., (Electrical Engineering)  
Sharif University of Technology, Tehran, Iran

SUPERVISOR: Dr. Shahin Sirouspour

NUMBER OF PAGES: xv, 246

*To My Parents*

# Acknowledgements

I owe my deepest gratitude to my supervisor, Dr. Shahin Sirouspour, for his endless support, guidance and encouragement. I want to thank him for his deep insight, broad knowledge and tremendous effort during all the stages of the program.

I am indebted to my colleagues at Telerobotics, Haptics, and Computational Vision Lab, for their kind helps and friendship. I would also like to thank my friends for their support, friendship and reminding me that there is life beyond school.

Last but not least, my sincere thanks go to my parents who always support and encourage me through my life. Their understanding and patience have made it possible to pass all the steps. Without their supports, completion of this thesis would not have been possible.

# Abstract

Prior research on time-delay bilateral teleoperation has mainly resulted in methods that favor the robust stability of the system at the expense of its transparency. In contrast, it is demonstrated in this thesis that carefully designed model-based predictive controllers are able to achieve high levels of transparency while maintaining teleoperation stability. This is accomplished by utilizing available information on system model and time delay within a predictive control framework. The performance objectives are delay-free position tracking between the master and slave and the establishment of a virtual mass-damper tool impedance between the user and environment. Three model-based predictive controllers are proposed in this thesis which utilize both force and position measurements at the master and slave sites. The first two controllers can only handle known and fixed time delays whereas the third controller is applicable to systems with fixed or variable delay.

First, building upon our recent work in [1, 2], a decentralized model-based predictive controller is introduced that can enhance the time-delay teleoperation transparency and robust stability by allowing the use of local delay-free measurements in local master/slave controllers. The stability of the system is analyzed using a frequency sweeping test. Numerical analysis demonstrates improved performance and robustness compared with the centralized controller in [2].

Next, a robust predictive controller is proposed to deal with modeling uncertainty, particularly in the operator and environment dynamics. In a two-step control approach, first local adaptive/nonlinear controllers are applied to linearize the system dynamics and to eliminate dependency on the master and slave parameters. Teleoperation coordination is then achieved by formulating an input/output (I/O) time-delay  $H_\infty$  robust control synthesis. The transparency and robust stability properties of the proposed method are examined via numerical analysis.

Although less sensitive to modeling uncertainty, the robust controller can still sacrifice teleoperation transparency in favor of its stability since it utilizes a fixed controller for the entire range of teleoperation. In an attempt to avoid such a trade-off, a stable adaptive predictive controller for teleoperation systems with constant and varying communication delay is proposed. The controller utilizes a model of the system dynamics and the time delay within a predictive control framework to achieve the desired transparency objectives while maintaining the system stability. The controller adapts to uncertainties in the system dynamics by estimating the model parameters in real time. A Lyapunov analysis of the performance and stability of the resulting system is presented.

The proposed controllers for time-delay bilateral teleoperation are implemented and experimentally evaluated. The results demonstrate the effectiveness of the proposed methods in providing a stable transparent interface for teleoperation under time delay.

# Contents

<b>Acknowledgements</b>	<b>iv</b>
<b>Abstract</b>	<b>v</b>
<b>1 Introduction and Problem Statement</b>	<b>1</b>
1.1 Background . . . . .	1
1.2 Motivation . . . . .	3
1.3 Summary of Thesis Contributions . . . . .	6
1.4 Organization of the Thesis . . . . .	12
1.5 Related Publications . . . . .	13
1.5.1 Journal Articles . . . . .	13
1.5.2 Conference Papers . . . . .	13
<b>2 Literature Review</b>	<b>15</b>
2.1 Introduction . . . . .	15
2.2 Teleoperation Control Architectures . . . . .	16
2.3 Control of Delay-free Teleoperation . . . . .	17
2.3.1 Robust Controllers . . . . .	21
2.3.2 Adaptive Controllers . . . . .	22

2.4	Time-delay Teleoperation Control . . . . .	24
2.4.1	Passivity-based Controllers . . . . .	25
2.4.2	Robust Controllers . . . . .	28
2.4.3	Predictive Controllers . . . . .	29
2.5	Time-delay Systems . . . . .	30
<b>3</b>	<b>Teleoperation Dynamics and Performance Objectives</b>	<b>34</b>
3.1	Introduction . . . . .	34
3.2	Robot Dynamics . . . . .	35
3.3	Teleoperation System Dynamics . . . . .	39
3.4	Performance of Master/Slave Teleoperation Systems . . . . .	42
<b>4</b>	<b>Model-based Decentralized Control of Time-delay Teleoperation Systems</b>	<b>46</b>
4.1	Introduction . . . . .	46
4.2	Linearization of Master/Slave Teleoperation Systems Dynamics . . . . .	48
4.3	Decentralized Time-delay Teleoperation System . . . . .	55
4.3.1	Free motion/soft contact . . . . .	59
4.3.2	Rigid contact . . . . .	62
4.4	Reduction and Control of Time-delay Systems . . . . .	65
4.4.1	Closed-loop Stability Analysis . . . . .	72
4.5	Performance and Robust Stability Analysis for Single-axis Teleoper- ation . . . . .	77
4.5.1	Robust stability analysis w.r.t parametric uncertainty . . . . .	79
4.5.2	Performance analysis . . . . .	81

4.5.3	Robust stability analysis w.r.t. perturbations in communication delay . . . . .	82
4.6	Experimental Results . . . . .	86
4.6.1	Decentralized controller with 100 ms delay . . . . .	88
4.6.2	Decentralized controller with 200 ms delay . . . . .	89
4.6.3	Decentralized controller with 300 ms delay . . . . .	90
4.7	Conclusions . . . . .	90
<b>5</b>	<b>Adaptive/Robust Control for Time-delay Teleoperation</b>	<b>93</b>
5.1	Introduction . . . . .	93
5.2	Master/Slave Local Adaptive Control . . . . .	94
5.3	Teleoperation Control Formulation . . . . .	99
5.4	$H_\infty$ Control of MIMO Systems with I/O time delay . . . . .	107
5.4.1	Problem Formulation . . . . .	109
5.4.2	Equivalent One-block Problem . . . . .	110
5.4.3	The Adobe Delay Problem . . . . .	112
5.4.4	Decomposition . . . . .	113
5.5	Design Example . . . . .	115
5.6	Experimental Results . . . . .	127
5.6.1	Teleoperation experiment with 100 msec delay . . . . .	128
5.6.2	Teleoperation experiment with 200 msec delay . . . . .	130
5.6.3	Teleoperation experiment with 300 msec delay . . . . .	131
5.7	Conclusions . . . . .	131
<b>6</b>	<b>Adaptive Control of Bilateral Time-delay Teleoperation</b>	<b>133</b>

6.1	Introduction . . . . .	133
6.2	Revised Time-delay Teleoperation System Formulation . . . . .	134
6.3	Modified Delay Reduction and Model-based State Prediction . . . . .	137
6.4	New Outputs Definition and Regulation . . . . .	143
6.5	System Stability and Parameters Adaptation Law . . . . .	148
6.5.1	Output Regulation . . . . .	155
6.6	Parameter Convergence and Composite Adaptive Control . . . . .	156
6.6.1	Composite Adaptive Control . . . . .	157
6.7	Adaptive Control of Teleoperation with Time-varying Delay . . . . .	162
6.7.1	Practical Implementation Issues for the Time-varying Controller in Packet Switched Networks . . . . .	169
6.8	Experimental Results . . . . .	171
6.8.1	Adaptive controller with 50 ms delay . . . . .	173
6.8.2	Adaptive controller with 100 ms delay . . . . .	175
6.8.3	Adaptive controller with 200 ms delay . . . . .	176
6.8.4	Adaptive controller with time-varying delay . . . . .	177
6.9	Conclusion . . . . .	178
<b>7</b>	<b>Conclusions and Future Work</b>	<b>180</b>
7.1	Conclusions . . . . .	180
7.1.1	Model-based Decentralized Controller . . . . .	181
7.1.2	Robust Controller . . . . .	182
7.1.3	Adaptive Controller . . . . .	183
7.2	Future Work . . . . .	184

<b>A</b>	<b>Master/Hand, Slave/Environment and Tool Dynamics in State-space Form</b>	<b>187</b>
<b>B</b>	<b>Teleoperation Dynamics in Chapter 4 in State-space Form</b>	<b>190</b>
	B.1 Free Motion/Soft Contact . . . . .	190
	B.2 Rigid Contact . . . . .	196
<b>C</b>	<b>Proof of Theorem 4.1</b>	<b>200</b>
	C.1 Stabilizability . . . . .	200
	C.2 Detectability . . . . .	205
<b>D</b>	<b>One-block Equivalent of a Four-block Time-delay Problem</b>	<b>209</b>
<b>E</b>	<b>Solution to the Adobe Delay Problem</b>	<b>214</b>
<b>F</b>	<b>Teleoperation Dynamics in Chapter 6 in State-space Form</b>	<b>217</b>
	F.1 Teleoperation Dynamics after Transformation . . . . .	219
	F.2 Teleoperation Dynamics in Chapter 6 in Closed-loop Form . . . . .	222
	F.3 Teleoperation Dynamics in Chapter 6 in Linear-in-parameter Form . . . . .	223
<b>G</b>	<b>The Persistency of Excitation Condition</b>	<b>225</b>
<b>H</b>	<b>Composite Adaptive Controller Matrices</b>	<b>227</b>

# List of Figures

1.1	(a) Unilateral teleoperation architecture with visual feedback and (b) bilateral architecture with additional kinesthetic and force feedback.	2
2.1	A general bilateral teleoperation control architecture.	16
2.2	Two-port network model of a teleoperation system.	17
3.1	Linear mass-spring-damper models of (a) the operator's arm and (b) the environment.	41
3.2	Operator and environment interaction through (a) ideally transparent teleoperation and (b) virtual intervening tool, with unity position and force scaling factors.	43
4.1	A centralized teleoperation architecture with controller at the master site.	47
4.2	Conceptual representation of the proposed model-predictive decentralized teleoperation controller: (a) Centralized teleoperation control at master or slave side; (b) Decentralized sub-controller design; (c) Decentralized controller implementation.	57
4.3	Multi-model decentralized controller for time-delay teleoperation.	75
4.4	Robust stability analysis results in free motion: (a), (b) and (c), and in rigid contact: (d), as a function of time delay.	80

4.5	Robust stability analysis results in free motion: (b) and (c), and in rigid contact: (a) and (d), for simultaneous variations in two parameters. . . . .	81
4.6	$\ H\ _2^2$ for the closed-loop system from $f_h^*$ to (a) position tracking error in free motion, (b) tool tracking error in free motion, (c) position tracking error in rigid contact, and (d) force tracking error in rigid contact. . . . .	83
4.7	Closed-loop decentralized teleoperation control subject to uncertainty in communication delay. . . . .	84
4.8	Maximum/minimum allowable time-delay variations to maintain stability. . . . .	85
4.9	The experimental setup. . . . .	87
4.10	Decentralized controller with 100 msec delay in experiment: (a) position tracking and (b) force tracking. . . . .	89
4.11	Decentralized controller with 200 msec delay in experiment: (a) position tracking and (b) force tracking. . . . .	90
4.12	Decentralized controller with 300 msec delay in experiment: (a) position tracking and (b) force tracking. . . . .	91
5.1	Block diagram of master (slave) dynamics after the application of local adaptive nonlinear controllers. . . . .	98
5.2	Linearized teleoperation control system. . . . .	101
5.3	A MIMO system with multiple I/O delays: (a) original; (b) after applying the wave transformations. . . . .	106

5.4	(a) Lower fractional transformation (LFT); (b) Scattering representation. . . . .	108
5.5	Equivalent one-block problem . . . . .	111
5.6	Controller reconstruction from a two-step adobe decomposition. . . . .	119
5.7	Closed-loop frequency response to the input $f_h^*$ for 100 msec delay and matched environment stiffness. . . . .	121
5.8	Closed-loop frequency response to the input $f_h^*$ for 100 msec delay and mismatched environment stiffness. . . . .	121
5.9	Closed-loop frequency response to the input $f_h^*$ for 200 msec delay and matched environment stiffness. . . . .	122
5.10	Closed-loop frequency response to the input $f_h^*$ for 200 msec delay and mismatched environment stiffness. . . . .	122
5.11	Closed-loop frequency response to the input $f_h^*$ for 300 msec delay and matched environment stiffness. . . . .	123
5.12	Closed-loop frequency response to the input $f_h^*$ for 300 msec delay and mismatched environment stiffness. . . . .	123
5.13	The closed-loop system subject to the environment stiffness uncertainty, $\delta k_e$ . . . . .	124
5.14	Nyquist plot of $R(s)$ for 100 msec of delay. . . . .	125
5.15	Nyquist plot of $R(s)$ for 200 msec of delay. . . . .	126
5.16	Nyquist plot of $R(s)$ for 300 msec of delay. . . . .	126
5.17	The two-stage teleoperation controller. . . . .	128
5.18	The controller with 100 ms delay in experiment: (a) position tracking; (b) force tracking; (c) estimated environment stiffness. . . . .	129

5.19	The controller with 200 ms delay in experiment: (a) position tracking; (b) force tracking; (c) estimated environment stiffness. . . . .	130
5.20	The controller with 300 ms delay in experiment: (a) position tracking; (b) force tracking; (c) estimated environment stiffness. . . . .	131
6.1	A centralized time-delay teleoperation control (a) without delay padding, (b) after delay padding, (c) after combining master/operator and slave/environment dynamics and (d) after moving all the delays to the input channels. . . . .	136
6.2	Communication over a packet switched network with (a) increasing delay and (b) decreasing delay. . . . .	170
6.3	Control action and master/slave devices running with a faster sampling rate than the communication packet transmission rate. . . . .	171
6.4	Time-delay teleoperation system with the proposed adaptive predictive controller . . . . .	172
6.5	Model-based adaptive controller with 50 msec delay in experiment: (a) position tracking and (b) force tracking. . . . .	174
6.6	Model-based adaptive controller with 100 msec delay in experiment: (a) position tracking and (b) force tracking. . . . .	175
6.7	Model-based adaptive controller with 200 msec delay in experiment: (a) position tracking and (b) force tracking. . . . .	176
6.8	The model-based adaptive controller with time-varying delay in (6.138): (a) position tracking and (b) force tracking. . . . .	178
6.9	The model-based adaptive controller with time-varying delay in (6.139): (a) position tracking and (b) force tracking. . . . .	179

# Chapter 1

## Introduction and Problem Statement

### 1.1 Background

Operator-in-the-loop control of robotic manipulators, widely known as teleoperation, has been an alternative to autonomous robotic operation in complex and unstructured environments. Teleoperation systems allow a human operator to extend his/her intelligence and manipulation skills to remote and/or hazardous environments. This is achieved through coordinated control of two robotic arms, i.e. a **master** hand-controller which is often a force-feedback enabled interface used by the **operator**, and a **slave** robot that manipulates the task **environment**. The coordination is carried out by master/slave **controllers** and by utilizing the position and force information exchanged over the linking **communication medium**. Figure 1.1 shows these six elements that usually constitute a teleoperation system.

After its initial introduction in 1940s, telerobotics has rapidly progressed from mechanically linked tele-manipulation to current advanced computer-controlled

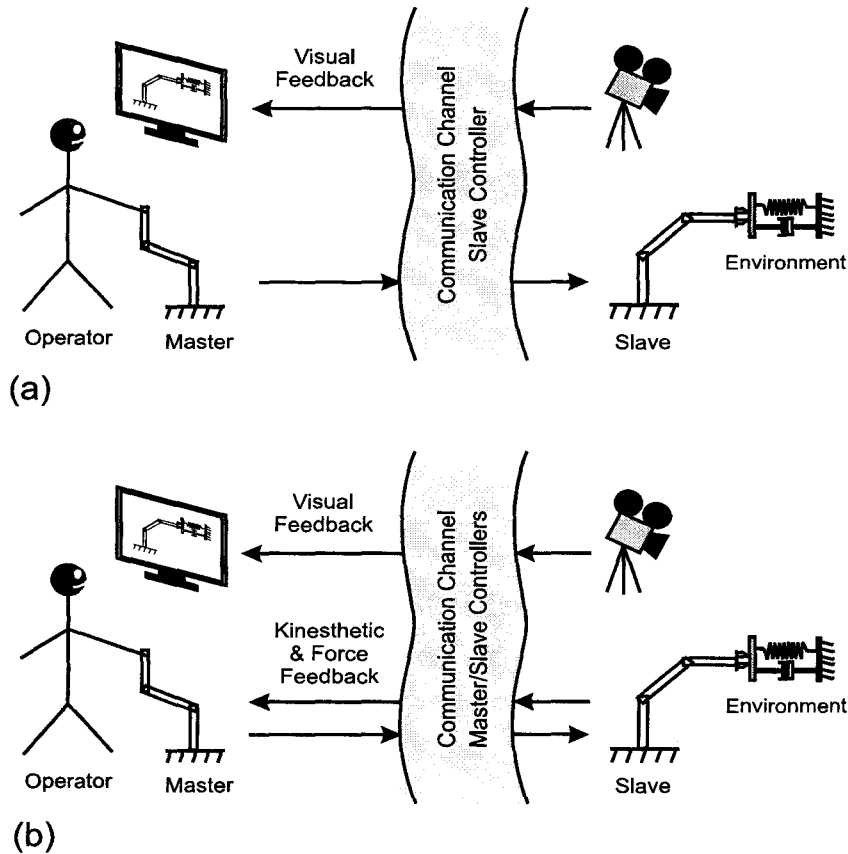


Figure 1.1: (a) Unilateral teleoperation architecture with visual feedback and (b) bilateral architecture with additional kinesthetic and force feedback.

teleoperation systems [3,4,5,6,7]. Over the past few decades, applications of teleoperation technology have grown in a number of different areas. These include but are not limited to space operation [8,9,10,11], underwater exploration [12,13], mining [14], nuclear material handling [15], toxic material handling, the entertainment industry, and more recently healthcare [16,17].

In unilateral teleoperation, the operator uses a passive hand-controller and merely relies on visual feedback from the remote environment to perform the task

(see Fig. 1.1(a)). In this context, the operator is an intelligent controller that utilizes the visual sensory feedback to control the slave arm and perform the task. In bilateral teleoperation, however, position and force information are communicated in both directions between the master and slave sites (see Fig. 1.1(b)). By providing force and kinesthetic feedback through a force-feedback enabled device, also known as a haptic interface, bilateral teleoperators can greatly facilitate task execution in inaccessible/remote environments. The ultimate goal of bilateral teleoperation is to convey to the operator a sense of direct interaction with the environment, a performance objective often denoted as *ideal transparency* in the literature [18].

## 1.2 Motivation

Teleoperation control design involves a trade-off between the often conflicting requirements of stability and performance [18]. From a control theory perspective, teleoperation is complicated due to a number of fundamental challenges which can be summarized as follows:

- **Communication channel latency:** Various transmission media can be utilized in a teleoperation setup such as wired transmission, e.g. coaxial cables and fiber optics, wireless transmission, e.g. satellite and free space optics, and the Internet. Depending on the medium of communication in a teleoperation application, the data exchange between the master and slave sites may suffer from several limitations. Among these, the communication channel delay is the main and the most challenging problem to be addressed in

the context of teleoperation control. This latency comprises of the switching and the data transfer latency. Constant or time-varying communication time-delay in telerobotic applications is a formidable barrier to achieving a high level of fidelity while maintaining the system stability. The time delay at which a teleoperation system would become unstable depends on factors such as master and slave dynamics, controller architecture and bandwidth, as well as the environment and operator dynamics.

Unilateral teleoperators are less sensitive to delay since their feedback loop is closed only through the human's visual perception and motor control system with a relatively small bandwidth. In contrast, bilateral teleoperators entail high bandwidth feedback loops that provide kinesthetic coupling and force tracking between the master and slave. This makes them prone to delay-induced instability. Several controllers have been proposed in the literature to deal with the delay problem which will be reviewed in Chapter 2. A major common disadvantage of many of these methods is that their robust stability is gained at the expense of the transparency of teleoperation.

Beside the delay, the communication channel can pose other potential control challenges. Data rate or bit rate is the maximum rate at which data can be transferred over the channel. Due to its widespread geographical reach, accessibility and simplicity, the Internet is becoming popular as the communication medium in teleoperation systems. In a packet switching network such as the Internet, data are collected and transferred in the form of packets. In such networks, the packet transfer rate is yet another constrain on the controller performance. A low control rate imposed by the limited packet

transfer rate can potentially result in instability of a discrete-time implementation of teleoperation controllers. Another drawback of a packet switching network is packet loss. The packet is considered lost if for any reason it is not delivered successfully to the recipient [19].

All of the above limitations can potentially decrease the fidelity of teleoperation systems or even cause instability [20, 21]. However, due to the advancements in network and communication technology in recent years, their impact has diminished significantly. The data and packet rates have been increased to the point that they are satisfactory for real-time control of robotics systems. Moreover, the reliability of communication networks has highly increased by utilizing advanced communication protocols as well as redundant transfer paths. Hence, these challenges are assumed to be relatively less important in comparison with the delay and are not being addressed by this thesis.

- **Uncertain nonlinear dynamics:** Master and slave manipulators are often multi-degree-of-freedom devices with highly nonlinear and possibly unknown dynamics. Large uncertainty is also introduced to the system dynamics through the interaction of the master and slave robots with unknown and widely varying user and environment dynamics. The teleoperation controller must maintain its stability amidst these dynamic uncertainty and still provide an acceptable level of transparency.
- **Decentralized sensing and control:** Teleoperation systems belong to the larger family of decentralized control systems since their sensing and actuation are distributed at the master and slave sites. Nevertheless, the vast majority of

existing decentralized control schemes attempt to weaken the interaction between the control sites rather than to coordinate their operation, as desired in teleoperation. Consequently such methods are not applicable to control of master/slave teleoperation systems.

- **Unknown exogenous input:** Unlike most conventional control systems in which unknown disturbances must be suppressed, in teleoperation the unknown user intension, which is usually modeled as an exogenous force, is the main cause of motion and should not be rejected. In fact the rejection of such disturbance would immobilize the master/slave system.

The main focus of all of the proposed controllers in this thesis is the issue of time-delay. As elaborated in the next chapter, the existing literature lacks systematic methods to approach these challenges and to balance the vital trade-off between the performance and the stability of time-delay teleoperation systems. The objective of this thesis is to develop new control schemes to achieve a well-balanced trade-off between robust stability and performance by carefully incorporating any knowledge about system model, time delay and modeling uncertainty in the control design. The contributions of the thesis can be summarized as follows.

### 1.3 Summary of Thesis Contributions

In this thesis, several new controllers have been developed to achieve improved transparency and stability in time-delay teleoperation. The use of model-based state-space control techniques in bilateral teleoperation had been investigated in some of our earlier contributions. In [1], a discrete-time state-space formulation of

teleoperation was presented in which the communication delay is augmented into the system states resulting in a delay-free output feedback control problem. To improve computational efficiency, a continuous-time formulation was later introduced in [2] utilizing new state/observation transformations to eliminate the delay in the input/output channels producing yet another delay-free dynamics suitable for output-feedback control. The teleoperation control was then achieved through the application of the Linear Quadratic Gaussian (LQG) control to the delay-free systems in discrete or continuous-time domain. Building and improving on these earlier results, the work of this thesis has resulted in several novel controllers for bilateral time-delay teleoperation as described below.

- **Model-based decentralized control:** The use of model and delay information in the model-based controllers in [1, 2] improves the transparency of time-delay teleoperation. However, the centralized structure of these controllers introduces an additional time delay in the control loop which can potentially increase their sensitivity with respect to uncertainty in the models of the operator and environment.

An alternative decentralized formulation of the delay reduction-based teleoperation controller is proposed in this thesis to improve its robust stability while maintaining a high level of transparency. In the proposed decentralized control approach, delay-free local and delayed remote measurements of position and force signals are used in two local controllers at the master and slave stations. Using similar state/observation transformations to those introduced in [2], and assuming delay-free control actions, delay-free dynamics/measurement equations are obtained for master and slave sub-systems.

Using the delay-reduced models, two centralized multi-model LQG output-feedback controllers, one based at the master and the other at the slave end are synthesized. It is shown that this suboptimal control approach results in a closed-loop dynamics with state delay perturbations the stability of which can be investigated using a frequency-sweeping test [22].

An extensive numerical performance and robust stability analysis indicates that, using the same set of design parameters, the decentralized controller exhibits improved performance and robustness when compared with the previous centralized controller in [2]. The teleoperation control formulation as an LQG optimal control design allows for the systematic optimization of the transparency measures while maintaining stability. The performance indices used include non-delayed position tracking, force tracking, and virtual tool impedance shaping.

- **Robust control:** The proposed decentralized model-based LQG controller can still be rather sensitive to modeling uncertainties such as master/slave modeling errors as well as variations in the environment and operator dynamics. Although the robustness of the controller has been increased using a multi-model switching control strategy, the stability of such switching controllers is difficult to prove.

Robust  $H_\infty$  and  $\mu$ -synthesis-based controllers have been widely used for the control of uncertain dynamical systems. The reader is referred to [23,24,25, 26] for a survey of linear and nonlinear robust control methods for robotic manipulators. By incorporating performance indices, disturbance signals, and uncertainty elements into the control design, these methods optimize an

$\ell_\infty$  norm of the closed-loop performance of the system while guaranteeing its stability under a worst-case uncertainty scenario [27, 28]. Robust  $H_\infty$ -based controllers have been used for delay-free teleoperation [29, 30], as well as time-delay teleoperation, using a *Padé* approximation of the delay [31] or by treating it as a perturbation to the system [32, 33]. *Padé* approximation is usually valid at low frequency and can lead to closed-loop instability due to its inaccuracy, unless very high-order approximations are used. High-order delay approximations, on the other hand, can cause difficulties in obtaining a solution to the  $H_\infty$  control problem. Moreover, the treatment of the delay as a perturbation to system dynamics is unrealistic and can yield overly conservative control designs specially for larger delays. It is expected that the inclusion of the time delay information into the design process would produce far less conservative results.

In this thesis a new mixed adaptive/robust controller is proposed for time-delay teleoperation. In the first step, local Lyapunov-based adaptive/nonlinear controllers [34] are used to eliminate the nonlinearities and dynamic uncertainties of the master and slave robots resulting in two linear subsystems with uncertainty only in the environment and operator dynamics. In the second step, a robust performance  $H_\infty$  optimization problem is formulated to enhance teleoperation fidelity using transparency-based performance indices while maintaining stability in the presence of uncertainty in the operator and environment dynamics. The performance indices include non-delayed position and force tracking. A robust coordinating controller is synthesized through recursive solutions to *adobe*-type problems based on the approach

proposed in [35]. The interaction between the local adaptive controllers and the robust coordinating controller is modeled by the introduction of appropriate disturbance signals in the  $H_\infty$  control problem formulation. Stability margins and performance characteristics of the proposed controller are analyzed via a design example and are further verified in experiment.

In brief, there are several novelties in this teleoperation control approach. It incorporates uncertain nonlinear models of master and slave robots, and the uncertainties of the operator and environment dynamics into the design process. Through the explicit integration of model and delay information as well as the aforementioned knowledge about system uncertainties in the control synthesis, this method provides a systematic mechanism for balancing the robust stability and haptic fidelity objectives in time-delay teleoperation. The trade-off is accomplished by the selection of a set of design filters in the  $H_\infty$  design framework. This is in contrast to most existing teleoperation controllers that are skewed towards one of these conflicting requirements. In particular, passivity-based methods usually sacrifice performance to achieve robust stability whereas purely model-based techniques with transparent nominal response often exhibit poor stability margins. The proposed method also avoids the difficulties associated with the delay approximation or the conservatism arising from its treatment as perturbation, as is the case with other linear robust teleoperation controllers in the literature. Moreover, unlike these methods, this controller can handle nonlinear dynamics of the master/slave robots in a demonstrably stable manner.

- **Adaptive control:** Adaptive controllers can avoid the trade-off between stability and performance by changing their parameters and/or structure in response to variations in system dynamics. The proposed robust controller is less sensitive to modeling uncertainties compared to our earlier model-based controllers. Nonetheless, given that a fixed teleoperation controller is used for the entire range of operation, the transparency may still be sacrificed particularly if large modeling uncertainty is considered in the design.

To address this problem, in this thesis a new adaptive controller for time-delay teleoperation is introduced. This approach represents a major step towards achieving higher transparency while maintaining the stability of a time-delay bilateral teleoperation system. The proposed method consists of a model-based predictive control scheme which uses the estimated model of the system to predict its future states. Using the predicted states, teleoperation coordination is achieved by defining new outputs that are regulated to zero within an output control framework. A Lyapunov analysis is used to demonstrate closed-loop stability and to derive the parameters adaptation law. Another advantage of this controller is its ability to handle known time-varying latencies in the design procedure.

The proposed method provides a provably stable adaptive predictive controller for teleoperation systems with communication delay. In order to achieve a high level of transparency, the model and delay information are utilized in design procedure. The transparency objectives include delay-free position tracking and tool impedance shaping. The controller also has the ability to

adapt to uncertainties and changes in user and environment dynamics. Experimental results demonstrate the effectiveness of the proposed approach for both constant and time-varying latencies.

It is important to mention that all the proposed controllers are designed in the continuous-time domain but are implemented in the discrete-time domain. Employing a fast sampling rate compared to the relatively slower dynamics of the mechanical system and the desired bandwidth of the tracking objectives ensures that the discrete-time implementation is a sufficiently accurate approximation of the original controller.

## 1.4 Organization of the Thesis

The rest of the thesis is organized as follows. Telerobotic literature has been reviewed in Chapter 2. Chapter 3 formulates the nonlinear dynamics of the master and slave robots. Model-based decentralized control of time-delay teleoperation systems is presented in Chapter 4. Chapter 5 introduces the robust control architecture for time-delay teleoperation. The adaptive controller for bilateral teleoperation under time delay is presented in Chapter 6. Simulations, robust stability analysis and experimental results under various scenarios are given for each of the methods in their corresponding chapters. The thesis is concluded in Chapter 7 where some possible directions for future research are also discussed.

## 1.5 Related Publications

### 1.5.1 Journal Articles

- A. Shahdi and S. Sirouspour, "Adaptive control for time-delay teleoperation," To be submitted to *IEEE Transactions on Robotics*.
- A. Shahdi and S. Sirouspour, "Model-based decentralized control of time delay teleoperation systems," *The International Journal of Robotics Research*, vol. 28, no.3, pp. 376-394, 2009.
- A. Shahdi and S. Sirouspour, "Adaptive/robust control for time delay teleoperation," *IEEE Transactions on Robotics*, vol. 25, no. 1, pp. 196-205, 2009.

### 1.5.2 Conference Papers

- A. Shahdi and S. Sirouspour, "Improved transparency in bilateral teleoperation with variable time delay," in *Proceedings of IEEE/RSJ International Conference on Intelligent Robots and Systems*, pp. 4616-4621, St. Louis, Missouri, 2009.
- A. Shahdi and S. Sirouspour, "Adaptive control of time delay teleoperation systems," in *Proceedings of Third Joint EuroHaptics Conference and Symposium on Haptic Interfaces for Virtual Environment and Teleoperator Systems*, pp. 308-313, Salt Lake City, Utah, 2009.
- A. Shahdi and S. Sirouspour, "Adaptive/robust control for enhanced teleoperation under communication time delay," in *Proceedings of IEEE/RSJ International Conference on Intelligent Robots and Systems*, pp. 2667-2672, San Diego,

California, 2007.

- A. Shahdi and S. Sirouspour, "A multi-model decentralized controller for teleoperation with time delay," in *Proceedings of IEEE/RSJ International Conference on Intelligent Robots and Systems*, pp. 496-501, San Diego, California, 2007.
- P. Setoodeh, S. Sirouspour and A. Shahdi, "Discrete-time multi-model control for cooperative teleoperation under time delay," in *Proceedings of IEEE International Conference on Robotics and Automation*, pp. 2921-2926, Orlando, Florida, 2006.

# Chapter 2

## Literature Review

### 2.1 Introduction

Teleoperation systems have been subject of extensive research in the past. Various control methods have been proposed and developed trying to achieve the two main and often conflicting objectives of teleoperation, i.e. robust stability and transparency. In a perfectly transparent system the operator feels as he/she is directly manipulating the task environment.

This chapter presents a survey of the teleoperation control literature under the following categories: (i) teleoperation control architectures, (ii) control of delay-free teleoperation systems, (iii) time-delay systems and (iv) time-delay teleoperation control.



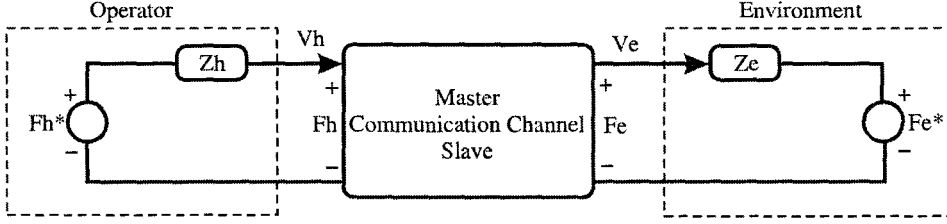


Figure 2.2: Two-port network model of a teleoperation system.

may adversely affect the stability and transparency of an ideal transparent teleoperation is the limitation on the sampling rate in the discrete-time implementation of the controller [38, 40, 41].

### 2.3 Control of Delay-free Teleoperation

Linear circuit theory and the concept of two-port networks have been utilized to model, design and analyze teleoperation controllers [36, 37, 42]. Fig. 2.2 depicts a master/slave teleoperation system modeled using a two-port network, where the master, slave, their controllers and the communication channel are all lumped as a single linear-time-invariant(LTI) two-port block. The operator and the environment are modeled using the following LTI models [36, 37]

$$F_h = F_h^* - Z_h V_h \quad (2.1)$$

$$F_e = F_e^* - Z_e V_e \quad (2.2)$$

where  $Z_h$  and  $Z_e$  and  $V_h$  and  $V_e$  are the hand and environment impedances and velocities, respectively.  $F_h$  and  $F_e$  and  $F_h^*$  and  $F_e^*$  represent hand and environment forces and exogenous inputs, respectively. Based on the choice of the input and

output signals, different network matrices can be defined as [43, 44]

$$\begin{bmatrix} F_h \\ F_e \end{bmatrix} = \begin{bmatrix} z_{11} & z_{12} \\ z_{21} & z_{22} \end{bmatrix} \begin{bmatrix} V_h \\ -V_e \end{bmatrix} \quad \text{Impedance } \mathcal{Z} \quad (2.3)$$

$$\begin{bmatrix} V_h \\ -V_e \end{bmatrix} = \begin{bmatrix} y_{11} & y_{12} \\ y_{21} & y_{22} \end{bmatrix} \begin{bmatrix} F_h \\ F_e \end{bmatrix} \quad \text{Admittance } \mathcal{Y} \quad (2.4)$$

$$\begin{bmatrix} F_h \\ -V_e \end{bmatrix} = \begin{bmatrix} h_{11} & h_{12} \\ h_{21} & h_{22} \end{bmatrix} \begin{bmatrix} V_h \\ F_e \end{bmatrix} \quad \text{Hybrid } \mathcal{H} \quad (2.5)$$

$$\begin{bmatrix} V_h \\ F_e \end{bmatrix} = \begin{bmatrix} g_{11} & g_{12} \\ g_{21} & g_{22} \end{bmatrix} \begin{bmatrix} F_h \\ -V_e \end{bmatrix} \quad \text{Inverse Hybrid } \mathcal{G}. \quad (2.6)$$

The transparency of a teleoperation system can be formulated using the mentioned two-port network representations. In a perfectly transparent system, the impedance reflected to the operator should be a match to the actual environment impedance, i.e. [18]

$$\left. \frac{F_h}{V_h} \right|_{F_e^*=0} = \left. \frac{F_e}{V_e} \right|_{F_e^*=0}. \quad (2.7)$$

In addition, the position/velocity of the master and slave devices should precisely track each other. Using the hybrid matrix parameters in (2.5) the transmitted impedance to the operator,  $Z_{to}$ , can be expressed as

$$Z_{to} = \frac{h_{11} + \Delta h Z_e}{1 + h_{22} Z_e} \quad (2.8)$$

where  $\Delta h$  is defined as

$$\Delta h = h_{11}h_{22} - h_{12}h_{21} \quad (2.9)$$

and  $Z_e$  is the environment impedance. The ideal transparency condition in (2.7) can be expressed in terms of the hybrid parameters as follows [37,42]

$$\begin{aligned} h_{11} &= h_{22} = 0 \\ h_{12} &= -h_{21} = 1. \end{aligned} \quad (2.10)$$

It is worth noticing that a perfect transparent system is marginally absolutely stable and requires acceleration measurements in its implementation. Hence, to achieve robust stability, ideal transparency has to be compromised. [18,42]

The concept of passivity has been utilized to guarantee the stability of teleoperation systems. Consider the two-port network depicted in Fig. 2.2. Such network is passive if and only if the following condition holds at any time  $t$  [45]

$$\int_{-\infty}^t F_h v_h - F_e v_e \geq -E_0 \quad (2.11)$$

where  $E_0$  is the initial energy stored in the network. In other words a passive system can only dissipate energy. The system is known to be lossless if the integral in (2.11) is equal to  $-E_0$  as  $t \rightarrow \infty$ . The passivity of the two-port network teleoperation in Fig. 2.2 ensures the stability of the system when it is attached to strictly passive operator and environment dynamics [36,18]. This is due to the fact that the connection of passive elements results in a passive system which directly implies its stability provided that  $F_h^*$  and  $F_e^*$  inputs are bounded [46]. The passivity of a two-port network modeled by (2.3) can be formulated in terms of the network

parameters using Raisbecks' passivity criteria as

$$\mathcal{R}\{z_{11}(j\omega)\} \geq 0, \quad (2.12)$$

$$\mathcal{R}\{z_{22}(j\omega)\} \geq 0, \quad (2.13)$$

$$4\mathcal{R}\{z_{11}(j\omega)\}\mathcal{R}\{z_{22}(j\omega)\} - (\mathcal{R}\{z_{12}(j\omega)\} + \mathcal{R}\{z_{21}(j\omega)\})^2 - (\mathcal{I}\{z_{12}(j\omega)\} - \mathcal{I}\{z_{21}(j\omega)\})^2 \geq 0 \quad (2.14)$$

for all  $\omega \geq 0$ , where  $\mathcal{R}\{\cdot\}$  and  $\mathcal{I}\{\cdot\}$  are equal to the real and imaginary value of their corresponding arguments.

Passivity condition is however rather conservative. Therefore, other less conservative techniques such as structured singular value condition [47] and absolute stability condition [44] have been utilized to ensure the stability of the system. Llewellyn's criteria states that a two-port network modeled by (2.3) is absolutely stable if and only if [43]

$$\mathcal{R}\{z_{11}(j\omega)\} \geq 0, \quad (2.15)$$

$$\mathcal{R}\{z_{22}(j\omega)\} \geq 0, \quad (2.16)$$

$$-\frac{\mathcal{R}\{z_{12}(j\omega)z_{21}(j\omega)\}}{|z_{12}(j\omega)z_{21}(j\omega)|} + 2\frac{\mathcal{R}\{z_{11}(j\omega)\}\mathcal{R}\{z_{22}(j\omega)\}}{|z_{12}(j\omega)z_{21}(j\omega)|} \geq 1 \quad (2.17)$$

for all  $\omega \geq 0$ , where  $|\cdot|$  represents the absolute value operator.

Researchers have used the two-port network model for teleoperation control design. Hannaford [37] proposed a bilateral impedance control architecture using a hybrid two-port model. Hashtrudi-zaad and Salcudean [42] gave a comprehensive review of the teleoperation controllers utilizing two-port network models. In

this article, the extension of the controller design from two-channel impedance controller to four-channel bilateral teleoperators with either impedance or admittance models is investigated. Also, the set of control parameters that provide the system with ideal transparency are calculated for each type of teleoperation. The surveyed control methods so far often sacrifice either the transparency or the stability of teleoperation in favor of the other. To facilitate a systematic approach to balance these conflicting teleoperation objectives, more sophisticated control architectures have been utilized in the literature.

### 2.3.1 Robust Controllers

Linear controllers based on the  $H_\infty$  and  $\mu$ -synthesis theories have been developed for the control of robotic manipulators to achieve robust stability and enhanced performance in the presence of uncertainties in the system dynamics. The reader is referred to [26] for a survey of linear and nonlinear robust control methods for robotic manipulators. By incorporating performance indices, disturbance signals, and uncertainty elements into the control design, these methods optimize an  $\ell_\infty$  norm of the closed-loop performance of the system while guaranteeing its stability under a worst-case uncertainty scenario [25, 24, 48, 49, 50].

In the context of teleoperation, these robust controller design methods have been utilized to achieve robust stability and transparency [32, 47, 31, 30]. Colgate [47] introduced an impedance shaping control technique for teleoperation systems. A general condition for the robustness of a bilateral teleoperator is calculated using the structured singular value( $\mu$ ). Kazerooni et. al. [29] proposed a control method based on  $H_\infty$ -optimal control for force-force teleoperation systems.

In [31], a general  $H_\infty$  framework has been proposed for four-channel bilateral teleoperation control. Hu et. al. [51] formulated the controller design as a multiple objective optimization problem and incorporated robust stability into the design of the controller. Recently, Sirouspour [52] proposed a robust controller for multi-master/multi-slave cooperative teleoperation based on  $\mu$ -synthesis.

Passivity based methods have been developed for the control of teleoperation systems in order to ensure robust stability in the presence of a wide range of uncertainties. Ryu et al. [53] have proposed an energy-based method for stable teleoperation using the time-domain passivity control under no communication delay. Based on the concept of passive decomposition, the authors in [54] proposed a non-linear controller that can provide useful task-specific dynamics for inertia scaling, motion guidance, and obstacle avoidance.

These robust control approaches can often lead to conservative controllers especially when the uncertainty range in the dynamics parameters are large which is usually the case in teleoperation systems. This is due to the fixed structure and/or parameters of the controller. Passivity-based control designs also often tend to sacrifice transparency objectives in favor of robust stability. This is due to the fact that these controllers have to maintain system's stability for all passive environment and arm dynamics.

### 2.3.2 Adaptive Controllers

Variable controller parameters and/or structure help adaptive controllers avoid the trade-off between system's performance and stability. Kress and Jansen [55] have introduced a tuning technique for a telerobotic arm controller which can

automatically determine the set of optimal controller gains for a simple PD controller by utilizing an intelligent search technique. Hashtrudi-zaad and Salcudean [56] have proposed a class of indirect adaptive bilateral control schemes. Their method uses measurements of master and slave position, velocity and acceleration to estimate the environment impedance. Shi et al. [57] have introduced new transparency concepts suitable for adaptive control of teleoperation systems with time varying parameters. In [34], local master/slave adaptive nonlinear position/force controllers have been combined with teleoperation coordinating controllers to guarantee stable teleoperation in the presence of dynamic uncertainty. The proposed method is applicable to both unilateral and bilateral teleoperation systems and in both position and rate control modes. The uncertainties in hand and environment dynamics are taken care of by adding these dynamics to the master and slave dynamics and applying the local adaptive controllers. Some other adaptive teleoperation control schemes can be found in [58,59].

In the decentralized control method proposed in this thesis, a multiple-model adaptive controller is used for teleoperation in unknown environments. Multiple-model controllers assume that system dynamics obey a model from a given finite set of models, with known or unknown parameters. These methods have previously been used for the control of robot manipulators. Ciliz and Narendra [60] utilized multiple models of a manipulator for identifying its unknown inertial parameters as well as the parameters of its load. Leaby and Sablan [61] augmented a mode-based controller with multiple-model adaptive estimation to minimize position trajectory tracking errors. Narendra and Balakrishnan [62] presented a general methodology for adaptive control using multiple models, switching and tuning.

They proposed specific performance indices in terms of model outputs and how to choose the best model using these indices. Zhang and Jiang [63] adopted interacting multiple model (IMM) filters to develop an active fault tolerant controller.

In the proposed decentralized method, the change in the slave/environment dynamics due to rigid contact, and parameter variations due to flexible contact, is handled with a multi-model control approach, in which mode-based controllers are designed for different phases of the operation. Switching between these mode-based control laws occurs according to the identified contact mode.

## 2.4 Time-delay Teleoperation Control

In applications in which the master and slave sites are at a distance from each other, communication time delay can severely degrade the transparency and stability of conventional teleoperation methods [18,64,8]. This latency imposes a trade-off between the conflicting requirements of stability and performance with the potential for instability increasing by the level of the performance [18,64]. A well-balanced trade-off between robust stability and performance can only be achieved by carefully incorporating knowledge about system model, time delay and modeling uncertainty in the control design process.

The trade-off between the stability and the transparency of time-delay teleoperation systems can be clearly noticed in the comparison of unilateral and bilateral controllers. Using high bandwidth position/velocity and/or force feedback loops, bilateral teleoperators can provide kinesthetic coupling and a more faithful rendering of the environment to the operator. However, this makes them far more susceptible to instability issues caused by the delay in communication channel.

On the other hand, unilateral teleoperators in which the operator merely receives visual feedback from the task environment are more robust with respect to the time delay [8].

In [64], the robust stability of a number of bilateral teleoperation architectures with respect to time delay is analyzed. Arcara and Melchiorri [65] have compared some existing teleoperation control schemes that address the issue of time delay from stability and performance perspectives. Imaida et. al. [66] have shown that, by providing sufficient damping at the master and slave ends, a delayed bilateral position-position teleoperation system can be stabilized, though at the expense of a sluggish response. In [67] a quantitative evaluation of operability has been investigated that depends on the communication time delay.

Lee and Lee [68] have proposed the concept of telemonitoring force feedback as a form of kinesthetic coupling for teleoperation under delays of up to a few seconds. The performance of the teleoperation system is optimized assuming delays of up to a known maximum value. In [69], state convergence has been used for time-delay teleoperation control design. In this method, master and slave manipulators are represented in linear state-space form and the delay is approximated using a first-order Taylor's expansion. Mirfakhrai and Payandeh [70] have developed a stochastic model for time delay over the Internet, which is becoming more popular as a communication medium.

### **2.4.1 Passivity-based Controllers**

A large number of existing time-delay teleoperation controllers employ the scattering theory and the concept of passivity to attain guaranteed stability, e.g. see [71,

72,73,74,75,76] among other references. A survey on passivity based controllers for time-delay teleoperation can be found in [77].

The introduction of wave variables enabled researchers to analyze and design stable force-reflecting teleoperation controllers. Based on the concepts of power and energy, wave variable transformation can handle large uncertainties and unknown models. A pair of wave variables,  $(u, w)$ , can be defined based on a pair of velocity and force signals,  $(v, f)$ , and using the following equations

$$u = \frac{bv + f}{\sqrt{2b}}, \quad (2.18)$$

$$w = \frac{bv - f}{\sqrt{2b}} \quad (2.19)$$

where  $b$  is positive scalar and can be used as a tuning parameter. Assuming the following power flow for a pair of velocity and force signals

$$P = v^T f \quad (2.20)$$

and using the definitions in (2.18) and (2.19), the power flow can be written as a function of the wave variables as

$$P = \frac{1}{2}u^T u - \frac{1}{2}w^T w. \quad (2.21)$$

It is worth mentioning that the contribution of the signal  $u$  is always positive and the contribution of the signal  $w$  is always negative.

The wave variable transformation and the concept of passivity have enabled researchers to develop stable controllers for time-delay teleoperation in presence

of uncertainties. In [71], it has been shown that for a time-delay teleoperation system, the master/slave control laws can be chosen such that the two-port model of the system is rendered passive. This ensures the stability of the system in contact with all passive arm and environment dynamics and irrespective of the amount of time delay. Niemeyer and Slotine [73] used the idea of passivity to provide energy conservation and to guarantee system's stability in the presence of an unknown time-delay. In [78], the authors have introduced an energy balance monitoring method to limit the generated energy by the system and achieve passivity in presence of time-varying communication delay.

Yokokohji et. al. [79] proposed a control scheme based on wave variables which minimizes the performance degradation in spite of time delay fluctuations. Benedetti et al. [80] introduced a force-feedback teleoperation controller based on wave-variables for variable time delays. In [81] a passivity-based controller was developed which can match the system parameters with changes in the delay by predicting the future values of delay. Ueda and Yoshikawa [76] presented a force-reflecting teleoperation controller with time delay using wave transmission methods. Conditions of stability for the proposed controller were also derived.

In passivity-based methods, enhanced robust stability is often gained at the expense of a highly reduced transparency. Consequently, several variations of the wave transformation-based control approach have been developed to improve its transparency. In [82], an adaptation of line terminating impedance functions was proposed to remedy the loss of transparency in bilateral teleoperation based on the scattering theory. In [83], a wave-based teleoperation controller has been combined with a Smith Predictor, a Kalman filter, and an energy regulator to improve

its transparency. The passivity has been used to enhance the performance of a proportional-derivative type time-delay teleoperation controller in [84].

In [85], new passive outputs were defined for master and slave robots which include position and velocity information. These outputs were then utilized to couple the master and slave devices and to enhance the teleoperation transparency. In [86], wave filtering and shaping have been employed to reduce the damping resulted from impedance matching. Furthermore, a high frequency force feedback at the slave side was used to increase the fidelity of teleoperation. Finally in [87], the authors have combined wave variables and a model-based slave predictor to achieve stability and reduce undesirable effects of the wave variable approach on the performance. A direct drift control scheme was also used to minimize the drift caused by the errors in the slave model.

## 2.4.2 Robust Controllers

Robust controllers have been utilized in the literature to control teleoperation systems in presence of time delay. In [31], a controller design based on the  $H_\infty$  theory has been presented. In this paper, a *Padé* approximation of the delay is employed. *Padé* approximation is usually valid at low frequency and can lead to closed-loop instability due to its inaccuracy, unless high-order approximations are used. High-order delay approximations, on the other hand, can lead to difficulties in obtaining a solution to the  $H_\infty$  control problem. In [32],  $H_\infty$  and  $\mu$ -synthesis methods have been used to design a stable teleoperation controller for a predefined delay maximum. Sename and Fattouh [33] have proposed a controller that stabilizes the teleoperation system in presence of environment uncertainties and independent of

the amount of time delay. In both [32, 33] the delay in teleoperation is treated as a perturbation to the system. The treatment of the delay as a perturbation to dynamics is unrealistic and can yield overly conservative control designs. This is due to the fact that the model of the system and delay are not being effectively used in the controller design.

### 2.4.3 Predictive Controllers

Heuristic techniques such as predictive displays and virtual environments rely on accurate models of the task environment to provide the operator with a realistic delay-free simulated response of the remote manipulator and environment for teleoperation under time delays up to several seconds [8, 88, 89, 90]. In [91], local models of the environment have been utilized to deliver predictive displays as well as delay-free simulated force-feedback to the operator. The local models utilized in the mentioned predictive display controllers can interact with the actual environment using the measurements received from the slave site through introducing the concept of time clutches [92, 93, 94]. The complexity of building accurate local models for unstructured environments and stability issues pertaining to real-time model identification and update limit the utility of such approaches in many applications.

Predictive control methods such as the Smith Predictor have also been developed for teleoperation [65, 83]. Ganjefar et al. [95] have discussed the behavior of Smith Predictor in teleoperation systems with respect to modelling and time delay errors. In [96] a predictive model-based controller has been proposed for

teleoperation with time-delay using state prediction. Different predictive force-feedback methods are also presented. References [97] and [98] have proposed predictive controller techniques for teleoperation with unbounded delays. Prekopiou et. al. [99] have developed a predictive controller for teleoperators based on a prediction of the user position and force. Polynomial or spline predictor have been used to predict the master's state. The method has shown a good performance in simulations, for short time delays and smooth hand movements. Nevertheless, excluding the arm dynamics in the control design can result in reduced transparency or even cause instability. Also, the stability of such predictive controller is not guaranteed.

Model-based predictive controllers have been successfully utilized in [1] and [2] to reduce the time-delay teleoperation system to a delay-free system in discrete and continuous-time, respectively. Linear Quadratic Gaussian controllers are then applied to the delay-free systems to achieve tracking objectives. Although multi-model switching strategies are used to increase the robustness of these controllers, they are still sensitive to modeling uncertainties, e.g. modeling errors in master/slave as well as operator arm and environment dynamics. Also, an additional time delay is introduced in the control loop due to the centralized structure of these controllers. The additional delay can potentially increase the controllers sensitivity to modeling uncertainties.

## 2.5 Time-delay Systems

There has been considerable effort in stability analysis and control synthesis for time-delay systems. This section is not a comprehensive review of the literature

on time-delay systems and focuses only on the approaches related to the methods proposed in this thesis. Interested reader is referred to the following survey papers on this topic [100, 101, 102]. Also, methods for robust stability analysis of systems with time delay can be found in the survey papers [103, 104].

Kwon et al. [105] and later Artstein [106] introduced a transformation to reduce an infinite-dimensional continuous-time linear control system with delayed control actions to an equivalent control system without delay. Consider a multi-input linear delay system with the following state-space dynamics

$$\dot{X}(t) = AX(t) + \sum_{j=1}^{n_I} B_j u_j(t - d_I^j) \quad (2.22)$$

where  $X(t)$  is the vector of states,  $u_j(t)$  is the  $j$ 'th input vector,  $n_I$  is the number of inputs and  $d_I^j$  is the delay in the  $j$ 'th input channel. By taking the derivative of a new state  $Z(t)$  defined below

$$Z(t) = X(t) + \sum_{j=1}^{n_I} \int_{t-d_I^j}^t e^{A(t-s-d_I^j)} B_j u_j(s) ds \quad (2.23)$$

and substituting  $\dot{X}(t)$  from (4.45), one may write

$$\dot{Z}(t) = AZ(t) + \sum_{j=1}^{n_I} e^{-Ad_I^j} B_j u_j(t). \quad (2.24)$$

The new system in (2.24) has no delay in its control signals and therefore, standard control methods such as state-feedback can be implemented for its stabilization. Systems with delays in both input and output channels can simply be converted

to an equivalent system with delays in inputs, if the delays in all output or all input ports are equal. However, teleoperation control systems involve non-identical delays in their input and output channels and this transformation in its original form is not suitable for such systems. A modified version of the transformation is introduced in this thesis and is utilized in the decentralized model-predictive teleoperation controller in Chapter 4.

An increased interest in the robust  $H_\infty$  control of time-delay systems since late 1990s has yielded several new results in this area, i.e. see [107, 108]. Most researchers have approached the problem as designing controllers for infinite-dimensional systems resulting in rather abstract and complex solutions unsuitable for the use in practical applications. In contrast in the work of [109] and [35], the treatment of the delay as a constraint on the controller has produced elegant tractable solutions to the  $H_\infty$  control of multi-input/multi-output (MIMO) systems with input/output (I/O) delays. In this method, a robust controller is synthesized through recursive solutions to *adobe*-type problems. Through explicit integration of model and delay information as well as the knowledge about system uncertainties in the control synthesis, this method provides a systematic mechanism for balancing the robust stability and performance objectives in time-delay systems.

Several schemes for adaptive control of time-delay systems have been proposed in the literature. Interested reader is referred to [110, 111] for a survey of such controllers. In [112], an adaptive controller for a class of input-delayed system has been presented. This control architecture depended on the relative degree of the plant transfer function. The stability of the closed-loop system is investigated through a Lyapunov-Krasovskii analysis. In [113] a modified reduction method

has been introduced which uses estimates of system parameters. These parameter estimates are updated by utilizing the measurements. However, this method is only applicable to single-input/single-output first-order systems and was never extended to more general forms of dynamics. In this thesis, we propose a new delay reduction technique which can be applied to an uncertain multi-input/multi-output system such as that in time-delay teleoperation.

# Chapter 3

## Teleoperation Dynamics and Performance Objectives

### 3.1 Introduction

This chapter studies the dynamics of the teleoperation system components, i.e. the master and slave robots as well as the operator's arm and the environment. In addition, the performance objectives in teleoperation control are discussed.

The chapter is organized as follows. In Section 3.1, the equations of motion of teleoperation subsystems are derived. Several properties of these dynamics are shown and at the end the combined nonlinear dynamics of the master/hand and slave/environment are presented. In Section 3.2, the performance objectives of teleoperation control are illustrated in the form of ideal transparency and its alternative, virtual tool impedance shaping.

## 3.2 Robot Dynamics

The master and slave robots in teleoperation are generally rigid multi-body mechanical manipulators. The dynamics of such manipulators can be expressed either in the *joint-space* or the *work-space* coordinates. Two different methods can be utilized to obtain the manipulator dynamics in the joint-space, i.e. the *Newton-Euler* recursive method and *Lagrange* formulation [114]. The Newton-Euler formulation is a numerical method and leads to a recursive type of solution for manipulator dynamics. It incorporates a forward recursion for propagating link velocities and accelerations and a backward recursion for propagating forces. On the other hand in the Lagrange method, the equations of motion are derived in a systematic way and independent of the reference coordinate frame and gives a closed-form solution for the dynamics. This method provides valuable insight about the nature of the system dynamics and is utilized in this thesis to obtain the dynamics of the teleoperation system.

For an  $n$ -degree-of-mobility robot, the *generalized coordinates* are defined as a set of variables  $\lambda_i, i = 1, \dots, n$ , which describe the link positions of the manipulator. Joint variables are the natural choice for the generalized coordinated for an open-chain mechanical manipulator

$$q = \begin{bmatrix} \lambda_1 \\ \vdots \\ \lambda_n \end{bmatrix}. \quad (3.1)$$

To derive the equations of motion of the mechanical system using the Lagrange

method, first the *Lagrangian* of the system is defined as a function of the generalized coordinates [114]

$$\mathcal{L}(q, \dot{q}) = \mathcal{T}(q, \dot{q}) - \mathcal{U}(q) \quad (3.2)$$

where  $\mathcal{T}$  and  $\mathcal{U}$  are the kinetic and potential energy of the system, respectively. The total kinetic energy of the  $n$ -link manipulator can be calculated using the following sum

$$\mathcal{T}(q, \dot{q}) = \sum_{i=1}^n (\mathcal{T}_{li} + \mathcal{T}_{mi}) \quad (3.3)$$

where  $\mathcal{T}_{li}$  and  $\mathcal{T}_{mi}$  are the kinetic energies of the link  $i$  and the link  $i$  actuator, and are functions of the joint positions and velocities, i.e.  $q$  and  $\dot{q}$ . The total potential energy stored in the manipulator is a function of joint positions and is obtained using the following sum

$$\mathcal{U}(q) = \sum_{i=1}^n (\mathcal{U}_{li} + \mathcal{U}_{mi}) \quad (3.4)$$

where  $\mathcal{U}_{li}$  and  $\mathcal{U}_{mi}$  are the contributions of the link  $i$  and its actuator to the potential energy. See [114] for the actual forms of the kinetic and potential energies in (3.3) and (3.4).

Using 3.2, the Lagrange's dynamics equations are formulated by the following equation set

$$\frac{d}{dt} \frac{\partial \mathcal{L}}{\partial \dot{\lambda}_i} - \frac{\partial \mathcal{L}}{\partial \lambda_i} = \xi_i, \quad i = 1, \dots, n \quad (3.5)$$

where  $\xi_i$  is the *generalized force* associated with the generalized coordinate  $\lambda_i$ . The generalized forces include the joint actuator torques, the joint friction torques, and

the torques induced by the forces at the end-effector in contact with the environment. It can be shown that using (3.2) and (3.5), the dynamics of an n-link manipulator in the joint-space can be written in the following compact matrix form

$$D(q)\ddot{q} + C(q, \dot{q})\dot{q} + G(q) = \tau - J^T(q)h \quad (3.6)$$

where  $D(q)$  is the inertia matrix,  $C(q, \dot{q})$  matrix represents velocity dependent elements such as Coriolis and centrifugal effects,  $G(q)$  corresponds to position-dependent forces such as the gravity,  $\tau$  is the vector of the joint actuator torques,  $J$  is the *geometric Jacobian* of the manipulator and  $h$  represents generalized external forces acting at the end-effector. The dynamics equations presented in (3.6) have the following properties [114,115,45].

**Property 1.** The inertia matrix,  $D(q)$ , is symmetric and uniformly positive-definite for  $\forall q \in \mathbb{R}^n$ . It also satisfies the following inequality

$$m_1\|\alpha\|^2 \leq \alpha^T D(q)\alpha \leq m_2\|\alpha\|^2 \quad \forall \alpha \in \mathbb{R}^n \quad (3.7)$$

where  $\|\cdot\|$  is standard euclidean norm, and  $m_1$  and  $m_2$  are known positive constants.

**Property 2.** For a particular choice of  $C(q, \dot{q})$  based on the *Christoffel symbols*, the following skew-symmetry property holds

$$\alpha^T \left( \frac{1}{2}\dot{D}(q) - C(q, \dot{q}) \right) \alpha = 0, \quad \forall \alpha \in \mathbb{R}^n. \quad (3.8)$$

For  $\alpha$  equal to  $\dot{q}$ , the property in (3.8) holds for all choices of the matrix  $C(q, \dot{q})$ .

**Property 3.** The dynamics in (3.6) can be expressed in the linear-in-parameter form as follows

$$D(q)\ddot{q} + C(q, \dot{q})\dot{q} + G(q) = Y(\ddot{q}, \dot{q}, q)\theta \quad (3.9)$$

where  $Y(\cdot)$  is a regressor matrix and is a function of joint positions, velocities and accelerations and  $\theta$  is a vector of unknown parameters.

**Property 4.** The norm of  $C(q, \dot{q})$  is bounded as

$$\|C(q, \dot{q})\| \leq \beta \|\dot{q}\| \quad (3.10)$$

where  $\beta$  is a positive constant.

In the work-space coordinates, the manipulator dynamics can be expressed in the following form [114]

$$D_A(X)\ddot{X} + C_A(X, \dot{X})\dot{X} + G_A(X) = \vartheta_A - h \quad (3.11)$$

where  $X \in \mathbb{R}^6$  is the generalized workspace position vector,  $h$  is defined in (3.6) and  $\vartheta_A$  is the contribution of the end-effector forces due to joint actuation,  $\tau$ .  $\vartheta_A$  and  $\tau$  are related by the geometric jacobian,  $J(q)$ , through the following equation

$$\tau = J^T(q)\vartheta_A. \quad (3.12)$$

Matrices  $D_A$ ,  $C_A$  and  $G_A$  in the work-space dynamics in (3.11) can be calculated

based on the matrices  $D$ ,  $C$  and  $G$  in the joint-space dynamics (3.6) as follows

$$\begin{aligned} D_A &= J^{-T} D J^{-1} \\ C_A \dot{x} &= J^{-T} C \dot{q} - D_A \dot{J} \dot{q} \\ G_A &= J^{-T} G. \end{aligned} \tag{3.13}$$

It can be shown that the work-space dynamics in (3.11) inherits all the properties of the joint-space dynamics in (3.7)-(3.10).

### 3.3 Teleoperation System Dynamics

The dynamics of the master ( $\gamma = m$ ) and slave ( $\gamma = s$ ) robots can be written in the form of (3.11) as

$$D_\gamma(X_\gamma) \ddot{X}_\gamma + C_\gamma(X_\gamma, \dot{X}_\gamma) \dot{X}_\gamma + G_\gamma(X_\gamma) = F_{c\gamma}^n - F_{ext,\gamma} \tag{3.14}$$

where  $F_{c\gamma}^n \in \mathbb{R}^6$  is the robots control force. The external end-effector forces on the master and slave robots correspond to  $F_h$  and  $F_e$  which are the hand and environment forces, respectively.

In general, the dynamics of the hand can be nonlinear, time-dependent, posture-dependent and subject-dependent [116,117,34]. Linear-time-invariant models have been employed by previous researchers in their work to approximate these dynamics. Such models have been effective in modeling and control of the manipulators while operated by the human arm [117, 34]. Based on these results, the following second-order decoupled linear-time-invariant (LTI) dynamics are considered for

the operator arm presented in the workspace coordinates

$$F_{ext,m} = -F_h = - \left( F_h^* - M_h \ddot{X}_m - B_h \dot{X}_m - K_h [X_m - X_{m0}] \right) \quad (3.15)$$

$$\|F_h^*\|_\infty \leq \alpha_h < +\infty, \quad \alpha_h > 0 \quad (3.16)$$

where  $M_h$ ,  $B_h$  and  $K_h$  are positive diagonal matrices corresponding to mass, damping and stiffness,  $F_h^*$  is the user exogenous force and  $X_{m0}$  represents the initial hand contact point. In (3.15), the user interaction force with the haptic device,  $F_h$ , is modeled by a bounded exogenous force,  $F_h^*$ , applied to a mass grounded by a spring-damper element at one end and attached to the end-effector at the other end, as depicted in Fig. 3.1(a). This linear mass-spring-damper element represents the passive dynamics of the user arm whereas the exogenous force models the user intentional force. Some of the nonlinearities involved in the arm dynamics can be captured by utilizing linear time-varying model for the operator arm, e.g. by allowing the model parameters to change over time. The proposed robust/adaptive and adaptive controllers in this thesis can handle such cases.

The dynamics of the environment is also modeled using the following second-order LTI system

$$F_{ext,s} = F_e = F_e^* + M_e \ddot{X}_s + B_e \dot{X}_s + K_e [X_s - X_{s0}] \quad (3.17)$$

$$\|F_e^*\|_\infty \leq \alpha_e < +\infty, \quad \alpha_e > 0 \quad (3.18)$$

where  $M_e$ ,  $B_e$  and  $K_e$  correspond to environment mass, damping and stiffness,  $F_e^*$  is the environment exogenous force, and  $X_{s0}$  represents the environment rest position. The environment mass-spring-damper model is shown in Fig 3.1(b).

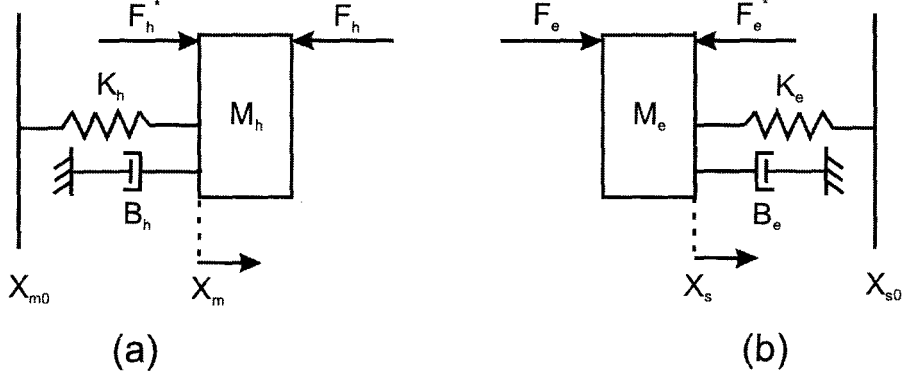


Figure 3.1: Linear mass-spring-damper models of (a) the operator's arm and (b) the environment.

Using (3.14), (3.15) and (3.17), the dynamics of the master robot incorporating the human operator and the dynamics of the slave robot incorporating the environment can be represented by

$$\begin{aligned} \mathcal{M}_m \ddot{X}_m + \mathcal{C}_m \dot{X}_m + \mathcal{G}_m &= F_{cm}^n + F_h^* & (3.19) \\ \mathcal{M}_m &= D_m(X_m) + M_h, \quad \mathcal{C}_m = C_m(\dot{X}_m, X_m) + B_h \\ \mathcal{G}_m &= G_m(X_m) + K_h[X_m - X_{m0}] \end{aligned}$$

and

$$\begin{aligned} \mathcal{M}_s \ddot{X}_s + \mathcal{C}_s \dot{X}_s + \mathcal{G}_s &= F_{cs}^n + F_e^* & (3.20) \\ \mathcal{M}_s &= D_s(X_s) + M_e, \quad \mathcal{C}_s = C_s(\dot{X}_s, X_s) + B_e \\ \mathcal{G}_s &= G_s(X_s) + K_e[X_s - X_{s0}]. \end{aligned}$$

It can be shown that the master/hand and slave/environment dynamics in (3.19) and (3.20) hold the properties in (3.7)-(3.10).

### 3.4 Performance of Master/Slave Teleoperation Systems

The performance of a bilateral teleoperation system is often measured by how well it is able to convey to the operator the perception of direct interaction with the actual or scaled task environment. Ideal *transparency*, also known as ideal kinesthetic coupling [38], can be described in terms of scaled position and force tracking between the master and slave robots [38,7], i.e.

$$f_h(t) = \alpha_f f_e(t) \quad (3.21)$$

$$x_m(t) = \alpha_p x_s(t) \quad (3.22)$$

where  $\alpha_f$  and  $\alpha_p$  denote the force and position scaling factors, respectively. Fig. 3.2(a) shows the interaction of the operator and the environment through an ideally transparent teleoperation system with unity position and force scaling factors. In this case there is a rigid dynamic-less connection between the operator arm and the environment. Acceleration measurement or equivalently force measurement, and an exact knowledge of the master and slave dynamics are required for achieving ideal transparency [38]. In practice, however, modeling and sensing errors, computation and control delays, and sampling rate limitations in a discrete-time implementation of the control can easily cause instability in an ideally transparent teleoperation system [38,41].

To alleviate these robustness issues with the ideal transparency, a virtual intervening tool can be introduced between the operator and the environment as

in (3.21)-(3.22), if  $k_t = 0$ . The virtual tool between the operator and the environment is depicted in Fig. 3.2(b).

As (3.23) and Fig. 3.2(b) suggest, in free motion the operator perceives the tool dynamics as he/she moves the master device. Also, in contact with the environment, the interaction between the operator and the environment feels like manipulating the environment through the virtual tool. Employing a tool with a high impedance would hinder the operator movements in free motion and interfere with the operator's perception of the environment in contact. Therefore, it is desired to keep the tool impedance as low as possible to achieve a more transparent response. However, as shown in [41], computation delays and sampling rate limitations in a discrete-time implementation limit the lowest achievable tool impedance.

It is worth noticing that the ideal transparency objectives introduced in this chapter are based on delay-free tracking measures. Alternatively, the desired performance objectives can be revised to include delayed force and position tracking. However, in this case the operator would perceive a distorted form of the environment impedance since the reflected force would be subject to a round-trip delay with respect to the position of the operator arm. Delay-free teleoperation, if achievable, would present the operator with the actual impedance of the remote environment. If needed, the visual display can also include a predictive element to avoid any discrepancy between visual and haptic feedback. The proposed controllers in this thesis will utilize model-based prediction mechanisms in attempt to approach such delay-free tracking goals by using any available model and sensor information. Achieving perfect prediction, however, requires an exact knowledge

of the system dynamics and more importantly the future of the hand and environment exogenous inputs to the system and is not possible in practice.

## Chapter 4

# Model-based Decentralized Control of Time-delay Teleoperation Systems

### 4.1 Introduction

In a centralized architecture the teleoperation controller resides either at the master or the slave side. Fig. 4.1 shows a general centralized teleoperation control with the controller at the master side. In our earlier contributions [1,2], model-based centralized controllers were proposed to enhance the performance of teleoperation by incorporating model and delay information in controller design. One drawback of such control schemes is the extra delay introduced either in the master or the slave control path. In Fig. 4.1, this extra delay can be clearly noticed between the slave measurement and control. By removing this delay through the use of two local controllers at each station, a decentralized control scheme can potentially lead to a system with higher stability margins and a better performance. Built on the earlier results in [2], in this chapter a model-based decentralized control scheme

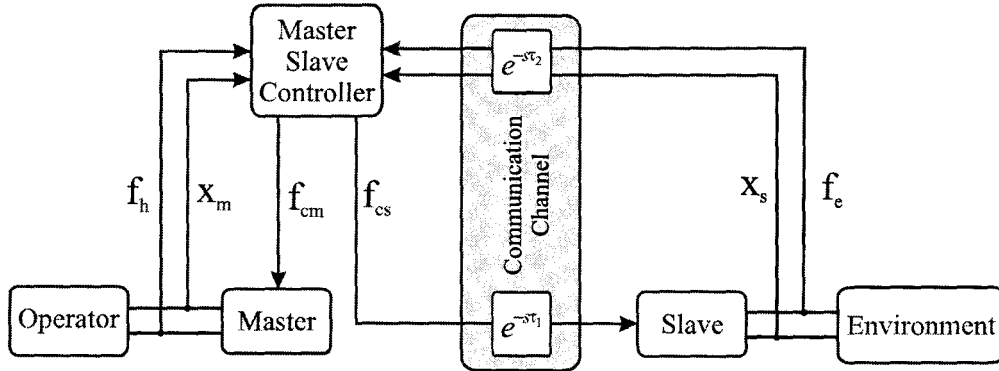


Figure 4.1: A centralized teleoperation architecture with controller at the master site.

for time-delay bilateral teleoperation is proposed to improve its robust stability while maintaining a high level of transparency. This is achieved through the use of delay-free local and delayed remote measurements by the two local controllers at the master and slave stations. Using the similar approach as in [2], a model-based delay reduction technique is utilized to obtain two centralized LQG output-feedback controllers. The stability margins of such control scheme is investigated using a frequency-sweeping test [22].

The chapter is organized as follows. An adaptive Lyapunov based linearization of the master and slave nonlinear dynamics is introduced in Section 4.2. The integration of the teleoperation dynamics and transparency objectives into a two-station decentralized control system is presented in Section 4.3. The proposed state/observation transformations for delay reduction and the two-station decentralized control of the resulting system are discussed in Section 4.4. The results of numerical performance and robust stability analysis are presented in Section 4.5. Experimental results are discussed in Section 4.6. The chapter is concluded in Section 4.7.

## 4.2 Linearization of Master/Slave Teleoperation Systems Dynamics

As demonstrated in (3.9) and to facilitate the development of adaptive Lyapunov-based linearization, the master device dynamics in (3.14) are rewritten in an equivalent linear-in-parameter format as follows [114]

$$D(X_m)\ddot{X}_m + C(X_m, \dot{X}_{m1})\dot{X}_{m2} + G(X_m) = Y(\ddot{X}_m, \dot{X}_{m1}, \dot{X}_{m2}, X_m)\theta \quad (4.1)$$

where  $Y(\cdot)$  is a regressor matrix function of motion variables and known constants, and  $\theta$  is a vector of unknown parameters. The following theorem is concerned with adaptive dynamic linearization of the nonlinear robot dynamics.

*Theorem 4.1:* Consider the robot dynamics in (3.14) and the following control law

$$F_{cm}^n = -F_h + Y(\ddot{X}_{mr}, \dot{X}_m, \dot{X}_{mr}, X_m)\hat{\theta} - K_d\rho_m \quad (4.2)$$

with

$$\begin{aligned} \dot{X}_{mr} &= \dot{X}_{md} - \Lambda\tilde{X}_m, & \tilde{X}_m &= X_m - X_{md}, & \rho_m &= \dot{\tilde{X}}_m + \Lambda\tilde{X}_m \\ X_{md} &= \mathcal{L}^{-1}\{(s^2M_m + sB_m + K_m)^{-1}(F_h + F_{cm})\} \end{aligned} \quad (4.3)$$

where  $M_m, B_m, K_m > 0$  are diagonal matrices,  $\mathcal{L}^{-1}\{\cdot\}$  is the inverse Laplace transform,  $s$  is the Laplace variable, and  $K_d > 0$ . Also  $\hat{\theta}$  is a parameter estimate vector

with the adaption law

$$\dot{\theta}_i = \begin{cases} 0 & \text{if } -[\Gamma Y^T \rho_m]_i > 0, \theta_i > \theta_i^{max} \\ 0 & \text{if } -[\Gamma Y^T \rho_m]_i < 0, \theta_i < \theta_i^{min} \\ -[\Gamma Y^T \rho_m]_i & \text{otherwise} \end{cases} \quad (4.4)$$

where  $\Gamma = \Gamma^T > 0$ ,  $[\cdot]_i$  denotes the  $i$ 'th element of the argument vector, and  $\theta_i^{min}$  and  $\theta_i^{max}$  are a priori known lower and upper bounds on the corresponding unknown parameter. Then the closed-loop dynamics are governed by

$$M_m \ddot{\bar{X}}_m + B_m \dot{\bar{X}}_m + K_m \bar{X}_m = \bar{F}_h + \bar{F}_{cm} + \eta_m. \quad (4.5)$$

In (4.5),  $\eta_m \in L_2 \cap L_\infty$  and  $\bar{X}_m, \bar{F}_h$  are produced by passing the corresponding variables through a linear low-pass filter with the transfer function

$$H(s) = \frac{c}{s + c} \quad (4.6)$$

and  $\bar{F}_{cm}$  is a new control signal related to  $F_{cm}$  in (4.3) via the filter  $H(s)$

$$\mathcal{L}\{\bar{F}_{cm}\} = H(s)\mathcal{L}\{F_{cm}\} \quad (4.7)$$

where the operator  $\mathcal{L}\{\cdot\}$  represents the Laplace transform.

*Proof:* Following steps similar to those in [118], first a candidate Lyapunov function

is defined as

$$V(t) = \frac{1}{2}\rho_m^T D(X_m)\rho_m + \frac{1}{2}\tilde{\theta}^T \Gamma^{-1}\tilde{\theta} \quad (4.8)$$

where

$$\tilde{\theta} = \hat{\theta} - \theta \quad (4.9)$$

is the parameter estimation error and  $\rho_m$  is defined in (4.3). By taking the derivative of  $V(t)$ , one can write

$$\dot{V}(t) = \frac{1}{2}\rho_m^T \dot{D}(X_m)\rho_m + \rho_m^T D(X_m)\dot{\rho}_m + \dot{\tilde{\theta}}^T \Gamma^{-1}\tilde{\theta}. \quad (4.10)$$

By finding this derivative along the system dynamics in (3.14), employing the control laws in (4.2) and the definitions in (4.3), it can be shown that

$$\dot{V}(t) = \frac{1}{2}\rho_m^T \dot{D}(X_m)\rho_m - \rho_m^T C(X_m, \dot{X}_m)\rho_m + \dot{\tilde{\theta}}^T \Gamma^{-1}\tilde{\theta} + \rho_m^T Y\tilde{\theta} - \rho_m^T K_d\rho_m. \quad (4.11)$$

After utilizing the adaptation law in (4.4) as well as the skew-symmetry property of  $\dot{D} - 2C$ , the following is derived

$$\dot{V}(t) \leq -\rho_m^T K_d\rho_m. \quad (4.12)$$

Considering (4.8) and (4.12), it can be concluded that  $\rho_m \in L_\infty$ . Also, integrating (4.12) yields

$$\int_0^t \dot{V}(t) \leq \int_0^t -\rho_m^T K_d\rho_m. \quad (4.13)$$

For  $t \rightarrow \infty$ , (4.13) can be rewritten as

$$V(0) - V(\infty) \geq \int_0^\infty \rho_m^T K_d \rho_m. \quad (4.14)$$

Moreover, (4.12) directly results in the following inequality

$$0 < V(0) - V(\infty) \leq V(0). \quad (4.15)$$

The inequality in (4.14) together with (4.15) show that  $\rho_m \in L_2$ . Consequently, from (4.3) it can be concluded that  $\tilde{X}_m, \dot{\tilde{X}}_m \in L_2 \cap L_\infty$  and therefore  $\tilde{X}_m \rightarrow 0$ . Now using the definition of  $\tilde{X}_m$  and  $X_{md}$  in (4.3), it is straightforward to show that Eq. (4.5) holds with

$$\eta_m = \mathcal{L}^{-1} \left\{ (s^2 M_m + s B_m + K_m) \frac{c}{s+c} \tilde{X}_m(s) \right\}. \quad (4.16)$$

Given that  $\tilde{X}_m, \dot{\tilde{X}}_m \in L_2 \cap L_\infty$ , it can be concluded that  $\eta_m \in L_2 \cap L_\infty$ . This error term can be incorporated into the proposed LQG-based control design framework as an external disturbance to the linearized dynamics in (4.5). The dynamics of the slave robot can be similarly linearized through the application of a local dynamic adaptive feedback linearizing control law resulting in

$$M_s \ddot{\bar{X}}_s + B_s \dot{\bar{X}}_s + K_s \bar{X}_s = \bar{F}_{cs} - \bar{F}_e + \eta_s \quad (4.17)$$

where  $\bar{F}_{cs}$  is a new control command for the linearized dynamics of the slave, and  $\bar{F}_e$  is the environment force filtered by  $H(s)$ . It should be noted that the master/slave robot position and velocity, and user and environment interaction forces

as well as  $\dot{\bar{F}}_{cm}$  and  $\dot{\bar{F}}_{cs}$  are required for the implementation of the proposed nonlinear control laws. The position/velocity and force signals are assumed to be directly available from sensors whereas  $\ddot{\bar{F}}_{cm}$  and  $\ddot{\bar{F}}_{cs}$  can also be computed, as will be seen later in this chapter.

In Section 4, the new LQG-based controllers will be developed using the linearized dynamics in (4.5) and (4.17) enforcing teleoperation transparency objectives based on the filtered master and slave position and force variables. Therefore in the selection of the bandwidth of the first-order low-pass filter  $H(s)$ , the choice of variable  $c$  in (4.6), one should be aware of its impact on teleoperation transparency in the frequency domain. A filter with a very low bandwidth can cause poor performance where the motion includes high frequency components. This is due to the fact that the controller is blind to those higher frequency parts of the measurement as they pass through the low-pass filter. Also, considering the relationship in (4.7), choosing a high bandwidth for  $H(s)$  can cause high frequency contents of  $\bar{F}_{cm}$  to be amplified in  $F_{cm}$ , resulting in a possibly noisy control input. In addition, choosing a filter with a high bandwidth in practice may cause noise amplification and even instability in case of discrete-time implementation of the controller. Finally, it must be pointed out that in the case that the master and slave have linear dynamics with known parameters, the dynamic linearization step can be simply skipped to avoid undue complexity.

The linearized master/slave dynamics in (4.5) and (4.17) become decoupled in different axes of motion if the user and environment dynamics are assumed decoupled. Such assumption leads to the decoupling of the control design into single-axis problems yielding considerable simplification in the control synthesis.

Therefore, throughout the rest of the chapter only a single-axis problem will be considered although the proposed solution can be generalized to the case in which the linearized dynamics are coupled among the axes of motion.

By dropping the bar symbol for notational simplicity, the linearized single-axis dynamics of master robot can be written as

$$m_m \ddot{x}_m(t) + b_m \dot{x}_m(t) + k_m x_m(t) = f_{cm}(t) + f_h(t) + \eta_m(t) \quad (4.18)$$

where  $m_m$ ,  $b_m$ , and  $k_m$  are mass, damping, and stiffness of the master interface, and  $x_m(t)$  is its position;  $f_{cm}(t)$  is the control signal and  $f_h(t)$  is the operator/device interaction force. The linear arm dynamics in (3.15) can be written in the following single-axis form

$$m_h \ddot{x}_m(t) + b_h \dot{x}_m(t) + k_h x_m(t) = f_h^*(t) - f_h(t). \quad (4.19)$$

In (4.19)  $m_h$ ,  $b_h$ , and  $k_h$  are respectively, mass, damping and stiffness of the operator's arm,  $x_m(t)$  has been defined in (4.18), and  $f_h^*(t)$  is a bounded exogenous input force. The arm dynamics in (4.19) can be combined with the master dynamics in (4.18) resulting in

$$(m_m + m_h) \ddot{x}_m(t) + (b_m + b_h) \dot{x}_m(t) + (k_m + k_h) x_m(t) = f_{cm}(t) + f_h^*(t) + \eta_m(t). \quad (4.20)$$

Similarly, the linearized dynamics of the slave robot in one axis can be written as

$$m_s \ddot{x}_s(t) + b_s \dot{x}_s(t) + k_s x_s(t) = f_{cs}(t) - f_e(t) + \eta_s(t) \quad (4.21)$$

where  $x_s(t)$  is the position of the slave,  $m_s$ ,  $b_s$ , and  $k_s$  are the slave mass, damping, and stiffness, respectively,  $f_{cs}(t)$  is the control signal and  $f_e(t)$  is the environment reaction force. The reaction force for compliant environments is modeled by (3.17) in single axis as

$$f_e(t) = \begin{cases} m_e \ddot{x}_s(t) + b_e \dot{x}_s(t) + k_e x_s(t) + f_e^*(t) & \text{in contact} \\ 0 & \text{free motion} \end{cases} \quad (4.22)$$

This environment model can be combined with the slave dynamics in (4.21) to obtain

$$(m_s + \sigma_f m_e) \ddot{x}_s(t) + (b_s + \sigma_f b_e) \dot{x}_s(t) + (k_s + \sigma_f k_e) x_s(t) = f_{cs}(t) - \sigma_f f_e^*(t) + \eta_s(t), \quad (4.23)$$

$$\sigma_f = \begin{cases} 1 & \text{slave in contact} \\ 0 & \text{slave in free motion} \end{cases} \quad (4.24)$$

During a rigid contact, the slave acceleration and velocity become zero and therefore the equations of motion can be simplified to

$$m_s(1 - \sigma_r) \ddot{x}_s(t) + b_s(1 - \sigma_r) \dot{x}_s(t) + k_s x_s(t) = f_{cs}(t) - \sigma_r f_e(t) + \eta_s(t) \quad (4.25)$$

and

$$\dot{x}_s(t) = (1 - \sigma_r) \dot{x}_s(t) \quad , \quad \ddot{x}_s(t) = (1 - \sigma_r) \ddot{x}_s(t) \quad (4.26)$$

with  $\sigma_r$  is similarly defined as in (4.24).

### 4.3 Decentralized Time-delay Teleoperation System

The performance objectives based on a virtual intervening tool as described in (3.23)-(3.25) are utilized in this chapter. By choosing the master position and velocity as state variables, the combined operator/master dynamics in (4.20) can be written in the following state-space form which is suitable for the application of the proposed output-feedback teleoperation controllers

$$\begin{aligned}\dot{X}_m(t) &= A_m X_m(t) + B_m f_{cm}(t) + G_m w_m(t) \\ y_m(t) &= C_m X_m(t) + D_m f_{cm}(t) + H_m w_m(t) + v_m(t)\end{aligned}\quad (4.27)$$

where  $X_m(t) = \begin{bmatrix} x_m(t) & v_m(t) \end{bmatrix}^T$  is the state vector and  $y_m(t) = \begin{bmatrix} x_m(t) & f_h(t) \end{bmatrix}^T$  is the output vector. The control signal  $f_{cm}(t)$  has been introduced in (4.18) and the disturbance signal is  $w_m(t) = \begin{bmatrix} f_h^*(t) & \tilde{f}_{cm}(t) \end{bmatrix}^T$  where  $\tilde{f}_{cm}(t)$  is the disturbance in the control signal  $f_{cm}(t)$  which also accounts for the adaptive control error  $\eta_m$  in (4.5);  $v_m(t)$  is a measurement noise vector. Similarly using (4.23)-(4.26), the state-space equations for the slave/environment subsystem can be written as

$$\begin{aligned}\dot{X}_s^i(t) &= A_s^i X_s^i(t) + B_s^i f_{cs}(t) + G_s^i w_s(t) \quad i = 1, 2, 3 \\ y_s^i(t) &= C_s^i X_s^i(t) + D_s^i f_{cs}(t) + H_s^i w_s(t) + v_s(t)\end{aligned}\quad (4.28)$$

where the indices 1, 2, 3 correspond to free motion, contact with a soft environment, and contact with a rigid environment, respectively;  $X_s^{1,2,3}(t) = \begin{bmatrix} x_s(t) & v_s(t) \end{bmatrix}^T$

and  $y_s(t) = \begin{bmatrix} x_s(t) & f_e(t) \end{bmatrix}$  is the measurement vector. The control signal is  $f_{cs}(t)$  and the disturbance vector is  $w_s(t) = \begin{bmatrix} f_e^*(t) & \tilde{f}_{cs}(t) \end{bmatrix}^T$ . The desired tool dynamics in (3.23) can also be written as

$$\begin{aligned} \dot{X}_t(t) &= A_t X_t(t) + B_t u_t(t) \\ y_t(t) &= X_t(t) \end{aligned} \quad (4.29)$$

where  $X_t(t) = \begin{bmatrix} x_t(t) & v_t(t) \end{bmatrix}^T$ ,  $u_t(t) = \begin{bmatrix} f_h(t) & f_e(t) \end{bmatrix}^T$  and  $y_t(t) = X_t(t)$ . The state-space matrices for the operator/master, slave/environment and tool dynamics are all presented in Appendix A.

Systematic output-feedback control schemes such as the LQG control are essentially centralized and must be stationed either at the master or slave site. For example, the top part of Fig. 4.2(a) depicts the case in which the centralized controller is placed at the master site hence having access to delay-free master and delayed slave position and force measurements. Similarly, the master control signal is delay-free whereas the slave control command is delayed because of its transmission over the communication channel. The bottom part of Fig. 4.2(a) displays the teleoperation system with the controller at the slave end. A centralized teleoperation architecture lends itself to the model-based delay-reduction and output-feedback control method proposed in [2]. The drawback, however, is that such architecture would introduce extra round-trip delay in the control loop, negatively affecting the trade-off between the performance and robust stability. For instance in the case of a centralized controller at the master site, local measurements at the slave site must undergo a round-trip delay before being used in the control of the

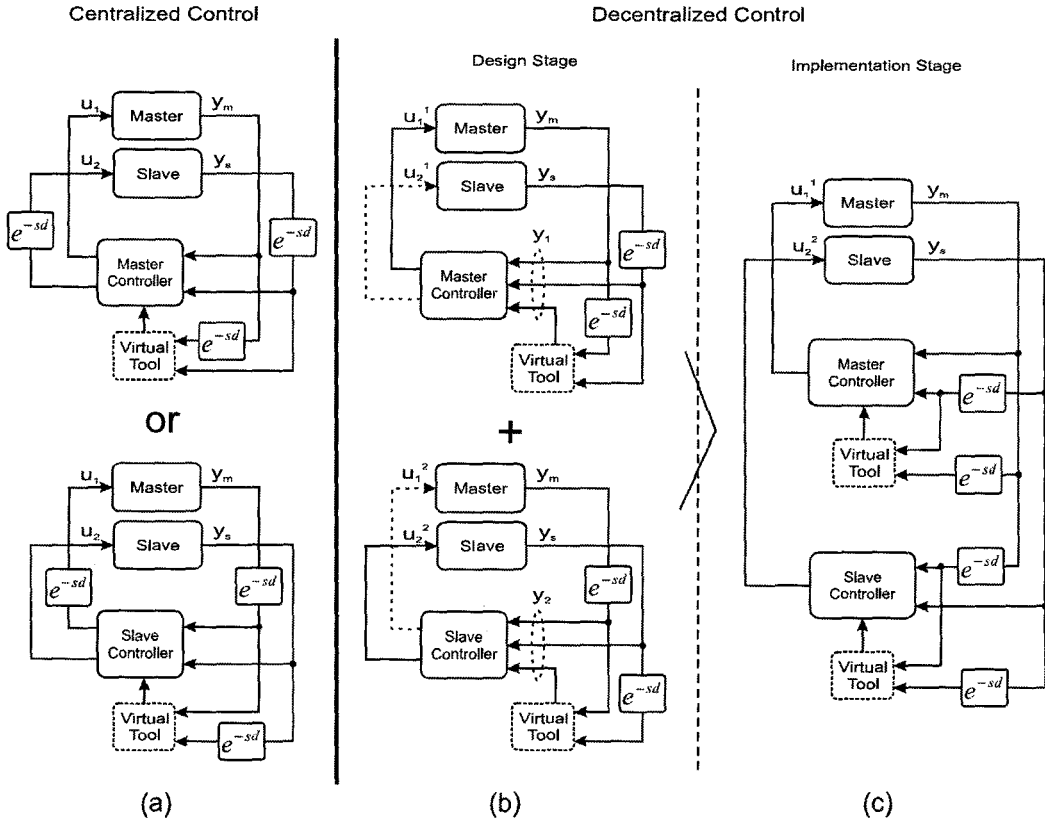


Figure 4.2: Conceptual representation of the proposed model-predictive decentralized teleoperation controller: (a) Centralized teleoperation control at master or slave side; (b) Decentralized sub-controller design; (c) Decentralized controller implementation.

slave robot.

To improve the performance-robustness trade-off of the delay reduction-based teleoperation controller in [2], a decentralized control architecture utilizing the proposed delay reduction technique is introduced here. The design concept is demonstrated in Fig. 4.2(b-c) in which the problem is divided into two centralized sub-controllers, one at the master and the other at the slave site. Each control

station has access to delay-free local and delayed remote position and force measurements. However unlike the case of the centralized controllers in Fig. 4.2(a), both control outputs of these sub-controllers are assumed to be delay-free. From the two control signals that are produced by each station, only the local control commands are used for the control of the master and slave robots as shown in Fig. 4.2(c), i.e.

$$f_{cm}(t) = u_1^1(t) , \quad f_{cs}(t) = u_2^2(t). \quad (4.30)$$

The remaining two control signals,  $u_2^1(t)$  and  $u_1^2(t)$ , are local estimates of the remote control forces at the master and slave sites and are not being used in the implementation. It should be pointed out that the stability of the closed-loop system with each individual sub-controller in Fig. 4.2(b) provides no guarantee of the stability of the actual system in Fig. 4.2(c). This will be thoroughly investigated later in this chapter.

The change in the slave/environment dynamics due to rigid contact and parameter variations due to soft contact can be handled within a multi-model control framework in which mode-based controllers are designed for different phases of the operation. In this strategy, dedicated controllers are designed for each mode of the operation and switching between controllers occurs according to the identified mode. Similar technique has been successfully employed in our previous contributions in [119, 1, 2] to handle the environment uncertainties.

### 4.3.1 Free motion/soft contact

The states of the system are obtained by combining the master, slave and tool sub-system dynamics. For the cases of free motion/soft contact, system states are defined as follows

$$X(t) = \begin{bmatrix} \alpha_p X_s(t) - X_m(t) & X_m(t) - X_t(t) & X_t(t) \end{bmatrix}^T \quad (4.31)$$

where  $X_m(t)$ ,  $X_s(t)$ , and  $X_t(t)$  have been introduced in (4.27), (4.28) and (4.29), and  $\alpha_f$  and  $\alpha_p$  have been defined in (3.23) and (3.24). The position tracking errors between the master and slave, and the master and virtual tool are included in the state vector. An application of output-feedback LQG control to regulate these tracking errors to zero would enforce the transparency objectives defined in (3.23)-(3.25). The evolution of the states is governed by

$$\begin{aligned} \dot{X}(t) &= AX(t) + Bu(t) + Gw(t) \\ u(t) &= \begin{bmatrix} f_{cm}(t) & f_{cs}(t) \end{bmatrix}^T \\ w(t) &= \begin{bmatrix} f_h^*(t) & f_e^*(t) & \tilde{f}_{cm}(t) & \tilde{f}_{cs}(t) \end{bmatrix}^T. \end{aligned} \quad (4.32)$$

It is straightforward to obtain the system matrices,  $A$ ,  $B$ , and  $G$  from  $A_m$ ,  $B_m$ ,  $C_m$ ,  $D_m$ ,  $G_m$ ,  $H_m$ ,  $A_s$ ,  $B_s$ ,  $C_s$ ,  $D_s$ ,  $G_s$ ,  $H_s$ ,  $A_t$ , and  $B_t$ . These matrices are presented in Appendix B. The measurement vectors are

$$\begin{aligned} y^1(t) &= \begin{bmatrix} y_m(t) & y_s(t-d) & y_t(t-d) \end{bmatrix}^T \\ y^2(t) &= \begin{bmatrix} y_m(t-d) & y_s(t) & y_t(t-d) \end{bmatrix}^T \end{aligned} \quad (4.33)$$

where  $y^1(t)$  and  $y^2(t)$  are the measurements received by master and slave sub-controllers, respectively, as shown in Fig. 4.2(b). The observations are the actual sensor readings  $x_m(t)$ ,  $f_h(t)$ ,  $x_s(t)$ , and  $f_e(t)$  as well as the virtual intervening tool states computed from (4.29). Note that the *delayed* virtual tool states are included in both measurement vectors in (4.33). This is due to the fact that tool states are produced by the control algorithm based on the desired tool dynamics and hand and environment forces according to (4.29). However as is evident in Fig. 4.2, the master and slave sub-controllers only have access to  $f_e(t - d)$  and  $f_h(t - d)$  and therefore must artificially delay their local force measurements to synchronize them with the delayed measurements. This is equivalent to the tool measurements being delayed by  $d$  in the master and slave sub-controllers. It is worth mentioning that the forward and backward delays are assumed to be equal. In case where these delays are not equal, this assumption can be relaxed by buffering those signals in the path with the smaller delay.

The operator's exogenous force  $f_h^*(t)$  is part of the unknown disturbance vector  $w(t)$  that excites the teleoperation control system and produces output error. In the LQG control design framework, the disturbances are modeled as white Gaussian noise with a flat power spectrum and the area under mixed weighted power spectrums of the output errors and the control signals under such excitation is minimized. The use of white noise model usually reflects a lack of information about the disturbance input in the control synthesis [120]. In teleoperation, however, it is reasonable to assume that the operator exogenous force has a low-pass power spectrum as the user cannot apply high-frequency intentional forces to the master device. This rather imprecise knowledge about the exogenous force can

be incorporated into the LQG framework using a simple pre-filtering technique as follows

$$\ddot{f}_h^*(t) + 2\alpha_{fh}\dot{f}_h^*(t) + \alpha_{fh}^2 f_h^*(t) = n_f(t) \quad (4.34)$$

where  $n_f(t)$  is a white Gaussian noise. While the proposed model has not been validated by human factors studies, our experience shows that in practice, it can significantly enhance the performance of the LQG-based teleoperation controller compared with a white noise model. This should not be surprising as using such model causes the controller to minimize the LQG cost function in the frequency range that operator force has most of its energy. In [121], a similar approach was successfully employed for the cancelation of biodynamic feedthrough in joystick-controlled machines.

The state-space equations of the system in free motion/soft contact after the augmentation of  $f_h^*$  and  $\dot{f}_h^*$  into the state vector are given by

$$\begin{aligned} \dot{X}_f(t) &= A_f X_f(t) + B_f u_f(t) + G_f w_f(t) \\ y_{f_k}^i(t) &= C_{f_k}^i X_f(t - d_O^k) + H_{f_k}^i w_f(t - d_O^k) + v_{f_k}^i(t - d_O^k) \\ i \text{ (station \#)} &= 1, 2 \quad k \text{ (output \#)} = 1, 2, 3 \end{aligned} \quad (4.35)$$

and

$$\begin{aligned}
X_f(t) &= \begin{bmatrix} X(t) & f_h^*(t) & \dot{f}_h^*(t) \end{bmatrix}^T \\
y_f^1(t) = y^1(t) &= \begin{bmatrix} y_m(t) & y_s(t-d) & y_t(t-d) \end{bmatrix}^T \\
y_f^2(t) = y^2(t) &= \begin{bmatrix} y_m(t-d) & y_s(t) & y_t(t-d) \end{bmatrix}^T \\
u_f(t) = u(t) &= \begin{bmatrix} f_{cm}(t) & f_{cs}(t) \end{bmatrix}^T \\
w_f(t) &= \begin{bmatrix} n_f(t) & f_e^*(t) & \tilde{f}_{cm}(t) & \tilde{f}_{cs}(t) \end{bmatrix}^T \\
v_f^1(t) = v_f^2(t) &= \begin{bmatrix} v_m(t) & v_s(t) & 0 \end{bmatrix}^T
\end{aligned} \tag{4.36}$$

where  $d_{\mathcal{O}}^k$  is the delay in the  $k$ 'th output channel. The reader is referred to Appendix B for the state-space matrices of the system dynamics in free motion/soft contact.

### 4.3.2 Rigid contact

When the slave is in rigid contact, its dynamics are governed by (4.25)-(4.26). In this case, the vector of states including the master and slave subsystems is chosen as

$$X(t) = [x_m(t) - \alpha_p x_s(t) \quad v_m(t) \quad x_s(t) \quad \tilde{f}_e(t) \quad \alpha_f \tilde{f}_e(t) - \tilde{f}_h(t)]^T \tag{4.37}$$

and the measurement vectors are

$$\begin{aligned} y^1(t) &= \begin{bmatrix} y_m(t) & x_s(t-d) & \tilde{f}_e(t-d) \end{bmatrix}^T \\ y^2(t) &= \begin{bmatrix} y_m(t-d) & x_s(t) & \tilde{f}_e(t) \end{bmatrix}^T. \end{aligned} \quad (4.38)$$

In (4.37),  $\tilde{f}_e(t)$  and  $\tilde{f}_h(t)$  are generated by passing force sensor measurements  $f_e(t)$  and  $f_h(t)$  through the following first-order filters with poles at  $-\beta$

$$\dot{\tilde{f}}_e(t) + \beta \tilde{f}_e(t) = \beta f_{cs}, \quad (4.39)$$

$$\dot{\tilde{f}}_h(t) + \beta \tilde{f}_h(t) = \beta f_h. \quad (4.40)$$

These first-order filters convert the algebraic equations of the rigid contact in (4.25)-(4.26) to dynamic-type equations involving new states  $\tilde{f}_e$  and  $\alpha_f \tilde{f}_e - \tilde{f}_h$ , enabling the application of the LQG control. The effect of the design parameter  $\beta$  is similar to the one described for the parameter  $c$  in (4.6). The dynamics of filtered force tracking error  $\alpha_f \tilde{f}_e - \tilde{f}_h$  can be easily derived from the filter equations above

$$\alpha_f \dot{\tilde{f}}_e(t) - \dot{\tilde{f}}_h(t) = -\beta(\alpha_f \tilde{f}_e(t) - \tilde{f}_h(t)) + \alpha_f \beta f_{cs} - \beta f_h \quad (4.41)$$

and  $f_h$  can be written in terms of the states and inputs. Assuming to be almost constant, the slave position in rigid contact,  $x_s(t)$ , is modeled by

$$\dot{x}_s(t) = w_{xs}(t) \quad (4.42)$$

where  $w_{xs}(t)$  is white Gaussian noise. The steps for incorporating the operator's exogenous force  $f_h^*(t)$  into the system states are similar to those in the previous case and will not be repeated here. The dynamics of the augmented system can be expressed by the following equations

$$\begin{aligned}\dot{X}_r(t) &= A_r X_r(t) + B_r u_r(t) + G_r w_r(t) \\ y_{r_k}^i(t) &= C_{r_k}^i X_r(t - d_O^k) + \sum_{j=1}^{n_I=2} D_{r_k j}^i u_{r_j}^j(t - d_O^k) + \\ &H_{r_k}^i w_r(t - d_O^k) + v_{r_k}^i(t - d_O^k)\end{aligned}\quad (4.43)$$

with

$$\begin{aligned}X_r(t) &= \begin{bmatrix} X(t) & f_h^*(t) & \dot{f}_h^*(t) \end{bmatrix}^T \\ y_r^1(t) = y^1(t) &= \begin{bmatrix} y_m(t) & y_s(t-d) & \tilde{f}_e(t-d) \end{bmatrix} \\ y_r^2(t) = y^2(t) &= \begin{bmatrix} y_m(t-d) & y_s(t) & \tilde{f}_e(t) \end{bmatrix} \\ u_r(t) &= \begin{bmatrix} f_{cm}(t) & f_{cs}(t) \end{bmatrix}^T \\ w_r(t) &= \begin{bmatrix} n_f(t) & \tilde{f}_{cm}(t) & \tilde{f}_{cs}(t) & w_{xs}(t) \end{bmatrix} \\ v_r^1(t) = v_r^2(t) &= \begin{bmatrix} v_m(t) & 0 \end{bmatrix}\end{aligned}\quad (4.44)$$

where  $n_I$  is the number of inputs. The state-space matrices in rigid contact are given in Appendix B.

## 4.4 Reduction and Control of Time-delay Systems

The dynamics of master/slave subsystems in (4.35) or (4.43) can be written as

$$\dot{X}(t) = AX(t) + \sum_{j=1}^{n_I=2} B_j u_j^j(t) + Gw(t), \quad (4.45)$$

$$y_k^i(t) = C_k^i X(t - d_O^k) + \sum_{j=1}^{n_I=2} D_{kj}^i u_j^j(t - d_O^k) + H_k^i w(t - d_O^k) + v_k^i(t - d_O^k), \quad k = 1, \dots, n_O = 3 \quad (4.46)$$

where  $X(t)$  is the vector of states,  $y_k^i(t)$  is the  $k$ 'th output vector at the  $i$ 'th station,  $w(t)$  and  $v_k^i(t)$  are process and measurement noise, respectively,  $n_I = 2$  and  $n_O = 3$  are the numbers of inputs and outputs.

The following state transformations must be defined

$$Z^i(t) = X(t - d) + W_m^i(t) \quad i = 1, 2 \quad (4.47)$$

where  $i$  is the station number,  $W_m^i(t)$  is associated with the output with the maximum latency with

$$W_k^i(t) = \sum_{j=1}^{n_I=2} \int_{t-d_O^k}^t e^{A(t-s-d_O^k)} B_j u_j^i(s) ds. \quad (4.48)$$

Taking the time derivative of (4.47) and replacing  $\dot{X}(t-d)$  from (4.45) yield

$$\begin{aligned}\dot{Z}^1(t) &= A_z Z^1(t) + B_{z1} u_1^1(t) + B_{z2} u_1^2(t) \\ &\quad - B_2 \{u_2^1(t-d) - u_2^2(t-d)\} + Gw(t-d) \\ \dot{Z}^2(t) &= A_z Z^2(t) + B_{z1} u_1^2(t) + B_{z2} u_2^2(t) \\ &\quad - B_1 \{u_1^2(t-d) - u_1^1(t-d)\} + Gw(t-d),\end{aligned}\quad (4.49)$$

$$A_z = A, \quad B_z = [e^{-Ad} B_1, e^{-Ad} B_2]. \quad (4.50)$$

For the system described in (4.45),  $X(t-d)$  can be written in terms of  $X(t-d_O^k)$  using standard results from the linear systems theory as follows [122]

$$\begin{aligned}X(t-d) &= e^{-Ad_O^k} X(t-d_O^k) - \sum_{j=1}^{n_I=2} \int_{t-d}^{t-d_O^k} e^{A(t-s-d)} B_j u_j^j(s) ds \\ &\quad - \int_0^{d_O^k} e^{-As} Gw(t-d+s) ds\end{aligned}\quad (4.51)$$

where  $d_O^k = d - d_O^k$ . Replacing  $X(t-d)$  in (4.47) from (4.51) for  $i = 1$ , and then multiplying both sides from left by  $C_k^1 e^{Ad_O^k}$ , one may write

$$\begin{aligned}C_k^1 e^{Ad_O^k} Z^1(t) &= C_k^1 X(t-d_O^k) - C_k^1 \int_{-d_O^k}^0 e^{-As} Gw(t+s) ds \\ &\quad + C_k^1 W_k^1 + \int_{t-d}^{t-d_O^k} C_k^1 e^{A(t-s-d_O^k)} B_2 (u_2^1(s) - u_2^2(s)) ds.\end{aligned}\quad (4.52)$$

It can be shown that in the case of teleoperation system, the last term in (4.52) is always zero for both free motion/soft contact and rigid contact cases and for every

$k$ , i.e.  $k = 1, 2, 3$ . Considering the first station output vectors in (4.33) and (4.38) for free motion/soft contact and rigid contact cases, the following is true

$$d_O^k = d, \quad k = 2, 3. \quad (4.53)$$

Therefore, the last term in (4.52) is equal to zero for  $k = 2, 3$  due to the equality of the integral bounds. For  $k = 1$ , the integral term represents an effect of the second input,  $f_{cs}$ , on the first output,  $y_m$ . Since the slave control action has no impact on the master outputs, the last term in (4.52) will also be equal to zero for  $k = 1$ . Similar results can be obtained for the second station by replacing  $X(t-d)$  in (4.47) from (4.51) for  $i = 2$ .

A new output vector for the  $k'$ th channel at station  $i$ ,  $y_{zk}^i(t)$ , is defined as

$$y_{zk}^i(t) = C_k^i e^{A d_o^{mk}} Z^i(t) + H_k^i w(t - d_O^k) + v_k^i(t - d_O^k) + C_k^i \int_{-d_o^{mk}}^0 e^{-As} G w(t+s) ds \quad (4.54)$$

or equivalently,

$$y_z^i(t) = C_z^i Z^i(t) + v_z^i(t) \quad i = 1, 2 \quad (4.55)$$

with

$$C_z^i = \left[ (C_1^i e^{A d_o^{m1}})^T \quad (C_2^i e^{A d_o^{m2}})^T \quad \dots \quad (C_{n_o}^i e^{A d_o^{mn_o}})^T \right]^T. \quad (4.56)$$

Using (4.46) and (4.52),  $y_{zk}^i(t)$  in (4.54) can be calculated from

$$y_{zk}^i(t) = y_k^i(t) - \sum_{j=1}^{n_I=2} D_{kj}^i u_j^i(t - d_O^k) + C_k^i W_k^i(t). \quad (4.57)$$

This completes the derivation of the reduced system dynamics and the output equations in (4.49) and (4.55). The calculation of the new observation vectors in (4.57) involves the computation of  $W_k^i(t)$ 's that can be obtained from

$$\begin{aligned} \dot{W}_k^i(t) &= A W_k^i(t) + \sum_{j=1}^{n_I=2} e^{-A d_O^k} B_j u_j^i(t) - \sum_{j=1}^{n_I=2} B_j u_j^i(t - d_O^k), \\ y_{wk}^i(t) &= C_k^i W_k^i(t), \quad W_k^i(0) = 0. \end{aligned} \quad (4.58)$$

Since the states of the system are not directly available, an observer/controller pair can be designed to control the reduced system based on the new measurements. The following theorem is needed for the control of the reduced system.

*Theorem 4.1:* The reduced system in (4.49) and (4.55) is stabilizable and detectable if the original system in (4.45) is stabilizable and detectable.

*Proof:* See Appendix C for the proof.

At each station  $i$ ,  $u_1^i$  and  $u_2^i$  are calculated using the local measurement according to the LQG control, to minimize the following cost function as  $T \rightarrow \infty$  [123]

$$J^i(u) = \frac{1}{T} E \left\{ \int_0^T [Z^i(t)^T Q Z^i(t) + u_1^i(t)^T R_1 u_1^i(t) + u_2^i(t)^T R_2 u_2^i(t)] dt \right\} \quad (4.59)$$

where  $E\{\cdot\}$  denotes the expected value, and  $Q \geq 0$ ,  $R_1 > 0$  and  $R_2 > 0$ .

The solution to (4.59) is a combination of a constant state-feedback gain produced by solving the corresponding deterministic Linear Quadratic (LQ) control and a *Kalman* filter state estimator for the  $i^{\text{th}}$  station, i.e.

$$u_1^i(t) = -K_1 \hat{Z}^i(t), \quad u_2^i(t) = -K_2 \hat{Z}^i(t). \quad (4.60)$$

The feedback gain  $K_1$  and  $K_2$  are given by

$$K_1 = R_1^{-1} B_z^{1T} S, \quad K_2 = R_2^{-1} B_z^{2T} S \quad (4.61)$$

and  $S$  is the solution to the following *Continuous-time Algebraic Riccati Equation* (CARE)

$$A_z^T S + S A_z - S \left( B_z^1 R_1^{-1} B_z^{1T} + B_z^2 R_2^{-1} B_z^{2T} \right) S + Q = 0. \quad (4.62)$$

The state estimate at the  $i^{\text{th}}$  station,  $\hat{Z}^i(t)$ , is the output of a *Kalman* filter with the following dynamics

$$\dot{\hat{Z}}^i(t) = A_z \hat{Z}^i(t) + B_z^1 u_1^i(t) + B_z^2 u_2^i(t) + L^i \left[ y_z^i(t) - C_z^i \hat{Z}^i(t) \right]. \quad (4.63)$$

The *Kalman* filter gain  $L^i$  is computed as follows [124]

$$L^i = P^i C_z^{iT} \Pi^{i-1} \quad (4.64)$$

where  $P^i$  is the solution to the following CARE

$$P^i A_z^T - P^i C_z^{iT} \Pi^{i-1} C_z^i P^i + A_z P^i + W = 0 \quad (4.65)$$

with

$$W = E \{ G w(t) w(t)^T G^T \} \quad (4.66)$$

and

$$\Pi^i = E \{ v_z^i(t) v_z^i(t)^T \} \quad (4.67)$$

being the covariances of the process and measurement noise, respectively. Certain conditions must be satisfied for the existence of a solution to the local LQG problems. These include the stabilizability of pair  $(A_z, B_z)$  and detectability of pair  $(C_z^i, A_z)$  among others. It can be shown that the teleoperation system satisfies all necessary requirements. Furthermore according to Theorem 4.1, the stabilizability and detectability are preserved under the proposed state/output transformations.

To achieve the teleoperation performance objectives, the  $Q$  and  $R$  matrices for free motion/soft contact are selected as

$$X_f(t)^T Q_f X_f(t) = q_1 (\alpha_p x_s(t) - x_m(t))^2 + q_2 (x_m(t) - x_t(t))^2 \quad (4.68)$$

with  $q_1 > 0$  and  $q_2 > 0$ . Similarly for rigid contact,

$$X_r(t)^T Q_r X_r(t) = q_1 (x_m(t) - \alpha_p x_s(t))^2 + q_2 (\alpha_f \tilde{f}_e(t) - \tilde{f}_h(t))^2. \quad (4.69)$$

The quadratic terms in (4.68) and (4.69) involve position and force tracking errors at concurrent sample times. Therefore despite the presence of the delay, the

#### 4.4.1 Closed-loop Stability Analysis

After replacing the inputs from (4.60) in the dynamic equations of the reduced system in (4.49), one may obtain

$$\begin{bmatrix} \dot{Z}^1(t) \\ \dot{Z}^2(t) \end{bmatrix} = \begin{bmatrix} A_z & 0 \\ 0 & A_z \end{bmatrix} \begin{bmatrix} Z^1(t) \\ Z^2(t) \end{bmatrix} + \begin{bmatrix} -B_z K & 0 \\ 0 & -B_z K \end{bmatrix} \begin{bmatrix} \hat{Z}^1(t) \\ \hat{Z}^2(t) \end{bmatrix} + \begin{bmatrix} B_2 K_2 & -B_2 K_2 \\ -B_1 K_1 & B_1 K_1 \end{bmatrix} \begin{bmatrix} \hat{Z}^1(t-d) \\ \hat{Z}^2(t-d) \end{bmatrix}. \quad (4.73)$$

Combining the reduced system dynamics in (4.73) with observer dynamics in (4.63) results in the following closed-loop dynamics

$$\begin{bmatrix} \dot{Z}(t) \\ \dot{\tilde{Z}}(t) \end{bmatrix} = \begin{bmatrix} A_z - B_z K & 0 & B_z K & 0 \\ 0 & A_z - B_z K & 0 & B_z K \\ 0 & 0 & A_z - L^1 C_z^1 & 0 \\ 0 & 0 & 0 & A_z - L^2 C_z^2 \end{bmatrix} \begin{bmatrix} Z(t) \\ \tilde{Z}(t) \end{bmatrix} + \begin{bmatrix} B_2 K_2 & -B_2 K_2 & -B_2 K_2 & B_2 K_2 \\ -B_1 K_1 & B_1 K_1 & B_1 K_1 & -B_1 K_1 \\ B_2 K_2 & -B_2 K_2 & -B_2 K_2 & B_2 K_2 \\ -B_1 K_1 & B_1 K_1 & B_1 K_1 & -B_1 K_1 \end{bmatrix} \begin{bmatrix} Z(t-d) \\ \tilde{Z}(t-d) \end{bmatrix} \quad (4.74)$$

where  $\tilde{Z}(t) = Z(t) - \hat{Z}(t)$ ,  $Z(t) = \begin{bmatrix} Z^1(t) & Z^2(t) \end{bmatrix}^T$  and  $\hat{Z}(t) = \begin{bmatrix} \hat{Z}^1(t) & \hat{Z}^2(t) \end{bmatrix}^T$ . It can be seen that the closed-loop dynamics are in the following general state-delayed form

$$\dot{x}(t) = A_0x(t) + A_1x(t - \tau) \quad (4.75)$$

with  $\tau = d$ . It is important to note that unlike in the case of the centralized delay reduction based controller in [2], the application of the decentralized delay reduction and control would not yield a completely delay-free system. The state delayed perturbation term  $A_1x(t - d)$  appearing in (4.74) is due to the difference between the actual control signal and their remote estimated counterparts in (4.49). Since the delay reduction and control process have utilized the model and delay information to provide an embedded predictive control element, the effect of the extra state-delay perturbation term on the system stability and performance is expected to be small compared with the case where the controller has no built-in predictor. In fact if  $u_1^1 = u_1^2$  and  $u_2^2 = u_2^1$ , this perturbation term would vanish from the closed-loop dynamics.

The closed-loop stability of a system in the form of (4.75) can be examined using the following theorem.

*Theorem* [Frequency-Sweeping Test]: For the state-delayed system in (4.75), provided that  $A_0$  is stable, the closed-loop stability is guaranteed for a maximum delay derived from

$$\tau = \min_i \left( \frac{\theta_i}{\omega_i} \right), \quad \forall \lambda_i(j\omega_i I - A_0, A_1) = e^{-j\theta_i} \quad (4.76)$$

where  $\lambda(A, B)$  denotes the generalized eigenvalues of matrices  $A$  and  $B$ .

*Proof:* See [22].

Note that the stability of matrix  $A_0$  in equation (4.74) is guaranteed owing to its upper triangular structure and the fact that the diagonal elements  $A_z - B_z K$ ,  $A_z - L^1 C_z^1$ , and  $A_z - L^2 C_z^2$  obtained from the LQ and Kalman filter design procedures have all of their eigenvalues in the left half of the complex plane. Provided that the maximum delay calculated from (4.76) is greater than the nominal delay assumed in the design, the stability of the reduced closed-loop system is guaranteed.

*Theorem:* If the reduced system is stabilized through a decentralized output-feedback controller, the original delayed system will also become stable.

*Proof:* The stability of the reduced system/observer implies that the reduced states  $Z^i(t)$  and their estimates  $\hat{Z}^i(t)$  remain bounded in the presence of bounded disturbance and noise. Hence, the control signal  $u^i(t)$  which is given by (4.60) is also bounded. From (4.47), the original system states can be written as

$$X(t-d) = Z^i(t) - W_m^i(t) \quad (4.77)$$

where

$$W_m^i(t) = \sum_{j=1}^{n_I} \int_{t-d}^t e^{A(t-s-d)} B_j u_j^i(s) ds \quad (4.78)$$

and  $W_m^i(t)$  is bounded as a result of boundedness of  $u^i(t)$ . Since both terms on the right hand side of (4.77) are bounded,  $X(t-d)$  and consequently  $X(t)$  are also bounded. Therefore the pair of observer/controller for the reduced system stabilizes the original system as well. Note that if *zero* is an asymptotically stable point for the reduced states  $Z^i(t)$ , then it would also be an asymptotically stable

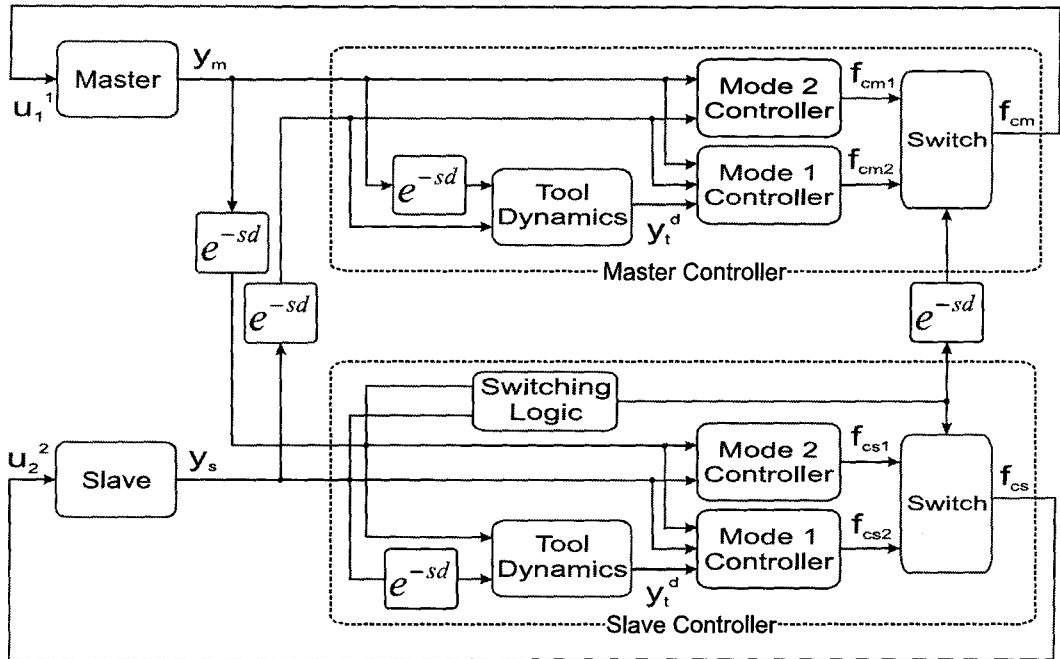


Figure 4.3: Multi-model decentralized controller for time-delay teleoperation.

point for the original states  $X(t)$ . Q.E.D.

A schematic of the proposed multi-model LQG-based teleoperation control system is displayed in Fig. 4.3. The sensor measurements are the master and slave positions as well as the hand and environment forces. Delayed hand and environment force signals are used to generate delayed virtual tool position and velocity at each station. These synthesized and actual observations enter the mode-based LQG controller blocks at the master and slave sites which produce the mode-based control signals. The switching logic, located at the slave side, uses the sensor measurements to identify the mode of operation and sends the result to the controller at the master side. This information is utilized in selecting the pair of control signals to be used by the master and slave actuators.

The disturbance signal  $f_h^*(t)$  is the cause of motion in teleoperation. The LQG design framework attempts to minimize the effect of the stochastic perturbations on the tracking errors, and as such coordinates the motions of master and slave robots. For example in free motion/soft contact, the disturbances drive the virtual tool dynamics in (4.29) which are not controllable by the control signals. Therefore, the controller must move the master and slave in response to operator's exogenous force such that the transparency objectives are achieved, i.e. the tracking errors among master, slave and tool are reduced.

Nominal model parameters of the operator, master robot, slave robot, and environment dynamics are used by the mode-based controllers. While the adaptive nonlinear controller in (4.2)-(4.4) renders the master and slave parameters constant, the operator and environment dynamics are usually unknown and time-varying. A deviation from the nominal parameters can degrade the system performance and even cause instability. Tightening the control loops through the adjustment of the LQ controller parameters could improve the performance by reducing the tracking errors and increasing the speed of the system response. However, this would be achieved at the expense of reduced stability margins and potential instability due to parametric uncertainty.

A careful selection of switching strategy can yield a smooth contact transition behavior. While the stability of mode-based controllers is guaranteed by the LQG design, it is difficult to prove the stability of the teleoperation system in the presence of control switching. This remains beyond the scope of the present thesis and will be a subject of future research. Interested reader is referred to [125] for an example of stability analysis of a gain-switching teleoperation controller.

As in [2], the control design can be extended to the case in which the delays in the forward and return paths of the master/slave communication link are different. The round-trip delay can be easily estimated by attaching time stamps to data packets. The one-way delays, if equal, are half of the round-trip delay. Otherwise, the master and slave computer clocks can be synchronized to an external universal time reference, e.g. Universal Coordinated Time, via GPS or special radio signals [126]. Once the computer clocks are synchronized, the data packets can be again time-stamped for delay estimation. Variable delays can be accommodated by adding buffers at the master and slave ends and delaying the signals to a maximum *a priori* known delay. The controller can then be designed for this constant delay.

## 4.5 Performance and Robust Stability Analysis for Single-axis Teleoperation

The proposed decentralized multi-model LQG control scheme is applied to a linear single-axis bilateral teleoperation system involving two similar masses. Since the master and slave dynamics are already linear and known, the adaptive nonlinear impedance controller is not needed in this example. Throughout the rest of the chapter, the delay values correspond to a round-trip communication unless otherwise noted. It is assumed that the operator manipulates the slave robot in free motion and in contact with a rigid environment and hence two mode-based controllers are designed.

The system parameters in Table 4.1 are based on the experimental setup which

System Parameters	
Master	$m_m = 1.0 \text{ kg}$ $b_m = 2.0 \text{ N.s/m}$ $k_m = 0 \text{ N/m}$
Slave	$m_s = 1.0 \text{ kg}$ $b_s = 2.0 \text{ N.s/m}$ $k_s = 0 \text{ N/m}$
Virtual Tool	$m_t = 1.0 \text{ kg}$ $b_t = 2.0 \text{ N.s/m}$ $k_t = 0 \text{ N/m}$
Arm	$m_h = 2.0 \text{ kg}$ $b_h = 2.0 \text{ N.s/m}$ $k_h = 30.0 \text{ N/m}$
Environment	$m_e = 0 \text{ kg}$ $b_e = 0 \text{ N.s/m}$ $k_e = 0 \text{ N/m}$
Other	$\alpha_f = 1$ $\alpha_p = 1$ $\alpha_{fh} = 0.01 \text{ rad/s}$ $\beta = 0.8 \text{ rad/s}$
LQG Controller Parameters	
Free Motion	
$q_1 = q_2 = 4 \times 10^5 \text{ m}^{-2}$	
$R = \text{diag}(0.1 \text{ N}^{-2}, 0.1 \text{ N}^{-2})$	
$E\{w_f w_f^T\} = \text{diag}(10^4 \text{ N}^2/\text{s}^4, 200 \text{ N}^2, 10^{-3} \text{ N}^2, 10^{-3} \text{ N}^2)$	
Rigid Contact	
$q_1 = 10^3 \text{ m}^{-2}$ $q_2 = 5.0 \text{ N}^{-2}$	
$R = \text{diag}(0.001 \text{ N}^{-2}, 0.001 \text{ N}^{-2})$	
$E\{w_r w_r^T\} = \text{diag}(10 \text{ N}^2/\text{s}^4, 10^{-4} \text{ N}^2, 10^{-6} \text{ N}^2, 10^{-5} \text{ m}^2/\text{s}^2)$	

Table 4.1: The system and the proposed decentralized controller parameters.

will be introduced in the next section. Typical values have been chosen for the arm mass, damping and stiffness. The LQG control parameters are also presented in this table. Among these, the values of measurement and disturbance noise powers were initially selected based on sensor and actuator specifications as well as a typical level of operator hand force and later refined based on simulation and experimental results. The  $Q$  and  $R$  in the LQG synthesis play a pivotal role in achieving a balance between performance and stability. A large  $Q$  and small  $R$  would generally yield faster poles, small tracking errors and enhanced performance at the expense of reduced robustness. These parameters have been manually tuned to strike a balance between these requirements.

In the forthcoming analysis, the stability margins and tracking performance of the decentralized controller with the above design parameters are numerically

calculated. The results are compared with those obtained from the centralized controller proposed in [2]. To allow for a fair comparison, the same set of parameters were employed in the design of both controllers.

#### 4.5.1 Robust stability analysis w.r.t parametric uncertainty

The robustness of the proposed controller with respect to parametric uncertainty can be investigated using classical linear analysis tools such as the Nyquist theorem. Among the model parameters, those of environment and operator are subject to uncertainty. In Fig. 4.4, the robustness of the mode-based controllers with respect to variations in individual parameters and as a function of communication latency is examined for both the decentralized and the centralized controllers. The environment stiffness in the design of the free-motion controller is set to 0 N/m.

The robustness of the controllers w.r.t. uncertainty in the environment stiffness is examined in Fig. 4.4(a) where the maximum stiffness for stability decreases by the amount of time delay from more than 4500 N/m for round-trip delays less than 20 ms to about 250 N/m for a delay of 250 ms. It can be seen that the decentralized controller exhibits a higher stability margin. In fact, this trend is evident in all other diagrams for free motion. In Fig. 4.4(c), the robustness of the free motion controller with respect to uncertainty in the operator's arm stiffness is demonstrated. The nominal value of stiffness used in the controller design is 30 N/m. In Figs. 4.4(b) and 4.4(d), the sensitivity of the free-motion and rigid-contact controllers with respect to variations in the operator's arm mass are examined where the nominal value of the arm mass used in the design is 2.0 kg according to Table 4.1. It can be seen that the arm mass stability margins in rigid contact are almost the same for

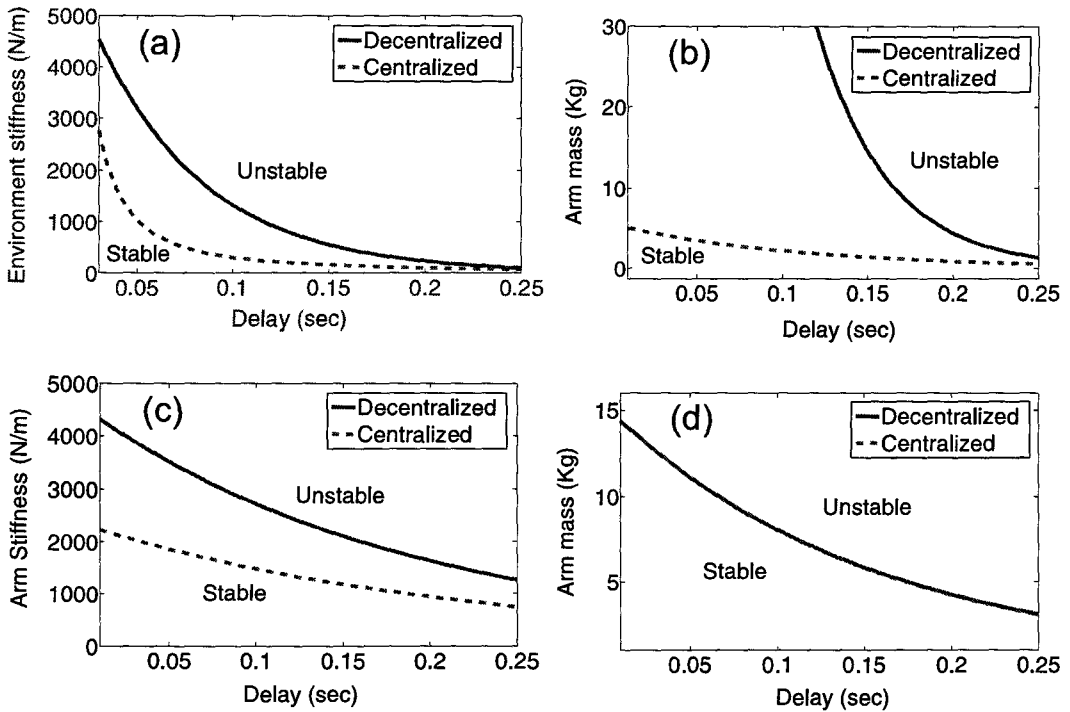


Figure 4.4: Robust stability analysis results in free motion: (a), (b) and (c), and in rigid contact: (d), as a function of time delay.

centralized and decentralized controllers. This trend is observed in the robustness of the rigid contact controllers with respect to changes in other parameters as well.

The robust stability analysis was also performed for simultaneous variations in two system parameters at a fixed delay of 125 ms, the results of which are given in Fig. 4.5. To obtain these graphs, one parameter was varied in fixed size steps while the stability bound on the second parameter was computed using the Nyquist criterion. Again it is evident that the decentralized controller enjoys higher or at least equal stability margins to those of the centralized controller.

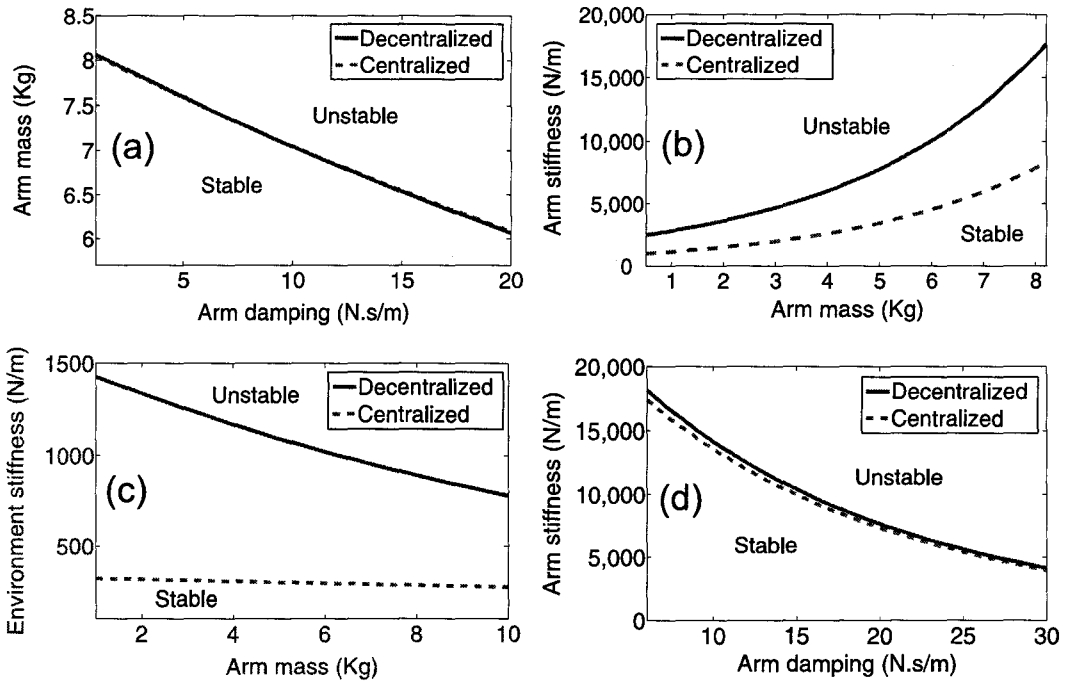


Figure 4.5: Robust stability analysis results in free motion: (b) and (c), and in rigid contact: (a) and (d), for simultaneous variations in two parameters.

#### 4.5.2 Performance analysis

The performances of the decentralized and centralized controllers formulated in terms of the  $H_2$  norm of the closed-loop system from the input  $f_h^*$ , to the tracking errors of interest are compared in this section. For a stable single-input/single-output transfer function  $H(s)$ , the square of the  $H_2$  norm is defined as [127]

$$\|H\|_2^2 = \frac{1}{\pi} \int_0^{+\infty} \|H(j\omega)\|^2 d\omega. \quad (4.79)$$

For low-pass systems, the upper limit of the integral can be replaced by a frequency  $\omega_f$  which is sufficiently above system bandwidth. This enables a numerical evaluation of the  $H_2$  norm.

The  $\|H\|_2^2$  norm of position and tool tracking errors in free motion, as well as position and force tracking errors in rigid contact are calculated using the frequency response of the closed-loop teleoperation system with the parameters given in Table 4.1. The results are presented in Fig. 4.6 as a function of the communication channel latency. From this figure, it is evident that using the same set of parameters, the decentralized clearly outperforms the centralized controller and exhibits smaller tracking errors in both free motion and rigid contact modes.

In summary, the preceding performance and stability analysis indicates that the proposed decentralized teleoperation controller, by avoiding an extra communication delay in the loop, yields tangible improvements over the centralized controller. That is it provides smaller tracking errors and higher stability margins with respect to parameter uncertainties.

### **4.5.3 Robust stability analysis w.r.t. perturbations in communication delay**

The proposed decentralized controller is designed based on the assumption of a known constant delay mainly for applications with a dedicated communication link. Under varying delay conditions, the measurement and control signals can be time-stamped, buffered and artificially delayed to maximum a priori known delay value, rendering the communication delay constant. This, however, may result in an excessively conservative design. A robustness analysis is performed

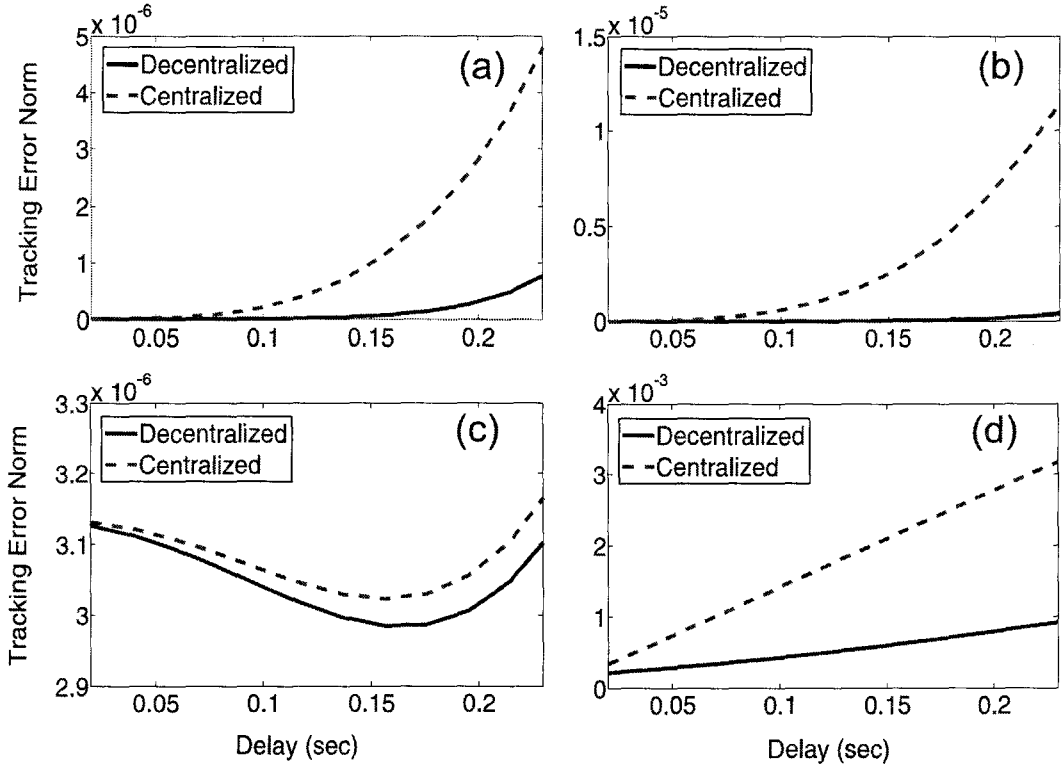


Figure 4.6:  $\|H\|_2^2$  for the closed-loop system from  $f_h^*$  to (a) position tracking error in free motion, (b) tool tracking error in free motion, (c) position tracking error in rigid contact, and (d) force tracking error in rigid contact.

to determine the maximum allowable variations in the delay to maintain the system stability. The value of the delay is assumed to be unknown and constant but different from that used in the design.

A model of the closed-loop decentralized teleoperation control system subject to uncertainty in communication delay is depicted in Fig. 4.7. The actual communication channel delay is equal to  $d + \Delta d$  where  $d$  is the nominal value used in the design and  $\Delta d$  is a delay perturbation. The stability margins, i.e. the maximum and minimum  $\Delta d$  for which the system remains stable, can be found using the

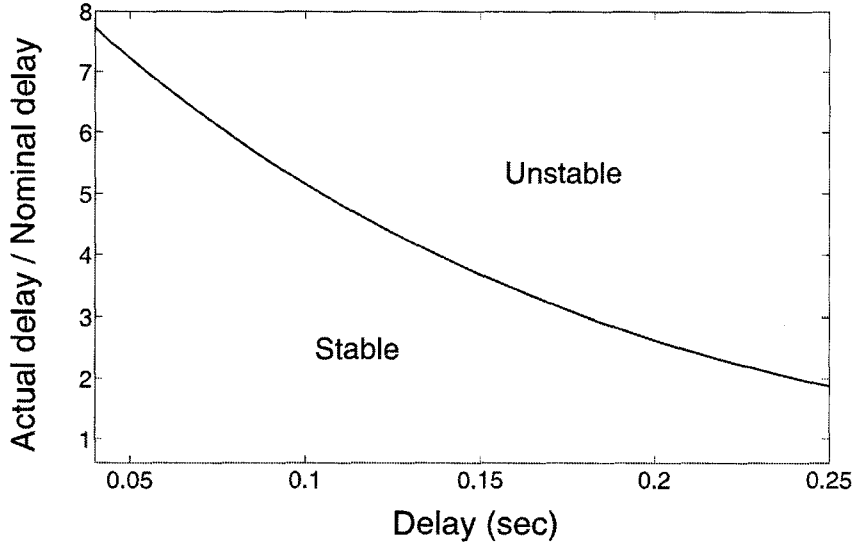


Figure 4.8: Maximum/minimun allowable time-delay variations to maintain stability.

is the perturbation to the communication channel delay. Since the proposed controller stabilizes the non-perturbed system, the stability margins can be found by sweeping  $\Delta d$  in the negative and positive directions and finding the first two points such that

$$\exists \omega > 0, p(j\omega, \Delta d) = 0. \quad (4.82)$$

Using the system and controller parameters in Table 4.1, the margins of stability for the decentralized controller in free motion are calculated and the results are plotted in Fig. 4.8. It can be seen from this figure that the system is stable for almost twice the nominal delay of 250 ms up to almost 8 times the nominal delay for delays smaller than 50 ms. The communication delay can also be reduced to zero while maintaining the stability.

## 4.6 Experimental Results

Fig. 4.9 depicts the teleoperation experimental setup. The system consists of two Quanser planar three-DOF pantographs powered by direct current motors employed as master and slave robots. The experiments were performed along one axis of motion while the other two axis were controlled by proportional-derivative controllers. These robots are equipped with *ATI Mini40* force sensors that measure the operator and environment forces. The control system runs on a PC platform under *Tornado/VxWorks* real-time operating system and is interfaced to the hardware by a *Q8* hardware-in-the-loop I/O board from Quanser. The control code is implemented using *Matlab Real-time Workshop* toolbox. The *ode1 (Euler)* integration routine of *Matlab/Simulink* is used for the discrete-time implementation of the proposed continuous-time controller. The control update rate is set to 2048 Hz, which is much higher than a typical closed-loop bandwidth of the teleoperation control system. Therefore, a discrete-time approximation of the continuous-time controller should be valid for practical purposes.

*Controller Switching:* The switching logic used in this method is simple. While in free motion, the controller enters the rigid mode if the magnitude of the measured environment force surpasses a predefined threshold. This will ensure that the force measurement noise cannot trigger a unintended switching event. To return to the free motion mode, the average slave velocity over a short window of time and the operator's measured force in the direction away from the contact must be below and above small predefined thresholds. Such logic reduces the possibility of erroneous switching due to the bouncing against the rigid environment during the

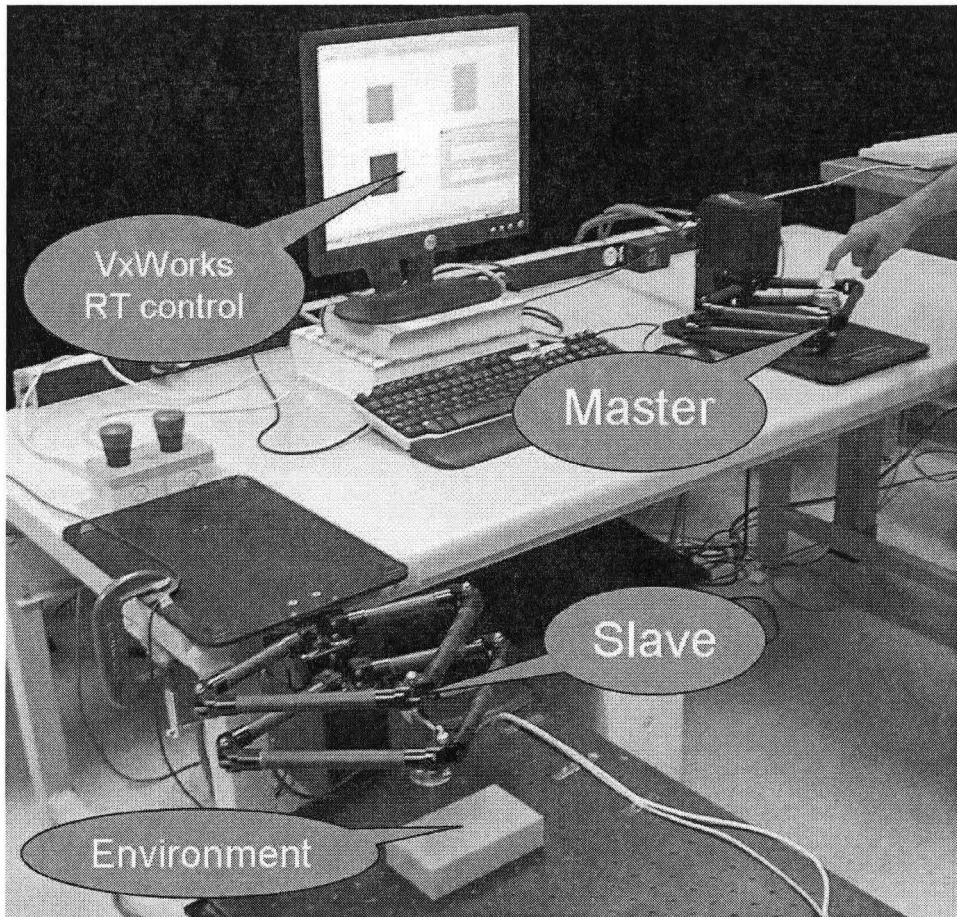


Figure 4.9: The experimental setup.

transition period. Also, the number of free-to-rigid bounces may be reduced simply by adding extra damping to the slave controller during the transition period. While in rigid contact, the virtual tool dynamics in Fig. 4.3 are disabled and the tool positions are reset to the slave position. This will enable a smooth transition from rigid contact to free motion.

In the experiments, the operator manipulates the slave robot in free motion and in contact with rigid environment. The experiments were conducted for three

different values of round-trip delay, i.e. 100 msec, 200 msec, and 300 msec. The delay was emulated by adding data buffers of appropriate size that store and delay the slave measurement and control signals. The system and controller parameters in the experiments are the same as those given in Table 4.1.

#### 4.6.1 Decentralized controller with 100 ms delay

In Fig. 4.10, the responses of the proposed controller under 100 ms of communication delay are plotted. The system is initially at rest until roughly  $t = 2\text{sec}$  when the operator begins moving the master/slave units in free motion. In free motion, the operator would feel the dynamics of the virtual tool as evident by the non-zero hand force observed in the free motion portions of Fig. 4.10. The positions of master, slave, and virtual tool closely follow each other in free motion which confirm that the performance objectives in (3.23) and (3.24) are both achieved with very high precision.

At  $t \simeq 18\text{sec}$ , the slave makes an initial contact with the rigid wall which triggers the controller to switch to the rigid mode. During the course of the first rigid contact from time 18-22 sec, the environment and hand forces as well as the master and slave positions closely track each other as can be seen in Fig. 4.10. The changes in forces are deliberately made by the operator to show the tracking performance of the controller. The contact is stable and is perceived rigid by the operator as is evident by the nearly constant master position despite the changes in the hand force. At  $t \simeq 22\text{ sec}$ , the operator withdraws the master and consequently the master/slave system returns to free motion following a smooth transition. Finally, a second rigid contact occurs at  $t \simeq 32\text{sec}$ .

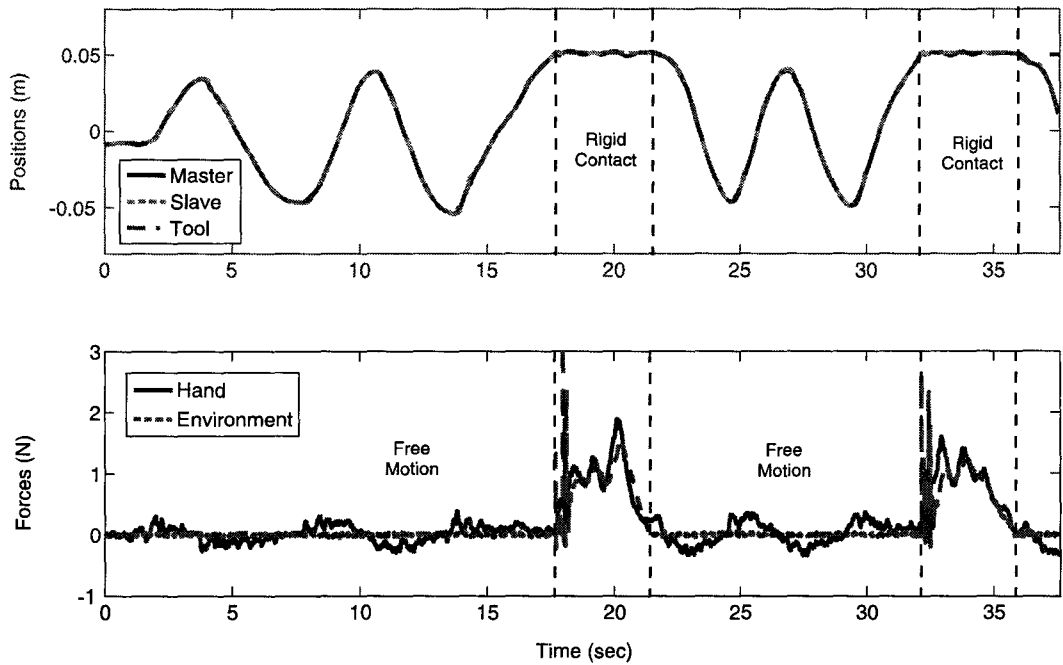


Figure 4.10: Decentralized controller with 100 msec delay in experiment: (a) position tracking and (b) force tracking.

#### 4.6.2 Decentralized controller with 200 ms delay

Fig. 4.11 illustrates the responses of the controller for a round-trip delay of 200 ms. As in the previous case, the experiments starts with the master/slave at rest, followed by a free motion operation and subsequent rigid contact and free motion phases. The transitions from free motion to rigid contact and vice versa are stable. The position tracking and virtual tool rendering in free motion as well as position and force tracking in rigid contact are quite satisfactory.

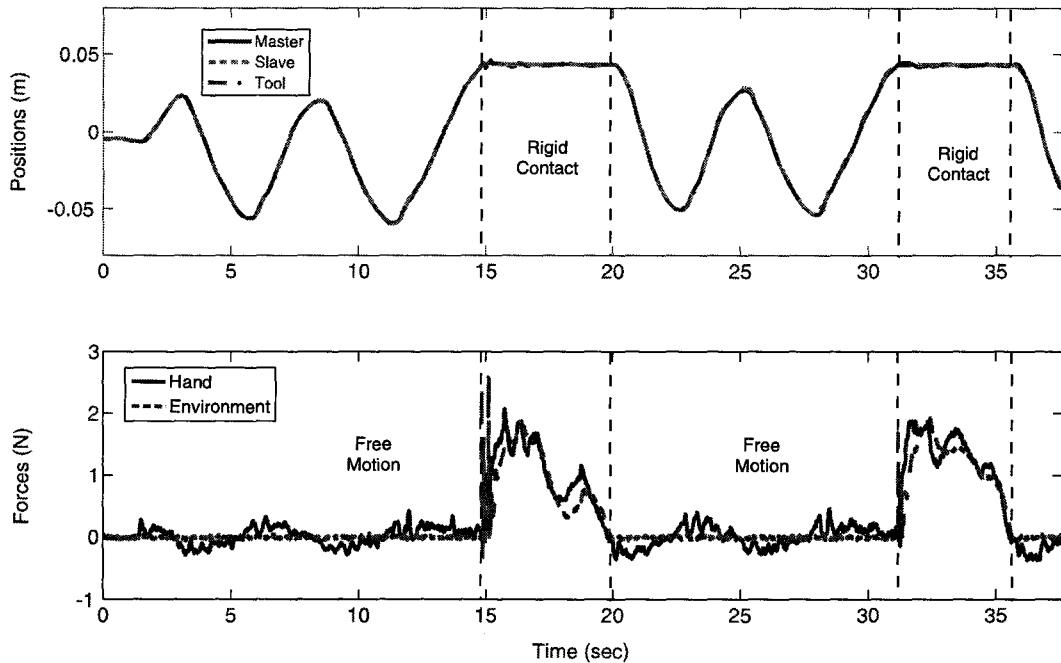


Figure 4.11: Decentralized controller with 200 msec delay in experiment: (a) position tracking and (b) force tracking.

### 4.6.3 Decentralized controller with 300 ms delay

In Fig. 4.12, the results of an experiment with the proposed teleoperation controller under 300 ms of communication latency are presented. Once again, the mode transitions are stable. Despite slight degradation in the performance of the free motion tracking, the results are still quite satisfactory.

## 4.7 Conclusions

The central idea of the proposed method in this chapter was to utilize system model and delay information to improve the stability-performance trade-off in

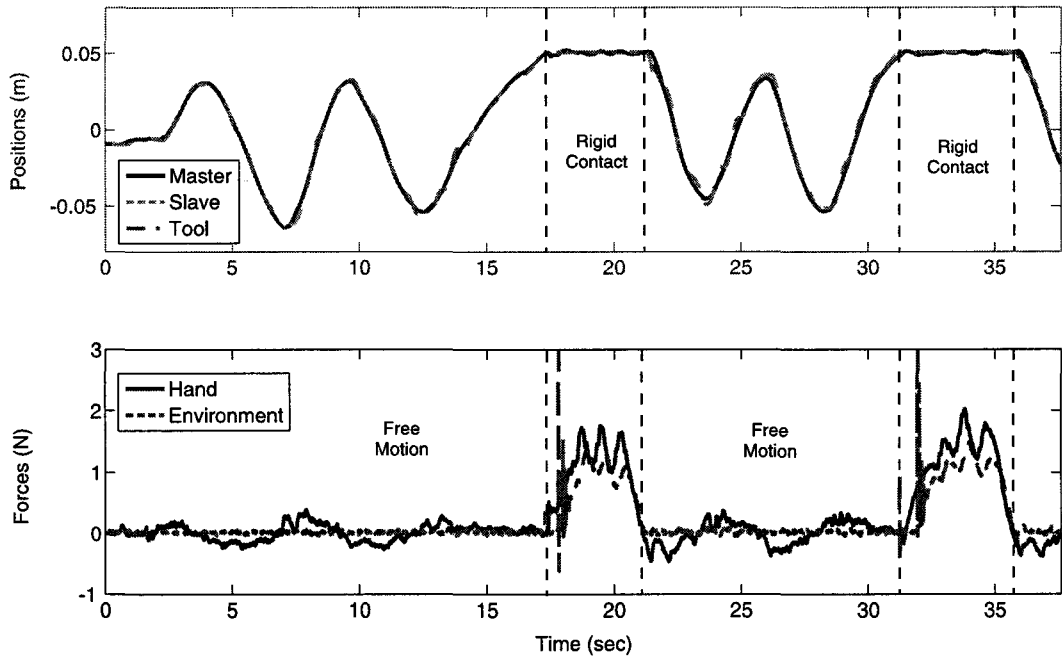


Figure 4.12: Decentralized controller with 300 msec delay in experiment: (a) position tracking and (b) force tracking.

time-delay bilateral teleoperation. To this end, a model-based decentralized controller was introduced. The application of a delay reduction method and LQG-based sub-controllers to the reduced dynamics at the master and slave sites resulted in a closed-loop dynamics with a state-delay perturbation term. A delay-dependent frequency sweeping test was employed to analyze the stability of these dynamics. Numerical robust stability and performance analysis demonstrated that, using the same set of design parameters, the new decentralized controller can provide enhanced performance and increased stability margins when compared with its centralized counterpart. Experimental studies with a single-axis teleoperation system also showed that the proposed approach is highly effective in improving teleoperation transparency under communication time delay.

The use of model and delay information in the proposed model-based decentralized control scheme improves the transparency of time-delay teleoperation. However, this controller can still be sensitive to modeling uncertainties such as master/slave modeling errors as well as variations in the environment and operator dynamics. Although the use of a multi-model control approach proved effective in handling large uncertainties in the environment dynamics, the stability of such switching control strategy must be carefully investigated. To systematically handle the modeling uncertainties, robust and adaptive control schemes are developed for time-delay teleoperation control and are presented in the following chapters.

# Chapter 5

## Adaptive/Robust Control for Time-delay Teleoperation

### 5.1 Introduction

To systematically balance the trade-off between the robust stability and performance in time-delay teleoperation, in this chapter a two-stage adaptive/robust control scheme is proposed. This method utilizes the model and delay information as well as the knowledge about the system uncertainties in the control synthesis process. In the first stage through the use of local Lyapunov-based adaptive controllers, the dynamics of the master and slave robots are linearized and are rendered independent from their parameters. Using these new dynamics, in the second stage teleoperation control is formulated as an  $H_\infty$  robust control synthesis with multiple I/O delays. The resulting problem is solved using decompositions into single-delay adobe-type problems.

This chapter is organized as follows. In Section 5.2, the local adaptive/nonlinear

controllers are introduced. The teleoperation control problem is formulated in Section 5.3. The solution to the  $H_\infty$  robust control of time-delay MIMO systems is discussed in Section 5.4. A numerical design example using the proposed method along with an analysis of performance and stability characteristics of the resulting solution are given in Section 5.5. Experimental results are provided in Section 5.6.

## 5.2 Master/Slave Local Adaptive Control

Consider the nonlinear combined dynamics of master/hand and slave/environment described in (3.19) and (3.20). Adaptive nonlinear controllers are employed at the master and slave sites to linearize these dynamics. These controllers are similar to those proposed in [34]. The local control laws for the master and slave robots are given by

$$F_{cm} = Y_m \hat{\Theta}_m + \mathcal{K}_m (V_{md} - V_m + A \tilde{F}_h - \beta X_m) + \alpha_h \text{sign}(V_{md} - V_m + A \tilde{F}_h - \beta X_m) \quad (5.1)$$

$$F_{cs} = Y_s \hat{\Theta}_s + \mathcal{K}_s (V_{sd} - V_s - A \tilde{F}_e - \beta X_s) \quad (5.2)$$

where  $V_{md}$  and  $V_{sd}$  are master and slave command vectors to be introduced later,  $V_m$  and  $V_s$  are master and slave velocity vectors,  $\mathcal{K}_m, \mathcal{K}_s > 0$ ,  $A > 0$  are diagonal matrices and  $\tilde{F}_\gamma$  is a filtered force obtained from

$$\dot{\tilde{F}}_\gamma = C(F_\gamma - \tilde{F}_\gamma) \quad (5.3)$$

where  $C > 0$  is diagonal. The use of filtered forces instead of the original signals in (5.1) and (5.2) eliminates the need for measurement force derivatives in the implementation. The effects of the filter bandwidth on system performance and stability are similar to the ones discussed for (4.6). In (5.1) and (5.2),  $\hat{\Theta}_\gamma$  denotes an estimate of  $\Theta_\gamma$  which contains all unknown dynamic parameters of the master ( $\gamma = m$ ) or slave ( $\gamma = s$ ). Furthermore,  $Y_m$  and  $Y_s$  are regressor matrices defined by

$$Y_s \Theta_s = \mathcal{M}_s \frac{d}{dt} [V_{sd} - A\tilde{F}_e - \beta X_s] + C_s [V_{sd} - A\tilde{F}_e - \beta X_s] + \mathcal{G}_s \quad (5.4)$$

$$Y_m \Theta_m = \mathcal{M}_m \frac{d}{dt} [V_{md} + A\tilde{F}_h - \beta X_m] + C_m [V_{md} + A\tilde{F}_h - \beta X_m] + \mathcal{G}_m. \quad (5.5)$$

The parameter adaptation laws are governed by

$$\dot{\hat{\Theta}}_{\gamma i} = \begin{cases} 0, & \hat{\Theta}_{\gamma i} \leq \Theta_{\gamma i}^- \text{ and } Y_{\gamma i}^T \rho_\gamma \leq 0 \\ 0, & \hat{\Theta}_{\gamma i} \geq \Theta_{\gamma i}^+ \text{ and } Y_{\gamma i}^T \rho_\gamma \geq 0 \\ \Gamma_{\gamma i} Y_{\gamma i}^T \rho_\gamma, & \text{otherwise} \end{cases} \quad (5.6)$$

$$\rho_s = V_{sd} - V_s - A\tilde{F}_e - \beta X_s \quad (5.7)$$

$$\rho_m = V_{md} - V_m + A\tilde{F}_h - \beta X_m \quad (5.8)$$

where  $\gamma i$  denotes the  $i$ th parameter of either master ( $\gamma = m$ ) or slave ( $\gamma = s$ ),  $\Gamma_{\gamma i} > 0$  is a parameter update gain,  $\Theta_{\gamma i}^-$  and  $\Theta_{\gamma i}^+$  denote the minimum and maximum allowable values of  $\Theta_{\gamma i}$ , and

$$\tilde{\Theta} = \hat{\Theta} - \Theta \quad (5.9)$$

is parameter estimation error.

The following Lyapunov function can be utilized for the master subsystem

$$W_m = \frac{1}{2}\rho_m^T \mathcal{M}_m \rho_m + \frac{1}{2}\tilde{\Theta}_m^T \Gamma_m^{-1} \tilde{\Theta}_m. \quad (5.10)$$

By taking the derivative of  $W_m$  one can write

$$\dot{W}_m = \frac{1}{2}\rho_m^T \dot{\mathcal{M}}_m \rho_m + \rho_m^T \mathcal{M}_m \dot{\rho}_m + \dot{\tilde{\Theta}}_m^T \Gamma_m^{-1} \tilde{\Theta}_m. \quad (5.11)$$

By finding this derivative along the system dynamics in (3.19), employing the control law in (5.1) and using the definition of  $\rho_m$  in (5.8), it can be shown that

$$\dot{W}_m = \frac{1}{2}\rho_m^T \dot{\mathcal{M}}_m \rho_m - \rho_m^T C_m \rho_m + \dot{\tilde{\Theta}}_m^T \Gamma_m^{-1} \tilde{\Theta}_m - \rho_m^T Y_m \tilde{\Theta}_m - \rho_m^T \mathcal{K}_m \rho_m. \quad (5.12)$$

Finally, the following can be derived

$$\dot{W}_m \leq -\rho_m^T \mathcal{K}_m \rho_m \quad (5.13)$$

where the adaptation law in (5.6) as well as the skew-symmetry property of  $\dot{\mathcal{M}}_m - 2C_m$  have been utilized. Similarly the following Lyapunov function is defined for the slave subsystem

$$W_s = \frac{1}{2}\rho_s^T \mathcal{M}_s \rho_s + \frac{1}{2}\tilde{\Theta}_s^T \Gamma_s^{-1} \tilde{\Theta}_s. \quad (5.14)$$

Again using (3.20), (5.2), (5.6), and the skew-symmetry of  $\dot{M}_s - 2C_s$ , one may obtain

$$\dot{W}_s \leq -\rho_s^T K_s \rho_s. \quad (5.15)$$

Using (5.10)-(5.15), it can be concluded that

$$\rho_s \in L_\infty, \quad \rho_m \in L_\infty. \quad (5.16)$$

By integrating (5.13) and (5.15), it can also be shown that the signals  $\rho_m$  and  $\rho_s$  have bounded energy and therefore

$$\rho_s \in L_2 \cap L_\infty, \quad \rho_m \in L_2 \cap L_\infty. \quad (5.17)$$

Considering (5.7), (5.8) and (5.17), and using the following LTI models of the hand and environment,

$$f_e = f_e^* + \hat{Z}_e x_s, \quad f_h = f_h^* - \hat{Z}_h x_m, \quad (5.18)$$

simplified linearized dynamics in the form of Fig. 5.1 can be derived for the master and slave subsystems. Here

$$\begin{aligned} \hat{Z}_h &= Z_h + \Delta Z_h \\ \hat{Z}_e &= Z_e + \Delta Z_e \end{aligned} \quad (5.19)$$

where  $Z_h$  and  $Z_e$  are nominal impedances of the user and environment with  $\Delta Z_h$  and  $\Delta Z_e$  being their associated uncertainty. Measurement noise  $n_{xm}(n_{xs})$  and  $n_{fh}(n_{fe})$

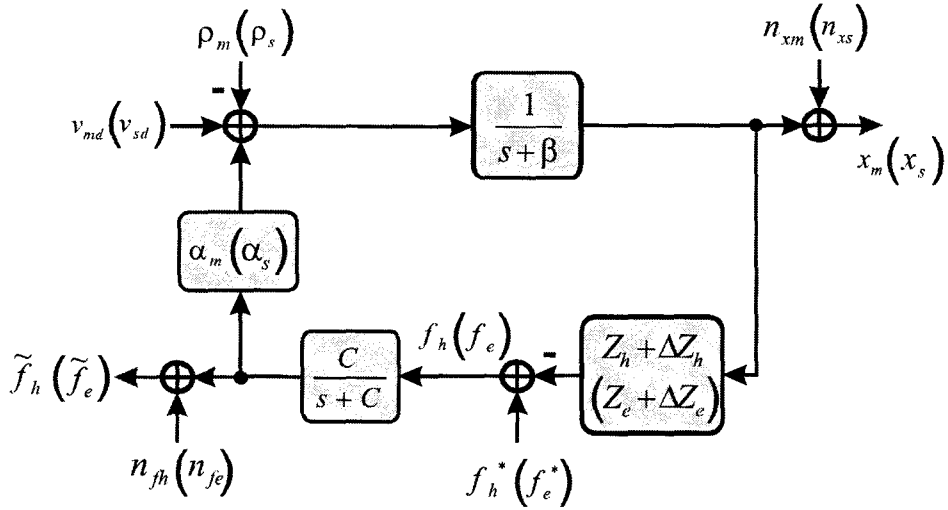


Figure 5.1: Block diagram of master (slave) dynamics after the application of local adaptive nonlinear controllers.

have been added to the position and force signals to facilitate the formulation of the robust control synthesis in the next section. The resulting dynamics are linear and decoupled in different axes of motion perturbed by disturbances in  $L_2 \cap L_\infty$  or  $L_\infty$ . Therefore, without loss of generality, only motion along a single axis is considered.

In the simplified dynamics, when the hand (environment) force is zero, the master (slave) position is determined through the response of a first-order filter with adjustable bandwidth  $\beta$  to the reference command  $v_{md}(v_{sd})$ . The adaptation manifests itself in the form of the decaying disturbance  $\rho_m \in L_2 \cap L_\infty$  ( $\rho_s \in L_2 \cap L_\infty$ ). At the other extreme, when the master (slave) position and velocity are zeros, e.g. in rigid contact, the hand (environment) force are directly determined by the control command  $v_{md}(v_{sd})$  and a decaying disturbance due to the adaptation. It is

clear that the application of local adaptive controllers greatly simplifies the master/slave dynamics. This is achieved by removing the nonlinearities and eliminating the system dependency on master/slave parameters. It should be noted, however, that these linearized dynamics are still subject to uncertainty in the form of the unknown perturbations to the operator and environment dynamics  $\Delta Z_h$  and  $\Delta Z_e$ .

A key point in the proposed two-step teleoperation approach is the decoupling of the local master and slave adaptive controls from an outer-loop time-delay coordinating controller introduced in the next section. The adaptation errors, shown to be bounded and having finite energy in (5.17), can be modeled as bounded disturbances in the robust control synthesis framework. The speed at which the local tracking errors decay could impact the overall fidelity of the teleoperation system in transition phases, but would not cause instability, at least from a theoretical point of view. While selecting large feedback and adaptation gains can accelerate the convergence of these tracking errors and reduce their effect on user perception, unmodeled dynamics such as drive flexibility, actuator dynamics, and nonlinear friction effects, as well as measurement noise can limit the gain values in practice.

### 5.3 Teleoperation Control Formulation

The coordination between master and slave robots must be achieved through the new control signals  $v_{md}$  and  $v_{sd}$  in Fig. 5.1. As stated in Chapter 3, the teleoperation control objectives can be expressed in terms of delay-free position and force tracking between the master and slave robots. Satisfying the transparency objectives in (3.21) and (3.22) would provide the operator with a seamless access to the

task environment. However in practice, robust stability constraints arising from the time delay and dynamic uncertainty prevent achieving ideal transparency. Instead, a compromise solution must be sought to balance the stability and performance requirements. To this end, a robust time-delay teleoperation control synthesis problem is formulated in this section.

A block diagram of the linearized teleoperation controllers with corresponding input, output, disturbance and measurement signals is shown in Fig. 5.2. The design objectives can be specified as reducing the filtered position and force tracking errors  $\bar{x}_m - \bar{x}_s$  and  $\bar{f}_h - \bar{f}_e$  in response to the two filtered exogenous forces  $\bar{f}_h^*$  and  $\bar{f}_e^*$  which are the cause of motion. The addition of the filtered noise signals  $\bar{n}_{xm}$ ,  $\bar{n}_{xs}$ ,  $\bar{n}_{fh}$ , and  $\bar{n}_{fe}$ , and the filtered control signals  $\bar{v}_{md}$  and  $\bar{v}_{sd}$  at the inputs and outputs, respectively, regularizes the design problem in order to attain a feasible solution. The adaptive control error signals  $\rho_m$  and  $\rho_s$ , as demonstrated in (5.17), belong to  $L_2 \cap L_\infty$  space. These errors can be integrated into the robust control formulation through the introduction of the filtered disturbance signals  $\bar{\rho}_m$  and  $\bar{\rho}_s$ . The frequency-dependent gains  $W_j s$  on the signals are used to emphasize their relative importance at various frequencies and must be carefully selected to balance the design objectives such as position and force tracking as well as robust stability. They are also employed to characterize the frequency content of the noise and disturbance signals as well as the cost associated with the control effort as a function of frequency.

Unlike the local adaptive controllers, the teleoperation coordinating controller is centralized and should be placed either at the master or at the slave site. In this thesis, the controller is assumed to be at the master site with forward and

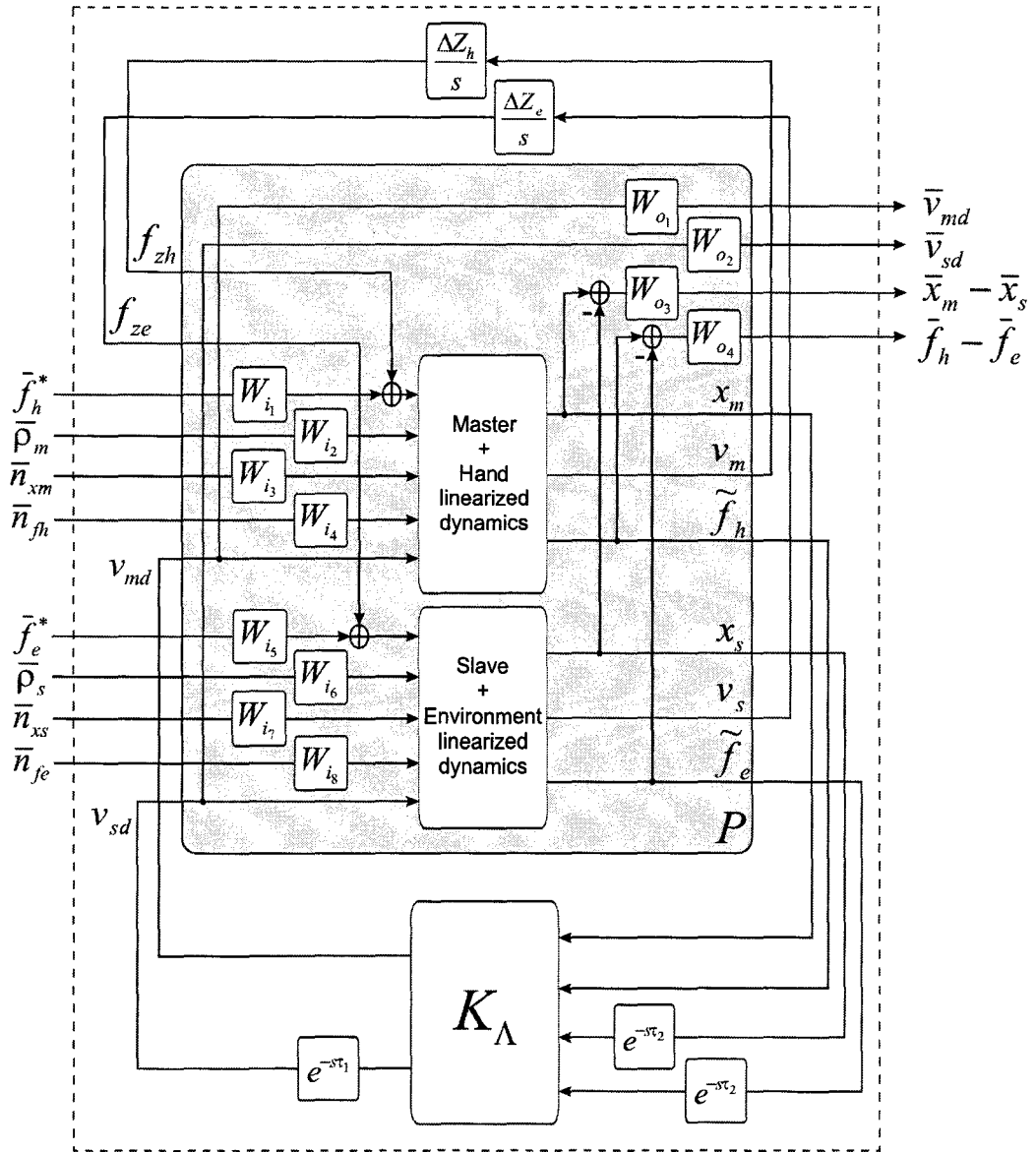


Figure 5.2: Linearized teleoperation control system.

return communication delays of  $\tau_1$  and  $\tau_2$  seconds, respectively. This is reflected in Fig. 5.2 where the slave control and measurement signals are delayed by  $\tau_1$  and  $\tau_2$ . The teleoperation control system in Fig. 5.2 can be redrawn in the general form of a MIMO system with multiple delays in I/O channels as shown in Fig. 5.3(a). In this figure

$$u(t) = \begin{bmatrix} v_{md} & v_{sd} \end{bmatrix}^T \quad (5.20)$$

$$y(t) = \begin{bmatrix} x_m & \tilde{f}_h & x_s & \tilde{f}_e \end{bmatrix}^T \quad (5.21)$$

$$w_1(t) = \begin{bmatrix} f_{zh}(t) & f_{ze}(t) \end{bmatrix}^T \quad (5.22)$$

$$w_2(t) = \begin{bmatrix} \bar{f}_h^* & \bar{f}_e^* & \bar{\rho}_m & \bar{\rho}_s & \bar{n}_{x_m} & \bar{n}_{f_h} & \bar{n}_{x_s} & \bar{n}_{f_e} \end{bmatrix}^T \quad (5.23)$$

$$z_1(t) = \begin{bmatrix} v_m(t) & v_s(t) \end{bmatrix}^T \quad (5.24)$$

$$z_2(t) = \begin{bmatrix} \bar{x}_m - \bar{x}_s & \bar{f}_h - \bar{f}_e & \bar{v}_{md} & \bar{v}_{sd} \end{bmatrix}^T \quad (5.25)$$

where  $u(t)$ ,  $y(t)$ ,  $w(t)$  and  $z(t)$  are the control action, measurement, disturbance, and output signals, respectively. Also,  $y_c$  and  $u_c$  are the input and the output of the controller block. The delays in control and measurement are represented by diagonal matrices  $\Lambda_u$  and  $\Lambda_y$  with appropriate dimensions. The diagonal entries of these matrices are either 1 or  $e^{-s\tau}$ , depending on whether delay exists in the

corresponding input (output) channel or not, i.e.

$$\Lambda_u(s) = \begin{bmatrix} e^{-h_{u,q}s} I_{m_q} & & & \\ & \ddots & & \\ & & e^{-h_{u,1}s} I_{m_1} & \\ & & & I_{m_0} \end{bmatrix} \quad (5.26)$$

and

$$\Lambda_y(s) = \begin{bmatrix} I_{p_0} & & & \\ & e^{-h_{y,1}s} I_{p_1} & & \\ & & \ddots & \\ & & & e^{-h_{y,r}s} I_{p_r} \end{bmatrix} \quad (5.27)$$

where diagonal entries are sorted in descending (ascending) order of the delay in input (output) channels, respectively. Note that a simple permutation of input and output channels can transform the system into this form, if needed.

The uncertainty in the hand and environment impedances is modeled as in (5.19). If the nominal impedances  $Z_h$  and  $Z_e$  are chosen based on the minimum expected mass, damping, and stiffness parameters of the operator and environment,  $\Delta Z_h/s$  and  $\Delta Z_e/s$  would become passive. However in this case, due to the unbounded  $\|\cdot\|_\infty$  of the uncertainty blocks  $\Delta Z_h/s$  and  $\Delta Z_e/s$ , robust control methods such as  $H_\infty$  and  $\mu$ -synthesis cannot be utilized directly. To resolve this issue, as proposed in [30], the following wave variables [73] are introduced

$$a_h = f_{zh} + \Delta Z_h^0 v_m, \quad b_h = f_{zh} - \Delta Z_h^0 v_m \quad (5.28)$$

where  $a_h$  and  $b_h$  are the output and input wave variables, respectively, and  $\Delta Z_h^0$  is an arbitrary resistive impedance. It can be shown that

$$b_h = [(\Delta Z_h - \Delta Z_h^0)(\Delta Z_h + \Delta Z_h^0)^{-1}] a_h = S_h a_h \quad (5.29)$$

where  $S_h$  is the scattering operator. For passive operator dynamics,  $\Delta Z_h/s$  is positive real [47], i.e.

$$\frac{1}{j\omega} [Z_h(j\omega) - Z_h^*(j\omega)] \geq 0 \quad (5.30)$$

and  $S_h$  is stable and bounded real, i.e.

$$\| S_h \|_\infty = \sup_\omega \bar{\sigma}[S_h(j\omega)] \leq 1 \quad (5.31)$$

where  $\bar{\sigma}[\cdot]$  is the maximum singular value. The environment wave variables  $a_e$ ,  $b_e$ , and the corresponding scattering operator  $S_e$  can be similarly defined based on  $f_{ze}$  and  $v_s$  signals. The new uncertainties elements  $S_h$  and  $S_e$  can be easily incorporated into the  $H_\infty$  design framework since they have bounded  $\| \cdot \|_\infty$ .

The application of the wave variable transformation results in a new open-loop plant dynamics  $\bar{P}(s)$ , whose elements can be expressed in terms of those of  $P(s)$ . Let the first and second inputs to  $P(s)$  be  $w_1(t)$  and  $\begin{bmatrix} w_2(t) & u(t) \end{bmatrix}^T$ , respectively, and the first and second outputs of  $P(s)$  be  $z_1(t)$  and  $\begin{bmatrix} z_2(t) & y(t) \end{bmatrix}^T$ , respectively. A state-space realization of  $P(s)$  in Fig. 5.3(a) can be written as

$$P(s) = \left[ \begin{array}{c|cc} A & B_1 & B_2 \\ \hline C_1 & 0 & D_1 \\ C_2 & 0 & D_2 \end{array} \right]. \quad (5.32)$$

It is straightforward to show that a corresponding state-space representation of the transformed system  $\bar{P}(s)$  in Fig. 5.3(b) after the application of the wave transformation in (5.28) is as follows

$$\bar{P}(s) = \left[ \begin{array}{c|cc} A + B_1 Z^0 C_1 & B_1 & B_2 + B_1 Z^0 D_1 \\ \hline 2Z^0 C_1 & I & 2Z^0 D_1 \\ C_2 & 0 & D_2 \end{array} \right] \quad (5.33)$$

where

$$Z^0 = \begin{bmatrix} Z_h^0 & 0 \\ 0 & Z_e^0 \end{bmatrix}. \quad (5.34)$$

The block diagram of the controller that uses the new variables is displayed in Fig. 5.3(b) where

$$a = \begin{bmatrix} a_h & a_e \end{bmatrix}^T, \quad b = \begin{bmatrix} b_h & b_e \end{bmatrix}^T. \quad (5.35)$$

Before proceeding further, it is helpful to comment on the operation of the robust controller particularly as it relates to its handling of the uncertainty in the operator and environment dynamics. Intuitively, the nominal operator and environment impedances will be used by the controller through an internal prediction mechanism to achieve the best delay-free tracking possible, subject to maintaining stability in the presence of  $\Delta Z_h$  and  $\Delta Z_e$ . However, the design could be rather conservative for two main reasons. First, passive  $\Delta Z_h/s$  and  $\Delta Z_e/s$  still cover a wide range of uncertainty in the operator and environment dynamics. Second, the  $H_\infty$  optimization ignores the structure of the uncertainty block.

The first problem can be partly remedied by restricting the uncertainty, e.g. to stiffness-type variations with *a priori* known bounds. This is reasonable since

assumption may not always be applicable [128]. The second problem can potentially be solved by the application of the  $\mu$ -synthesis and the structured singular value for incorporating the structure of the uncertainty into the control synthesis. This will reduce some of the conservatism inherent in the  $H_\infty$ -based approach due to ignoring the form and type of the perturbation.

## 5.4 $H_\infty$ Control of MIMO Systems with I/O time delay

First a couple of notations that will be used throughout the rest of this chapter are introduced. In Fig. 5.4(a), a generic feedback control system is displayed. For this system, the lower fractional transformation, i.e. the mapping from  $w$  to  $z$  when the lower loop is closed by

$$u = Ky \tag{5.37}$$

is denoted by  $\mathcal{F}_l(P, K)$ . Also, the time-delay  $H_\infty$  control method mainly relies on the so called scattering representation of systems as shown in Fig. 5.4(b). Here

$$Q = \mathcal{C}_r(G, K) \tag{5.38}$$

denotes the unique closed-loop mapping from  $\eta$  to  $\xi$  where

$$\begin{bmatrix} \xi \\ \eta \end{bmatrix} = G \begin{bmatrix} u \\ y \end{bmatrix} \tag{5.39}$$

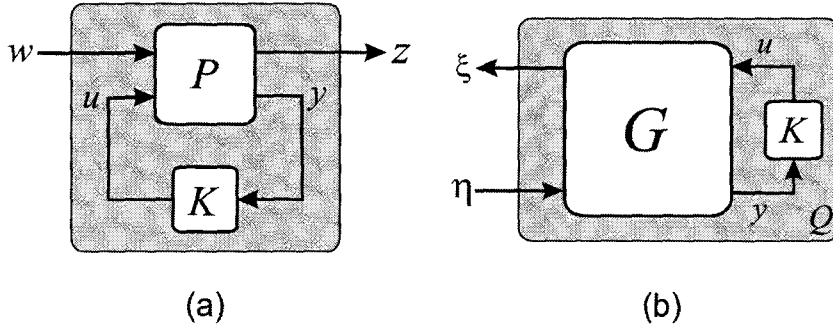


Figure 5.4: (a) Lower fractional transformation (LFT); (b) Scattering representation.

and when the loop is closed by  $u = Ky$ . In the case of  $\eta$  and  $y$  being of the same dimension, one may write

$$C_r(G, K) = (G_{11}K + G_{12})(G_{21}K + G_{22})^{-1}. \quad (5.40)$$

The objective of the design is to find a stabilizing controller  $K_\Lambda$  in Fig. 5.3 that would minimize the  $L_\infty$  norm of the closed-loop transfer function, i.e.

$$\text{minimize } \|\mathcal{F}_l(P, \Lambda_u K_\Lambda \Lambda_y)\|_\infty \quad (5.41)$$

from the input

$$w(t) = \begin{bmatrix} w_1(t) & w_2(t) \end{bmatrix}^T \quad (5.42)$$

to the output

$$z(t) = \begin{bmatrix} z_1(t) & z_2(t) \end{bmatrix}^T \quad (5.43)$$

in Fig. 5.3(a), or from the input

$$w(t) = \begin{bmatrix} b(t) & w_2(t) \end{bmatrix}^T \quad (5.44)$$

to the output

$$z(t) = \begin{bmatrix} a(t) & z_2(t) \end{bmatrix}^T \quad (5.45)$$

in Fig. 5.3(b). Recently in [35], Meinsma and Mirkin proposed a solution to the  $H_\infty$  control of MIMO systems with multiple I/O delays as depicted in Fig. 5.3. This method is adopted here to solve the  $H_\infty$  control synthesis problem posed in Fig. 5.2. A summary of this method is presented below. The reader is referred to [35] for further details.

### 5.4.1 Problem Formulation

Consider the feedback system in Fig. 5.3(a) with the following state-space realization for  $P(s)$

$$P(s) = \left[ \begin{array}{c|cc} A & B_1 & B_2 \\ \hline C_1 & D_{11} & D_{12} \\ C_2 & D_{21} & D_{22} \end{array} \right] \quad (5.46)$$

where the input is  $\begin{bmatrix} w(t) & u(t) \end{bmatrix}^T$  and the output is  $\begin{bmatrix} z(t) & y(t) \end{bmatrix}^T$ . It is assumed that

- (i)  $(C_2, A, B_2)$  is stabilizable and detectable,
- (ii)  $D'_{12}D_{12} > 0$  and
- (iii)  $D_{21}D'_{21} > 0$ .

The goal now is to find a proper  $K_\Lambda$  such that

$$K \triangleq \Lambda_u K_\Lambda \Lambda_y \quad (5.47)$$

internally stabilizes the system and

$$\|\mathcal{F}_l(P, \Lambda_u K_\Lambda \Lambda_y)\|_\infty < \gamma \quad (5.48)$$

for a given  $\gamma > 0$ . It is evident that  $K_\Lambda$  cannot be calculated simply by inverting the mapping in (5.47) since this would result in a *non-causal* controller  $K_\Lambda$ .

### 5.4.2 Equivalent One-block Problem

Time delay imposes additional constraints on the controller  $K_\Lambda$  in Fig. 5.3, and therefore, the problem has a solution only if it does the delay-free problem. The original four-block delay problem can be reduced to an equivalent one-block delay problem using the solution to the delay-free problem [35, 129]. The resulting one-block problem is in the form of Fig. 5.5, where  $G(s)$  is a bistable transfer matrix with an identity feedthrough term. The solution to the delay-free  $H_\infty$  problem as well as the definition of the transfer matrix  $G(s)$  are given in Appendix D. The joint input-output delay operator is defined as

$$\Lambda = \begin{bmatrix} \Lambda_u & \\ & \Lambda_y^{-1} \end{bmatrix} \quad (5.49)$$

where  $\Lambda_u$  and  $\Lambda_y$  are defined in (5.26) and (5.27), respectively. The noncausal elements in  $\Lambda$  can be eliminated by multiplying it with the scalar operator  $e^{-h_{y,r}s}$ ,

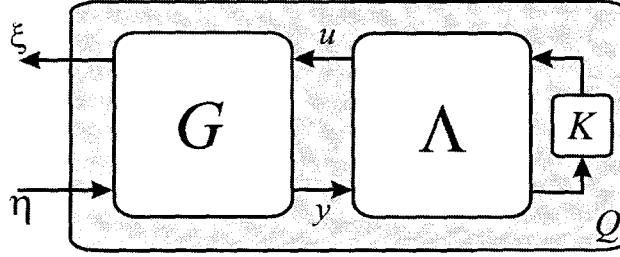


Figure 5.5: Equivalent one-block problem

without affecting the  $(\eta, \zeta)$  mapping. Therefore,  $\Lambda$  can be written as

$$\Lambda \triangleq \begin{bmatrix} e^{-h_{q+r}s} I_{n_{q+r}} & & & \\ & \dots & & \\ & & e^{-h_1 s} I_{n_1} & \\ & & & I_{n_0} \end{bmatrix} \quad (5.50)$$

where  $0 < h_1 < \dots < h_{q+r}$  and  $h_{q+r} = h_{u,q} + h_{y,r}$ .

The solution to the one-block problem is a controller  $K$  which yields

$$\|C_r(G\Lambda, K)\|_\infty < 1. \quad (5.51)$$

The original four-block problem solution,  $K_\Lambda$ , can be obtained from  $K$  using [35]

$$K_\Lambda = C_r(D_\Lambda^{-1}, K) \quad (5.52)$$

where  $D_\Lambda$  is bistable, causally invertible and is defined as

$$D_\Lambda \triangleq \Lambda^{-1} D_\infty \Lambda. \quad (5.53)$$

The definition of  $D_\infty$  can be found in Appendix D.

The solution to the  $H_\infty$  control of MIMO systems with multiple I/O delays in (5.51) can be obtained by successively splitting the one-block problem with multiple delays into a combination of simpler one-block problems with single-delay, the so called *adobe* delay problems.

### 5.4.3 The Adobe Delay Problem

A delay operator with the following structure

$$\Lambda = \begin{bmatrix} e^{-hs} I_\mu & 0 \\ 0 & I_\rho \end{bmatrix} \quad (5.54)$$

for some

$$\mu < n_u + n_y \quad (5.55)$$

$$\rho = n_u + n_y - \mu \quad (5.56)$$

is denoted as adobe delay structure. Note that if only some of the input channels are delayed equally and the rest of the channels are delay free,  $\mu \leq n_u$ . Similarly, in the case that only some of the output channels are delayed equally,  $\mu \geq n_u$ .

A one-block problem as shown in Fig. 5.5 with an adobe delay structure (5.54) is called an *adobe* delay problem. The solution to such a problem,  $K$ , can be obtained by [35]

$$K = C_r \left( \begin{bmatrix} I & 0 \\ \Pi & I \end{bmatrix} \tilde{G}^{-1}, \tilde{Q} \right) \quad (5.57)$$

where  $\tilde{G}(s)$  is a bistable transfer matrix,  $\Pi(s)$  is an Finite-Impulse-Response (FIR) operator, and  $\tilde{Q}$  is contractive, i.e.

$$\|\tilde{Q}\|_{\infty} < 1. \quad (5.58)$$

The reader is referred to Appendix E for the actual forms of  $\Pi$ ,  $\tilde{G}$ , and  $\tilde{Q}$ . Alternatively, it can be shown that

$$\tilde{Q} = c_r \left( \tilde{G} \begin{bmatrix} I & 0 \\ -\Pi & I \end{bmatrix}, K \right) \quad (5.59)$$

is a contraction.

#### 5.4.4 Decomposition

The multiple-delay one-block problem  $(G, \Lambda)$ , as shown in Fig 5.5, can be decomposed to a series of single-delay adobe problems, the solution of which was presented in the last subsection. The delay operator  $\Lambda$  in (5.50) includes  $q + r$  ordered delay blocks referred to as  $(q + r)$ -delay operator. It can be easily shown that [35]

$$\Lambda = \Lambda_1 \tilde{\Lambda} \quad (5.60)$$

where

$$\Lambda_1 \triangleq \begin{bmatrix} e^{-h_1 s} I_{\mu_1} & 0 \\ 0 & I_{\rho_1} \end{bmatrix}, \quad \rho_1 = n_0 \quad (5.61)$$

is a delay operator of the adobe form and  $\tilde{\Lambda}$  is a  $(q + r - 1)$ -delay operator with  $(n_0 + n_1)$  delay-free channels. Using (5.60), one may write

$$\mathcal{C}_r(G\Lambda, K) = \mathcal{C}_r\left(G\Lambda_1, \mathcal{C}_r(\tilde{\Lambda}, K)\right). \quad (5.62)$$

Therefore, the original multiple-delay problem  $(G, \Lambda)$  has solution only if the adobe delay problem  $(G, \Lambda_1)$  has one, i.e.

$$\tilde{Q} \triangleq \mathcal{C}_r\left(\tilde{G} \begin{bmatrix} I & 0 \\ -\Pi & I \end{bmatrix}, \mathcal{C}_r(\tilde{\Lambda}, K)\right) \quad (5.63)$$

is a contraction. By absorbing the term  $\begin{bmatrix} I & 0 \\ -\Pi & I \end{bmatrix}$  into the controller one can write

$$\tilde{Q} = \mathcal{C}_r(\tilde{G}\tilde{\Lambda}, \tilde{K}) \quad (5.64)$$

where

$$\tilde{K} = \mathcal{C}_r\left(\tilde{\Lambda}^{-1} \begin{bmatrix} I & 0 \\ -\Pi & I \end{bmatrix} \tilde{\Lambda}, K\right). \quad (5.65)$$

Due to the fact that  $\begin{bmatrix} I & 0 \\ -\Pi & I \end{bmatrix}$  has a lower triangular structure and the delays in  $\tilde{\Lambda}$  are ordered descendantly, the term  $\tilde{\Lambda}^{-1} \begin{bmatrix} I & 0 \\ -\Pi & I \end{bmatrix} \tilde{\Lambda}$  is bistable with an identity feedthrough term. Therefore,  $K$  is proper if and only if  $\tilde{K}$  is proper. Hence, a

proper choice of  $K$  can make  $\tilde{Q}$  contractive if and only if there is a  $\tilde{K}$  such that

$$\|\mathcal{C}_r(\tilde{G}\tilde{\Lambda}, \tilde{K})\|_\infty < 1. \quad (5.66)$$

In other words, the original multiple-delay problem is equivalent to a combination of a single-delay adobe problem and a multiple-delay problem with an order less than that of the original problem given in (5.66). This iterative procedure is continued until a one-block problem with (0)-delay operator is resulted, the solution of which can be obtained by inverting its transfer function.

## 5.5 Design Example

The proposed mixed adaptive/robust controller is applied to a two-axis teleoperation system involving two kinematically and dynamically similar two-degree-of-freedom robots. Due to the decoupling of dynamics through the first-stage adaptive controllers, only the design and analysis of the robust controller along a single axis is discussed here. The mechanical design of the robots, which will be introduced in the next section, is such that linear mass-damper-spring models with unknown parameters can sufficiently described their dynamics. Therefore, such models are used in the local adaptive controllers.

The system and controller parameters are given in Table 5.1. The system parameters reflect those of the experimental setup. It should be noted that no knowledge of the master and slave robot parameters is required by the controller because of the use of the local adaptive controllers. Typical values have been selected for the

System Parameters	
Master	$m_m = 0.4 \text{ kg}$ $b_m = 1.2 \text{ N.s/m}$ $k_m = 0 \text{ N/m}$
Slave	$m_s = 0.4 \text{ kg}$ $b_s = 1.6 \text{ N.s/m}$ $k_s = 0 \text{ N/m}$
Arm	$m_h = 0.3 \text{ kg}$ $b_h = 2 \text{ N.s/m}$ $k_h = 70.0 \text{ N/m}$
Environment	$m_e = 0.02 \text{ kg}$ $b_e = 0 \text{ N.s/m}$ $k_e = 900 \text{ N/m}$
Controller Parameters	
Filters	
Inputs	Outputs
$W_{i_1} = \frac{10}{s+10}$ $W_{i_2} = W_{i_6} = \frac{0.2(s+1)}{s+20}$ $W_{i_3} = W_{i_7} = \frac{0.005(s+1)}{s+10}$ $W_{i_4} = W_{i_8} = \frac{0.05(s+1)}{s+10}$ $W_{i_5} = 1$	$W_{o_1} = W_{o_2} = \frac{0.001(s+1)}{s+10}$ $W_{o_3} = \frac{1350}{(s^2+4.2s+9)(s^2+16.8s+144)}$ $W_{o_4} = \frac{5}{(s^2+4.2s+9)(s^2+16.8s+144)}$
Adaptive controllers parameters	
Master	Slave
$\hat{\Theta}_m^0 = [0.3 \text{ kg} \quad 4 \text{ N.s/m} \quad 5 \text{ N/m} \quad 0 \text{ N}]$ $\hat{\Theta}_m^- = [0.2 \text{ kg} \quad 2 \text{ N.s/m} \quad 0 \text{ N/m} \quad -10 \text{ N}]$ $\hat{\Theta}_m^+ = [0.5 \text{ kg} \quad 8 \text{ N.s/m} \quad 20 \text{ N/m} \quad 10 \text{ N}]$ $\Gamma_m = [50 \quad 350 \quad 350 \quad 250]$ $\mathcal{K}_m = 50$ $C_m = 12.5 \text{ rad/sec}$ $\alpha_m = 0.02$ $\beta_m = 10$	$\hat{\Theta}_s^0 = [0.3 \text{ kg} \quad 4 \text{ N.s/m} \quad 0 \text{ N/m}]$ $\hat{\Theta}_s^- = [0.2 \text{ kg} \quad 1 \text{ N.s/m} \quad 0 \text{ N/m}]$ $\hat{\Theta}_s^+ = [0.5 \text{ kg} \quad 8 \text{ N.s/m} \quad 5000 \text{ N/m}]$ $\Gamma_s = [100 \quad 250 \quad 5e8]$ $\mathcal{K}_s = 50$ $C_s = 12.5 \text{ rad/sec}$ $\alpha_s = 0.02$ $\beta_s = 10$

Table 5.1: System and controller parameters.

arm mass, damping and stiffness. The nominal environment stiffness has been deliberately chosen at roughly 1/3rd of its actual value to demonstrate the robustness of the controller with respect to uncertainty in the environment stiffness.

The filters used in the robust control design are also presented in Table 5.1. These were initially selected based on the sensor and actuator specifications, typical level and bandwidth of the operator hand force, desired level and bandwidth of position and force tracking errors, as well as the expected uncertainty in the environment stiffness. For example, low-pass filtering of the position and force

tracking errors emphasizes on transparency at low frequency whereas high pass-filtering of the noise inputs reflects the fact that the noise power is mostly concentrated at high frequency. Moreover, high-pass filtering of the control commands at the output penalizes undesirable high frequency control activities. The initial filters were further adjusted based on simulation and experimental results to achieve a balance between the robust stability and performance requirements. For instance, increasing the gains and bandwidth of the position and force tracking error filters, while enhancing transparency, can reduce the stability margin with respect to variations in the environment stiffness. This could also result in excessively tight control loops with high-frequency modes that would require high sampling rates for discrete-time implementation.

The original four-block delay problem of the teleoperation control system is shown in Fig. 5.2. The equivalent one-block delay problem can be obtained using the delay-free solution and following the steps outlined in the previous section and Appendix D. In this case, the input and output delay operators are

$$\Lambda_u = \begin{bmatrix} e^{-s\tau_1} & \\ & 1 \end{bmatrix} \quad (5.67)$$

and

$$\Lambda_y = \begin{bmatrix} I_2 & \\ & e^{-s\tau_2} I_2 \end{bmatrix}. \quad (5.68)$$

Using (5.49) and after eliminating the noncausal elements, the joint input/output

delay operator can be written as

$$\Lambda = \begin{bmatrix} e^{-s(\tau_1+\tau_2)} & & \\ & e^{-s\tau_2} I_3 & \\ & & I_2 \end{bmatrix}. \quad (5.69)$$

This can then be decomposed into two single-delay delay operators using (5.60) and (5.61) as follows

$$\Lambda = \underbrace{\begin{bmatrix} e^{-s\tau_2} I_4 & \\ & I_2 \end{bmatrix}}_{\Lambda_1} \underbrace{\begin{bmatrix} e^{-s\tau_1} & \\ & I_5 \end{bmatrix}}_{\tilde{\Lambda}}. \quad (5.70)$$

Using the decomposition in (5.62), the solution can be obtained by solving two single-delay adobe problems, first with  $\mu_1 = 4$ ,  $\rho_1 = 2$  and second with  $\mu_2 = 1$ ,  $\rho_2 = 5$ . This is due to the fact that both  $\Lambda_1$  and  $\tilde{\Lambda}$  are already in the adobe delay form. The solution of the first adobe delay problem,  $(G, \Lambda_1)$  produces  $\tilde{G}$ ,  $\Pi_1$  and  $\tilde{Q}$ . Following the steps of the last subsection, the second adobe delay problem  $(\tilde{G}, \tilde{\Lambda})$  can be formulated as in (5.66), the solution of which generates  $\bar{G}$ ,  $\Pi_2$  and  $\bar{Q}$ .

The controller can be reconstructed following reverse steps of the decomposition procedure resulting in the structure shown in Fig. 5.6, where  $\tilde{\Lambda}$  is defined in (5.70),  $D_\Lambda$  is defined in (5.53), and  $\bar{G}^{-1}$  is the inverse transfer function of the solution to the last adobe delay problem. The FIR filters  $\Pi_1$  and  $\Pi_2$  are partitioned

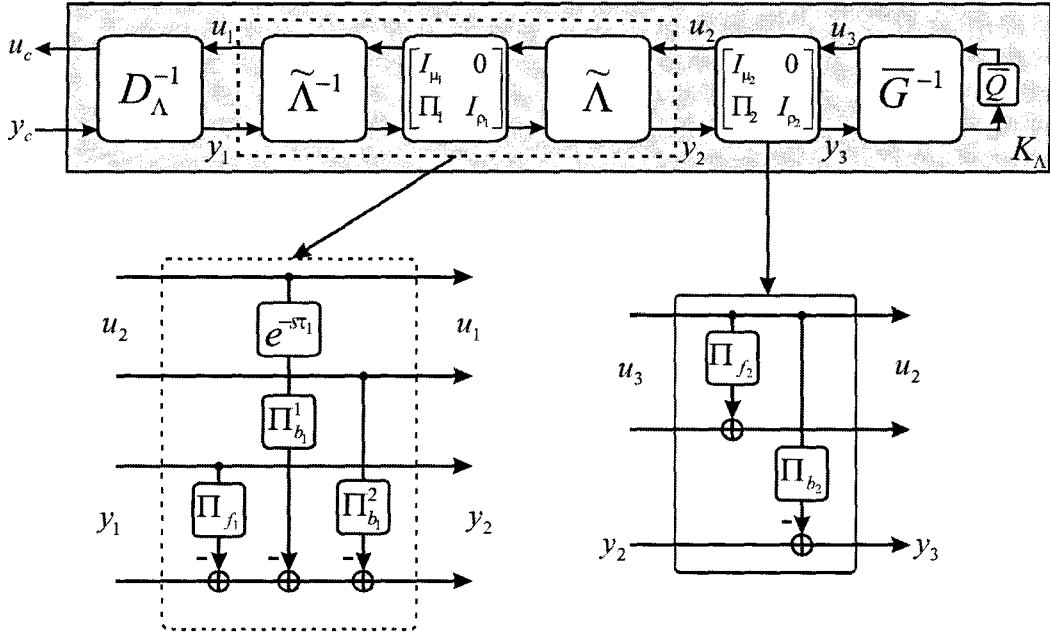


Figure 5.6: Controller reconstruction from a two-step adobe decomposition.

compatibly as

$$\begin{bmatrix} I_{\mu_1} & 0 \\ \Pi_1 & I_{\rho_1} \end{bmatrix} = \left[ \begin{array}{cc|cc} I_{n_u} & & 0 & 0 \\ & & I_{n_y - \rho_1} & 0 \\ \hline & \Pi_{b_1}^1 & \Pi_{b_1}^2 & \Pi_{f_1} & I_{\rho_1} \end{array} \right] \quad (5.71)$$

and

$$\begin{bmatrix} I_{\mu_2} & 0 \\ \Pi_2 & I_{\rho_2} \end{bmatrix} = \left[ \begin{array}{cc|cc} I_{\mu_2} & & 0 & 0 \\ \Pi_{f_2} & I_{n_u - \mu_2} & & 0 \\ \hline \Pi_{b_2} & & 0 & I_{n_y} \end{array} \right] \quad (5.72)$$

where  $\mu_1, \rho_1, \mu_2$  and  $\rho_2$  have been defined earlier,  $n_y = 4$  is the number of measurements and  $n_u = 2$  is the number of the control signals. The mapping from  $y_c$  to  $u_c$  is the synthesized robust controller  $K_\Lambda$ . The controller is parameterized in

terms of a contractive mapping  $\bar{Q}$  which is chosen to be zero. It is worth noticing that the local adaptive controllers require  $\dot{u} = \begin{bmatrix} \dot{v}_{md} & \dot{v}_{sd} \end{bmatrix}^T$  in their implementation. This can be calculated using the linearity of the robust controller and based on  $\dot{y}$ . The definition of  $y$  in Fig. 5.3 reveals that only velocity and force signals are required for the implementation. Alternatively, given that there is no feedthrough term from the measurement to control in the robust controller, the derivatives can also be computed based on  $y_c$  and a revised dynamics derived from the controller.

Throughout the rest of the chapter, the communication delay in both directions are assumed equal, i.e.  $\tau_1 = \tau_2 = \tau$  msec. Also, the delay values correspond to a round-trip delay unless otherwise stated. The closed-loop frequency responses from the user exogenous force input  $f_h^*$  to the system outputs  $x_m$ ,  $x_s$ ,  $f_h$ , and  $f_e$  for three different delays, i.e. 100 msec, 200 msec and 300 msec, are displayed in Figs. 5.7-5.12. Two cases have been considered for each delay, first when the actual environment stiffness matches that used in the design, i.e.  $\hat{k}_e = k_e = 900$  N/m (Figs. 5.7, 5.9, 5.11) and then when there is a mismatch between these values, i.e.  $\hat{k}_e = 2000$  N/m (actual) and  $k_e = 900$  N/m (design)(Figs. 5.8, 5.10, 5.12). From these figures, it can be seen that the transparency objectives have been met for frequencies up to 4.0 ~ 6.0 Hz for the matched environment stiffness. This is above the average hand voluntary movement frequency range of 0 ~ 2 Hz reported in the literature [130]. Although the system transparency would degrade to some extent in the mismatch case and by increase in communication delay, the results are still satisfactory and demonstrate robust performance of the controller.

The robust controller has been designed for a nominal environment stiffness of  $k_e = 900$  N/m. The stability margins of the controller with respect to variations

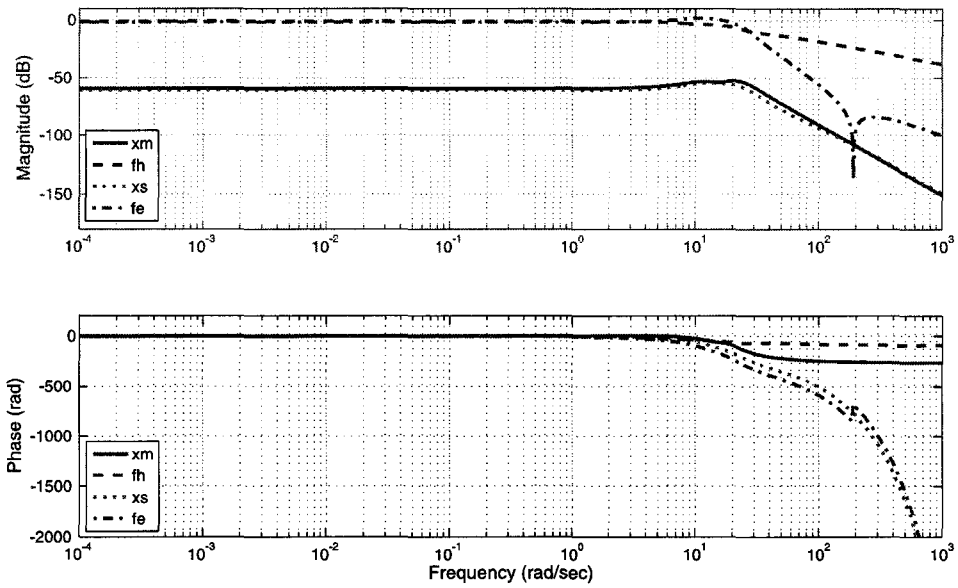


Figure 5.7: Closed-loop frequency response to the input  $f_h^*$  for 100 msec delay and matched environment stiffness.

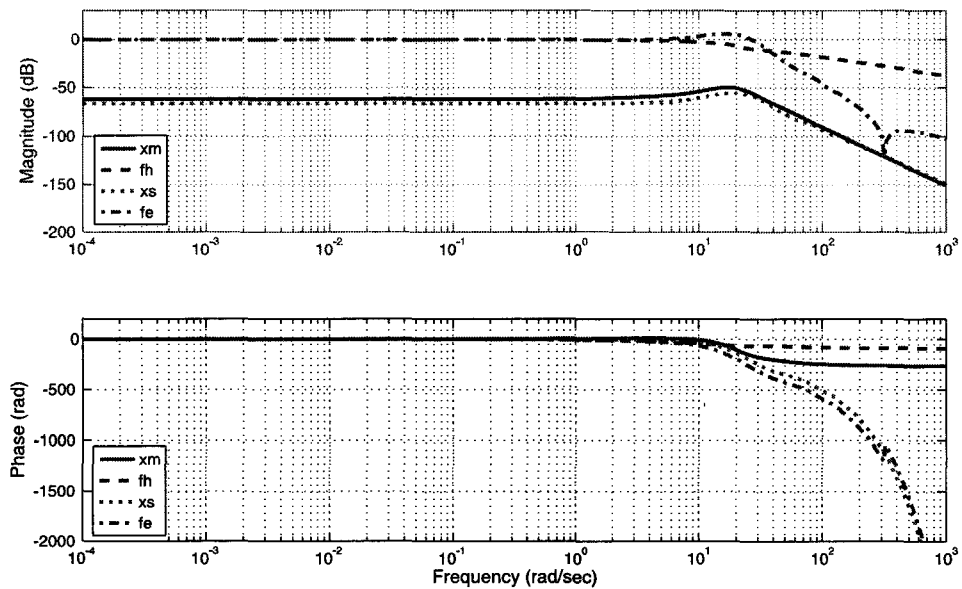


Figure 5.8: Closed-loop frequency response to the input  $f_h^*$  for 100 msec delay and mismatched environment stiffness.

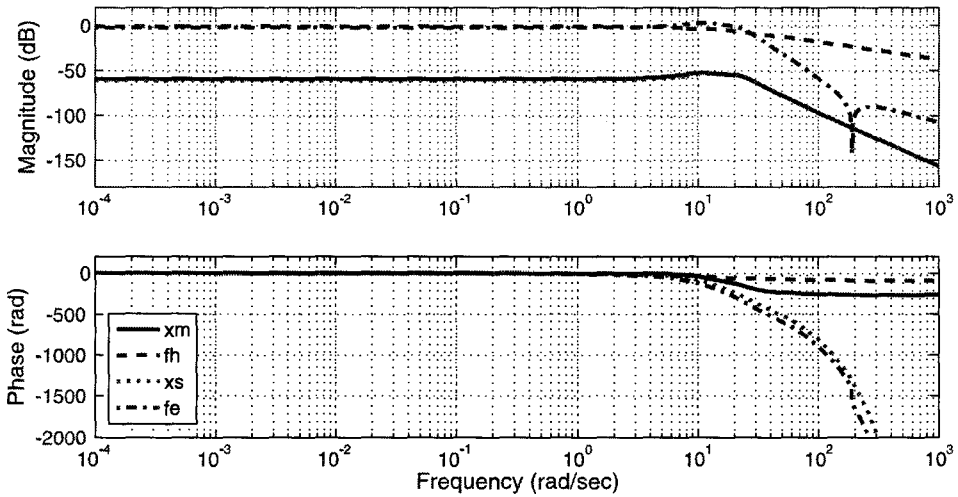


Figure 5.9: Closed-loop frequency response to the input  $f_h^*$  for 200 msec delay and matched environment stiffness.

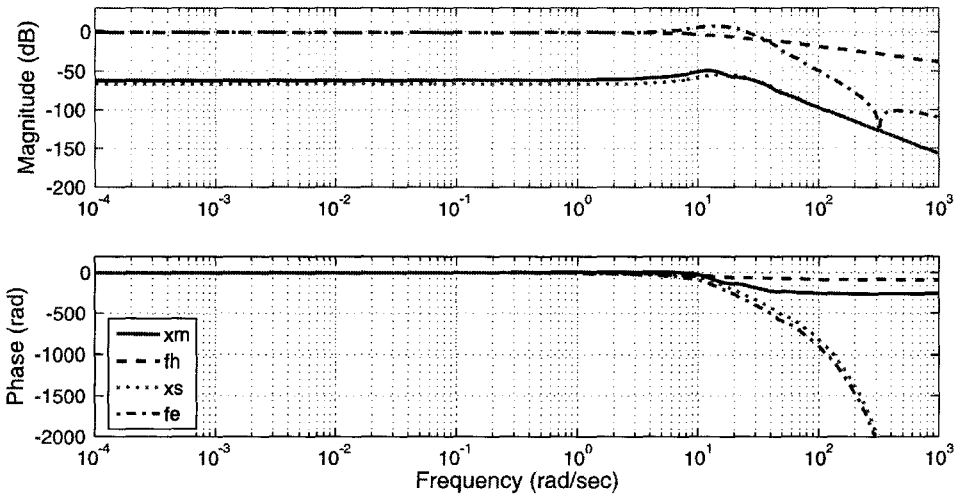


Figure 5.10: Closed-loop frequency response to the input  $f_h^*$  for 200 msec delay and mismatched environment stiffness.

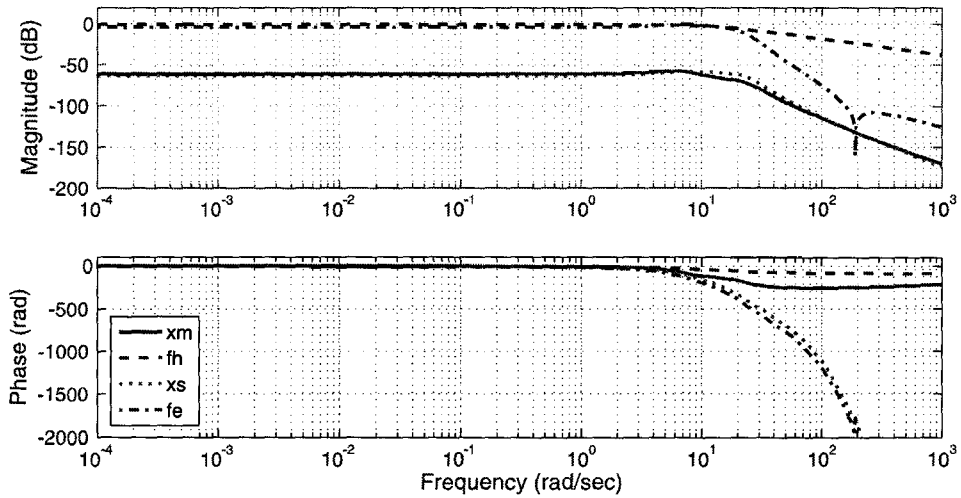


Figure 5.11: Closed-loop frequency response to the input  $f_h^*$  for 300 msec delay and matched environment stiffness.

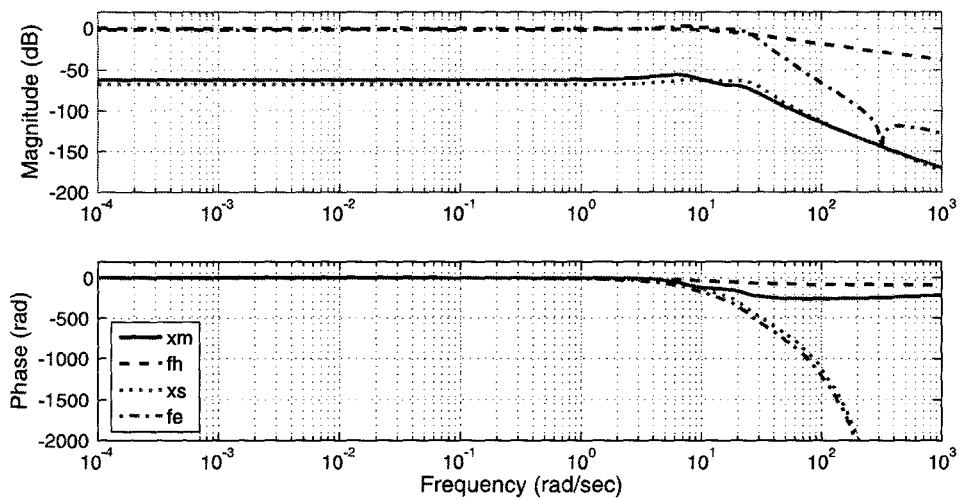


Figure 5.12: Closed-loop frequency response to the input  $f_h^*$  for 300 msec delay and mismatched environment stiffness.

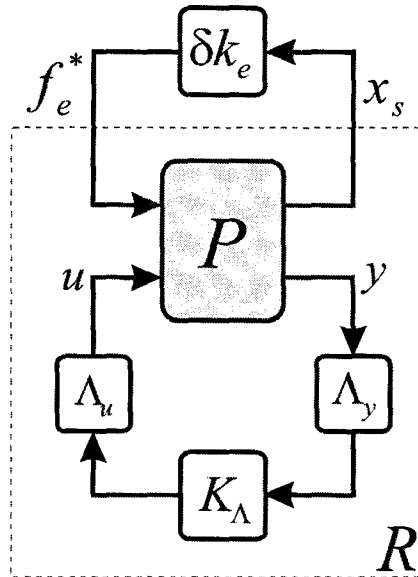


Figure 5.13: The closed-loop system subject to the environment stiffness uncertainty,  $\delta k_e$ .

in the environment stiffness can be examined with the aid of the Nyquist analysis. A model of closed-loop system subject to the stiffness uncertainty is displayed in Fig. 5.13. The characteristic equation of the perturbed system is given by

$$1 - \delta k_e R(s) = 0. \quad (5.73)$$

The Nyquist plots of  $R(s)$  for delays of 100, 200, and 300 msec are depicted in Fig. 5.14-5.16. Given that the unperturbed system is stable, it can be concluded that the system remains stable as long as the Nyquist plot of  $R(s)$  does not encircle  $1/\delta k_e$ . Therefore, the system stability is guaranteed for perturbations in the

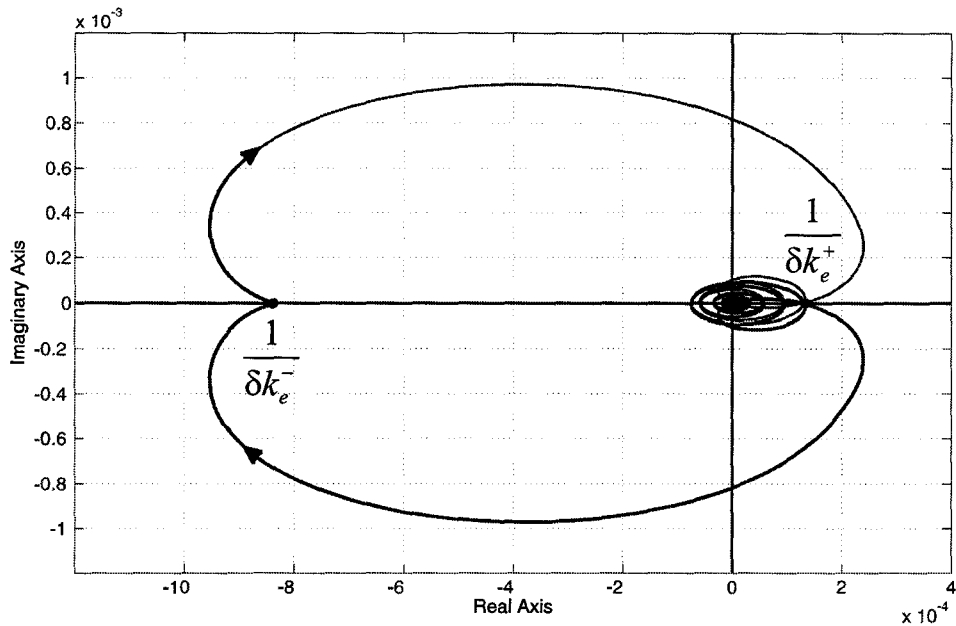


Figure 5.14: Nyquist plot of  $R(s)$  for 100 msec of delay.

following range

$$\delta k_e^- < \delta k_e < \delta k_e^+. \quad (5.74)$$

Using (5.74) and the Nyquist plots in Fig. 5.14-5.16, the ranges of the environment stiffness for guaranteed stability were calculated to be  $-293 \sim 8500$ ,  $-370 \sim 6210$ , and  $-454 \sim 4970$  N/m for delays of 100, 200, and 300 msec, respectively. In practice, the stability margins may be smaller due to discrete-time implementation of the continuous-time controller and the presence of other forms of uncertainties in the system. Nevertheless, it still can be concluded that the controller is fairly robust with respect to perturbations in the environment stiffness. Obviously, the stability margins can be altered by adjusting the design filters in the robust control

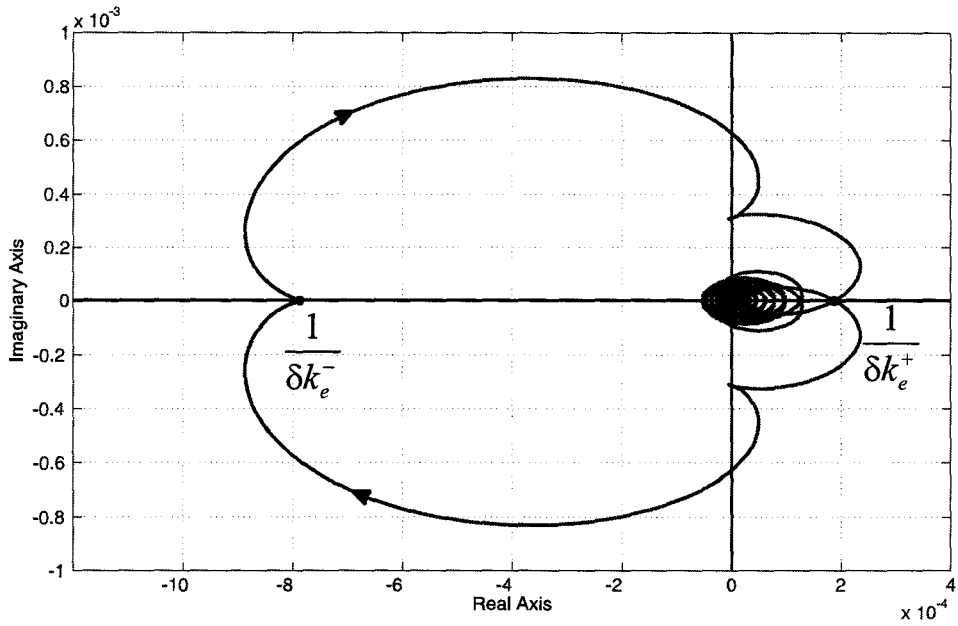


Figure 5.15: Nyquist plot of  $R(s)$  for 200 msec of delay.

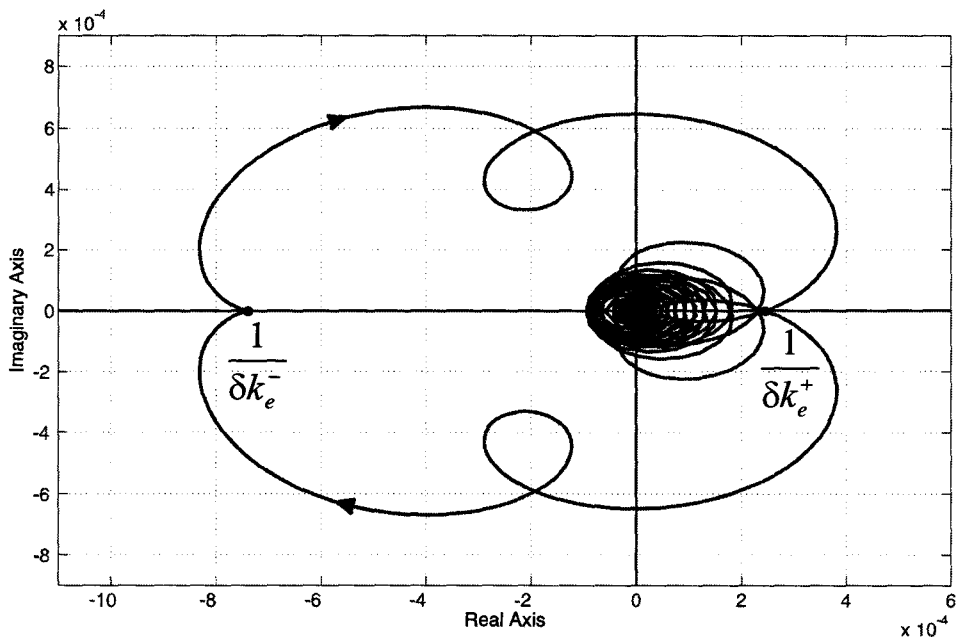


Figure 5.16: Nyquist plot of  $R(s)$  for 300 msec of delay.

formulation to achieve a new trade-off between transparency and robust stability.

## 5.6 Experimental Results

The same experimental setup, as shown in Fig. 4.9, has been utilized here to verify the effectiveness of the proposed control method. A block diagram of the proposed two-stage controller is shown in Fig. 5.17. The local adaptive controllers are implemented using the procedure outlined in Section 2 and based on the parameters given in Table 5.1. The parameters and filters used in the design of the outer-loop robust controller are also given in this table. The implementation of the robust controller involves two FIR filters  $\Pi_1$  and  $\Pi_2$  in Fig. 5.6 with the form given in (E.82)-(E.84) in Appendix E. These filters require buffering and multiplications of signals at a number of samples proportional to the amount of the time delay, i.e. the length of their impulse response, and the control update rate. In the particular example of this chapter, the length of the FIR filters are 100, 200, and 300 samples for round-trip delays of 100, 200, and 300 msec, respectively. The other component of the controller is the plant  $\bar{G}(s)^{-1}$  in Fig. 5.17 which has 23 states, six(6) inputs, and six(6) outputs in the design example.

In the experiments, the operator manipulates the slave robot in free motion and in contact with an environment with an stiffness of 2000-3000 N/m. However, as noted in Table 5.1, the nominal environment stiffness was chosen to be  $K_e = 900$  N/m in the design. In general, interaction with stiffer environments would require a higher design stiffness compromising the performance in interaction with softer environments and in free motion. Alternatively the robust stability margin with respect to the environment stiffness can be enlarged at the expense of

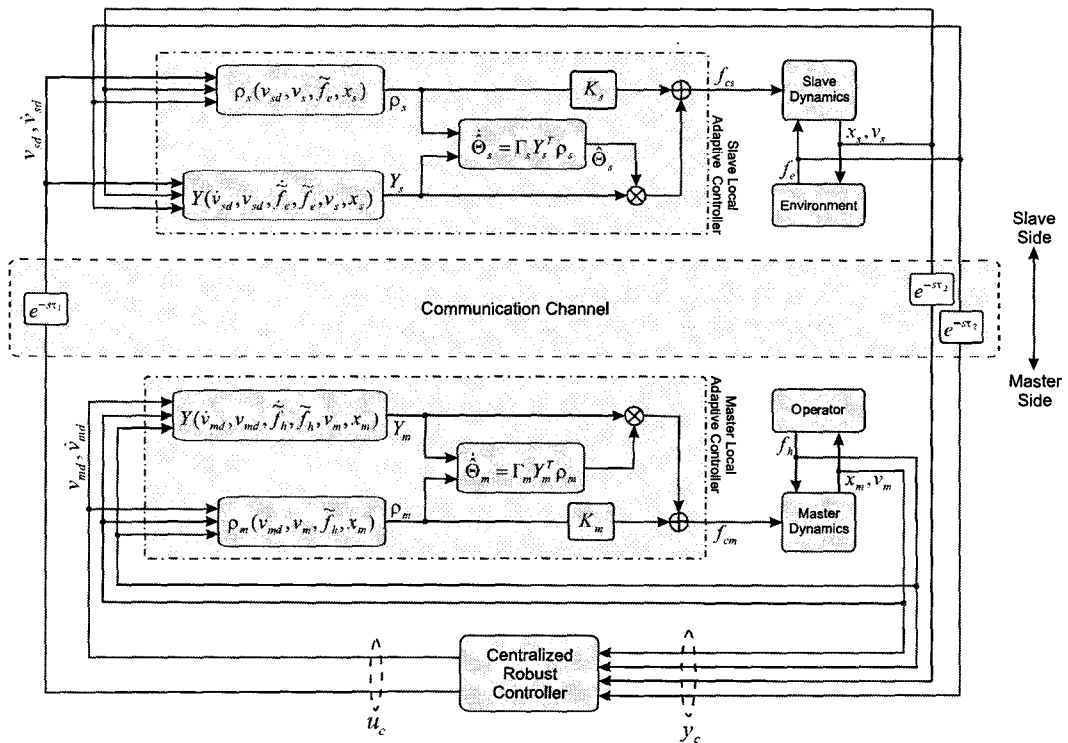


Figure 5.17: The two-stage teleoperation controller.

a reduced transparency to enable contact with stiffer environments.

The experiments were conducted for three different values of delay, i.e. 100 msec, 200 msec, and 300 msec. The delay was emulated by adding data buffers of appropriate size that store and delay the slave measurement and control signals.

### 5.6.1 Teleoperation experiment with 100 msec delay

In Fig. 5.18, the responses of the proposed controller along a single axis under 100 msec of communication delay are plotted. The system is initially at rest until roughly at  $t = 4$  sec when the operator begins moving the master/slave units in

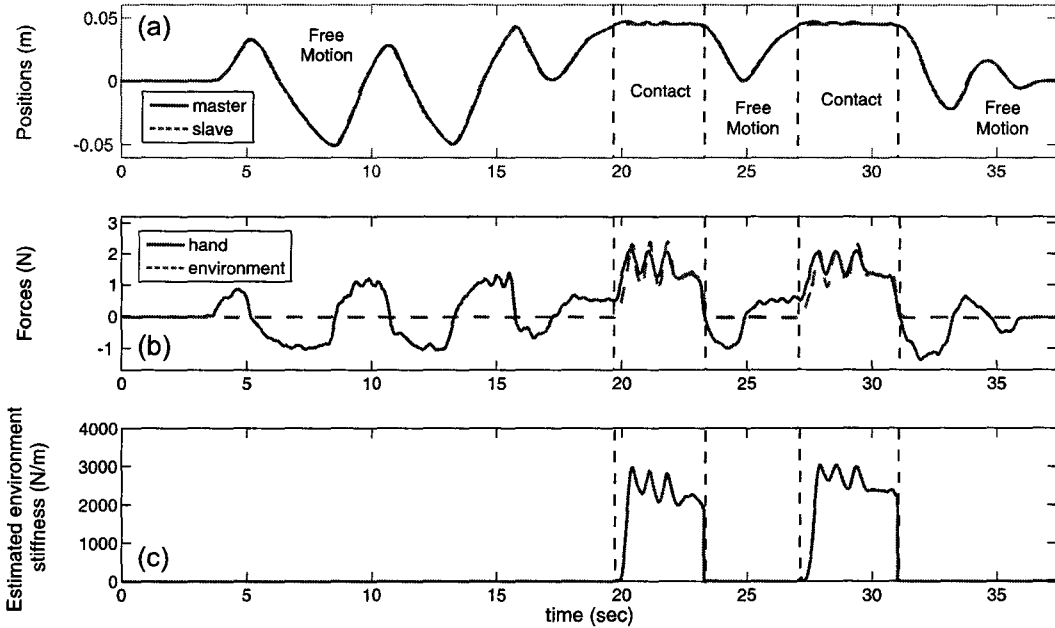


Figure 5.18: The controller with 100 ms delay in experiment: (a) position tracking; (b) force tracking; (c) estimated environment stiffness.

free motion. The positions of master and slave robots follow each other in free motion with high accuracy. Although ideally the user force must be zero in free motion, in practice, a nonzero force is needed to move the robots due to the trade-off involved in balancing performance against robust stability.

At  $t \simeq 19.5$ sec, the slave makes an initial contact with the environment. During the course of the first contact from time 19.5-23.5 sec, the environment and hand forces as well as the master and slave positions closely track each other as can be seen in Fig. 5.18. The variations in the contact force signals are deliberately induced by the operator in order to demonstrate the tracking performance. At  $t \simeq 23.5$  sec, the operator withdraws the master and consequently the master/slave system returns to free motion following a smooth transition. A second stable contact occurs

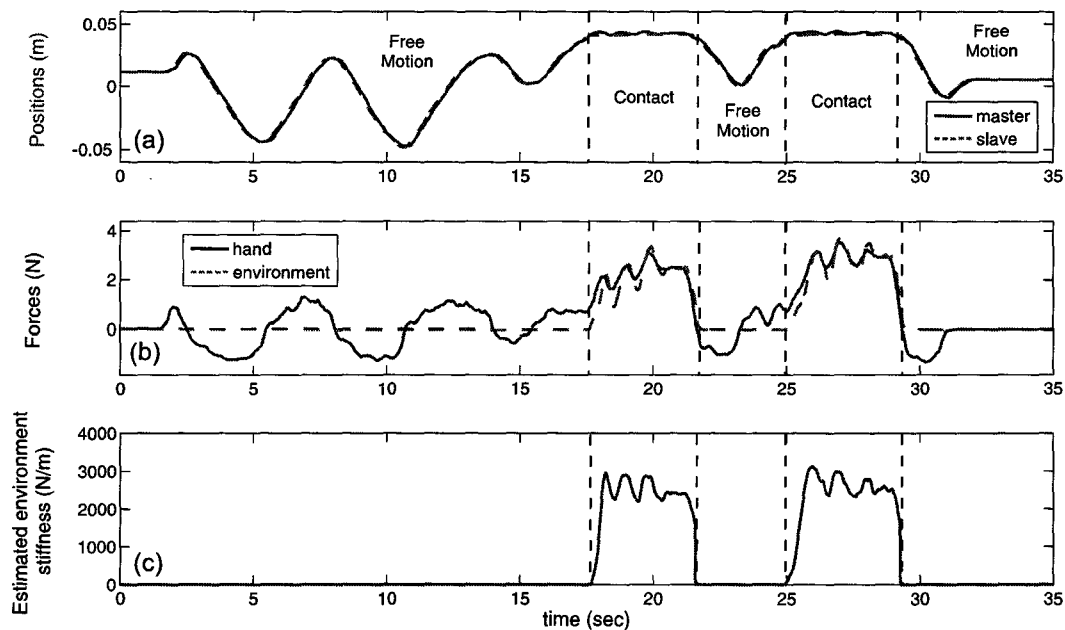


Figure 5.19: The controller with 200 ms delay in experiment: (a) position tracking; (b) force tracking; (c) estimated environment stiffness.

at  $t \approx 27$ sec followed by another period of free motion. The estimated environment stiffness is plotted in Fig. 5.18(c) from which it is evident that the local adaptive controller rapidly copes with the variations in the environment stiffness.

### 5.6.2 Teleoperation experiment with 200 msec delay

Fig. 5.19 illustrates the responses of the controller for a round-trip delay of 200 msec. As in the previous case, the experiments starts with the master/slave at rest, followed by a free motion operation and subsequent contact and free motion phases. The transitions from free motion to contact and vice versa are stable. The position tracking in free motion as well as position and force tracking in contact are quite satisfactory. The stiffness adaption is also demonstrated in Fig. 5.19(c).

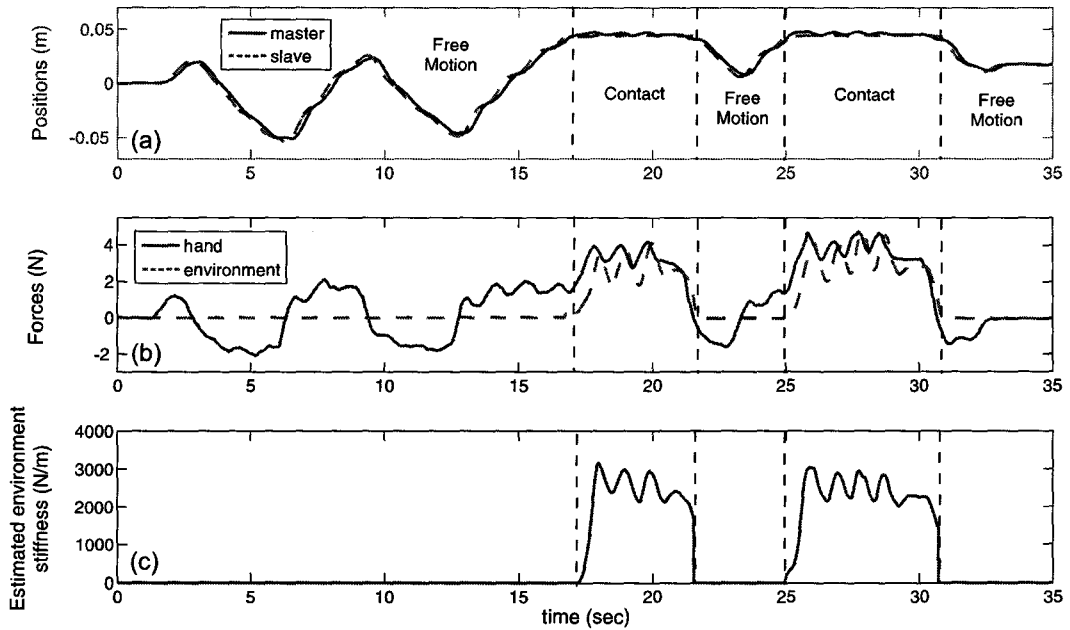


Figure 5.20: The controller with 300 ms delay in experiment: (a) position tracking; (b) force tracking; (c) estimated environment stiffness.

### 5.6.3 Teleoperation experiment with 300 msec delay

In Fig. 5.20, the results of an experiment with the proposed teleoperation controller under 300 msec of communication latency are presented. Once again, the transitions are stable and despite a slight degradation in the tracking results, the performance of the system is still satisfactory.

## 5.7 Conclusions

In this chapter, a two-stage adaptive/robust control was introduced to balance the performance and stability requirements in time-delay teleoperation. Through the use of local Lyapunov-based adaptive controllers, the dynamics of the master

and slave robots were linearized and rendered independent from their parameters. Using these new dynamics, teleoperation control for achieving transparency and robust stability was formulated as an  $H_\infty$  robust control synthesis with multiple I/O delays. The resulting problem was solved using decompositions into single-delay adobe-type problems. The interaction between the local adaptive/nonlinear controllers and the robust controller was accounted for in the proposed modeling and control synthesis.

The results of performance and stability analysis as well as experiments with a teleoperation setup demonstrated the effectiveness of the proposed adaptive/robust controller. Compared to our earlier proposed model-based controllers, the robust controller in this chapter is less sensitive to modeling uncertainties. Nevertheless, since it uses fixed structure and parameters for the entire range of operation, its transparency may be sacrificed in favor of robust stability, particularly if large modeling uncertainty is considered in the design stage.

# Chapter 6

## Adaptive Control of Bilateral Time-delay Teleoperation

### 6.1 Introduction

The robust controller proposed in the previous chapter has less sensitivity to uncertainties compared to the earlier decentralized and centralized model-based controllers in Chapter 4 and [1,2]. However, it utilizes a fixed controller for the entire range of operation, forcing a compromise between transparency and robust stability. By varying its structure and/or parameters an adaptive controller can potentially achieve a better transparency-stability trade-off in bilateral teleoperation. This chapter introduces a new adaptive model-predictive controller for teleoperation systems with constant and time-varying communication delay. The proposed method uses the model and delay information and can adapt to uncertainties in user and environment dynamics in order to achieve delay-free position tracking and tool impedance shaping. A delay reduction formulation is developed which

channel that is subject to delay. The slave measurements will arrive at the controller site with  $\tau_2$  time delay, and the slave control action is delayed by  $\tau_1$ . Note that in general the communication delays can be a function of time.

The combined nonlinear dynamics of master/hand and slave/environment have previously been presented in (3.19) and (3.20), respectively. Following the same steps as those in Section 4.2, these nonlinear dynamics can be linearized using an adaptive Lyapunov-based method. By choosing the master and slave position and velocity as state variables, the linearized dynamics can be written in state-space form as presented in Appendix A.

In the proposed adaptive control framework, all the input and all the output channels should include the same amount of latency. Therefore, the master measurements and the master control action are padded by extra  $\tau_2$  and  $\tau_1$  delay, respectively. Since the system dynamics have been linearized, the delay in the output measurement channels can be relocated to the input channels resulting in a system with  $d = \tau_1 + \tau_2$  delay in all of the control signals, as illustrated in Fig. 6.1. The round-trip delay,  $d$ , in general is variable and can be expressed as a function of time, i.e.

$$d(t) = \tau_1(t) + \tau_2(t). \quad (6.1)$$

The teleoperation transparency objectives used in the proposed method are the same as those used in Chapter 4, i.e. position tracking and virtual tool impedance shaping in (3.23)-(3.25). Here the states of the system are defined as combination of the master, slave, and tool states as follows

$$X(t) = \left[ X_s(t) \quad \alpha_p X_s(t) - X_m(t) \quad X_m(t) - X_t(t) \right]^T \quad (6.2)$$

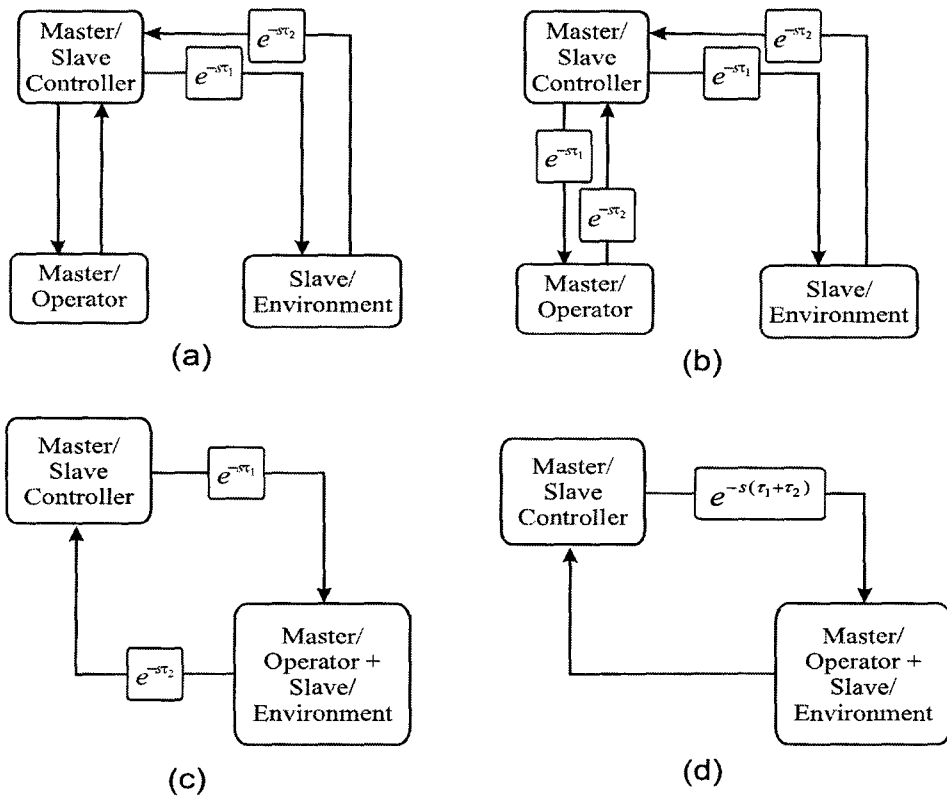


Figure 6.1: A centralized time-delay teleoperation control (a) without delay padding, (b) after delay padding, (c) after combining master/operator and slave/environment dynamics and (d) after moving all the delays to the input channels.

where  $X_m(t)$ ,  $X_s(t)$ , and  $X_t(t)$  have been introduced in (4.27), (4.28) and (4.29);  $\alpha_f$  and  $\alpha_p$  have been defined in (3.23) and (3.24). The position tracking errors between the master and slave, and the master and virtual tool are included in the state vector. In an output regulation control framework, the transparency objectives in (3.23)-(3.25) can be enforced by regulating these tracking errors to zero. As mentioned earlier, the system is assumed to have a round-trip delay of  $d(t)$  in all

the input channels. The evolution of the states is governed by

$$\begin{aligned}\dot{X}(t) &= AX(t) + Bu(t - d(t)) + B_{f_h^*} f_h^*(t) \\ u(t) &= \begin{bmatrix} f_{cs}(t) & f_{cm}(t) \end{bmatrix}^T.\end{aligned}\quad (6.3)$$

The system matrices,  $A$  and  $B$ , and  $B_{f_h^*}$  can be obtained from  $A_m$ ,  $B_m$ ,  $A_s$ ,  $B_s$ ,  $A_t$ , and  $B_t$ . These matrices are presented in Appendix F. Note that  $f_h^*(t)$  represents the operator exogenous input at time  $t$ .

### 6.3 Modified Delay Reduction and Model-based State Prediction

In this section the case of a constant round-trip delay, i.e.  $d(t) = d$ , is considered. Later in the chapter, the method will be extended to accommodate variable delays. An input-delayed system with the following dynamics

$$\dot{X}(t) = AX(t) + Bu(t - d) \quad (6.4)$$

where  $A$  and  $B$  are fixed known matrices can be reduced to a delay-free system using the reduction method introduced by Artstein [106]. The reduced state,  $Z(t)$ , is calculated using

$$Z(t) = X(t) + \int_{t-d}^t \Phi(t, s + d) B(s + d) u(s) ds \quad (6.5)$$

where  $\Phi(t_1, t_2)$  is the system state transition matrix from time  $t_2$  to  $t_1$  [122]. We introduced a multi-input multi-output variation of this reduction method in [2] which can be employed in teleoperation control. Both the original and the modified reduction method assume the knowledge of the system matrices, i.e.  $A$  and  $B$ . However in applications such as teleoperation, the system parameters are unknown and can change by time. This motivates the need for an adaptive version of the approach to handle unknown parameters. In [113] a reduction method was introduced which uses estimates of system parameters. However, this method is only applicable to single-input/single-output first-order systems and was never extended to more general forms of dynamics. In this chapter, we propose a new delay reduction technique which can be applied to an uncertain multi-input/multi-output system such as time-delay teleoperation.

For a system with the dynamics shown in (6.4), the delay reduced state in our approach is defined as

$$\hat{Z}(t) = \bar{X}(t) + \int_{t-d}^t \hat{\Phi}(t, s+d) \hat{B}(s) u(s) ds \quad (6.6)$$

where  $\hat{\Phi}$  and  $\hat{B}$  are the estimated values of  $\Phi$  and  $B$  matrices and  $\bar{X}$  is the state of an observer with the following dynamics

$$\dot{\bar{X}}(t) = \hat{A}(t-d) \bar{X}(t) + \hat{B}(t-d) u(t-d) + L(t) e(t). \quad (6.7)$$

Here  $\hat{A}$  is an estimation of the matrix  $A$  and  $L(t)$  is a time-varying observer gain matrix which will be introduced shortly. The signal  $e(t)$  is the state observation

error, i.e.

$$e(t) = X(t) - \bar{X}(t). \quad (6.8)$$

By applying the new reduction method to the teleoperation system defined in (6.3), one can write

$$\hat{Z}(t) = \bar{X}(t) + \int_{t-d}^t \hat{\Phi}(t, s+d) \hat{B}(s) u(s) ds + \int_{t-d}^t \hat{\Phi}(t, s+d) \hat{B} f_h^*(s) ds \quad (6.9)$$

and

$$\dot{\hat{X}}(t) = \hat{A}(t-d) \bar{X}(t) + \hat{B}(t-d) u(t-d) + \hat{B} f_h^*(t-d) + L(t) e(t) \quad (6.10)$$

where  $\hat{B} f_h^*(t-d)$  is the estimation of  $B_{f_h^*} f_h^*(t)$  at time  $t-d$ . Equations (6.9) and (6.10) use the estimated values of the system parameters the calculation of which will be discussed in the following sections. The dynamics of the reduced system can be calculated by finding the derivative of  $\hat{Z}(t)$  in (6.9) and by using the Leibniz integral rule [131] as

$$\begin{aligned} \dot{\hat{Z}}(t) = & \dot{\bar{X}}(t) + \hat{\Phi}(t, t+d) \hat{B}(t) u(t) + \hat{\Phi}(t, t+d) \hat{B} f_h^*(t) \\ & - \hat{B}(t-d) u(t-d) - \hat{B} f_h^*(t-d) \\ & + \int_{t-d}^t \frac{\partial}{\partial t} \hat{\Phi}(t, s+d) \hat{B}(s) u(s) ds + \int_{t-d}^t \frac{\partial}{\partial t} \hat{\Phi}(t, s+d) \hat{B} f_h^*(s) ds. \end{aligned} \quad (6.11)$$

The estimated system transition matrix,  $\hat{\Phi}(t, s)$ , satisfies the following

$$\frac{\partial \hat{\Phi}(t, s)}{\partial t} = \hat{A}(t-d)\hat{\Phi}(t, s) \quad , \quad \hat{\Phi}(s, s) = I \quad (6.12)$$

where  $\hat{A}$  is an estimation of the matrix  $A$ . Using the definition in (6.12) and Equation (6.9), the dynamics of the reduced state in (6.11) can be written as

$$\begin{aligned} \dot{\hat{Z}}(t) = & \dot{\hat{X}}(t) + \hat{\Phi}(t, t+d)\hat{B}(t)u(t) + \hat{\Phi}(t, t+d)\hat{B}f_h^*(t) \\ & - \hat{B}(t-d)u(t-d) - \hat{B}f_h^*(t-d) + \hat{A}(t-d) \left( \hat{Z}(t) - \bar{X}(t) \right). \end{aligned} \quad (6.13)$$

By substituting  $\dot{\hat{X}}$  from (6.10), one can write

$$\dot{\hat{Z}}(t) = \hat{A}(t-d)\hat{Z}(t) + \hat{\Phi}(t, t+d)\hat{B}(t)u(t) + \hat{\Phi}(t, t+d)\hat{B}f_h^*(t) + L(t)e(t). \quad (6.14)$$

The predicted state of the system in future,  $\hat{X}(t+d)$ , is calculated from the reduced state,  $\hat{Z}(t)$ , using the following equation

$$\hat{X}(t+d) = \hat{\Phi}(t+d, t)\hat{Z}(t). \quad (6.15)$$

The vector  $\hat{X}(t+d)$  represents the predicted future state of the system which is calculated based on the current state of the system, current information of the model parameters and the future inputs to the system. Future inputs up to the time  $t+d$  are available since the computed control action is buffered and applied to the system with a delay  $d$ . Using (6.15), the derivative of the predicted state can

be obtained by

$$\dot{X}(t+d) = \dot{\hat{\Phi}}(t+d, t)\hat{Z}(t) + \hat{\Phi}(t+d, t)\dot{\hat{Z}}(t). \quad (6.16)$$

To find the derivative of the system transfer matrix,  $\hat{\Phi}(t+d, t)$  in (6.16), the following properties are being utilized [122]

$$\hat{\Phi}(t+d, t) = \hat{\Phi}(t+d, \tau)\hat{\Phi}(\tau, t), \quad (6.17)$$

$$\hat{\Phi}(t, \tau)\hat{\Phi}(\tau, t) = I \quad (6.18)$$

where  $\tau$  is an arbitrary time and  $I$  is the identity matrix of the appropriate dimension. The derivative of the equation in (6.18) is calculated as

$$\frac{\partial \hat{\Phi}(t, \tau)}{\partial t} \hat{\Phi}(\tau, t) + \hat{\Phi}(t, \tau) \frac{\partial \hat{\Phi}(\tau, t)}{\partial t} = 0. \quad (6.19)$$

Using the definitions in (6.12) and (6.18), Equation (6.19) can be rewritten as

$$\hat{A}(t-d) + \hat{\Phi}(t, \tau) \frac{\partial \hat{\Phi}(\tau, t)}{\partial t} = 0. \quad (6.20)$$

After multiplying both sides of (6.20) by  $\hat{\Phi}(\tau, t)$  from left, one can write

$$\frac{\partial \hat{\Phi}(\tau, t)}{\partial t} = -\hat{\Phi}(\tau, t)\hat{A}(t-d). \quad (6.21)$$

Now taking the derivative of (6.17), one may write

$$\dot{\hat{\Phi}}(t+d, t) = \frac{\partial \hat{\Phi}(t+d, \tau)}{\partial t} \hat{\Phi}(\tau, t) + \hat{\Phi}(t+d, \tau) \frac{\partial \hat{\Phi}(\tau, t)}{\partial t}. \quad (6.22)$$

Using the definition in (6.12) and the result in (6.21), (6.22) can be rewritten as

$$\dot{\hat{\Phi}}(t+d, t) = \hat{A}(t)\hat{\Phi}(t+d, t) - \hat{\Phi}(t+d, t)\hat{A}(t-d). \quad (6.23)$$

The dynamics of the predicted state,  $\hat{X}(t+d)$ , can now be found using (6.16) and by replacing  $\dot{\hat{\Phi}}(t+d, t)$  and  $\dot{\hat{Z}}(t)$  from (6.23) and (6.14) as

$$\begin{aligned} \dot{\hat{X}}(t+d) = & \left( \hat{A}(t)\hat{\Phi}(t+d, t) - \hat{\Phi}(t+d, t)\hat{A}(t-d) \right) \hat{Z}(t) \\ & + \hat{\Phi}(t+d, t) \left( \hat{A}(t-d)\hat{Z}(t) + \hat{\Phi}(t, t+d)\hat{B}(t)u(t) \right. \\ & \left. + \hat{\Phi}(t, t+d)\hat{B}f_h^*(t) + L(t)e(t) \right). \end{aligned} \quad (6.24)$$

Simplifying this equation results in the following dynamics for the predicted state

$$\dot{\hat{X}}(t+d) = \hat{A}(t)\hat{X}(t+d) + \hat{B}(t)u(t) + \hat{B}f_h^*(t) + \hat{\Phi}(t+d, t)L(t)e(t). \quad (6.25)$$

The estimated predicted state,  $\hat{X}(t+d)$ , has the same structure as  $X(t)$  in (6.2), i.e.

$$\hat{X}(t+d) = \begin{bmatrix} \hat{x}_s(t+d) \\ \hat{v}_s(t+d) \\ \hat{x}_s(t+d) - \hat{x}_m(t+d) \\ \hat{v}_s(t+d) - \hat{v}_m(t+d) \\ \hat{x}_m(t+d) - \hat{x}_t(t+d) \\ \hat{v}_m(t+d) - \hat{v}_t(t+d) \end{bmatrix}. \quad (6.26)$$

## 6.4 New Outputs Definition and Regulation

The proposed reduction method removes the delay from the system and results in the delay-free dynamics of the predicted state in (6.25). It is important to mention that the dynamics equation in (6.25) is not just a time shifted version of the system dynamics in (6.3) since  $\hat{X}(t+d)$  is actually available for calculating the control action  $u$  at time  $t$ .

The predicted state of the system,  $\hat{X}(t+d)$ , can be regulated to zero using various types of state regulation methods. This is, however, not desired in teleoperation since regulating the entire state vector to zero would prevent master and slave devices from moving. Instead, to achieve the transparency objectives in (3.24) and (3.25), the following outputs are defined based on a part of the state vector and will be regulated to zero

$$\hat{y}_1(t+d) \triangleq \hat{X}_4(t+d) + \lambda \hat{X}_3(t+d), \quad (6.27)$$

$$\hat{y}_2(t+d) \triangleq \hat{X}_6(t+d) + \lambda \hat{X}_5(t+d). \quad (6.28)$$

Here  $\lambda$  is a positive scalar and  $\hat{X}_i(t+d)$  is the  $i$ th element of the predicted state in (6.26). As specified in (6.26), the third and the fourth states correspond to the master/slave tracking error and its derivative and the fifth and sixth states correspond to the master/tool tracking error and its derivative.

To facilitate the calculation of the output regulating control action,  $u(t)$ , the vector of states in (6.26) is transformed through a non-singular transformation  $T$

to a new set of state variables which include the newly defined outputs, i.e.

$$\hat{X}_T(t+d) = \begin{bmatrix} \hat{x}_s(t+d) \\ \hat{v}_s(t+d) \\ \hat{x}_s(t+d) - \hat{x}_m(t+d) \\ \hat{x}_m(t+d) - \hat{x}_t(t+d) \\ \hat{y}_1(t+d) \\ \hat{y}_2(t+d) \end{bmatrix}. \quad (6.29)$$

The dynamics of the transformed state,  $\hat{X}_T(t+d)$ , can be found from the dynamics of  $\hat{X}(t+d)$  and using the transformation matrix  $T$  as

$$\dot{\hat{X}}_T(t+d) = \hat{A}_T(t)\hat{X}_T(t+d) + \hat{B}_T(t)u(t) + B_T\hat{f}_h^*(t) + T\hat{\Phi}(t+d, t)L(t)e(t) \quad (6.30)$$

where  $\hat{A}_T(t)$ ,  $\hat{B}_T(t)$  and  $B_T\hat{f}_h^*(t)$  can be calculated from  $\hat{A}(t)$ ,  $\hat{B}(t)$  and  $B\hat{f}_h^*(t)$  using

$$\hat{A}_T(t) = T\hat{A}(t)T^{-1}, \quad (6.31)$$

$$\hat{B}_T(t) = T\hat{B}(t), \quad (6.32)$$

$$B_T\hat{f}_h^*(t) = TB\hat{f}_h^*(t). \quad (6.33)$$

The reader can refer to Appendix F.1 for the details of the calculations. As stated in

this appendix, the matrices  $\hat{A}_T(t)$ ,  $\hat{B}_T(t)$  and  $B_T \hat{f}_h^*(t)$  have the following structures

$$\hat{A}_T(t) = \begin{bmatrix} \hat{A}_s(t) & 0 & 0 \\ 0 & \Lambda & I \\ \hat{A}_1(t) & \hat{A}_2(t) & \hat{A}_3(t) \end{bmatrix}, \quad (6.34)$$

$$\hat{B}_T(t) = \begin{bmatrix} \hat{B}_s(t) \\ 0 \\ \hat{B}_y(t) \end{bmatrix}, \quad (6.35)$$

$$B_T \hat{f}_h^*(t) = \begin{bmatrix} 0 \\ 0 \\ B \hat{f}_{hy}^*(t) \end{bmatrix} \quad (6.36)$$

where

$$\Lambda = \begin{bmatrix} -\lambda & 0 \\ 0 & -\lambda \end{bmatrix} \quad (6.37)$$

and  $\lambda$  is defined in (6.27) and (6.28).

Assume the following control action

$$u(t) = \hat{B}_y^{-1}(t) \left( \Omega \hat{y}(t+d) - \hat{A}_1(t) \hat{X}_{T1}(t+d) - \hat{A}_2(t) \hat{X}_{T2}(t+d) \right. \\ \left. - \hat{A}_3(t) \hat{X}_{T3}(t+d) - B \hat{f}_{hy}^*(t) - T_3 \hat{\Phi}(t+d, t) L(t) e(t) \right) \quad (6.38)$$

where  $T_3$  is a part of the transformation matrix  $T$  and is defined in (F.87),  $\Omega$  is a

diagonal negative definite matrix in the form of

$$\Omega = \begin{bmatrix} -\omega_1 & 0 \\ 0 & -\omega_2 \end{bmatrix}, \quad \omega_1, \omega_2 > 0 \quad (6.39)$$

and

$$\hat{y}(t+d) \triangleq \begin{bmatrix} \hat{y}_1(t+d) \\ \hat{y}_2(t+d) \end{bmatrix}. \quad (6.40)$$

The inverse of the matrix  $\hat{B}_y$  in (6.38) always exists due to its special structure as shown in Appendix F.1. It is worth noticing that the control action in (6.38) is a function of the parameter estimates, the calculated predicted state of the system based on observations up to time  $t$ ,  $\hat{X}(t+d)$ , and the state observation error,  $e(t)$ . Applying this control action to the open-loop dynamics in (6.30) results in the following closed-loop output dynamics

$$\dot{\hat{y}}(t+d) = \Omega \hat{y}(t+d). \quad (6.41)$$

By substituting the control action from (6.38) into the system dynamics in (6.30), one can obtain

$$\dot{\hat{X}}_T(t+d) = \hat{A}_{T_d}(t) \hat{X}_T(t+d) + \hat{B} \hat{f}_{hd}^*(t) + T_d(t) \hat{\Phi}(t+d, t) L(t) e(t) \quad (6.42)$$

where

$$\hat{A}_{T_{cl}}(t) = \begin{bmatrix} \hat{A}_s(t) - \hat{B}_s(t)\hat{B}_y^{-1}(t)\hat{A}_1(t) & -\hat{B}_s(t)\hat{B}_y^{-1}(t)\hat{A}_2(t) & -\hat{B}_s(t)\hat{B}_y^{-1}(t)(\hat{A}_3(t) - \Omega) \\ 0 & \Lambda & I \\ 0 & 0 & \Omega \end{bmatrix}, \quad (6.43)$$

$$\hat{B}f_{h_{cl}}^*(t) = \begin{bmatrix} -\hat{B}_s(t)\hat{B}_y^{-1}(t)\hat{B}f_{hy}^*(t) \\ 0 \\ 0 \end{bmatrix} \quad (6.44)$$

and

$$T_{cl}(t) = \begin{bmatrix} T_1 - \hat{B}_s(t)\hat{B}_y^{-1}(t)T_3 \\ T_2 \\ 0 \end{bmatrix}. \quad (6.45)$$

The definition of  $T_1$ ,  $T_2$  and  $T_3$  and the closed-loop matrices in (6.42) are given in (F.87) and (F.90), respectively. It is worth mentioning that the eigenvalues of the closed-loop state matrix,  $\hat{A}_{T_{cl}}(t)$ , vary with time. However as shown in Appendix F.2, these eigenvalues which are the union of the eigenvalues of the diagonal elements of the state matrix, will always have negative real parts. Nonetheless, in the case of a time-varying system this is not sufficient to prove the stability of the system.

## 6.5 System Stability and Parameters Adaptation Law

The dynamics of the state observation error,  $e(t)$ , can be obtained by taking the derivative of (6.8) and substituting  $\dot{X}(t)$  and  $\dot{\hat{X}}(t)$  from (6.3) and (6.10) as

$$\dot{e}(t) = \left( \hat{A}(t-d) - L(t) \right) e(t) + \tilde{A}(t-d)X(t) + \tilde{B}(t-d)u(t-d) + \tilde{B}f_h^*(t-d) \quad (6.46)$$

where the *tilde* variables represent the estimation errors, i.e. the error between the actual and the estimated value of the corresponding variables

$$\tilde{A} = A - \hat{A}, \quad (6.47)$$

$$\tilde{B} = B - \hat{B}, \quad (6.48)$$

$$\tilde{B}f_h^* = B_{f_h^*}f_h^* - \hat{B}f_h^*. \quad (6.49)$$

The user-defined observer gain  $L(t)$  is chosen to be

$$L(t) = \hat{A}(t-d) - \Upsilon \quad (6.50)$$

where  $\Upsilon < 0$  is a constant matrix. Substituting  $L(t)$  from (6.50) in (6.46) results in the following state observation error dynamics

$$\dot{e}(t) = \Upsilon e(t) + \tilde{A}(t-d)X(t) + \tilde{B}(t-d)u(t-d) + \tilde{B}f_h^*(t-d). \quad (6.51)$$

To facilitate the use of adaptive control, the dynamics of  $e(t)$  in (6.51) are rewritten in an equivalent linear-in-parameter form as

$$\dot{e}(t) = \Upsilon e(t) + Y(t)\tilde{\theta}(t-d) \quad (6.52)$$

where  $Y(t)$  is a regressor matrix which is a function of the measurements and  $\tilde{\theta}(t)$  is the vector of parameter estimation errors, i.e.

$$\tilde{\theta}(t) = \theta - \hat{\theta}(t). \quad (6.53)$$

The system dynamics in linear-in-parameter form are presented in Appendix F.3. It is important to mention that the vector of system parameters,  $\theta$ , which includes the user exogenous force, is assumed to be constant. Such assumption is shown to be valid in experiments since the prediction horizon is relatively short with respect to the rate of change in hand exogenous input. To remove the delay from the estimation error vector,  $\tilde{\theta}(t-d)$ , as initially proposed by [113] a new signal,  $w(t)$ , is defined based on the following dynamics

$$\dot{w}(t) = \Upsilon w(t) - Y(t)\hat{\theta}(t) + Y(t)\hat{\theta}(t-d). \quad (6.54)$$

The signal  $w(t)$  will be added to the error signal  $e(t)$  resulting in the definition of a new variable

$$r(t) \triangleq e(t) + w(t). \quad (6.55)$$

Using (6.52) and (6.54), the dynamics of  $r(t)$  can be obtained as

$$\dot{r}(t) = \Upsilon r(t) + Y(t)\tilde{\theta}(t). \quad (6.56)$$

A Lyapunov analysis is employed to prove the stability of the observation error in (6.56) and to find the parameter adaptation law. The following theorem has been utilized in the Lyapunov analysis.

*Theorem 6.1:* Consider a matrix  $\Upsilon$  where all the eigenvalues have negative real parts. For any matrix  $Q = Q^T > 0$ , there exists a unique matrix  $P = P^T > 0$  that solves the following Lyapunov equation

$$\Upsilon^T P + P \Upsilon = -Q. \quad (6.57)$$

*Proof:* See [122].

Using the solution to the Lyapunov equation in (6.57), the following candidate Lyapunov function is defined

$$V(t) = \frac{1}{2} r^T(t) P r(t) + \frac{1}{2} \tilde{\theta}^T(t) \Gamma^{-1} \tilde{\theta}(t) \quad (6.58)$$

where  $\Gamma$  is a symmetric positive definite matrix, i.e.  $\Gamma = \Gamma^T > 0$ . The derivative of  $V(t)$  in (6.58) can be computed along the system state trajectory by replacing  $\dot{r}(t)$  from the dynamics equation in (6.56) as

$$\dot{V}(t) = \frac{1}{2} r^T(t) (\Upsilon^T P + P \Upsilon) r(t) + r^T(t) P Y(t) \tilde{\theta}(t) + \dot{\tilde{\theta}}^T(t) \Gamma^{-1} \tilde{\theta}(t). \quad (6.59)$$

Assuming that the actual parameters vector,  $\theta$ , is constant and using the equation (6.53), the following projection based adaptation law is proposed

$$\dot{\hat{\theta}}_i(t) = -\dot{\tilde{\theta}}_i(t) = \begin{cases} 0 & \hat{\theta}_i \leq \theta_i^- \\ \Gamma_i^T Y_i^T(t) P^T r(t) & \theta_i^- \leq \hat{\theta}_i \leq \theta_i^+ \\ 0 & \theta_i^+ \leq \hat{\theta}_i \end{cases} \quad (6.60)$$

where  $i$  denotes the  $i$ th parameter of the system,  $\Gamma$  is the parameter update gain, and  $\theta_i^-$  and  $\theta_i^+$  represent the minimum and maximum allowable bounds on the parameter estimate  $\hat{\theta}_i$ . The application of this adaptation law results in the following inequality for the sum of the last two terms on the right side of (6.59)

$$r^T(t) P Y(t) \tilde{\theta}(t) + \dot{\tilde{\theta}}^T(t) \Gamma^{-1} \tilde{\theta}(t) \leq 0. \quad (6.61)$$

Considering (6.57) and (6.61), it can be shown that

$$\dot{V}(t) \leq -\frac{1}{2} r^T(t) Q r(t) < 0. \quad (6.62)$$

It can be concluded from (6.58) and (6.62) that  $r(t)$  is bounded, i.e.  $r(t) \in L_\infty$ . Moreover, by integrating (6.62) it can be shown that  $r(t) \in L_2$ .

*Theorem 6.2:* The parameter estimation vector  $\hat{\theta}(t)$  converges to a constant value as  $t \rightarrow \infty$ .

*Proof:* The proof is along the same lines as Theorem 2 in [113]. First it must be shown that

$$r^T(t) P Y(t) \tilde{\theta}(t) \in L_1. \quad (6.63)$$

This can be achieved by multiplying the dynamics of  $r(t)$  in (6.56) by  $r^T(t)P$  from left, integrating from 0 to  $t$ , and applying the boundedness of the Lyapunov function. Now consider the following derivative

$$\frac{d}{dt} \left( \frac{1}{2} \tilde{\theta}^T(t) \Gamma^{-1} \tilde{\theta}(t) \right) = \tilde{\theta}^T(t) \Gamma^{-1} \dot{\tilde{\theta}}(t). \quad (6.64)$$

Using the parameter adaptation law in (6.60), one can rewrite (6.64) as

$$\frac{d}{dt} \left( \frac{1}{2} \tilde{\theta}^T(t) \Gamma^{-1} \tilde{\theta}(t) \right) = \tilde{\theta}^T(t) Y^T(t) P^T r(t) \quad (6.65)$$

and therefore for any arbitrary bounded  $k$  the following can be obtained

$$\tilde{\theta}^T(t) \Gamma^{-1} \tilde{\theta}(t) = \tilde{\theta}^T(t-k) \Gamma^{-1} \tilde{\theta}(t-k) + 2 \int_{t-k}^t \tilde{\theta}^T(s) Y^T(s) P^T r(s) ds. \quad (6.66)$$

Given the fact that the operand of the integral in (6.66) is in  $L_1$  space as shown in (6.63), for any finite  $k$  the following can be concluded

$$\lim_{t \rightarrow \infty} \left( \tilde{\theta}^T(t) \Gamma^{-1} \tilde{\theta}(t) - \tilde{\theta}^T(t-k) \Gamma^{-1} \tilde{\theta}(t-k) \right) = 0, \quad (6.67)$$

and therefore  $\tilde{\theta}(t)$  converges to a constant value as  $t \rightarrow \infty$ .

*Theorem 6.3:* The error signal  $e(t)$  is bounded as a result of the boundedness of the signal  $r(t)$ .

*Proof:* To prove Theorem 6.3 the same steps as those in Lemma 4 of [113] should be

followed. The proof is based on the definition of  $r(t)$  in (6.55) and by showing that

$$\lim_{t \rightarrow \infty} w(t) = 0. \quad (6.68)$$

This is achieved by demonstrating the dynamics of  $w(t)$  in (6.54) to satisfy the following equation

$$\dot{w}(t) = \Upsilon w(t) + L(t) + v(t) \quad (6.69)$$

where the signals  $L(t)$  and  $v(t)$  satisfy

$$|L(t)| \leq p(t)|w_t| \quad (6.70)$$

and

$$\lim_{t \rightarrow \infty} p(t) = 0, \quad (6.71)$$

$$\lim_{t \rightarrow \infty} v(t) = 0. \quad (6.72)$$

The norm of  $w_t$  in (6.70) is defined as

$$|w_t| = \sup_{-d \leq s \leq 0} |w(t+s)| \quad (6.73)$$

Theorem 6.2 and the fact that the matrix  $\Upsilon$  is Hurwitz are employed to obtain (6.69)-(6.73). The reader is referred to [113] and the references within for the details of the proof.

*Lemma 6.1:* A linear time-varying system with the state transition matrix  $A(t)$  is stable if all the eigenvalues of  $A(t)$  always have negative real values and converge

to constant values as  $t \rightarrow \infty$ .

*Proof:* See [132].

Now consider the closed-loop dynamics in (6.42). The matrix  $\hat{A}_{T_{cl}}(t)$  as stated in Appendix F.2 satisfies all the conditions of Lemma 6.1. Using the boundedness of  $e(t)$  and the estimated parameters of the system from Theorems 6.3 and 6.2, respectively, it can be concluded that the dynamics equation in (6.42) represents a stable system with bounded inputs. Hence, the vector of the states,  $\hat{X}_T(t+d)$ , is bounded. The boundedness of  $\hat{X}(t+d)$  is concluded directly as a result of a non-singular transformation  $T$ .

The control action,  $u(t)$ , which is calculated using (6.38) depends only on  $\hat{X}(t+d)$  and  $e(t)$ . By applying Theorem 6.3 and the boundedness of  $\hat{X}(t+d)$ , it can be concluded that the control action is bounded. The boundedness of the states of the system,  $X(t)$ , can be shown as a result of the bounded inputs and the structure of the teleoperation system which essentially consists of two mass-spring-damper systems as stated in (4.20) and (4.23). As a result, the regressor matrix  $Y(t)$ , which comprises of system measurements and inputs, is bounded.

The second derivative of  $V(t)$  in (6.58) can be calculated as

$$\ddot{V} = -r^T(t)Q\dot{r}(t). \quad (6.74)$$

By substituting  $\dot{r}(t)$  from (6.56) one can write

$$\ddot{V} = -r^T(t)Q \left( \Upsilon r(t) + Y(t)\tilde{\theta}(t) \right). \quad (6.75)$$

Using the boundedness of  $r(t)$ ,  $Y(t)$  and  $\tilde{\theta}(t)$  it can be concluded that  $\ddot{V}$  is also bounded. Given the boundedness of  $\ddot{V}$  and (6.58) and by employing the Barbalat's Lemma [45] it can be proven that  $r(t)$  converges to zero. It is also straightforward to show the convergence of the signal  $e(t)$  to zero as a result of  $w(t)$  going to zero.

### 6.5.1 Output Regulation

Consider the definition of the outputs in (6.27) and (6.28). These outputs can be rewritten using the dynamics of  $\hat{X}(t+d)$  in (6.25) as

$$\begin{aligned}\hat{y}_1(t+d) &= \hat{X}_4(t+d) + \lambda\hat{X}_3(t+d) \\ &= \dot{\hat{X}}_3(t+d) + \lambda\hat{X}_3(t+d) - \hat{\Phi}_3(t+d, t)L(t)e(t),\end{aligned}\quad (6.76)$$

$$\begin{aligned}\hat{y}_2(t+d) &= \hat{X}_6(t+d) + \lambda\hat{X}_5(t+d) \\ &= \dot{\hat{X}}_5(t+d) + \lambda\hat{X}_5(t+d) - \hat{\Phi}_5(t+d, t)L(t)e(t).\end{aligned}\quad (6.77)$$

The closed-loop output dynamics in (6.41) guarantee the convergence of  $\hat{y}_1(t+d)$  and  $\hat{y}_2(t+d)$  to zero. Moreover since  $e(t)$  also converges to zero, it can be concluded that

$$\dot{\hat{X}}_3(t+d) + \lambda\hat{X}_3(t+d) \rightarrow 0, \quad (6.78)$$

$$\dot{\hat{X}}_5(t+d) + \lambda\hat{X}_5(t+d) \rightarrow 0 \quad (6.79)$$

and therefore

$$\hat{X}_3(t+d) \rightarrow 0, \quad (6.80)$$

$$\hat{X}_5(t+d) \rightarrow 0. \quad (6.81)$$

It should be noted that delay-free transparent response can only be achieved if the mapping between the current state of the system,  $X(t)$ , and the predicted state,  $\hat{X}(t+d)$ , is close to the actual mapping. The accuracy of this mapping directly depends on the accuracy of parameter estimation. Several methods are proposed in the following sections in order to enhance the parameter estimation performance. In addition, perfect transparency requires the user and environment parameters, including the user exogenous force to be constant. Changes in these parameters may generate a transient error which would be corrected by the controller. The decay rate of these transient errors can be increased by increasing the adaptation gains. However, these gains can not be increased indefinitely due to the effect of measurement noise and a finite sampling rate on system performance and stability.

## 6.6 Parameter Convergence and Composite Adaptive Control

As mentioned earlier, achieving perfect tracking in time-delay teleoperation requires the exact knowledge of the system parameters as well as the exogenous inputs to the system. The tracking errors can be made smaller by increasing the gain  $\lambda$  in (6.27) and (6.28). The parameter adaptation speed can also be increased

by increasing the gain  $\Gamma$  in (6.60). Although increasing these gains decrease the bounds on the tracking errors, in practice noise amplification and instability due to limited sampling rate limit these gains. As shown in Theorem 6.2 the parameter estimates converge to constant values. However, these values may be different from the actual system parameters. To converge to actual parameter values the input signal requires to satisfy a certain condition, often referred to as *persistence of excitation* in the adaptive control literature.

Consider the dynamics equation in (6.56). As proved in the last section, the signal  $r(t)$  approaches zero as  $t \rightarrow \infty$ . As a result the last term on the right hand side of (6.56) goes to zero, i.e.

$$Y(t)\tilde{\theta}(t) \rightarrow 0. \quad (6.82)$$

This however does not ensure that the parameter estimation error,  $\tilde{\theta}(t)$ , converges to zero. The persistency of excitation condition [45] guarantees the convergence of the parameter estimation errors to zero as  $t \rightarrow \infty$ . The details of this condition and its proof are given in Appendix G.

### 6.6.1 Composite Adaptive Control

The parameter adaptation law in (6.60) utilizes the tracking error signal  $r(t)$  to estimate the system parameters. However, this is not the only source of information available on the parameters. The hand and environment forces also contain valuable information on the parameters which can be used in parameter estimation. A composite adaptation scheme will be utilized to use this extra source of information in parameter adaptation. The application of the composite adaptive scheme will result in a faster and more accurate parameter adaptation and consequently

smaller tracking errors.

Consider the linear second-order operator hand dynamics in (4.19). The error between the actual and the estimated hand force can be written as

$$e_h(t) = f_h(t) - \hat{f}_h(t) \quad (6.83)$$

where

$$f_h(t) = f_h^* - m_h \ddot{x}_m(t) - b_h \dot{x}_m(t) - k_h x_m(t), \quad (6.84)$$

$$\hat{f}_h(t) = \hat{f}_h^* - \hat{m}_h \ddot{x}_m(t) - \hat{b}_h \dot{x}_m(t) - \hat{k}_h x_m(t). \quad (6.85)$$

To avoid the acceleration terms, filtered actual and estimated hand forces are being used where the forces are passed through a first-order filter. The filtered error between the actual and the estimated hand force can be calculated as

$$\bar{e}_h(t) = \bar{f}_h(t) - \bar{\hat{f}}_h(t) \quad (6.86)$$

where

$$\bar{f}_h(t) = f_h^* - m_h \bar{\ddot{x}}_m(t) - b_h \bar{\dot{x}}_m(t) - k_h \bar{x}_m(t), \quad (6.87)$$

$$\bar{\hat{f}}_h(t) = \hat{f}_h^* - \hat{m}_h \bar{\ddot{x}}_m(t) - \hat{b}_h \bar{\dot{x}}_m(t) - \hat{k}_h \bar{x}_m(t). \quad (6.88)$$

The filtered error  $\bar{e}_h$  in (6.86) can be written in the following linear-in-parameter

form

$$\bar{e}_h(t) = \begin{pmatrix} 1 & -\bar{x}_m(t) & -\bar{x}_m(t) & -\bar{x}_m(t) \end{pmatrix} \begin{pmatrix} \tilde{f}_h^* \\ \tilde{m}_h \\ \tilde{b}_h \\ \tilde{k}_h \end{pmatrix} = Y_h(t)\tilde{\theta}_h(t) \quad (6.89)$$

where *tilde* variables again represent the error between the actual and the estimated parameters. Let the vector of hand parameters,  $\theta_h$ , be written as a function of the full vector of the system parameters,  $\theta$ , as

$$\theta_h = f_h(\theta). \quad (6.90)$$

Note that  $f_h(\theta)$  is nonlinear since the elements of the system parameters vector,  $\theta$ , are nonlinear combinations of hand/environment parameters. This function is presented in Appendix H and can be linearized around the estimated parameters as

$$f_h(\theta) = f_h(\hat{\theta}(t)) + \frac{\partial f_h}{\partial \theta} \Big|_{\theta=\hat{\theta}(t)} (\theta - \hat{\theta}(t)) + \dots \quad (6.91)$$

By ignoring the high order terms, (6.91) can be approximated as

$$\tilde{\theta}_h(t) \simeq J_h(t)\tilde{\theta}(t) \quad (6.92)$$

where

$$J_h(t) = \frac{\partial f_h}{\partial \theta} \Big|_{\theta=\hat{\theta}(t)} \quad (6.93)$$

is given in Appendix H. Now from (6.89) and (6.92) the following can be derived

$$\bar{e}_h(t) \simeq Y_h(t)J_h(t)\tilde{\theta}(t). \quad (6.94)$$

The same calculations can be performed for the error between the actual and the estimated environment forces. Assuming a zero environment mass, one can write

$$e_e(t) = f_e(t) - \hat{f}_e(t) \quad (6.95)$$

where

$$f_e(t) = b_e\dot{x}_s(t) + k_ex_s(t), \quad (6.96)$$

$$\hat{f}_e(t) = \hat{b}_e\dot{x}_s(t) + \hat{k}_ex_s(t). \quad (6.97)$$

The error  $e_e(t)$  in (6.95) can be expressed in the following linear-in-parameter form

$$e_e(t) = \begin{pmatrix} \dot{x}_s(t) & x_s(t) \end{pmatrix} \begin{pmatrix} \tilde{b}_e(t) \\ \tilde{k}_e(t) \end{pmatrix} = Y_e(t)\tilde{\theta}_e(t). \quad (6.98)$$

Using the similar calculations as in (6.90)-(6.93), the following can be obtained

$$e_e(t) \simeq Y_e(t)J_e(t)\tilde{\theta}(t) \quad (6.99)$$

where  $J_e(t)$  is given in Appendix H.

The composite parameter adaptation law can be derived by modifying the

adaptation law in (6.60) and by utilizing  $\bar{e}_h(t)$  and  $e_e(t)$  as

$$\dot{\hat{\theta}}(t) = \Gamma^T [Y^T(t)P^T r(t) + c_h J_h^T(t)Y_h^T(t)\bar{e}_h(t) + c_e J_e^T(t)Y_e^T(t)e_e(t)] \quad (6.100)$$

where  $c_h > 0$  and  $c_e > 0$  are the composite adaptation gains. These gains can be used to increase or decrease the contribution of the hand and environment forces estimation errors.

The next step is to show the stability of the system after utilizing the composite adaptive scheme. Consider again the derivative of the Lyapunov function in (6.59). Replacing  $\dot{\hat{\theta}}(t)$  from (6.100) results in

$$\begin{aligned} \dot{V}(t) = & \frac{1}{2}r^T(t) (\Upsilon^T P + P\Upsilon) r(t) + r^T(t)PY(t)\tilde{\theta}(t) \\ & - (Y^T(t)P^T r(t) + c_h J_h^T(t)\bar{Y}_h^T(t)\bar{e}_h(t) + c_e J_e^T(t)Y_e^T(t)e_e(t))^T \tilde{\theta}(t) \end{aligned} \quad (6.101)$$

Using (6.57), this can be rewritten as

$$\dot{V}(t) = -\frac{1}{2}r^T(t)Qr(t) - (c_h J_h^T(t)\bar{Y}_h^T(t)\bar{e}_h(t) + c_e J_e^T(t)Y_e^T(t)e_e(t))^T \tilde{\theta}(t) \quad (6.102)$$

After substituting  $\bar{e}_h(t)$  and  $e_e(t)$  from (6.94) and (6.99), one can write

$$\begin{aligned} \dot{V}(t) = & -\frac{1}{2}r^T(t)Qr(t) \\ & - \tilde{\theta}^T(t) (c_h J_h^T(t)\bar{Y}_h^T(t)\bar{Y}_h(t)J_h(t) + c_e J_e^T(t)Y_e^T(t)Y_e(t)J_e(t)) \tilde{\theta}(t) \end{aligned} \quad (6.103)$$

Given that  $Q > 0$  and  $c_h$  and  $c_e$  are positive scalars it can be concluded that

$$\dot{V}(t) < 0 \quad (6.104)$$

Hence the composite adaptation law stated in (6.100) stabilizes the time-delay teleoperation system. It can also be shown that the signal  $r(t)$ , the parameter estimate errors,  $\tilde{\theta}(t)$ , as well as the system states,  $X(t)$ , are bounded. As a result, the second derivative of the Lyapunov function,  $\ddot{V}(t)$ , will be bounded and employing the Barbalat's Lemma proves that  $\dot{V}(t)$  goes to zero. From (6.103), it can then be concluded that  $r(t)$  and  $\tilde{\theta}(t)$  converge to zero as  $t \rightarrow \infty$ . In other words the parameter estimates will converge to their actual values. It is important to mention that if the approximations in (6.94) and (6.99) are not accurate, i.e. the initial values of the parameter estimates are far off the actual values, the parameter estimates can potentially converge to values different than the actual parameters of the system.

## 6.7 Adaptive Control of Teleoperation with Time-varying Delay

In the case of time-varying latencies, the dynamics of the teleoperation system can be written in the following form

$$\dot{X}(t) = AX(t) + Bu(t - d(t)) + B_{f_h^*} f_h^*. \quad (6.105)$$

For notational convenience, the argument of the control action in (6.105) is defined as

$$m(t) \triangleq t - d(t). \quad (6.106)$$

It is assumed that the argument is always increasing by time, i.e.

$$\dot{m}(t) = 1 - \dot{d}(t) > 0 \quad (6.107)$$

which leads to the following constraint on the time-varying time delay  $d(t)$

$$\dot{d}(t) < 1. \quad (6.108)$$

Finally the inverse of  $m(\cdot)$ , which is also a function itself, is defined as

$$q(m(t)) = t. \quad (6.109)$$

For the teleoperation system with time-varying delay as shown in (6.105), the delay-reduced state is defined as

$$\hat{Z}(t) = \bar{X}(t) + \int_{m(t)}^t \hat{\Phi}(t, q(s)) \frac{\partial q(s)}{\partial s} \hat{B}(s) u(s) ds + \int_{m(t)}^t \hat{\Phi}(t, q(s)) \frac{\partial q(s)}{\partial s} \hat{B} f_h^*(s) ds \quad (6.110)$$

where  $m(\cdot)$  and  $q(\cdot)$  have been defined in (6.106) and (6.109) and  $\bar{X}$  is the state of an observer with the following dynamics

$$\dot{\bar{X}}(t) = \hat{A}(m(t))\bar{X}(t) + \hat{q}(m(t))\hat{B}(m(t))u(m(t)) + \hat{q}(m(t))\hat{B}f_h^*(m(t)) + L(t)e(t) \quad (6.111)$$

where  $e(t)$  is defined in (6.8). Note that

$$\dot{q}(m(t)) = \left. \frac{dq(s)}{ds} \right|_{s=m(t)} \quad (6.112)$$

is different than  $\frac{d}{dt} \{q(m(t))\}$  which is equal to one according to (6.109).

The dynamics of the reduced system can be calculated by taking the derivative of (6.110) as

$$\begin{aligned} \dot{\hat{Z}}(t) = & \dot{\hat{X}}(t) + \hat{\Phi}(t, q(t))\dot{q}(t)\hat{B}(t)u(t) + \hat{\Phi}(t, q(t))\dot{q}(t)B\hat{f}_h^*(t) \\ & - \dot{q}(m(t))\hat{B}(m(t))u(m(t)) - \dot{q}(m(t))B\hat{f}_h^*(m(t)) \\ & + \int_{m(t)}^t \frac{\partial}{\partial t} \hat{\Phi}(t, q(s)) \frac{\partial q(s)}{\partial s} \hat{B}(s)u(s)ds + \int_{m(t)}^t \frac{\partial}{\partial t} \hat{\Phi}(t, q(s)) \frac{\partial q(s)}{\partial s} B\hat{f}_h^*(s)ds. \end{aligned} \quad (6.113)$$

Similar to (6.12), the estimated system transition matrix in the case of a time-varying delay satisfies

$$\frac{\partial \hat{\Phi}(t, s)}{\partial t} = \hat{A}(m(t))\hat{\Phi}(t, s) \quad , \quad \hat{\Phi}(s, s) = I \quad (6.114)$$

Using (6.110) and (6.114), the dynamics of the reduced state can be written as

$$\begin{aligned} \dot{\hat{Z}}(t) = & \dot{\hat{X}}(t) + \hat{\Phi}(t, q(t))\dot{q}(t)\hat{B}(t)u(t) + \hat{\Phi}(t, q(t))\dot{q}(t)B\hat{f}_h^*(t) \\ & - \dot{q}(m(t))\hat{B}(m(t))u(m(t)) - \dot{q}(m(t))B\hat{f}_h^*(m(t)) \\ & + \hat{A}(m(t)) \left( \hat{Z}(t) - \hat{X}(t) \right). \end{aligned} \quad (6.115)$$

By substituting  $\dot{\hat{X}}$  from (6.111), one can write

$$\dot{\hat{Z}}(t) = \hat{A}(m(t))\hat{Z}(t) + \hat{\Phi}(t, q(t))\dot{q}(t)\hat{B}(t)u(t) + \hat{\Phi}(t, q(t))\dot{q}(t)\hat{B}f_h^*(t) + L(t)e(t) \quad (6.116)$$

The predicted state of the system is defined as

$$\hat{X}(q(t)) \triangleq \hat{\Phi}(q(t), t)\hat{Z}(t). \quad (6.117)$$

Using this definition, the dynamics of the predicted state can be calculated using

$$\dot{\hat{X}}(q(t)) = \dot{\hat{\Phi}}(q(t), t)\hat{Z}(t) + \hat{\Phi}(q(t), t)\dot{\hat{Z}}(t). \quad (6.118)$$

Following the similar steps as in (6.17)-(6.22), one can write

$$\dot{\hat{\Phi}}(q(t), t) = \dot{q}(t)\hat{A}(t)\hat{\Phi}(q(t), t) - \hat{\Phi}(q(t), t)\hat{A}(m(t)). \quad (6.119)$$

Using (6.118), (6.119) and (6.116), the dynamics of the predicted state can be written as

$$\begin{aligned} \dot{\hat{X}}(q(t)) = & \left( \dot{q}(t)\hat{A}(t)\hat{\Phi}(q(t), t) - \hat{\Phi}(q(t), t)\hat{A}(m(t)) \right) \hat{Z}(t) \\ & + \hat{\Phi}(q(t), t) \left( \hat{A}(m(t))\hat{Z}(t) + \hat{\Phi}(t, q(t))\dot{q}(t)\hat{B}(t)u(t) \right. \\ & \left. + \hat{\Phi}(t, q(t))\dot{q}(t)\hat{B}f_h^*(t) + L(t)e(t) \right). \quad (6.120) \end{aligned}$$

Simplifying this equation and using (6.117) result in the following dynamics

$$\dot{\hat{X}}(q(t)) = \dot{q}(t)\hat{A}(t)\hat{X}(q(t)) + \dot{q}(t)\hat{B}(t)u(t) + \dot{q}(t)\hat{B}f_h^*(t) + \hat{\Phi}(q(t), t)L(t)e(t). \quad (6.121)$$

Again new outputs are defined based on the predicted state of the system as follows

$$\hat{y}_1(q(t)) \triangleq \hat{X}_4(q(t)) + \lambda \hat{X}_3(q(t)) \quad (6.122)$$

$$\hat{y}_2(q(t)) \triangleq \hat{X}_6(q(t)) + \lambda \hat{X}_5(q(t)) \quad (6.123)$$

where  $\lambda > 0$  is a scalar. The predicted state of the system is transformed using the same transformation as in (6.29). The dynamics of the transformed state,  $\hat{X}_T(q(t))$ , can be calculated as

$$\dot{\hat{X}}_T(q(t)) = \dot{q}(t)\hat{A}_T(t)\hat{X}_T(q(t)) + \dot{q}(t)\hat{B}_T(t)u(t) + \dot{q}(t)\hat{B}_T f_h^*(t) + T\hat{\Phi}(q(t), t)L(t)e(t). \quad (6.124)$$

where  $\hat{A}_T(t)$ ,  $\hat{B}_T(t)$  and  $\hat{B}_T f_h^*(t)$  have exactly the same structure as those shown in (6.34)-(6.37).

Consider the following control action

$$u(t) = \hat{B}_y^{-1}(t) \left( \frac{1}{\dot{q}(t)} \Omega \hat{y}(q(t)) - \hat{A}_1(t)\hat{X}_{T1}(q(t)) - \hat{A}_2(t)\hat{X}_{T2}(q(t)) - \hat{A}_3(t)\hat{X}_{T3}(q(t)) - B\hat{f}_{hy}^*(t) - \frac{1}{\dot{q}(t)} T_3 \hat{\Phi}(q(t), t)L(t)e(t) \right) \quad (6.125)$$

where  $\Omega$  is defined in (6.39). Substituting (6.125) into (6.124) results in the following output dynamics

$$\dot{\hat{y}}(q(t)) = \Omega \hat{y}(q(t)). \quad (6.126)$$

Moreover, the closed-loop dynamics of the transformed state in (6.124) can be written as

$$\dot{\hat{X}}_T(q(t)) = \dot{q}(t)\hat{A}_{T_{cl}}(t)\hat{X}_T(q(t)) + \dot{q}(t)\hat{B}f_{h_{cl}}^*(t) + T_{cl}(t)\hat{\Phi}(q(t), t)L(t)e(t) \quad (6.127)$$

where  $\hat{A}_{T_{cl}}(t)$ ,  $\hat{B}f_{h_{cl}}^*(t)$  and  $T_{cl}(t)$  are given in (6.43)-(6.45).

The dynamics of the state observation error can be obtained using (6.8), (6.105) and (6.111) as

$$\dot{e}(t) = \left(\hat{A}(m(t)) - L(t)\right)e(t) + \tilde{A}(m(t))X(t) + \tilde{B}(m(t))u(m(t)) + \tilde{B}f_h^*(m(t)) \quad (6.128)$$

where the *tilde* variables represent the error between the actual and the estimated value of the corresponding variables. Choosing the gain  $L(t)$  as

$$L(t) = \hat{A}(m(t)) - \Upsilon \quad (6.129)$$

where  $\Upsilon < 0$  is a constant matrix results in the following observation error dynamics

$$\dot{e}(t) = \Upsilon e(t) + \tilde{A}(m(t))X(t) + \tilde{B}(m(t))u(m(t)) + \tilde{B}f_h^*(m(t)). \quad (6.130)$$

These dynamics can be rewritten in linear-in-parameter form as

$$\dot{e}(t) = \Upsilon e(t) + Y(t)\tilde{\theta}(m(t)) \quad (6.131)$$

Similar to (6.54) and to remove the delay from the observation error dynamics

in (6.134), a new signal  $w(t)$  with the following dynamics is defined

$$\dot{w}(t) = \Upsilon w(t) - Y(t)\hat{\theta}(t) + Y(t)\hat{\theta}(m(t)). \quad (6.132)$$

The signal  $w(t)$  will be added to the error signal  $e(t)$  resulting in the definition of a new variable  $r(t)$

$$r(t) \triangleq e(t) + w(t) \quad (6.133)$$

with the following dynamics

$$\dot{r}(t) = \Upsilon r(t) + Y(t)\tilde{\theta}(t) \quad (6.134)$$

These dynamics are exactly the same as those in (6.56). Hence the same Lyapunov function can be utilized to prove the stability of the system and to derive the parameter adaptation law. These steps will not be repeated here in the interest of space.

In case where the delay is constant,  $d(t) = d$ , the controller for the variable delay will reduce to the one proposed for the constant delay case. For a constant delay, one can write

$$m(t) = t - d, \quad (6.135)$$

$$q(t) = t + d, \quad (6.136)$$

and therefore

$$\dot{q}(t) = \dot{q}(m(t)) = 1. \quad (6.137)$$

### 6.7.1 Practical Implementation Issues for the Time-varying Controller in Packet Switched Networks

In the proposed controller for teleoperation with time-varying delay, it is assumed that a model of time delay is available in the form of  $m(t)$  in (6.106), satisfying the condition in (6.108). In practice, such model can be constructed numerically from a real-time measurement of the round-trip delay. However, potential problems can arise in a discrete-time implementation of the controller over a packet switched network communication channel such as the Internet.

When the communication channel packet rate is similar to the sampling rate at the receiving side and the delay is increasing, there will be a train of samples with equal delay followed by one or more black-out samples. This is illustrated in Fig. 6.2(a) where  $P_1$  represents the black-out period. During these black-out samples the latest received data packet could be used for control. However, the rate of change of the delay,  $\dot{d}(t)$ , would be zero (delay is constant) for several samples and it would be one for the black-out samples. This results in  $\dot{q}(t)$  being zero and infinity, reflectively, which can cause problems in calculating the control action. This issue can be partially remedied by having a faster sampling rate at the receiving end than the packet rate of the channel as shown in Fig. 6.2(a). In this case, an estimation of  $\dot{q}(t)$  can be calculated since the packet arrival time is available to the controller with a higher resolution. Note that such an assumption is indeed practical since the channel packet rate is often slower than the local controller sampling rate.

In case where the delay is decreasing multiple packets may arrive within one sample time in which case all but the most recent packet may be discarded. This

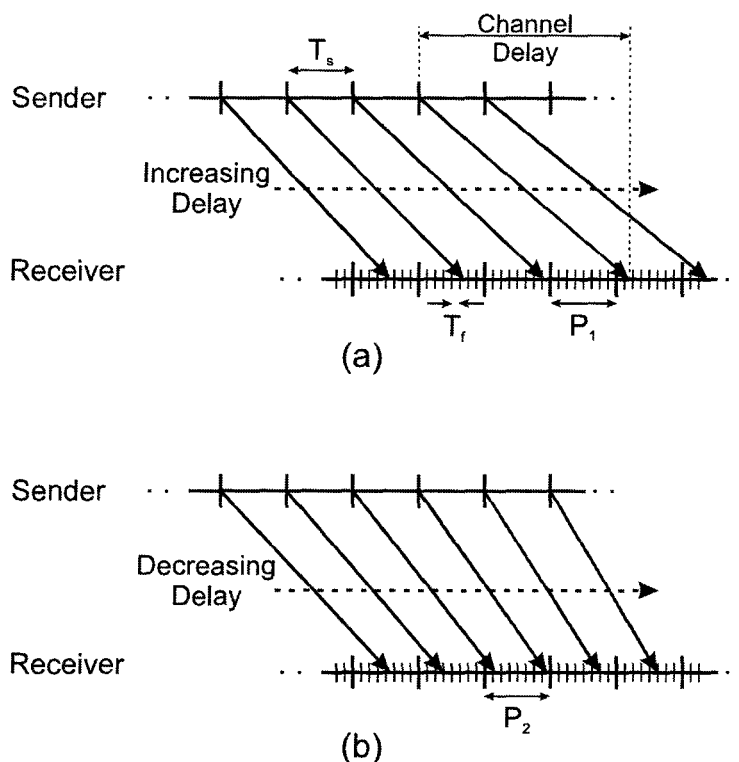


Figure 6.2: Communication over a packet switched network with (a) increasing delay and (b) decreasing delay.

case is illustrated in Fig. 6.2(b) where  $P_2$  represents the period with more than one received packets. Again, if similar sampling and packet rates are being employed the model of the delay can not be constructed properly. Running the receiving end model with faster sampling rate as shown in Fig. 6.2(b) can solve the problem by enabling the controller to calculate an estimate of  $\dot{q}(t)$  using the available information on packets arrival time.

Fig. 6.3 demonstrates how the proposed multi-rate solution can be implemented in the case of our adaptive centralized control for time-delay teleoperation. As shown in this figure, the control action calculations as well as the master/slave

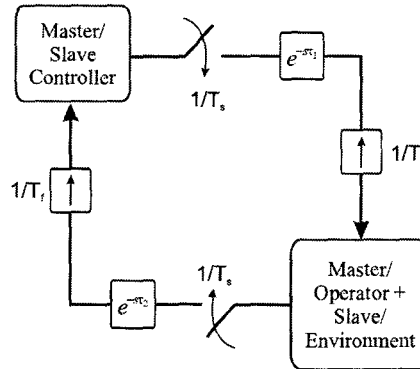


Figure 6.3: Control action and master/slave devices running with a faster sampling rate than the communication packet transmission rate.

devices are operating with a higher sampling rate  $\frac{1}{T_f}$ , while the communication channel is running at a slower rate  $\frac{1}{T_s}$ .

## 6.8 Experimental Results

Fig. 6.4 shows the schematic of the proposed adaptive predictive controller for a general teleoperation system with time-varying delay. Assuming the centralized controller resides at the master side, the slave control action and measurements are subject to time-varying delays of  $\tau_1(t)$  and  $\tau_2(t)$  seconds. As mentioned previously, the proposed adaptive control framework requires equal amount of latencies in input channels and output channels. To accommodate for this, master control action and measurements should be padded with  $\tau_1(t)$  and  $\tau_2(t)$  seconds of delay, respectively.

The virtual tool position and velocity are generated using delayed hand and environment force signals. These synthesized observations, along with the actual observations, enter the model-based predictive controller block at the master site

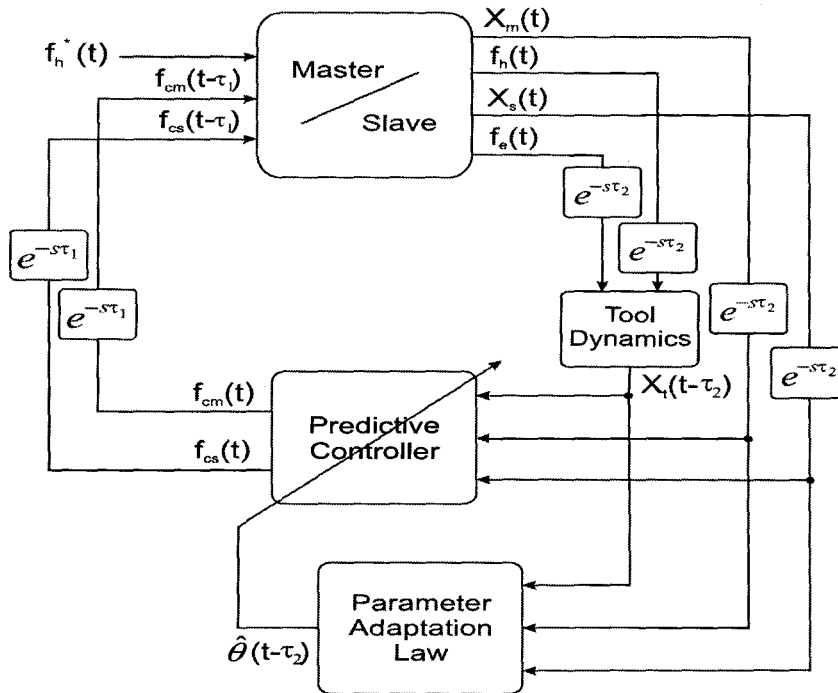


Figure 6.4: Time-delay teleoperation system with the proposed adaptive predictive controller

which produces the control signals. Estimated model of the system is updated using the measurements and by applying the parameter adaptation law.

To verify the effectiveness of the proposed control method, the same experimental setup as in Fig. 4.9 is utilized here. This setup consists of two three-DOF manipulators equipped with force sensors. The controller code is implemented using *Matlab/Simulink* environment and runs in real-time on a PC platform using *Quanser's WinCon* software. The controller runs with a sampling rate of 1000 Hz, which is high enough in teleoperation applications to achieve a valid discrete-time approximation of the continuous-time controller. It is important to mention that the experiments are not performed on a packet-switched network in order to avoid

the practical issues with such a network in the time-varying case as stated in 6.7.1. The parameters of the adaptive predictive controller are given in Table 6.1. Note that the composite adaptive controller proposed in 6.6.1 is utilized in the experiments with the parameters stated in Table 6.1.

In the experiments, the operator manipulates the slave robot in free motion and in contact with an unknown environment. The experiments are conducted for three different constant values of round-trip delay, i.e. 50 msec, 100 msec, and 200 msec as well as two time-varying delays, i.e.  $d(t) = 0.1 - 0.1 \cos(\pi t/10)$  and  $d(t) = 0.1 - 0.05 \cos(\pi t/5)$ . The time-varying delays satisfy the condition in (6.108). These delays are emulated by adding data buffers of appropriate size that store and delay the measurement and control signals.

### 6.8.1 Adaptive controller with 50 ms delay

Fig. 6.5 illustrates the responses of the proposed controller along a single axis with 50 msec time-delay. At  $t \simeq 4$ sec the operator starts moving the master/slave devices in free motion. As evident by the non-zero hand force in free motion portions of the response in Fig. 6.5(b), the operator feels the dynamics of the virtual tool in free motion. The positions of master, slave, and virtual tool closely follow each other which confirms that the performance objectives in (3.24) and (3.25) are both

Controller Parameters		
$P = \text{diag}(10, 10, 10, 10, 10, 10)$ ,	$\Upsilon = \text{diag}(-50, -50, -50, -50, -50, -50)$	
$\Omega = \text{diag}(-50, -50)$ ,	$\lambda_1 = \lambda_2 = 10$ ,	$c_h = c_e = 0.5$
$\Gamma = (1e3, 1e3, 1e2, 1e2)$		

Table 6.1: Adaptive predictive controller parameters.

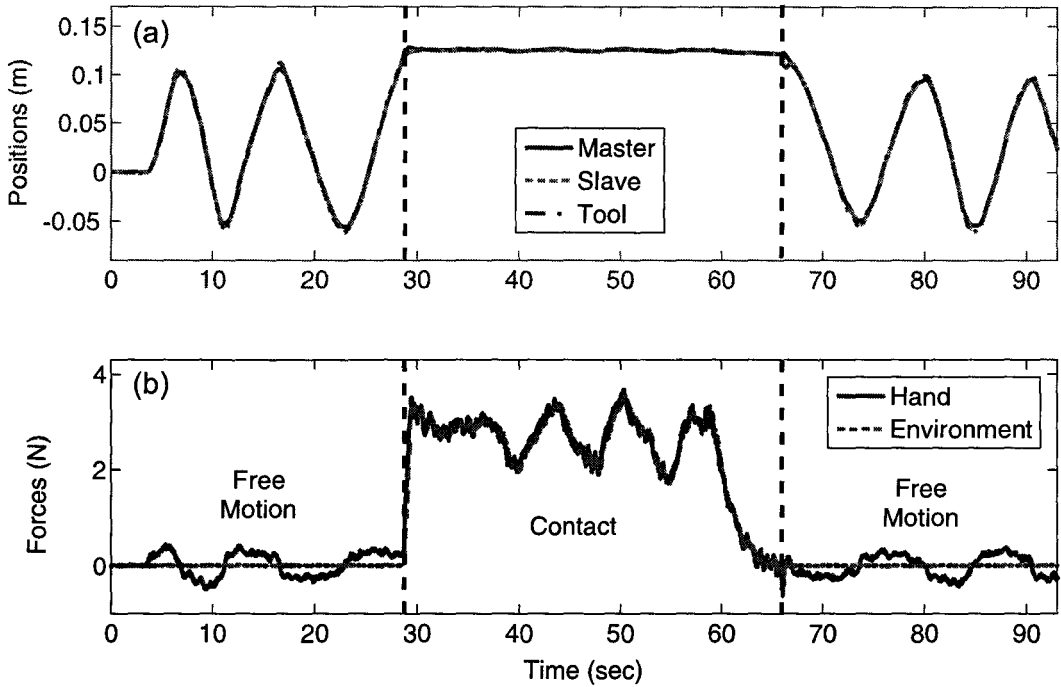


Figure 6.5: Model-based adaptive controller with 50 msec delay in experiment: (a) position tracking and (b) force tracking.

achieved with very high precision. At around  $t = 28$ sec, the slave contacts with the unknown environment after which the adaptive controller adapts to this change in system parameters. During the course of contact, the environment and hand forces as well as the master and slave positions closely track each other as shown in Fig. 6.5. This demonstrates that the tracking objectives in (3.24) and (3.25) are accurately achieved throughout the contact. The changes in the hand and environment forces while in contact are made deliberately by the operator to demonstrate the performance of the controller. At  $t \approx 66$  sec, the operator withdraws the master which returns the master/slave system to free motion.

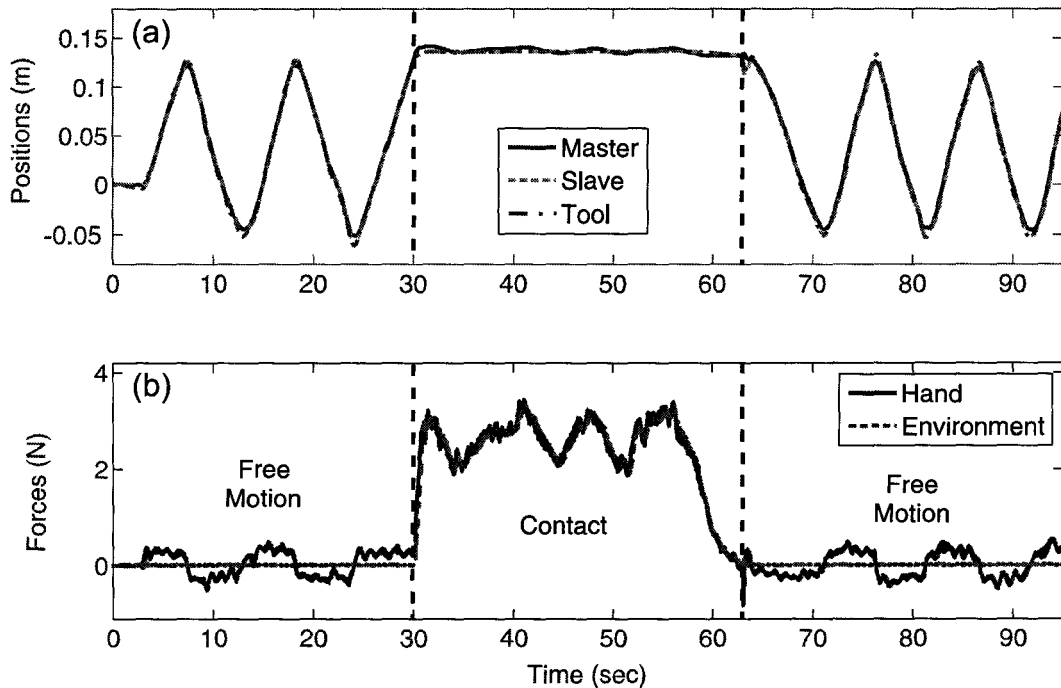


Figure 6.6: Model-based adaptive controller with 100 msec delay in experiment: (a) position tracking and (b) force tracking.

## 6.8.2 Adaptive controller with 100 ms delay

Fig. 6.6 demonstrates the responses of the adaptive controller for a round-trip delay of 100 msec. Similar to the previous case, the operator begins the experiment while the master and slave devices are at rest. He/she then moves the system in free motion and subsequently brings it to the contact with an unknown environment. Again, the adaptive controller adapts to changes in the system parameters as the master/slave transit from free motion to contact phases and vice versa. As illustrated in Fig. 6.6, the position tracking in free motion and contact as well as the force tracking in contact are quite satisfactory.

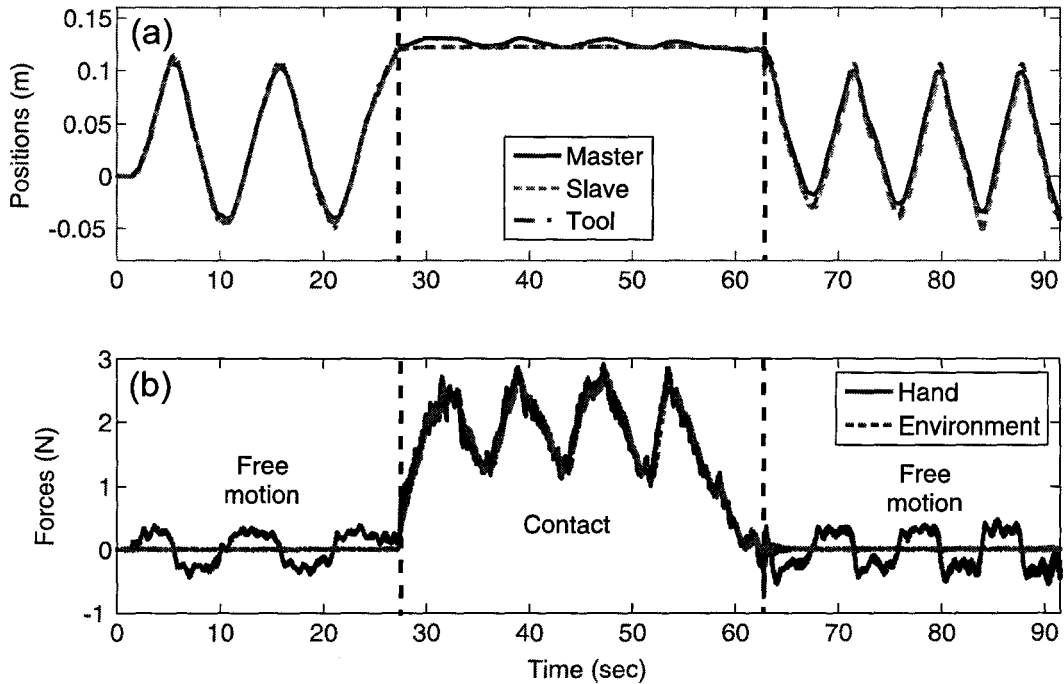


Figure 6.7: Model-based adaptive controller with 200 msec delay in experiment: (a) position tracking and (b) force tracking.

### 6.8.3 Adaptive controller with 200 ms delay

The results of the experiment using the proposed adaptive controller under 200 msec of communication latency are given in Fig. 6.7. Despite a slight degradation in performance, the position and force tracking in free motion and in contact with an unknown environment are still satisfactory. Note that such a degradation is expected as the round-trip delay grows larger. This is due to the fact that the controller utilizes the system parameter estimates to predict the future state of the system. Hence, a slight error in these estimations can potentially cause greater tracking errors if the delay is longer.

#### 6.8.4 Adaptive controller with time-varying delay

The experiments are repeated for two cases of time-varying delay. These delays are calculated from the following equations

$$d_1(t) = 0.1 - 0.1 \cos(\pi t/10), \quad (6.138)$$

$$d_2(t) = 0.1 - 0.05 \cos(\pi t/5). \quad (6.139)$$

The second delay,  $d_2(t)$ , has a smaller range comparing to the first one but it changes more rapidly. Similar to the cases with constant delay, the operator moves the master/slave system in free motion and in contact with an unknown environment. Figs. 6.8 and 6.9 show the experimental results for the two cases of varying time-delay. As is evident in these figures, the adaptive controller performs very well in case of time-varying delay. Master, slave and virtual tool position tracking in free motion as well as hand and environment force tracking in contact with the environment are all achieved with a high level of accuracy using the proposed adaptive predictive controller. Also the transitions between the free motion and contact phases are smooth and stable. The experiments with time-varying delays were also repeated where the adaptive controller was designed for a constant time delay. Delay values of 20, 100 and 200 msec were employed. The results showed that the constant delay controller would become unstable if the actual delay is time varying.

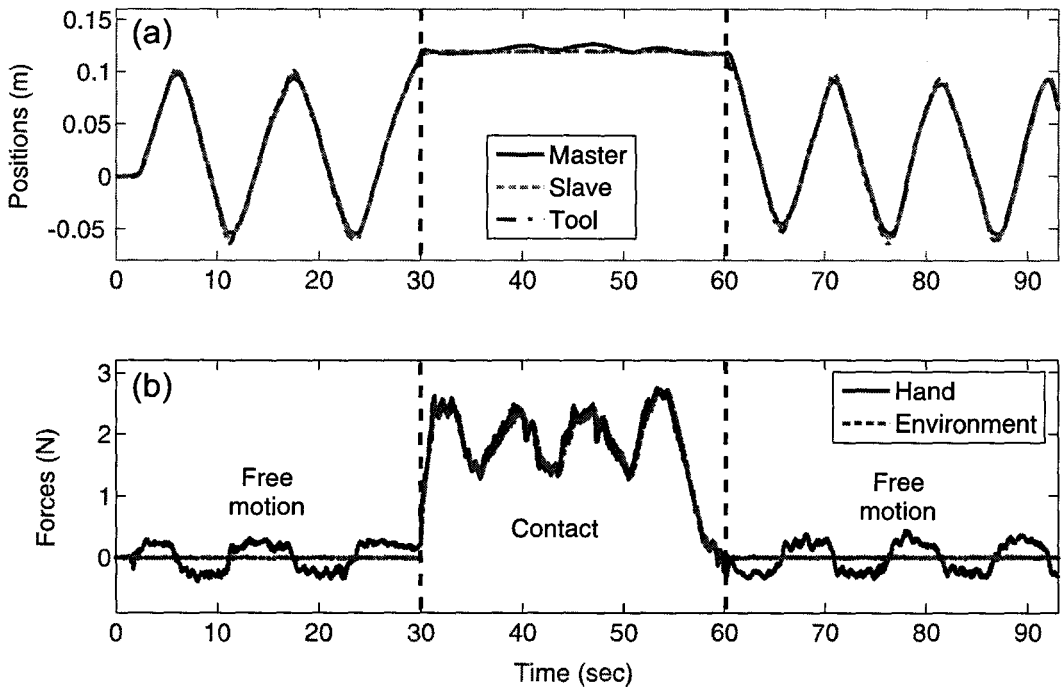


Figure 6.8: The model-based adaptive controller with time-varying delay in (6.138): (a) position tracking and (b) force tracking.

## 6.9 Conclusion

In this chapter, a provably stable adaptive model-based predictive controller was proposed for constant and variable time-delay teleoperation. The controller uses available information about system model and time delay to improve the transparency of teleoperation while maintaining its stability. A delay reduction method was developed that utilizes estimated model parameters and an auxiliary state observer. The teleoperation performance objectives, i.e. non-delayed virtual tool impedance shaping and position tracking were achieved within an output-regulation control framework and using the delay-reduced dynamics. The stability of the system was proven using a Lyapunov analysis which also generated the parameters

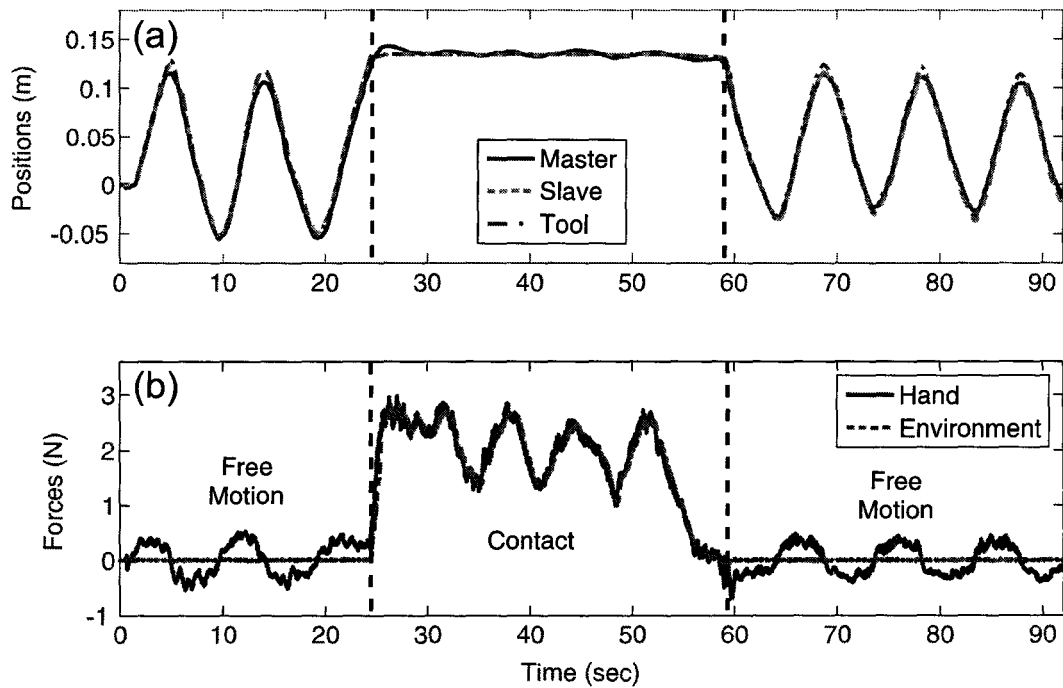


Figure 6.9: The model-based adaptive controller with time-varying delay in (6.139): (a) position tracking and (b) force tracking.

adaptation law. The effectiveness of the proposed controller was demonstrated in the experiments for both constant and time-varying delays.

# Chapter 7

## Conclusions and Future Work

### 7.1 Conclusions

Time delay in communication channel and dynamic uncertainty are major barriers to achieving transparency and robust stability in bilateral teleoperation. Most existing teleoperation control techniques sacrifice transparency objectives in order to gain robust stability in the presence of system uncertainty and communication delay. The central idea of this thesis was to utilize available system model and delay information in the controller in order to improve the stability-performance trade-off in time-delay bilateral teleoperation. To this end, three new model-based controllers were proposed and experimentally evaluated. These controllers were designed to employ position and force measurements at both the master and slave sites.

### 7.1.1 Model-based Decentralized Controller

First, a model-based decentralized controller was introduced that improved upon our earlier work on model-based time-delay teleoperation in [2]. In this controller, master and slave measurements are used locally in the control of their respective robots hence eliminating an extra delay from the loop that existed in the controller of [2]. Teleoperation control was formulated as an output-feedback state-space control problem incorporating performance objectives such as non-delayed virtual tool impedance shaping, position tracking, and force tracking. To enable the application of a decentralized control scheme, two output-delayed subsystems at the master and slave site were considered in which local measurements are delay-free whereas remote measurements are delayed. The application of a delay reduction method and LQG-based sub-controllers to the reduced dynamics at the master and slave sites resulted in a closed-loop dynamics with a state-delay perturbation term. A delay-dependent frequency sweeping test was employed to analyze the stability of these dynamics. Extensive robust stability and performance analysis demonstrated that, using the same set of design parameters, the new decentralized controller can provide enhanced performance and increased stability margins when compared with its centralized counterpart in [2]. Experimental studies with a single-axis teleoperation system also showed that the proposed approach is effective in improving teleoperation transparency under communication time delay.

### 7.1.2 Robust Controller

Mode-based predictive controllers can utilize the system model and the delay information to improve the transparency in time-delay bilateral teleoperation. However uncertainty in the system dynamics, particularly variations in the user and environment dynamics can affect the robustness of such controllers. The use of a multi-model control approach in the previous method proved effective in handling uncertainties in the environment dynamics. Nevertheless, it is difficult to guarantee the stability of such switching control strategy. Also, the number of modes must increase if contact with a wide range of environments is considered which further complicates the controller/switching strategy.

The second controller proposed in this thesis was a robust controller for time-delay teleoperation. Through the use of local Lyapunov-based adaptive controllers, the dynamics of the master and slave robots were linearized and rendered independent from their parameters. However, uncertainty still existed in the form of unknown linear operator and environment dynamics. Using the linearized dynamics, teleoperation control for achieving transparency and robust stability was formulated as an  $H_\infty$  robust control synthesis with multiple I/O delays. The resulting problem was solved using decompositions into single-delay adobe-type problems. The interaction between the local adaptive/nonlinear controllers and the robust controller was fully accounted for in the proposed modeling and control synthesis.

The proposed approach explicitly incorporates information about model, delay, and uncertainty into the design process and allows the designer to balance

transparency against robust stability through the selection of a set of design filters. Due to the use of local adaptive nonlinear controllers, modeling uncertainty only appears in the form of perturbations in the user and environment parameters. The ability to systematically optimize performance and stability trade-off in time-delay teleoperation is rather unique to the proposed approach. This offers a real advantage over existing methods that are often biased towards one of the conflicting design requirements of performance or robust stability. The controller is also distinct from the previous  $H_\infty$  and  $\mu$ -synthesis based teleoperation controllers in that it can accommodate the nonlinear dynamics of the master and slave robots, and more importantly, that it explicitly incorporates the delay into the design process, providing an internal prediction mechanism. The results of performance and stability analysis as well as experiments with a teleoperation setup demonstrated the effectiveness of the proposed adaptive/robust controller.

### 7.1.3 Adaptive Controller

Although the proposed robust controller is less sensitive to modeling uncertainties, it can still potentially sacrifice the performance of the system in favor of its robust stability. This is due to the fact that a constant controller is employed throughout all phases of teleoperation. The third proposed controller in this thesis was an adaptive model-based predictive controller for constant and time-varying time-delay teleoperation. This controller further improved on our earlier model-based controllers by providing an adaptation mechanism to the user and environment parameters within a provably stable framework. The proposed adaptive controller

could also handle both constant and time-varying delay in communication channel.

Unlike the majority of existing time-delay teleoperation controllers which sacrifice the performance of the system in favor of its stability, the new adaptive controller uses available information about system model and time delay to improve the transparency of teleoperation while maintaining its stability. In this process, the estimates of the system parameters are updated by using the measurements.

A delay reduction method was developed that utilizes estimated model parameters and an auxiliary state observer to transform the system dynamics into a delay-free form. The teleoperation performance objectives, i.e. non-delayed virtual tool impedance shaping and position tracking were achieved within an output-regulation control framework. The stability of the system was proven using a Lyapunov analysis which also generated the parameters adaptation law. The effectiveness of the proposed controller was demonstrated through experimental studies for both constant and variable time-delay.

## 7.2 Future Work

In future, research can be carried out to improve upon the proposed controllers in this thesis. Some recommendations for future research are as follows:

- **Decentralized Controller:** The use of a multi-model control approach in the proposed decentralized controller proved effective in handling environment uncertainties. However, the stability of such switching control strategy must

be carefully investigated in future. Particularly, a formal analysis of the stability of the proposed switching control strategy can be performed.

- **Robust Controller:** Our original problem formulation in Fig. 5.2 was based on a rather general model of the uncertainty considering passive  $\Delta Z_h/s$  and  $\Delta Z_e/s$  disturbances to the system dynamics. Such large uncertainties in the system model could result in a conservative robust controller hence reducing the transparency. This issue was partly addressed by restricting the uncertainty to stiffness type variations in the environment dynamics. Also, the problem could be aggravated by the fact that  $H_\infty$  control framework would disregard the structure of the uncertainty blocks. The use of  $\mu$ -synthesis can be investigated in order to account for the structure of the uncertainty in the controller synthesis. Using D-K iterations,  $\mu$ -synthesis method solves the controller design problem by breaking it into a sequence of scaled  $H_\infty$  synthesis problems. In case of a time-delay system, each step can be solved using the introduced *adobe*-based method in 5.4.
- **Adaptive Controller:** In the proposed adaptive controller, it was assumed that the delay in all the input and output channels are equal. The controller could be modified to remove this restriction as well as the need for extra delay padding of the signals. Moreover, a decentralized version of the controller may be developed in future. Such a controller can avoid the extra delay that is imposed on the control loop by the centralized scheme. This can potentially result in faster and more accurate adaptation which further improves the transparency of teleoperation. Also, the implementation issues concerning packet-switched networks can be investigated more thoroughly

and the proposed solutions in the thesis can be further developed, implemented and experimentally verified.

Future work may also involve a comprehensive experimental comparison of the performance of the proposed controllers with that of other existing time-delay teleoperation controllers. In addition, the stability and the performance of the proposed methods can be further tested by implementing the controllers on a multi-axis teleoperation setup where the unmodeled dynamics and/or couplings among the axes can potentially cause practical issues. Also, the effect of the improved transparency on user performance in various time-delay teleoperation tasks can be assessed by conducting human factors studies.

# Appendix A

## Master/Hand, Slave/Environment and Tool Dynamics in State-space Form

The combined master and arm linearized dynamics in (4.27) can be written in the following state-space form

$$\begin{bmatrix} \dot{x}_m(t) \\ \dot{v}_m(t) \end{bmatrix} = \begin{bmatrix} 0 & 1 \\ -\frac{k_m+k_h}{m_m+m_h} & -\frac{b_m+b_h}{m_m+m_h} \end{bmatrix} \begin{bmatrix} x_m(t) \\ v_m(t) \end{bmatrix} + \begin{bmatrix} 0 \\ \frac{1}{m_m+m_h} \end{bmatrix} f_{cm}(t) + \begin{bmatrix} 0 & 0 \\ \frac{1}{m_m+m_h} & \frac{1}{m_m+m_h} \end{bmatrix} \begin{bmatrix} f_h^*(t) \\ \tilde{f}_{cm}(t) \end{bmatrix} \quad (\text{A.1})$$

$$\begin{aligned}
\begin{bmatrix} \dot{x}_m(t) \\ \dot{f}_h(t) \end{bmatrix} &= \begin{bmatrix} 1 & 0 \\ \frac{m_h(k_m+k_h)}{m_m+m_h} - k_h & \frac{m_h(b_m+b_h)}{m_m+m_h} - b_h \end{bmatrix} \begin{bmatrix} x_m(t) \\ v_m(t) \end{bmatrix} + \begin{bmatrix} 0 \\ -\frac{m_h}{m_m+m_h} \end{bmatrix} f_{cm}(t) \\
&+ \begin{bmatrix} 0 & 0 \\ 1 - \frac{m_h}{m_m+m_h} & -\frac{m_h}{m_m+m_h} \end{bmatrix} \begin{bmatrix} f_h^*(t) \\ \tilde{f}_{cm}(t) \end{bmatrix} + \begin{bmatrix} v_{xm}(t) \\ v_{fh}(t) \end{bmatrix}. \quad (\text{A.2})
\end{aligned}$$

The state-space equivalents of the combined slave and compliant environment dynamics in (4.28) and for  $i = 1, 2$  are as follows

$$\begin{aligned}
\begin{bmatrix} \dot{x}_s(t) \\ \dot{v}_s(t) \end{bmatrix} &= \begin{bmatrix} 0 & 1 \\ -\frac{k_s+\sigma_f k_e}{m_s+\sigma_f m_e} & -\frac{b_s+\sigma_f b_e}{m_s+\sigma_f m_e} \end{bmatrix} \begin{bmatrix} x_s(t) \\ v_s(t) \end{bmatrix} + \begin{bmatrix} 0 \\ \frac{1}{m_s+\sigma_f m_e} \end{bmatrix} f_{cs}(t) \\
&+ \begin{bmatrix} 0 & 0 \\ \frac{-\sigma_f}{m_s+\sigma_f m_e} & \frac{1}{m_s+\sigma_f m_e} \end{bmatrix} \begin{bmatrix} f_e^*(t) \\ \tilde{f}_{cs}(t) \end{bmatrix} \quad (\text{A.3})
\end{aligned}$$

$$\begin{aligned}
\begin{bmatrix} \dot{x}_s(t) \\ \dot{f}_e(t) \end{bmatrix} &= \begin{bmatrix} 1 & 0 \\ \frac{\sigma_f m_e(k_s+k_e)}{m_s+m_e} - \sigma_f k_e & \frac{\sigma_f m_e(b_s+b_e)}{m_s+m_e} - \sigma_f b_e \end{bmatrix} \begin{bmatrix} x_m(t) \\ v_m(t) \end{bmatrix} + \begin{bmatrix} 0 \\ -\frac{\sigma_f m_e}{m_s+\sigma_f m_e} \end{bmatrix} \\
&+ f_{cs}(t) + \begin{bmatrix} 0 & 0 \\ -\sigma_f \left(1 - \frac{m_e}{m_s+m_e}\right) & -\frac{\sigma_f m_e}{m_s+\sigma_f m_e} \end{bmatrix} \begin{bmatrix} f_e^*(t) \\ \tilde{f}_{cs}(t) \end{bmatrix} + \begin{bmatrix} v_{xs}(t) \\ v_{fe}(t) \end{bmatrix}. \quad (\text{A.4})
\end{aligned}$$

In the case of contact with rigid environment, i.e.  $i = 3$  in (4.28), the combined slave and environment linearized dynamics can be written in the state-space form

as follows

$$\begin{bmatrix} \dot{x}_s(t) \\ \dot{v}_s(t) \end{bmatrix} = \begin{bmatrix} 0 & 1 - \sigma_r \\ -(1 - \sigma_r)\frac{k_s}{m_s} & -(1 - \sigma_r)\frac{b_s}{m_s} \end{bmatrix} \begin{bmatrix} x_s(t) \\ v_s(t) \end{bmatrix} + \begin{bmatrix} 0 \\ \frac{1 - \sigma_r}{m_s} \end{bmatrix} f_{cs}(t) + \begin{bmatrix} 0 & 0 \\ 0 & \frac{1 - \sigma_r}{m_s} \end{bmatrix} \begin{bmatrix} f_e^*(t) \\ \tilde{f}_{cs}(t) \end{bmatrix} \quad (\text{A.5})$$

$$\begin{bmatrix} x_s(t) \\ f_e(t) \end{bmatrix} = \begin{bmatrix} 1 & 0 \\ 0 & 0 \end{bmatrix} \begin{bmatrix} x_s(t) \\ v_s(t) \end{bmatrix} + \begin{bmatrix} 0 \\ \sigma_r \end{bmatrix} f_{cs} + \begin{bmatrix} 0 & 0 \\ 0 & \sigma_r \end{bmatrix} \begin{bmatrix} f_e^*(t) \\ \tilde{f}_{cs}(t) \end{bmatrix} + \begin{bmatrix} v_{x_s}(t) \\ v_{f_e}(t) \end{bmatrix}. \quad (\text{A.6})$$

The tool dynamics in (4.29) can also be presented in the state-space, i.e.

$$\begin{bmatrix} \dot{x}_t(t) \\ \dot{v}_t(t) \end{bmatrix} = \begin{bmatrix} 0 & 1 \\ -\frac{k_t}{m_t} & -\frac{b_t}{m_t} \end{bmatrix} \begin{bmatrix} x_t(t) \\ v_t(t) \end{bmatrix} + \begin{bmatrix} 0 & 0 \\ \frac{1}{m_t} & -\frac{1}{m_t} \end{bmatrix} \begin{bmatrix} f_h(t) \\ f_e(t) \end{bmatrix} \quad (\text{A.7})$$

$$y_t(t) = \begin{bmatrix} 1 & 0 \\ 0 & 1 \end{bmatrix} \begin{bmatrix} x_t(t) \\ v_t(t) \end{bmatrix}. \quad (\text{A.8})$$

# Appendix B

## Teleoperation Dynamics in Chapter 4 in State-space Form

### B.1 Free Motion/Soft Contact

Based on the state definition in (4.31), the dynamics of the teleoperation in free motion/soft contact in (4.32) can be presented in the following state-space form

$$\begin{bmatrix} \dot{x}_s(t) - \dot{x}_m(t) \\ \dot{v}_s(t) - \dot{v}_m(t) \\ \dot{x}_m(t) - \dot{x}_t(t) \\ \dot{v}_m(t) - \dot{v}_t(t) \\ \dot{x}_t(t) \\ \dot{v}_t(t) \end{bmatrix} = \begin{bmatrix} 0 & 1 & 0 \\ -\frac{k_{se}}{m_{se}} & -\frac{b_{se}}{m_{se}} & -\frac{k_{se}}{m_{se}} + \frac{k_{mh}}{m_{mh}} \\ 0 & 0 & 0 \\ -\frac{m_e k_{se}}{m_{se} m_t} + \frac{k_e}{m_t} & -\frac{m_e b_{se}}{m_{se} m_t} + \frac{b_e}{m_t} & -\frac{k_{mh}}{m_{mh}} - \frac{m_e k_{se}}{m_{se} m_t} + \frac{k_e}{m_t} & \dots \\ 0 & 0 & -\frac{m_h k_{mh}}{m_{mh} m_t} + \frac{k_h}{m_t} \\ 0 & 0 & 0 \\ \frac{m_e k_{se}}{m_{se} m_t} - \frac{k_e}{m_t} & \frac{m_e b_{se}}{m_{se} m_t} - \frac{b_e}{m_t} & \frac{m_e k_{se}}{m_{se} m_t} - \frac{k_e}{m_t} \\ & & + \frac{m_h k_{mh}}{m_{mh} m_t} - \frac{k_h}{m_t} \end{bmatrix}$$

$$\begin{aligned}
& \left[ \begin{array}{ccc}
0 & 0 & 0 \\
-\frac{b_{se}}{m_{se}} + \frac{b_{mh}}{m_{mh}} & -\frac{k_{se}}{m_{se}} + \frac{k_{mh}}{m_{mh}} & -\frac{b_{se}}{m_{se}} + \frac{b_{mh}}{m_{mh}} \\
1 & 0 & 0 \\
-\frac{b_{mh}}{m_{mh}} - \frac{m_e b_{se}}{m_{se} m_t} + \frac{b_e}{m_t} & -\frac{k_{mh}}{m_{mh}} - \frac{m_e k_{se}}{m_{se} m_t} + \frac{k_e}{m_t} & -\frac{b_{mh}}{m_{mh}} - \frac{m_e b_{se}}{m_{se} m_t} + \frac{b_e}{m_t} \\
\dots & & \\
-\frac{m_h b_{mh}}{m_{mh} m_t} + \frac{b_h}{m_t} & -\frac{m_h k_{mh}}{m_{mh} m_t} + \frac{k_h}{m_t} + \frac{k_t}{m_t} & -\frac{m_h b_{mh}}{m_{mh} m_t} + \frac{b_h}{m_t} + \frac{b_t}{m_t} \\
0 & 0 & 1 \\
\frac{m_e b_{se}}{m_{se} m_t} - \frac{b_e}{m_t} & \frac{m_e k_{se}}{m_{se} m_t} - \frac{k_e}{m_t} & \frac{m_e b_{se}}{m_{se} m_t} - \frac{b_e}{m_t} \\
+\frac{m_h b_{mh}}{m_{mh} m_t} - \frac{b_h}{m_t} & +\frac{m_h k_{mh}}{m_{mh} m_t} - \frac{k_h}{m_t} - \frac{k_t}{m_t} & +\frac{m_h b_{mh}}{m_{mh} m_t} - \frac{b_h}{m_t} - \frac{b_t}{m_t}
\end{array} \right] \\
& \cdot \left[ \begin{array}{c}
x_s(t) - x_m(t) \\
v_s(t) - v_m(t) \\
x_m(t) - x_t(t) \\
v_m(t) - v_t(t) \\
x_t(t) \\
v_t(t)
\end{array} \right] + \left[ \begin{array}{cc}
0 & 0 \\
-\frac{1}{m_{mh}} & \frac{1}{m_{se}} \\
0 & 0 \\
\frac{1}{m_{mh}} + \frac{m_h}{m_{mh} m_t} & \frac{m_e}{m_{se} m_t} \\
0 & 0 \\
-\frac{m_h}{m_{mh} m_t} & -\frac{m_e}{m_{se} m_t}
\end{array} \right] \left[ \begin{array}{c}
f_{cm}(t) \\
f_{cs}(t)
\end{array} \right] \\
& + \left[ \begin{array}{cccc}
0 & 0 & 0 & 0 \\
-\frac{1}{m_{mh}} & -\frac{1}{m_{se}} & -\frac{1}{m_{mh}} & \frac{1}{m_{se}} \\
0 & 0 & 0 & 0 \\
\frac{1}{m_{mh}} + \frac{m_h}{m_{mh} m_t} - \frac{1}{m_t} & -\frac{m_e}{m_{se} m_t} + \frac{1}{m_t} & \frac{1}{m_{mh}} + \frac{m_h}{m_{mh} m_t} & \frac{m_e}{m_{se} m_t} \\
0 & 0 & 0 & 0 \\
-\frac{m_h}{m_{mh} m_t} + \frac{1}{m_t} & \frac{m_e}{m_{se} m_t} - \frac{1}{m_t} & -\frac{m_h}{m_{mh} m_t} & -\frac{m_e}{m_{se} m_t}
\end{array} \right] \left[ \begin{array}{c}
f_h^*(t) \\
f_e^*(t) \\
\tilde{f}_{cm}(t) \\
\tilde{f}_{cs}(t)
\end{array} \right] \quad (B.9)
\end{aligned}$$

with the output equation

$$\begin{aligned}
 \begin{bmatrix} x_m(t) \\ f_h(t) \\ x_s(t) \\ f_e(t) \\ x_t(t) \\ v_t(t) \end{bmatrix} &= \begin{bmatrix} 0 & 0 & 1 & 0 & 1 \\ 0 & 0 & \frac{m_h k_{mh}}{m_{mh}} - k_h & \frac{m_h b_{mh}}{m_{mh}} - b_h & \frac{m_h k_{mh}}{m_{mh}} - k_h \\ 1 & 0 & 1 & 0 & 1 \\ -\frac{m_e k_{se}}{m_{se}} + k_e & -\frac{m_e b_{se}}{m_{se}} + b_e & -\frac{m_e k_{se}}{m_{se}} + k_e & -\frac{m_e b_{se}}{m_{se}} + b_e & -\frac{m_e k_{se}}{m_{se}} + k_e & \dots \\ 0 & 0 & 0 & 0 & 1 \\ 0 & 0 & 0 & 0 & 0 \end{bmatrix} \\
 &\quad \begin{bmatrix} 0 \\ \frac{m_h b_{mh}}{m_{mh}} - b_h \\ 0 \\ \dots -\frac{m_e b_{se}}{m_{se}} + b_e \\ 0 \\ 1 \end{bmatrix} \begin{bmatrix} x_s(t) - x_m(t) \\ v_s(t) - v_m(t) \\ x_m(t) - x_t(t) \\ v_m(t) - v_t(t) \\ x_t(t) \\ v_t(t) \end{bmatrix} + \begin{bmatrix} 0 & 0 & 0 & 0 \\ 1 - \frac{m_h}{m_{mh}} & 0 & -\frac{m_h}{m_{mh}} & 0 \\ 0 & 0 & 0 & 0 \\ 0 & 1 - \frac{m_e}{m_{se}} & 0 & \frac{m_e}{m_{se}} \\ 0 & 0 & 0 & 0 \\ 0 & 0 & 0 & 0 \end{bmatrix} \\
 &\quad \cdot \begin{bmatrix} f_h^*(t) \\ f_e^*(t) \\ \tilde{f}_{cm}(t) \\ \tilde{f}_{cs}(t) \end{bmatrix} + \begin{bmatrix} v_{xm}(t) \\ v_{fh}(t) \\ v_{xs}(t) \\ v_{fe}(t) \\ 0 \\ 0 \end{bmatrix} \quad (\text{B.10})
 \end{aligned}$$

where  $\alpha_p$  in (4.31) is assumed to be equal to one. The state-space equations in free motion/soft contact in (4.35) after the augmentation of  $f_h^*$  and  $\tilde{f}_{cs}^*$  into the state

vector can be presented as

$$\begin{bmatrix} \dot{x}_s(t) - \dot{x}_m(t) \\ \dot{v}_s(t) - \dot{v}_m(t) \\ \dot{x}_m(t) - \dot{x}_t(t) \\ \dot{v}_m(t) - \dot{v}_t(t) \\ \dot{x}_t(t) \\ \dot{v}_t(t) \\ \ddot{f}_h^*(t) \\ \ddot{f}_h^*(t) \end{bmatrix} = \begin{bmatrix} 0 & 1 & 0 \\ -\frac{k_{se}}{m_{se}} & -\frac{b_{se}}{m_{se}} & -\frac{k_{se}}{m_{se}} + \frac{k_{mh}}{m_{mh}} \\ 0 & 0 & 0 \\ -\frac{m_e k_{se}}{m_{se} m_t} + \frac{k_e}{m_t} & -\frac{m_e b_{se}}{m_{se} m_t} + \frac{b_e}{m_t} & -\frac{k_{mh}}{m_{mh}} - \frac{m_e k_{se}}{m_{se} m_t} + \frac{k_e}{m_t} \\ 0 & 0 & -\frac{m_h k_{mh}}{m_{mh} m_t} + \frac{k_h}{m_t} \\ 0 & 0 & 0 \\ \frac{m_e k_{se}}{m_{se} m_t} - \frac{k_e}{m_t} & \frac{m_e b_{se}}{m_{se} m_t} - \frac{b_e}{m_t} & \frac{m_e k_{se}}{m_{se} m_t} - \frac{k_e}{m_t} \\ 0 & 0 & +\frac{m_h k_{mh}}{m_{mh} m_t} - \frac{k_h}{m_t} \\ 0 & 0 & 0 \\ 0 & 0 & 0 \\ 0 & 0 & 0 \\ -\frac{b_{se}}{m_{se}} + \frac{b_{mh}}{m_{mh}} & -\frac{k_{se}}{m_{se}} + \frac{k_{mh}}{m_{mh}} & -\frac{b_{se}}{m_{se}} + \frac{b_{mh}}{m_{mh}} \\ 1 & 0 & 0 \\ -\frac{b_{mh}}{m_{mh}} - \frac{m_e b_{se}}{m_{se} m_t} + \frac{b_e}{m_t} & -\frac{k_{mh}}{m_{mh}} - \frac{m_e k_{se}}{m_{se} m_t} + \frac{k_e}{m_t} & -\frac{b_{mh}}{m_{mh}} - \frac{m_e b_{se}}{m_{se} m_t} + \frac{b_e}{m_t} \\ -\frac{m_h b_{mh}}{m_{mh} m_t} + \frac{b_h}{m_t} & -\frac{m_h k_{mh}}{m_{mh} m_t} + \frac{k_h}{m_t} + \frac{k_t}{m_t} & -\frac{m_h b_{mh}}{m_{mh} m_t} + \frac{b_h}{m_t} + \frac{b_t}{m_t} \\ \dots & 0 & 1 \\ \frac{m_e b_{se}}{m_{se} m_t} - \frac{b_e}{m_t} & \frac{m_e k_{se}}{m_{se} m_t} - \frac{k_e}{m_t} & \frac{m_e b_{se}}{m_{se} m_t} - \frac{b_e}{m_t} \\ +\frac{m_h b_{mh}}{m_{mh} m_t} - \frac{b_h}{m_t} & +\frac{m_h k_{mh}}{m_{mh} m_t} - \frac{k_h}{m_t} - \frac{k_t}{m_t} & +\frac{m_h b_{mh}}{m_{mh} m_t} - \frac{b_h}{m_t} - \frac{b_t}{m_t} \\ 0 & 0 & 0 \\ 0 & 0 & 0 \end{bmatrix} \dots$$

(B.11)

$$\begin{aligned}
 & \begin{bmatrix} 0 & 0 \\ -\frac{1}{m_{mh}} & 0 \\ 0 & 0 \\ \frac{1}{m_{mh}} + \frac{m_h}{m_{mh}m_t} - \frac{1}{m_t} & 0 \\ \dots & 0 \\ -\frac{m_h}{m_{mh}m_t} + \frac{1}{m_t} & 0 \\ 0 & 1 \\ -\alpha_{fh}^2 & -2\alpha_{fh} \end{bmatrix} \begin{bmatrix} x_s(t) - x_m(t) \\ v_s(t) - v_m(t) \\ x_m(t) - x_t(t) \\ v_m(t) - v_t(t) \\ x_t(t) \\ v_t(t) \\ f_h^*(t) \\ \dot{f}_h^*(t) \end{bmatrix} + \begin{bmatrix} 0 & 0 \\ -\frac{1}{m_{mh}} & \frac{1}{m_{se}} \\ 0 & 0 \\ \frac{1}{m_{mh}} + \frac{m_h}{m_{mh}m_t} & \frac{m_e}{m_{se}m_t} \\ 0 & 0 \\ -\frac{m_h}{m_{mh}m_t} & -\frac{m_e}{m_{se}m_t} \\ 0 & 0 \\ 0 & 0 \end{bmatrix} \\
 & \cdot \begin{bmatrix} f_{cm}(t) \\ f_{cs}(t) \end{bmatrix} + \begin{bmatrix} 0 & 0 & 0 & 0 \\ 0 & -\frac{1}{m_{se}} & -\frac{1}{m_{mh}} & \frac{1}{m_{se}} \\ 0 & 0 & 0 & 0 \\ 0 & -\frac{m_e}{m_{se}m_t} + \frac{1}{m_t} & \frac{1}{m_{mh}} + \frac{m_h}{m_{mh}m_t} & \frac{m_e}{m_{se}m_t} \\ 0 & 0 & 0 & 0 \\ 0 & \frac{m_e}{m_{se}m_t} - \frac{1}{m_t} & -\frac{m_h}{m_{mh}m_t} & -\frac{m_e}{m_{se}m_t} \\ 0 & 0 & 0 & 0 \\ 1 & 0 & 0 & 0 \end{bmatrix} \begin{bmatrix} n_f(t) \\ f_e^*(t) \\ \tilde{f}_{cm}(t) \\ \tilde{f}_{cs}(t) \end{bmatrix} \quad (\text{B.12})
 \end{aligned}$$

where the output is given by

$$\begin{bmatrix} x_m(t) \\ f_h(t) \\ x_s(t) \\ f_e(t) \\ x_t(t) \\ v_t(t) \end{bmatrix} = \begin{bmatrix} 0 & 0 & 1 & 0 & 1 \\ 0 & 0 & \frac{m_h k_{mh}}{m_{mh}} - k_h & \frac{m_h b_{mh}}{m_{mh}} - b_h & \frac{m_h k_{mh}}{m_{mh}} - k_h \\ 1 & 0 & 1 & 0 & 1 \\ -\frac{m_e k_{se}}{m_{se}} + k_e & -\frac{m_e b_{se}}{m_{se}} + b_e & -\frac{m_e k_{se}}{m_{se}} + k_e & -\frac{m_e b_{se}}{m_{se}} + b_e & -\frac{m_e k_{se}}{m_{se}} + k_e \dots \\ 0 & 0 & 0 & 0 & 1 \\ 0 & 0 & 0 & 0 & 0 \end{bmatrix}$$

$$\begin{bmatrix} 0 & 0 & 0 \\ \frac{m_h b_{mh}}{m_{mh}} - b_h & 1 - \frac{m_h}{m_{mh}} & 0 \\ 0 & 0 & 0 \\ \dots & -\frac{m_e b_{se}}{m_{se}} + b_e & 0 & 0 \\ 0 & 0 & 0 \\ 1 & 0 & 0 \end{bmatrix} \begin{bmatrix} x_s(t) - x_m(t) \\ v_s(t) - v_m(t) \\ x_m(t) - x_t(t) \\ v_m(t) - v_t(t) \\ x_t(t) \\ v_t(t) \\ f_h^*(t) \\ \dot{f}_h^*(t) \end{bmatrix} + \begin{bmatrix} 0 & 0 & 0 & 0 \\ 0 & 0 & -\frac{m_h}{m_{mh}} & 0 \\ 0 & 0 & 0 & 0 \\ 0 & 1 - \frac{m_e}{m_{se}} & 0 & \frac{m_e}{m_{se}} \\ 0 & 0 & 0 & 0 \\ 0 & 0 & 0 & 0 \end{bmatrix}$$

$$\cdot \begin{bmatrix} n_f(t) \\ f_e^*(t) \\ \tilde{f}_{cm}(t) \\ \tilde{f}_{cs}(t) \end{bmatrix} + \begin{bmatrix} v_{xm}(t) \\ v_{fh}(t) \\ v_{xs}(t) \\ v_{fe}(t) \\ 0 \\ 0 \end{bmatrix} \quad (\text{B.13})$$

## B.2 Rigid Contact

Considering the state definition in (4.37) for the case of rigid contact and assuming the scaling factors,  $\alpha_p$  and  $\alpha_f$ , to be equal to one, the system's dynamics in (4.43) can be written in the following state-space form

$$\begin{aligned}
 \begin{bmatrix} \dot{x}_m(t) - \dot{x}_s(t) \\ \dot{v}_m(t) \\ \dot{x}_s(t) \\ \dot{\tilde{f}}_e(t) \\ \dot{\tilde{f}}_e(t) - \dot{\tilde{f}}_h(t) \end{bmatrix} &= \begin{bmatrix} 0 & 1 & 0 & 0 & 0 \\ -\frac{k_{mh}}{m_{mh}} & -\frac{b_{mh}}{m_{mh}} & -\frac{k_{mh}}{m_{mh}} & 0 & 0 \\ 0 & 0 & 0 & 0 & 0 \\ 0 & 0 & 0 & -\beta & 0 \\ \frac{-\beta m_h k_{mh}}{m_{mh}} + \beta k_h & \frac{-\beta m_h b_{mh}}{m_{mh}} + \beta b_h & \frac{-\beta m_h k_{mh}}{m_{mh}} + \beta k_h & 0 & -\beta \end{bmatrix} \\
 &\cdot \begin{bmatrix} x_m(t) - x_s(t) \\ v_m(t) \\ x_s(t) \\ \tilde{f}_e(t) \\ \tilde{f}_e(t) - \tilde{f}_h(t) \end{bmatrix} + \begin{bmatrix} 0 & 0 \\ \frac{1}{m_{mh}} & 0 \\ 0 & 0 \\ 0 & \beta \\ \frac{\beta m_h}{m_{mh}} & \beta \end{bmatrix} \begin{bmatrix} f_{cm}(t) \\ f_{cs}(t) \end{bmatrix} \\
 &+ \begin{bmatrix} 0 & 0 & 0 & -1 \\ \frac{1}{m_{mh}} & \frac{1}{m_{mh}} & 0 & 0 \\ 0 & 0 & 0 & 1 \\ 0 & 0 & \beta & 0 \\ -\beta + \frac{\beta m_h}{m_{mh}} & \frac{\beta m_h}{m_{mh}} & \beta & 0 \end{bmatrix} \begin{bmatrix} f_h^*(t) \\ \tilde{f}_{cm}(t) \\ \tilde{f}_{cs}(t) \\ w_{xs}(t) \end{bmatrix} \quad (\text{B.14})
 \end{aligned}$$

with the following output equation

$$\begin{aligned}
 \begin{bmatrix} x_m(t) \\ f_h(t) \\ x_s(t) \\ \tilde{f}_e(t) \end{bmatrix} &= \begin{bmatrix} 1 & 0 & 1 & 0 & 0 \\ \frac{m_h k_{mh}}{m_{mh}} - k_h & \frac{m_h b_{mh}}{m_{mh}} - b_h & \frac{m_h k_{mh}}{m_{mh}} - k_h & 0 & 0 \\ 0 & 0 & 1 & 0 & 0 \\ 0 & 0 & 0 & 1 & 0 \end{bmatrix} \begin{bmatrix} x_m(t) - x_s(t) \\ v_m(t) \\ x_s(t) \\ \tilde{f}_e(t) \\ \tilde{f}_e(t) - \tilde{f}_h(t) \end{bmatrix} \\
 &+ \begin{bmatrix} 0 & 0 \\ -\frac{m_h}{m_{mh}} & 0 \\ 0 & 0 \\ 0 & 0 \end{bmatrix} \begin{bmatrix} f_{cm}(t) \\ f_{cs}(t) \end{bmatrix} + \begin{bmatrix} 0 & 0 & 0 & 0 \\ 1 - \frac{m_h}{m_{mh}} & -\frac{m_h}{m_{mh}} & 0 & 0 \\ 0 & 0 & 0 & 0 \\ 0 & 0 & 0 & 0 \end{bmatrix} \\
 &\quad \cdot \begin{bmatrix} f_h^*(t) \\ \tilde{f}_{cm}(t) \\ \tilde{f}_{cs}(t) \\ w_{xs}(t) \end{bmatrix} + \begin{bmatrix} v_{xm}(t) \\ v_{fh}(t) \\ 0 \\ 0 \end{bmatrix} \quad (B.15)
 \end{aligned}$$

After augmenting  $f_h^*$  and  $\dot{f}_h^*$  into the state vector, the state-space equations in rigid contact in (4.43) can be written as

$$\begin{aligned}
 & \begin{bmatrix} \dot{x}_m(t) - \dot{x}_s(t) \\ \dot{v}_m(t) \\ \dot{x}_s(t) \\ \dot{\tilde{f}}_e(t) \\ \dot{\tilde{f}}_e(t) - \dot{\tilde{f}}_h(t) \\ \dot{f}_h^*(t) \\ \dot{\tilde{f}}_h^*(t) \end{bmatrix} = \begin{bmatrix} 0 & 1 & 0 & 0 & 0 \\ -\frac{k_{mh}}{m_{mh}} & -\frac{b_{mh}}{m_{mh}} & -\frac{k_{mh}}{m_{mh}} & 0 & 0 \\ 0 & 0 & 0 & 0 & 0 \\ 0 & 0 & 0 & -\beta & 0 \dots \\ \frac{-\beta m_h k_{mh}}{m_{mh}} + \beta k_h & \frac{-\beta m_h b_{mh}}{m_{mh}} + \beta b_h & \frac{-\beta m_h k_{mh}}{m_{mh}} + \beta k_h & 0 & -\beta \\ 0 & 0 & 0 & 0 & 0 \\ 0 & 0 & 0 & 0 & 0 \end{bmatrix} \\
 & \begin{bmatrix} 0 & 0 \\ \frac{1}{m_{mh}} & 0 \\ 0 & 0 \\ \dots & 0 \\ -\beta + \frac{\beta m_h}{m_{mh}} & 0 \\ 0 & 1 \\ -\alpha_{fh}^2 & -2\alpha_{fh} \end{bmatrix} \begin{bmatrix} x_m(t) - x_s(t) \\ v_m(t) \\ x_s(t) \\ \tilde{f}_e(t) \\ \tilde{f}_e(t) - \tilde{f}_h(t) \\ f_h^*(t) \\ \tilde{f}_h^*(t) \end{bmatrix} + \begin{bmatrix} 0 & 0 \\ \frac{1}{m_{mh}} & 0 \\ 0 & 0 \\ 0 & \beta \\ \frac{\beta m_h}{m_{mh}} & \beta \\ 0 & 0 \\ 0 & 0 \end{bmatrix} \begin{bmatrix} f_{cm}(t) \\ f_{cs}(t) \end{bmatrix} \\
 & + \begin{bmatrix} 0 & 0 & 0 & -1 \\ 0 & \frac{1}{m_{mh}} & 0 & 0 \\ 0 & 0 & 0 & 1 \\ 0 & 0 & \beta & 0 \\ 0 & \frac{\beta m_h}{m_{mh}} & \beta & 0 \\ 0 & 0 & 0 & 0 \\ 1 & 0 & 0 & 0 \end{bmatrix} \begin{bmatrix} n_f(t) \\ \tilde{f}_{cm}(t) \\ \tilde{f}_{cs}(t) \\ w_{xs}(t) \end{bmatrix} \quad (\text{B.16})
 \end{aligned}$$

where the output is given by

$$\begin{aligned}
 \begin{bmatrix} x_m(t) \\ f_h(t) \\ x_s(t) \\ \tilde{f}_e(t) \end{bmatrix} &= \begin{bmatrix} 1 & 0 & 1 & 0 & 0 & 0 & 0 \\ \frac{m_h k_{mh}}{m_{mh}} - k_h & \frac{m_h b_{mh}}{m_{mh}} - b_h & \frac{m_h k_{mh}}{m_{mh}} - k_h & 0 & 0 & 1 - \frac{m_h}{m_{mh}} & 0 \\ 0 & 0 & 1 & 0 & 0 & 0 & 0 \\ 0 & 0 & 0 & 1 & 0 & 0 & 0 \end{bmatrix} \\
 &\cdot \begin{bmatrix} x_m(t) - x_s(t) \\ v_m(t) \\ x_s(t) \\ \tilde{f}_e(t) \\ \tilde{f}_e(t) - \tilde{f}_h(t) \\ f_h^*(t) \\ \tilde{f}_h^*(t) \end{bmatrix} + \begin{bmatrix} 0 & 0 \\ -\frac{m_h}{m_{mh}} & 0 \\ 0 & 0 \\ 0 & 0 \end{bmatrix} \begin{bmatrix} f_{cm}(t) \\ f_{cs}(t) \end{bmatrix} \\
 &+ \begin{bmatrix} 0 & 0 & 0 & 0 \\ 0 & -\frac{m_h}{m_{mh}} & 0 & 0 \\ 0 & 0 & 0 & 0 \\ 0 & 0 & 0 & 0 \end{bmatrix} \begin{bmatrix} n_f(t) \\ \tilde{f}_{cm}(t) \\ \tilde{f}_{cs}(t) \\ w_{xs}(t) \end{bmatrix} + \begin{bmatrix} v_{xm}(t) \\ v_{fh}(t) \\ 0 \\ 0 \end{bmatrix}. \quad (\text{B.17})
 \end{aligned}$$

# Appendix C

## Proof of Theorem 4.1

### C.1 Stabilizability

The controllability matrix of the original system with pair  $(A, B)$  can be written as

$$U = [B \ AB \ A^2B \ \dots \ A^{n-1}B] = [B_1 \ \dots \ B_{n_I} | AB_1 \ \dots \ AB_{n_I} | \dots | A^{n-1}B_1 \ \dots \ A^{n-1}B_{n_I}] \quad (\text{C.18})$$

where the rank of  $U$  is

$$\rho(U) = n_c \leq n. \quad (\text{C.19})$$

Using the canonical decomposition theorem [122], there exists a transformation  $\bar{X} = PX$ , which transforms pair  $(A, B)$  to  $(\bar{A}, \bar{B})$

$$\bar{A} = PAP^{-1} = \begin{bmatrix} \bar{A}^c & \bar{A}^{12} \\ 0 & \bar{A}^{\bar{c}} \end{bmatrix} \quad (\text{C.20})$$

$$\bar{B} = PB = \begin{bmatrix} \bar{B}^c \\ 0 \end{bmatrix} \quad (\text{C.21})$$

such that the pair  $(\bar{A}^c, \bar{B}^c)$  is controllable. The state transformation matrix  $P$  is defined as

$$P^{-1} \triangleq Q = [q_1 \cdots q_{n_c} \cdots q_n] \quad (\text{C.22})$$

where  $q_1 \cdots q_{n_c}$  are  $n_c$  linearly independent columns of matrix  $U$  and the last  $n - n_c$  columns are arbitrarily chosen vectors that make the matrix  $Q$  nonsingular. Since the original system is assumed stabilizable,  $\bar{A}^c$  would contain all unstable modes, if any.

From (4.50), the controllability matrix of the transformed system represented by the pair  $(A_z, B_z)$  is given by

$$U_z = [B_z \ A_z B_z \ A_z^2 B_z \ \cdots \ A_z^{n-1} B_z] = \\ [e^{-Ah_1^m} B_1 \ \cdots \ e^{-Ah_{n_I}^m} B_{n_I} | e^{-Ah_1^m} A B_1 \ \cdots \ e^{-Ah_{n_I}^m} A B_{n_I} | \cdots \\ | e^{-Ah_1^m} A^{n-1} B_1 \ \cdots \ e^{-Ah_{n_I}^m} A^{n-1} B_{n_I}] \quad (\text{C.23})$$

where the commutability of matrices  $A$  and  $e^{-Ah}$  has been used. The following lemma is needed to continue the proof.

*Lemma A.1:*

$$\rho(U_z) = \rho(U). \quad (\text{C.24})$$

*Proof:* Reordering the columns of a matrix will not alter its rank, so from (C.23)

$$\rho(U_z) = \rho([e^{-Ah_1^m} [B_1 AB_1 \cdots A^{n-1}B_1] | \cdots | e^{-Ah_{n_I}^m} [B_{n_I} AB_{n_I} \cdots A^{n-1}B_{n_I}]]). \quad (\text{C.25})$$

Note that since  $e^{-Ah_j^m}$  is a full rank square matrix, for each  $j$ ,

$$\rho([e^{-Ah_j^m} [B_j AB_j \cdots A^{n_I-1}B_j]]) = \rho([B_j AB_j \cdots A^{n_I-1}B_j]). \quad (\text{C.26})$$

To proceed, we use the *Caley-Hamilton* theorem which states that each matrix satisfies its own characteristic polynomial [122], i.e.

$$f(A) = a_n A^n + a_{n-1} A^{n-1} + \cdots + a_0 = 0 \quad (\text{C.27})$$

and therefore,

$$A^n = b_{n-1} A^{n-1} + \cdots + b_0 \quad (\text{C.28})$$

and consequently, all the powers of  $A$  greater than or equal to  $n$  can be written as

a linear combination of  $A^k$ , for  $k < n$ . Using this theorem and the *Taylor* series expansion of  $e^{-Ah_j^m}$ , one can write

$$e^{-Ah_j^m} = c_0I + c_1A + c_2A^2 + \cdots + c_{n-1}A^{n-1}. \quad (\text{C.29})$$

Using (C.29),

$$\begin{aligned} e^{-Ah_j^m} A^k B_j &= (c_0I + c_1A + c_2A^2 + \cdots + c_{n-1}A^{n-1})A^k B_j \\ &= l_0B_j + l_1AB_j + l_2A^2B_j + \cdots + l_{n-1}A^{n-1}B_j. \end{aligned} \quad (\text{C.30})$$

Considering (C.26) and (C.30), one can conclude that for each  $j$ ,  $[B_j \ AB_j \ \cdots \ A^{n-1}B_j]$  and  $e^{-Ah_j^m} [B_j \ AB_j \ \cdots \ A^{n-1}B_j]$  span the same space. Therefore,  $U$  and  $U_z$  are of the same rank and the proof of Lemma A.1 is complete. Q.E.D.

The canonical form of the reduced system represented by the pair  $(\bar{A}_z, \bar{B}_z)$  can be generated using the same transformation  $P$  in (C.22) for the original system, i.e.

$$\bar{A}_z = PA_zP^{-1} \quad (\text{C.31})$$

$$\bar{B}_z = PB_z \text{ or } P^{-1}\bar{B}_z = B_z. \quad (\text{C.32})$$

Substituting  $A_z$  and  $B_z$  from (4.50), results in

$$\bar{A}_z = PAP^{-1} = \begin{bmatrix} \bar{A}^c & \bar{A}^{12} \\ 0 & \bar{A}^e \end{bmatrix} \quad (\text{C.33})$$

$$P^{-1} [\bar{b}_z^1 \cdots \bar{b}_z^{n_I}] = [e^{-Ah_1^m} B_1 \cdots e^{-Ah_{n_I}^m} B_{n_I}]. \quad (\text{C.34})$$

For the  $j$ th column of (C.34), one can write

$$P^{-1} \bar{b}_z^j = e^{-Ah_j^m} B_j. \quad (\text{C.35})$$

Replacing  $e^{-Ah_j^m}$  from (C.29)

$$P^{-1} \bar{b}_z^j = (c_0 I + c_1 A + c_2 A^2 + \cdots + c_{n-1} A^{n-1}) B_j. \quad (\text{C.36})$$

From the definition of  $P^{-1}$  in (C.22), the first  $n_c$  columns of  $P^{-1}$  are the basis of the controllability matrix  $U$  in (C.18). Considering (C.36), the right hand side of (C.34) can be written in terms of first  $n_c$  columns of  $P^{-1}$ , i.e.

$$\bar{B}_z = \begin{bmatrix} \bar{B}_z^c \} n_c \\ 0 \end{bmatrix}. \quad (\text{C.37})$$

Using (C.33) and (C.37), the controllability matrix of the pair  $(\bar{A}_z, \bar{B}_z)$  can be written as

$$\bar{U}_z = \begin{bmatrix} \bar{B}_z^c & \bar{A}_z \bar{B}_z^c & \cdots & \bar{A}_z^{n-1} \bar{B}_z^c \} n_c \\ 0 & 0 & \cdots & 0 \end{bmatrix}. \quad (\text{C.38})$$

According to Lemma A.1,  $\rho(U_z) = \rho(U) = n_c$ . Also, since the transformation  $P$  is nonsingular,  $U_z$  and  $\bar{U}_z$  have equal ranks, i.e.

$$\rho(\bar{U}_z) = n_c \quad (\text{C.39})$$

and consequently, the pair  $(\bar{A}^c, \bar{B}_z^c)$  is controllable where  $\bar{A}^c$  contains all the unstable poles.

## C.2 Detectability

The proof follows the same lines as in the case of stabilizability. The observability matrix of the original system  $(A, B)$  can be written as

$$V = \begin{bmatrix} C \\ CA \\ CA^2 \\ \vdots \\ CA^{n-1} \end{bmatrix} = \begin{bmatrix} C_1 \\ \vdots \\ C_{n_o} \\ \text{---} \\ C_1 A \\ \vdots \\ C_{n_o} A \\ \text{---} \\ \vdots \\ \text{---} \\ C_1 A^{n-1} \\ \vdots \\ C_{n_o} A^{n-1} \end{bmatrix} \quad (\text{C.40})$$

where the rank of  $V$  is

$$\rho(V) = n_{ob} \leq n. \quad (\text{C.41})$$

Using the canonical decomposition theorem [122], there exists a transformation  $\bar{X} = PX$ , which transforms pair  $(A, C)$  to  $(\bar{A}, \bar{C})$

$$\bar{A} = PAP^{-1} = \begin{bmatrix} \bar{A}^o & 0 \\ \bar{A}^{21} & \bar{A}^o \end{bmatrix} \quad (\text{C.42})$$

$$\bar{C} = CP^{-1} = \begin{bmatrix} \bar{C}^o & 0 \end{bmatrix} \quad (\text{C.43})$$

and the pair  $(\bar{A}^o, \bar{C}^o)$  is observable. The matrix  $P$  is defined as

$$P \triangleq \begin{bmatrix} r_1 \\ \vdots \\ r_{n_o} \\ \vdots \\ r_n \end{bmatrix} \quad (\text{C.44})$$

where  $r_1 \cdots r_{n_{ob}}$  are  $n_{ob}$  independent rows of  $V$  and the last  $n - n_{ob}$  rows are arbitrarily chosen vectors such that the matrix  $P$  is nonsingular. The detectability of the original system requires all unstable modes to be observable. Therefore,  $\bar{A}^o$  should contain all unstable modes. The canonical representation of the reduced system  $(\bar{A}_z, \bar{C}_z)$  can be obtained using transformation  $P$  in (C.44) from the original system as

$$\bar{A}_z = PA_zP^{-1} \quad (\text{C.45})$$

$$\bar{C}_z = C_z P^{-1} \text{ or } \bar{C}_z P = C_z. \quad (\text{C.46})$$

Substituting  $A_z$  and  $C_z$  from (4.50) and (4.56), results in

$$\bar{A}_z = P A P^{-1} = \begin{bmatrix} \bar{A}^o & 0 \\ \bar{A}^{21} & \bar{A}^{\bar{o}} \end{bmatrix} \quad (\text{C.47})$$

$$\begin{bmatrix} \bar{C}_z^1 \\ \vdots \\ \bar{C}_z^{m_o} \end{bmatrix} P = \begin{bmatrix} C_1 e^{A_d^{m_1}} \\ C_2 e^{A_d^{m_2}} \\ \vdots \\ C_{n_o} e^{A_d^{m_{n_o}}} \end{bmatrix}. \quad (\text{C.48})$$

For the  $j$ th row of (C.48), one can write

$$\bar{C}_z^j P = C_j e^{A_d^{m_j}}. \quad (\text{C.49})$$

Using the Caley-Hamilton theorem,

$$\bar{C}_z^j P = C_j (a_0 I + a_1 A + a_2 A^2 + \cdots + a_{n-1} A^{n-1}). \quad (\text{C.50})$$

From the definition of  $P$  in (C.44), the first  $n_{ob}$  rows of  $P$  are the basis of matrix  $V$  in (C.40). Therefore, the right hand side of (C.48) can be written in terms of the first  $n_{ob}$  rows of  $P$ , i.e.

$$\bar{C}_z = \begin{bmatrix} \bar{C}_z^o & 0 \end{bmatrix}. \quad (\text{C.51})$$

Using (C.47) and (C.51), the observability matrix of the pair  $(\bar{A}_z, \bar{C}_z)$  can be written as

$$\bar{V}_z = \begin{bmatrix} \bar{C}_z^o & 0 \\ \bar{C}_z^o \bar{A}_o & 0 \\ \vdots & \\ \bar{C}_z^o \bar{A}_o^{n-1} & 0 \end{bmatrix}. \quad (\text{C.52})$$

Using the dual arguments of Lemma A.1,  $\rho(\bar{V}_z) = n_{ob}$ , and hence the pair  $(\bar{A}^o, \bar{C}_z^o)$  is observable. Also from the canonical decomposition theorem,  $\bar{A}^o$  encompasses all unstable poles. Consequently, the reduced system is detectable. Q.E.D.

# Appendix D

## One-block Equivalent of a Four-block Time-delay Problem

This appendix discusses the details of reducing a time-delay four-block problem in (5.46) and (5.48) to the equivalent one-block problem using the solution to the problem where the delay is ignored. The following are the conditions that need to be satisfied for the delay-free problem to have a solution [35]

$$\max\{\gamma_z, \gamma_w\} < \gamma \tag{D.53}$$

$$H_X \in \text{dom Ric} \quad , \quad X \triangleq \text{Ric}(H_X) \geq 0 \tag{D.54}$$

$$H_Y \in \text{dom Ric} \quad , \quad Y \triangleq \text{Ric}(H_Y) \geq 0 \tag{D.55}$$

$$\rho(XY) < \gamma \tag{D.56}$$

where

$$\begin{aligned}\gamma_z &\triangleq \| (I - D_{12}(D'_{12}D_{12})^{-1}D'_{12})D_{11} \| \\ \gamma_w &\triangleq \| D_{11}(I - D'_{21}(D_{21}D'_{21})^{-1}D_{21}) \| \end{aligned} \quad (\text{D.57})$$

and

$$\begin{aligned}H_X &\triangleq \begin{bmatrix} A & 0 \\ -C'_1C_1 & -A' \end{bmatrix} - \begin{bmatrix} B_1 & B_2 \\ -C'_1D_{11} & -C'_1D_{12} \end{bmatrix} \\ &\times \begin{bmatrix} D'_{11}D_{11} - \gamma^2 I & D'_{11}D_{12} \\ D'_{12}D_{11} & D'_{12}D_{12} \end{bmatrix}^{-1} \begin{bmatrix} D'_{11}C_1 & B'_1 \\ D'_{12}C_1 & B'_2 \end{bmatrix} \end{aligned} \quad (\text{D.58})$$

$$\begin{aligned}H_Y &\triangleq \begin{bmatrix} A' & 0 \\ -B_1B'_1 & -A \end{bmatrix} - \begin{bmatrix} C'_1 & C'_2 \\ -B_1D'_{11} & -B_1D'_{21} \end{bmatrix} \\ &\times \begin{bmatrix} D_{11}D'_{11} - \gamma^2 I & D_{11}D'_{21} \\ D_{21}D'_{11} & D_{21}D'_{21} \end{bmatrix}^{-1} \begin{bmatrix} D_{11}B'_1 & C_1 \\ D_{21}B'_1 & C_2 \end{bmatrix}. \end{aligned} \quad (\text{D.59})$$

Assuming

$$\Theta_z \triangleq \begin{bmatrix} D'_{11}D_{11} - \gamma^2 I & D'_{11}D_{12} \\ D'_{12}D_{11} & D'_{12}D_{12} \end{bmatrix} \quad (\text{D.60})$$

$$\Theta_w \triangleq \begin{bmatrix} D_{11}D'_{11} - \gamma^2 I & D_{11}D'_{21} \\ D_{21}D'_{11} & D_{21}D'_{21} \end{bmatrix} \quad (\text{D.61})$$

the following matrices can be defined

$$F = \begin{bmatrix} F_1 \\ F_2 \end{bmatrix} \triangleq -\Theta_z^{-1} \left( \begin{bmatrix} B'_1 \\ B'_2 \end{bmatrix} X + \begin{bmatrix} D'_{11} \\ D'_{12} \end{bmatrix} C_1 \right) \quad (\text{D.62})$$

$$L = \begin{bmatrix} L_1 & L_2 \end{bmatrix} \triangleq - \left( Y \begin{bmatrix} C'_1 & C'_2 \end{bmatrix} + B_1 \begin{bmatrix} D'_{11} & D'_{21} \end{bmatrix} \right) \Theta_w^{-1}. \quad (\text{D.63})$$

Providing that the conditions in (D.53)-(D.56) holds, it can be shown that

$$Z \triangleq (I - \gamma^{-2} Y X)^{-1} \quad (\text{D.64})$$

is well defined and the matrices

$$\begin{aligned} A_F &\triangleq A + B_1 F_1 + B_2 F_2, \\ A_L &\triangleq A + L_1 C_1 + L_2 C_2 \end{aligned} \quad (\text{D.65})$$

are Hurwitz.

The resulting one-block problem transfer matrix,  $G(s)$ , can be calculated by

$$G(s) = \left[ \begin{array}{c|c} A_L & B_\infty D_\infty^{-1} \\ \hline D_\infty C_\infty Z^{-1} & I \end{array} \right] \quad (\text{D.66})$$

where

$$\begin{aligned} B_\infty &\triangleq \begin{bmatrix} -(B_2 + L_1 D_{12} + L_2 D_{22}) & L_2 \end{bmatrix} \\ C_\infty &\triangleq \begin{bmatrix} F_2 \\ C_2 + D_{21} F_1 + D_{22} F_2 \end{bmatrix}. \end{aligned} \quad (\text{D.67})$$

$D_\infty$  in (D.66) can be calculated using the Parrott's theorem [133]. Based on this theorem, there exists a matrix  $D_K$  such that

$$\tilde{D}_{11} \triangleq \mathcal{F}_l \left( \begin{bmatrix} D_{11} & D_{12} \\ D_{21} & D_{22} \end{bmatrix}, D_K \right) \quad (\text{D.68})$$

is well defined and  $\|\tilde{D}_{11}\| < \gamma$ .  $D_\infty$  can then be chosen in the form of

$$D_\infty = V \begin{bmatrix} I & -D_K \\ 0 & I \end{bmatrix} \quad (\text{D.69})$$

where  $V$  is a lower triangular matrix defined as

$$V = \gamma \begin{bmatrix} V_1 & 0 \\ V_2(I - D_{22}D_K)^{-1}V_3 & V_2 \end{bmatrix}. \quad (\text{D.70})$$

$V_1$ ,  $V_2$  and  $V_3$  in (D.70) are found by the following lower triangular Cholesky factorizations

$$V_1'V_1 = -(I - D'_{22}D'_K)^{-1}D'_{12}\tilde{\Theta}_{11}^{-1}D_{12}(I - D_KD_{22})^{-1} \quad (\text{D.71})$$

$$V_2'V_2 = -(I - D'_K D'_{22})\Delta^{-1}(I - D_{22}D_K) \quad (\text{D.72})$$

$$V_3 \triangleq \tilde{\Theta}_{21}\tilde{\Theta}_{11}^{-1}D_{12}(I - D_KD_{22})^{-1} - D_{22} \quad (\text{D.73})$$

where

$$\Delta \triangleq \tilde{\Theta}_{22} - \tilde{\Theta}_{21}\tilde{\Theta}_{11}^{-1}\tilde{\Theta}_{12} \quad (\text{D.74})$$

$$\tilde{\Theta} = \begin{bmatrix} \tilde{\Theta}_{11} & \tilde{\Theta}_{12} \\ \tilde{\Theta}_{21} & \tilde{\Theta}_{22} \end{bmatrix} \triangleq \begin{bmatrix} \tilde{D}_{11}\tilde{D}'_{11} - \gamma^2 I & \tilde{D}_{11}D'_{21} \\ D_{21}\tilde{D}'_{11} & D_{21}D'_{21} \end{bmatrix}. \quad (\text{D.75})$$

# Appendix E

## Solution to the Adobe Delay Problem

The solution to an *adobe* delay problem, i.e. a one-block problem shown in Fig. 5.5 with the adobe delay structure (5.54), is calculated in this appendix based on the results from [35]. Transfer function  $G(s)$  in (D.66) can be rewritten as

$$G(s) \triangleq \left[ \begin{array}{c|cc} A_L & B_\mu & B_\rho \\ \hline C_\mu & I_\mu & 0 \\ C_\rho & 0 & I_\rho \end{array} \right] \quad (\text{E.76})$$

where  $G(s)$  is partitioned compatibly with the adobe delay structure in (5.54). Let

$$\begin{aligned}
 J &\triangleq \begin{bmatrix} I_{n_u} & 0 \\ 0 & -I_{n_y} \end{bmatrix} \\
 J_\mu &\triangleq \begin{bmatrix} I_\mu & 0 \end{bmatrix} J \begin{bmatrix} I_\mu \\ 0 \end{bmatrix} \\
 J_\rho &\triangleq \begin{bmatrix} 0 & I_\rho \end{bmatrix} J \begin{bmatrix} 0 \\ I_\rho \end{bmatrix}.
 \end{aligned} \tag{E.77}$$

Define  $\Sigma(t)$  as

$$\Sigma(t) = \begin{bmatrix} \Sigma_{11}(t) & \Sigma_{12}(t) \\ \Sigma_{21}(t) & \Sigma_{22}(t) \end{bmatrix} \triangleq e^{Ht} \tag{E.78}$$

and the Hamiltonian matrix  $H$  as

$$H = \begin{bmatrix} H_{11}(t) & H_{12}(t) \\ H_{21}(t) & H_{22}(t) \end{bmatrix} \triangleq \begin{bmatrix} A_L - B_\rho C_\rho & -B_\rho J_\rho B'_\rho \\ -C'_\mu J_\mu B_\mu & -A'_L + C'_\rho B'_\rho \end{bmatrix}. \tag{E.79}$$

The adobe delay problem has a solution if and only if  $\Sigma_{22}(t)$  is nonsingular for  $\forall t \in [0, h]$ . The controller  $K$  can then be obtained by

$$K = C_r \left( \begin{bmatrix} I & 0 \\ \Pi & I \end{bmatrix} \tilde{G}^{-1}, \tilde{Q} \right) \tag{E.80}$$

where

$$\tilde{G}(s) = \left[ \begin{array}{c|cc} A_L & \Sigma'_{22}B_\mu + \Sigma'_{12}C'_\mu J_\mu & B_\rho \\ \hline C_\mu \Sigma'^{-1}_{22} & I_\mu & 0 \\ C_\rho - J_\rho B'_\rho \Sigma'^{-1}_{22} \Sigma_{21} & 0 & I_\rho \end{array} \right] \quad (\text{E.81})$$

is a bistable transfer matrix and

$$\Pi(s) = \pi_h \left\{ e^{-hs} \left[ \begin{array}{c|cc} H_{11} & H_{12} & B_\rho \\ \hline H_{21} & H_{22} & -C'_\mu J_\mu \\ C_\rho & J_\rho B'_\rho & 0 \end{array} \right] \right\} \quad (\text{E.82})$$

is a FIR operator.  $\tilde{Q}$  in (E.80) is a contractive matrix and  $\Sigma = \Sigma(h)$ .

The completion operator,  $\pi_h$  in (E.82), is defined as follows [109]. Assuming a  $h$ -delayed system,  $e^{-hs}P$ , with

$$P = \left[ \begin{array}{c|c} A & B \\ \hline C & 0 \end{array} \right] \quad (\text{E.83})$$

the completion operator is calculated by

$$\pi_h(e^{-hs}P) = \left[ \begin{array}{c|c} A & B \\ \hline Ce^{-Ah} & 0 \end{array} \right] - e^{-hs} \left[ \begin{array}{c|c} A & B \\ \hline C & 0 \end{array} \right]. \quad (\text{E.84})$$

# Appendix F

## Teleoperation Dynamics in Chapter 6 in State-space Form

Based on the state definition in (6.2), the dynamics of the teleoperation system in (6.3) can be presented in the following state-space form

$$\begin{bmatrix} \dot{x}_s(t) \\ \dot{v}_s(t) \\ \dot{x}_s(t) - \dot{x}_m(t) \\ \dot{v}_s(t) - \dot{v}_m(t) \\ \dot{x}_m(t) - \dot{x}_t(t) \\ \dot{v}_m(t) - \dot{v}_t(t) \end{bmatrix} = \begin{bmatrix} 0 & 1 & 0 \\ -\frac{k_e}{m_s} & -\frac{b_{se}}{m_s} & 0 \\ 0 & 0 & 0 \\ -\frac{k_e}{m_s} + \frac{k_h}{m_{mh}} & -\frac{b_{se}}{m_s} + \frac{b_{mh}}{m_{mh}} & -\frac{k_h}{m_{mh}} & \dots \\ 0 & 0 & 0 \\ -\frac{k_h}{m_{mh}} + \frac{k_t}{m_t} & -\frac{b_{mh}}{m_{mh}} + \frac{b_t}{m_t} & \frac{k_h}{m_{mh}} - \frac{k_t}{m_t} \\ \frac{k_e}{m_t} & \frac{b_e}{m_t} & \frac{m_h k_h}{m_{mh} m_t} - \frac{k_h}{m_t} \\ -\frac{m_h k_h}{m_{mh} m_t} + \frac{k_h}{m_t} & -\frac{m_h b_{mh}}{m_{mh} m_t} + \frac{b_h}{m_t} & \frac{m_h k_h}{m_{mh} m_t} - \frac{k_h}{m_t} \end{bmatrix} \quad (\text{F.85})$$

$$\begin{aligned}
 & \dots \begin{bmatrix} 0 & 0 & 0 \\ 0 & 0 & 0 \\ 1 & 0 & 0 \\ -\frac{b_{mh}}{m_{mh}} & 0 & 0 \\ 0 & 0 & 1 \\ \frac{b_{mh}}{m_{mh}} - \frac{b_t}{m_t} & -\frac{k_t}{m_t} & -\frac{b_t}{m_t} \\ \frac{m_h b_{mh}}{m_{mh} m_t} - \frac{b_h}{m_t} & & \end{bmatrix} \begin{bmatrix} x_s(t) \\ v_s(t) \\ x_s(t) - x_m(t) \\ v_s(t) - v_m(t) \\ x_m(t) - x_t(t) \\ v_m(t) - v_t(t) \end{bmatrix} \\
 & + \begin{bmatrix} 0 & 0 \\ \frac{1}{m_s} & 0 \\ 0 & 0 \\ \frac{1}{m_s} & -\frac{1}{m_{mh}} \\ 0 & 0 \\ 0 & \frac{1}{m_{mh}} + \frac{m_h}{m_{mh} m_t} \end{bmatrix} \begin{bmatrix} f_{cs}(t - d(t)) \\ f_{cm}(t - d(t)) \end{bmatrix} + \begin{bmatrix} 0 \\ 0 \\ 0 \\ -\frac{1}{m_{mh}} \\ 0 \\ \frac{1}{m_{mh}} - \frac{1}{m_t} + \frac{m_h}{m_{mh} m_t} \end{bmatrix} f_h^* \quad (\text{F.86})
 \end{aligned}$$

Note that in these state-space equations the environment mass,  $m_e$ , and the master and slave stiffnesses,  $k_m$  and  $k_s$ , are assumed to be zero.

## F.1 Teleoperation Dynamics after Transformation

After applying the non-singular transformation

$$T = \begin{bmatrix} 1 & 0 & 0 & 0 & 0 & 0 \\ 0 & 1 & 0 & 0 & 0 & 0 \\ \hline 0 & 0 & 1 & 0 & 0 & 0 \\ 0 & 0 & 0 & 0 & 1 & 0 \\ \hline 0 & 0 & \lambda & 1 & 0 & 0 \\ 0 & 0 & 0 & 0 & \lambda & 1 \end{bmatrix} \triangleq \begin{bmatrix} T_1 \\ T_2 \\ T_3 \end{bmatrix} \quad (\text{F.87})$$

where  $\lambda$  is defined in (6.27) and (6.28), the dynamics of the transformed state in (6.30) can be written in the following form

$$\begin{bmatrix} \hat{x}_s(t+d) \\ \hat{v}_s(t+d) \\ \hat{x}_s(t+d) - \hat{x}_m(t+d) \\ \hat{x}_m(t+d) - \hat{x}_t(t+d) \\ \hat{y}_1(t+d) \\ \hat{y}_2(t+d) \\ \dots \\ 0 \\ 0 \\ -\lambda \\ 0 \\ -\frac{k_h}{m_{mh}} + \lambda \frac{b_{mh}}{m_{mh}} - \lambda^2 \\ \frac{k_h}{m_{mh}} - \frac{k_t}{m_t} - \lambda \frac{b_{mh}}{m_{mh}} + \lambda \frac{b_t}{m_t} \\ \frac{m_h k_h}{m_{mh} m_t} - \frac{k_h}{m_t} - \lambda \frac{m_h b_{mh}}{m_{mh} m_t} + \lambda \frac{b_h}{m_t} \end{bmatrix} = \begin{bmatrix} 0 & 1 \\ -\frac{k_e}{m_s} & -\frac{b_{se}}{m_s} \\ 0 & 0 \\ 0 & 0 & \dots \\ -\frac{k_e}{m_s} + \frac{k_h}{m_{mh}} & -\frac{b_{se}}{m_s} + \frac{b_{mh}}{m_{mh}} \\ -\frac{k_h}{m_{mh}} + \frac{k_t}{m_t} + \frac{k_e}{m_t} & -\frac{b_{mh}}{m_{mh}} + \frac{b_t}{m_t} + \frac{b_e}{m_t} \\ -\frac{m_h k_h}{m_{mh} m_t} + \frac{k_h}{m_t} & -\frac{m_h b_{mh}}{m_{mh} m_t} + \frac{b_h}{m_t} \\ 0 & 0 & 0 & 0 \\ 0 & 0 & 0 & 0 \\ 0 & 0 & 1 & 0 \\ 0 & -\lambda & 0 & 1 \\ 0 & 0 & -\frac{b_{mh}}{m_{mh}} + \lambda & 0 \\ -\frac{k_t}{m_t} + \lambda \frac{b_t}{m_t} - \lambda^2 & \frac{b_{mh}}{m_{mh}} - \frac{b_t}{m_t} & -\frac{b_t}{m_t} + \lambda \\ \frac{m_h b_{mh}}{m_{mh} m_t} - \frac{b_h}{m_t} & \frac{m_h b_{mh}}{m_{mh} m_t} - \frac{b_h}{m_t} & \dots \end{bmatrix}$$

$$\begin{bmatrix} \hat{x}_s(t+d) \\ \hat{v}_s(t+d) \\ \hat{x}_s(t+d) - \hat{x}_m(t+d) \\ \hat{x}_m(t+d) - \hat{x}_t(t+d) \\ \hat{y}_1(t+d) \\ \hat{y}_2(t+d) \end{bmatrix} + \begin{bmatrix} 0 & 0 \\ \frac{1}{m_s} & 0 \\ 0 & 0 \\ 0 & 0 \\ \frac{1}{m_s} & -\frac{1}{m_{mh}} \\ 0 & \frac{1}{m_{mh}} + \frac{m_h}{m_{mh} m_t} \end{bmatrix} \begin{bmatrix} f_{cs}(t) \\ f_{cm}(t) \end{bmatrix}$$

$$+ \begin{bmatrix} 0 \\ 0 \\ 0 \\ 0 \\ -\frac{1}{m_{mh}} \\ \frac{1}{m_{mh}} - \frac{1}{m_t} + \frac{m_h}{m_{mh}m_t} \end{bmatrix} f_h^* + T\hat{\Phi}(t+d, t)L(t)e(t). \quad (\text{F.88})$$

$\hat{B}_y(t)$  in (6.35) which is defined as the last two rows of  $\hat{B}_T(t)$  in (6.30) is in the following form

$$\hat{B}_y(t) = \begin{bmatrix} \frac{1}{m_s} & -\frac{1}{m_{mh}} \\ 0 & \frac{1}{m_{mh}} + \frac{m_h}{m_{mh}m_t} \end{bmatrix}. \quad (\text{F.89})$$

Because the masses in (F.89) are non-zero the determinant of the matrix  $\hat{B}_y(t)$  is always non-zero and therefore this matrix is always invertible.

## F.2 Teleoperation Dynamics in Chapter 6 in Closed-loop Form

The closed-loop dynamics in (6.42) can be stated in the following state-space form

$$\begin{bmatrix} \hat{x}_s(t+d) \\ \hat{v}_s(t+d) \\ \hat{x}_s(t+d) - \hat{x}_m(t+d) \\ \hat{x}_m(t+d) - \hat{x}_t(t+d) \\ \hat{y}_1(t+d) \\ \hat{y}_2(t+d) \end{bmatrix} = \begin{bmatrix} 0 & 1 & 0 \\ -\frac{k_{tch}}{m_{th}} & -\frac{b_{tch}}{m_{th}} & \frac{k_{th}}{m_{th}} - \lambda \frac{b_{th}}{m_{th}} + \lambda^2 \\ 0 & 0 & -\lambda \\ 0 & 0 & 0 & \dots \\ 0 & 0 & 0 \\ 0 & 0 & 0 \end{bmatrix} \begin{bmatrix} 0 \\ 0 \\ 0 \\ \frac{k_t}{m_{th}} - \lambda \frac{b_t}{m_{th}} + \lambda^2 \frac{m_t}{m_{th}} & \frac{b_{th}}{m_{th}} - \lambda - \omega_1 & \frac{b_t}{m_{th}} - \lambda \frac{m_t}{m_{th}} - \omega_2 \frac{m_t}{m_{th}} \\ 0 \\ \dots & -\lambda & 0 & 1 \\ 0 & -\omega_1 & 0 \\ 0 & 0 & -\omega_2 \end{bmatrix} + \begin{bmatrix} \hat{x}_s(t+d) \\ \hat{v}_s(t+d) \\ \hat{x}_s(t+d) - \hat{x}_m(t+d) \\ \hat{x}_m(t+d) - \hat{x}_t(t+d) \\ \hat{y}_1(t+d) \\ \hat{y}_2(t+d) \end{bmatrix} + \begin{bmatrix} 0 \\ \frac{1}{m_{th}} \\ 0 \\ 0 \\ 0 \\ 0 \end{bmatrix} f_h^*$$

$$+ \begin{bmatrix} 1 & 0 & 0 & 0 & 0 & 0 \\ 0 & 1 & -\lambda & -1 & -\lambda \frac{m_t}{m_{th}} & -\frac{m_t}{m_{th}} \\ 0 & 0 & 1 & 0 & 0 & 0 \\ 0 & 0 & 0 & 0 & 1 & 0 \\ 0 & 0 & 0 & 0 & 0 & 0 \\ 0 & 0 & 0 & 0 & 0 & 0 \end{bmatrix} \hat{\Phi}(t+d, t) L(t) e(t). \quad (\text{F.90})$$

### F.3 Teleoperation Dynamics in Chapter 6 in Linear-in-parameter Form

The last three term on the right hand side of the equation (6.51) can be written as a multiplication of a regressor matrix,  $Y(t)$ , and a vector of parameter estimation

errors,  $\tilde{\theta}(t)$ . This results in the following linear-in-parameter form

$$Y(t)\tilde{\theta}(t) = \begin{bmatrix} 0 & 0 & 0 & 0 & 0 & 0 & 0 \\ -x_s(t) & -v_s(t) & 0 & 0 & 0 & 0 & 0 \\ 0 & 0 & 0 & 0 & 0 & 0 & 0 & \dots \\ -x_s(t) & -v_s(t) & x_m(t) & v_m(t) & 0 & 0 & 0 \\ 0 & 0 & 0 & 0 & 0 & 0 & 0 \\ 0 & 0 & -x_m(t) & -v_m(t) & x_t(t) & x_s(t) & -x_m(t) \\ 0 & 0 & 0 & 0 & 0 & 0 & 0 \\ 0 & 0 & 0 & 0 & 0 & f_{cs}(t-d) & 0 \\ \dots & 0 & 0 & 0 & 0 & 0 & 0 & \dots \\ 0 & 0 & 0 & 0 & 0 & f_{cs}(t-d) & -f_{cm}(t-d) \\ 0 & 0 & 0 & 0 & 0 & 0 & 0 \\ x_m(t) & v_t(t) & v_s(t) & -v_m(t) & v_m(t) & 0 & f_{cm}(t-d) \\ 0 & 0 & 0 \\ 0 & 0 & 0 \\ \dots & 0 & 0 & 0 \\ 0 & -1 & 0 \\ 0 & 0 & 0 \\ f_{cm}(t-d) & 1 & 1 \\ \dots & \frac{b_t}{m_t} & \frac{b_e}{m_t} & \frac{m_h b_{mh}}{m_{mh} m_t} & \frac{b_h}{m_t} & \frac{1}{m_s} & \frac{1}{m_{mh}} & \frac{m_h}{m_{mh} m_t} & \frac{1}{m_{mh}} f_h^* & -\frac{m_m}{m_{mh} m_t} f_h^* \end{bmatrix} \cdot \begin{bmatrix} \frac{k_e}{m_s} & \frac{b_{se}}{m_s} & \frac{k_h}{m_{mh}} & \frac{b_{mh}}{m_{mh}} & \frac{k_t}{m_t} & \frac{k_e}{m_t} & \frac{m_h k_h}{m_{mh} m_t} & \frac{k_h}{m_t} & \dots \end{bmatrix}^T \quad (\text{F.91})$$

# Appendix G

## The Persistency of Excitation Condition

*Theorem:* The parameter estimation errors approaches zero as  $t \rightarrow \infty$  if there exist positive scalars  $\alpha$  and  $T$  such that the following holds

$$\int_t^{t+T} Y^T(s)Y(s)ds > \alpha I. \quad (\text{G.92})$$

where  $I$  is the identity matrix with the appropriate dimension.

*Proof:* Considering the fact that  $r(t)$  in (6.56) approaches zero as  $t \rightarrow \infty$  and by employing Theorem 6.2 one can write

$$Y(t)\tilde{\theta}_e = 0 \quad (\text{G.93})$$

where  $\tilde{\theta}_e$  represents the final value of the parameter estimation errors as  $t \rightarrow \infty$ .

Now multiplying both sides of (G.93) by  $Y^T(t)$  from left and integrating the result from  $t$  to  $t + T$  yields

$$\int_t^{t+T} Y^T(s)Y(s)ds \tilde{\theta}_e = 0. \quad (\text{G.94})$$

Considering the inequality in (G.92), the condition in (G.94) holds if and only if

$$\tilde{\theta}_e = 0 \quad (\text{G.95})$$

and therefore parameters should converge to their actual values as  $t \rightarrow \infty$ .

# Appendix H

## Composite Adaptive Controller

### Matrices

The nonlinear function  $f_h(\theta)$  in (6.90) can be written in the following form

$$f_h(\theta) = \begin{bmatrix} \frac{1}{2} \left( \frac{\theta_{16}}{\theta_{14}} \right) + \frac{1}{2} \left( \frac{\theta_{17}}{\theta_{15} - \frac{1}{m_t}} \right) \\ \frac{1}{3} \left( \frac{\theta_{15} m_t}{\theta_{14}} \right) + \frac{1}{3} \left( \frac{\theta_{11} m_t}{\theta_4} \right) + \frac{1}{3} \left( \frac{\theta_7 m_t}{\theta_3} \right) \\ \theta_{12} m_t \\ \frac{1}{3} (\theta_8 m_t) + \frac{1}{3} \left( \frac{\theta_7}{\theta_{15}} \right) + \frac{1}{3} \left( \frac{\theta_3}{\theta_{14}} \right) \end{bmatrix} \quad (\text{H.96})$$

where  $\theta_i$  represents the  $i$ th element of the system parameters vector in (F.91). Similarly,  $f_e(\theta)$  can be written as

$$f_e(\theta) = \begin{bmatrix} \theta_{10} m_t \\ \frac{1}{2} (\theta_6 m_t) + \frac{1}{2} \left( \frac{\theta_1}{\theta_{13}} \right) \end{bmatrix} \quad (\text{H.97})$$

After linearization,  $J_h$  and  $J_e$  in (6.93) and (6.99) can be calculated as follows

$$J_h = \begin{bmatrix} 0 & 0 & 0 & 0 & 0 & 0 & 0 & 0 & 0 & 0 & 0 & 0 & -\frac{\theta_{16}}{2\theta_{14}^2} \\ 0 & 0 & -\frac{\theta_7 m_t}{3\theta_3^2} & -\frac{\theta_{11} m_t}{3\theta_4^2} & 0 & 0 & \frac{m_t}{3\theta_3} & 0 & 0 & 0 & \frac{m_t}{3\theta_4} & 0 & 0 & -\frac{\theta_{15} m_t}{3\theta_{14}^2} & \dots \\ 0 & 0 & 0 & 0 & 0 & 0 & 0 & 0 & 0 & 0 & m_t & 0 & 0 & 0 & \\ 0 & 0 & \frac{1}{3\theta_{14}} & 0 & 0 & 0 & \frac{1}{3\theta_{15}} & \frac{m_t}{3} & 0 & 0 & 0 & 0 & 0 & -\frac{\theta_3}{3\theta_{14}^2} \\ & & & & & & & & & & -\frac{\theta_{17}}{2(\theta_{15} - \frac{1}{m_t})^2} & \frac{1}{2\theta_{14}} & \frac{1}{2(\theta_{15} - \frac{1}{m_t})} \\ & & & & & \dots & \frac{m_t}{3\theta_{14}} & 0 & 0 & & 0 & 0 & 0 & & \\ & & & & & & 0 & 0 & 0 & & 0 & 0 & 0 & & \\ & & & & & & -\frac{\theta_7}{3\theta_{15}^2} & 0 & 0 & & 0 & 0 & 0 & & \end{bmatrix} \quad (\text{H.98})$$

and

$$J_e = \begin{bmatrix} 0 & 0 & 0 & 0 & 0 & 0 & 0 & 0 & 0 & m_t & 0 & 0 & 0 & 0 & 0 & 0 & 0 & 0 \\ \frac{1}{2\theta_{13}} & 0 & 0 & 0 & 0 & \frac{m_t}{2} & 0 & 0 & 0 & 0 & 0 & 0 & -\frac{\theta_1}{2\theta_{13}^2} & 0 & 0 & 0 & 0 & 0 \end{bmatrix}. \quad (\text{H.99})$$

# Bibliography

- [1] S. Sirouspour and A. Shahdi, "Discrete-time linear quadratic gaussian control for teleoperation under communication time delay," *The International Journal of Robotics Research*, vol. 25, pp. 187–202, 2006.
- [2] S. Sirouspour and A. Shahdi, "Model predictive control for transparent teleoperation under communication time-delay," *IEEE Transactions on Robotics*, vol. 22, no. 6, pp. 1131–1145, 2006.
- [3] T. Sheridan, "Telerobotics," *Automatica*, vol. 25, no. 4, pp. 487–507, 1989.
- [4] C. Melchiorri and A. Eusebi, "Telemanipulation: System aspects and control issues," *Proceedings of the International Summer School in Modelling and Control of Mechanisms and Robots*, pp. 149–183, 1996.
- [5] T. Sheridan, *Teletobotics, Automation, and Human Supervisory Control*. Cambridge, Massachusetts: The MIT Press, 1992.
- [6] P. F. Hokayem. and M. W. Spong, "Bilateral teleoperation: An historical survey," *Automatica*, vol. 42, pp. 2035–2057, 2006.

- [7] S. Salcudean, "Control for teleoperation and haptic interfaces," *Control Problems in Robotics and Automation LNCIS230*, B. Siciliano and K.P. Valavanis (Eds.). Springer, pp. 51–66, 1998.
- [8] T. Sheridan, "Space teleoperation through time delay: review and prognosis," *IEEE Transactions on Robotics and Automation*, vol. 9, no. 5, pp. 592–606, 1993.
- [9] K. Landzettel, B. Brunner, A. Beyer, E. Kramer, and C. Preusche, "Rokviss verification of advanced telepresence concepts for future space missions," in *7th ESA Workshop on Advances Space Technologies for Robotics and Automation' ASTRA2002'*, Noordwijk, Netherlands, 2002.
- [10] G. Hirzinger, G. Grunwald, B. Brunner, and J. Heindl, *A sensor-based telerobotic system for the space robot experiment ROTEX*. Springer, 1993.
- [11] M. Oda, "Coordinated control of spacecraft attitude and its manipulator," in *Proceedings of IEEE International Conference on Robotics and Automation*, pp. 732 – 738, 1996.
- [12] C. Stoker, D. Barch, B. Hine, and J. Barry, "Antarctic undersea exploration using a robotic submarine with a telepresence user interface," *IEEE Expert*, vol. 10, no. 6, pp. 14–23, 1995.
- [13] D. Kwon, J. Ryu, P. Lee, and S. Hong, "Design of a teleoperation controller for an underwater manipulator," in *Proceedings of IEEE International Conference on Robotics and Automation*, pp. 3114 – 3119, 2000.

- [14] A. Kwitowski, W. Mayercheck, and A. Brautigam, "Teleoperation for continuous miners and haulage equipment," *IEEE Transactions on Industry Applications*, vol. 28, no. 5, pp. 1118–1125, 1992.
- [15] J. Park, K. Kim, H. Lee, and M. Yang, "Robotic contamination cleaning system," in *Proceedings of IEEE/RSJ International Conference on Intelligent Robots and Systems*, pp. 1874 – 1879, 2002.
- [16] R. Taylor and D. Stoianovici, "Medical robotics in computer-integrated surgery," *IEEE Transactions on Robotics and Automation*, vol. 19, no. 5, pp. 765–781, 2003.
- [17] A. Madhani, G. Niemeyer, and J. Salisbury, "The black falcon: A teleoperated surgical instrument for minimally invasive surgery," in *Proceedings of IEEE/RSJ International Conference on Intelligent Robots and Systems*, pp. 936 – 944, 1998.
- [18] D. Lawrence, "Stability and transparency in bilateral teleoperation," *IEEE Transactions on Robotics and Automation*, vol. 9, pp. 624–637, October 1993.
- [19] N. Kularatna and D. Dias, *Essentials of modern telecommunications systems*. Artech House Publishers, 2004.
- [20] A. Rojas, J. Braslavsky, and R. Middleton, "Fundamental limitations in control over a communication channel," *Automatica*, vol. 44, no. 12, pp. 3147–3151, 2008.

- [21] J. Baillieul and P. Antsaklis, "Control and communication challenges in networked real-time systems," *Proceedings of the IEEE*, vol. 95, no. 1, pp. 9–28, 2007.
- [22] K. Gu, V. L. Kharitonov, and J. Chen, *Stability of Time-Delay Systems*. Boston: Birkhauser, 2003.
- [23] J. Slotine, "The robust control of robot manipulators," *The International Journal of Robotics Research*, vol. 4, no. 2, pp. 49–64, 1985.
- [24] C. Abdallah, D. Dawson, P. Dorato, and M. Jamshidi, "Survey of robust control for rigid robots," *IEEE Control Systems Magazine*, vol. 11, no. 2, pp. 24–30, 1991.
- [25] M. Spong, "On the robust control of robot manipulators," *IEEE Transactions on Automatic Control*, vol. 37, no. 11, pp. 1782–1786, 1992.
- [26] H. Sage, M. De Mathelin, and E. Ostertag, "Robust control of robot manipulators: a survey," *International Journal of Control*, vol. 72, no. 16, pp. 1498–1522, 1999.
- [27] J. Doyle, B. Francis, and A. Tannenbaum, *Feedback control theory*. Macmillan New York, 1992.
- [28] A. Isidori and W. Kang, " $H_\infty$  control via measurement feedback for general nonlinear systems," *IEEE Transactions on Automatic Control*, vol. 40, no. 3, pp. 466–472, 1995.

- [29] H. Kazerooni, T. Tsay, and K. Hollerbach, "A controller design framework for telerobotic systems," *IEEE Transactions on Control Systems Technology*, vol. 1, no. 1, pp. 50–62, 1993.
- [30] S. Sirouspour, "Modeling and control of cooperative teleoperation systems," *IEEE Transactions on Robotics*, vol. 21, no. 6, pp. 1220–1225, 2005.
- [31] J. Yan and S. Salcudean, "Teleoperation controller design using  $H_\infty$ -optimization with application to motion-scaling," *IEEE Transactions on Control Systems Technology*, vol. 4, no. 3, pp. 244–258, 1996.
- [32] G. Leung, B. Francis, and J. Apkarian, "Bilateral controller for teleoperators with time delay via mu-synthesis," *IEEE Transactions on Robotics and Automation*, vol. 11, no. 1, pp. 105–116, 1995.
- [33] O. Sename and A. Fattouh, "Robust  $H_\infty$  control of bilateral teleoperation systems under communication time-delay," *Applications of Time Delay Systems*. J. Chiasson and J. J. Loiseau (Eds.). Springer, pp. 99–116, 2007.
- [34] W.-H. Zhu and S. Salcudean, "Stability guaranteed teleoperation: an adaptive motion/force control approach," *IEEE Transactions on Automatic Control*, vol. 45, no. 11, pp. 1951–1969, 2000.
- [35] G. Meinsma and L. Mirkin, " $H^\infty$  control of systems with multiple I/O delays via decomposition to adobe problems," *IEEE Transactions on Automatic Control*, vol. 50, no. 2, pp. 199–211, 2005.

- [36] G. Raju, G. Verghese, and T. Sheridan, "Design issues in 2-port network models of bilateral remote teleoperation," in *Proceedings of IEEE International Conference on Robotics and Automation*, pp. 1317–1321, 1989.
- [37] B. Hannaford, "A design framework for teleoperators with kinesthetic feedback," *IEEE Transactions on Robotics and Automation*, vol. 5, no. 4, pp. 426–434, 1989.
- [38] Y. Yokokohji and T. Yoshikawa, "Bilateral control of master-slave manipulators for ideal kinesthetic coupling-formulation and experiment," *IEEE Transactions on Robotics and Automation*, vol. 10, no. 5, pp. 605–620, 1994.
- [39] K. Hastrudi-Zaad and S. Salcudean, "On the use of local force feedback for transparent teleoperation," in *Proceedings of IEEE International Conference on Robotics and Automation*, vol. 3, 1999.
- [40] M. Tavakoli, A. Aziminejad, R. Patel, and M. Moallem, "Discrete-time bilateral teleoperation: modelling and stability analysis," *IET Control Theory & Applications*, vol. 2, no. 6, pp. 496–512, 2008.
- [41] A. Abdossalami and S. Sirouspour, "Adaptive Control for Improved Transparency in Haptic Simulations," *IEEE Transactions on Haptics*, vol. 2, no. 1, pp. 2–14, 2009.
- [42] K. Hashtrudi-Zaad and S. Salcudean, "Analysis of control architectures for teleoperation systems with impedance/admittance master and slave manipulators," *The International Journal of Robotics Research*, vol. 20, no. 6, pp. 419–445, 2001.

- [43] S. Haykin, *Active network theory*. Addison-Wesley Reading, Massachusetts, USA, 1970.
- [44] R. Adams and B. Hannaford, "Stable haptic interaction with virtual environments," *IEEE Transactions on robotics and Automation*, vol. 15, no. 3, pp. 465–474, 1999.
- [45] J.-E. Slotine and W. Li, *Applied Nonlinear Control*. New Jersey: Prentice-Hall Inc., 1991.
- [46] C. Desoer and M. Vidyasagar, *Feedback systems: input-output properties*. Academic Press, Inc. Orlando, FL, USA, 1975.
- [47] J. Colgate, "Robust impedance shaping telemanipulation," *IEEE Transactions on Robotics and Automation*, vol. 9, no. 4, pp. 374–384, 1993.
- [48] H. Lu and W. Lin, "Robust controller with disturbance rejection for hydraulic servo systems," *IEEE Transactions on Industrial Electronics*, vol. 39, no. 1, pp. 157–162, 1993.
- [49] N. Niksefat and N. Sepehri, "Robust force controller design for an electrohydraulic actuator based on nonlinear model," in *Proceedings of IEEE International Conference on Robotics and Automation*, pp. 200–206, 1999.
- [50] N. Sadegh and R. Horowitz, "Stability and robustness analysis of a class of adaptive controllers for robotic manipulators," *The International Journal of Robotics Research*, vol. 9, no. 3, pp. 74–92, 1990.

- [51] Z. Hu, S. Salcudean, and P. Loewen, "Robust controller design for teleoperation systems," in *Proceedings of IEEE International Conference on Systems, Man and Cybernetics*, vol. 3, pp. 2127–2132, 1995.
- [52] S. Sirouspour and A. Shahdi, "Bilateral teleoperation under communication time delay using an LQG controller," in *Proceedings of IEEE Conference on Control Applications*, pp. 1257–1262, 2005.
- [53] J. Ryu, D. Kwon, and B. Hannaford, "Stable Teleoperation with Time-domain Passivity Control," *IEEE Transactions on Robotics and Automation*, vol. 20, pp. 365–373, 2004.
- [54] D. Lee and P. Li, "Passive bilateral control and tool dynamics rendering for nonlinear mechanical teleoperators," *IEEE Transactions on Robotics*, vol. 21, no. 5, pp. 936–951, 2005.
- [55] R. Kress and J. Jansen, "Automatic tuning for a teleoperated arm controller," in *Proceedings of IEEE Conference on Decision and Control*, pp. 2692–2695, 1992.
- [56] K. Hashtrudi-Zaad and S. Salcudean, "Adaptive transparent impedance reflecting teleoperation," in *Proceedings of IEEE International Conference on Robotics and Automation*, pp. 1369 – 1374, 1996.
- [57] M. Shi, G. Tao, H. Liu, and J. H. Downs, "Adaptive control of teleoperation systems," in *Proceedings of IEEE Conference on Decision and Control*, pp. 791 – 796, 1999.

- [58] H. K. Lee, M. H. Shin, and M. J. Chung, "Adaptive control of master-slave systems for transparent teleoperation," *Journal of Robotic Systems*, vol. 15, pp. 465–475, 1998.
- [59] L. Love and W. Book, "Force reflecting teleoperation with adaptive impedance control," *IEEE Transactions on Systems, Man, and Cybernetics*, vol. 34, no. 1, pp. 159–165, 2004.
- [60] K. Ciliz and K. Narendra, "Multiple model based adaptive control of robotic manipulators," in *Proceedings of IEEE Conference on Decision and Control*, pp. 1305–1310, 1994.
- [61] M. Leahy Jr and S. Sablan, "Multiple model-based control of robotic manipulators: an overview," in *Proceedings of IEEE Conference on Decision and Control*, pp. 1976–1977, 1990.
- [62] K. Narendra and J. Balakrishnan, "Adaptive control using multiple models," *IEEE Transactions on Automatic Control*, vol. 42, no. 2, pp. 171–187, 1997.
- [63] Y. Zhang and J. Jiang, "Integrated active fault-tolerant control using IMM approach," *IEEE Transactions on Aerospace and Electronic Systems*, vol. 37, no. 4, pp. 1221–1235, 2001.
- [64] K. Hashtrudi-Zaad and S. Salcudean, "Transparency in time-delayed systems and the effect of local force feedback for transparent teleoperation," *IEEE Transactions on Robotics and Automation*, vol. 18, no. 1, pp. 108–114, 2002.

- [65] P. Arcara and C. Melchiorri, "Control schemes for teleoperation with time delay: A comparative study," *Robotics and Autonomous Systems*, vol. 38, no. 1, pp. 49–64, 2002.
- [66] T. Imaida, Y. Yokokohji, T. Doi, M. Oda, and T. Yoshikawa, "Ground-space bilateral teleoperation of ETS-VII robot arm by direct bilateral coupling under 7-s time delay condition," *IEEE Transactions on Robotics and Automation*, vol. 20, no. 3, pp. 499–511, 2004.
- [67] N. Ando, J. Lee, and H. Hashimoto, "A study on influence of time delay in teleoperation," in *Proceedings of IEEE/ASME International Conference on Advanced Intelligent Mechatronics*, pp. 317–322, 1999.
- [68] S. Lee and H. Lee, "Modeling, design, and evaluation of advanced teleoperator controlsystems with short time delay," *IEEE Transactions on Robotics and Automation*, vol. 9, no. 5, pp. 607–623, 1993.
- [69] J. Azorin, O. Reinoso, R. Aracil, and M. Ferre, "Generalized control method by state convergence for teleoperation systems with time delay," *Automatica*, vol. 40, pp. 1575–1582, 2004.
- [70] T. Mirfakhrai and S. Payandeh, "A model for time-delays for teleoperation over the Internet," in *Proceedings of IEEE International Symposium on Computational Intelligence in Robotics and Automation*, pp. 236–241, 2001.
- [71] R. Anderson and M. Spong, "Bilateral control of teleoperators with time delay," *IEEE Transactions on Automatic Control*, vol. 34, no. 5, pp. 494–501, 1989.

- [72] S. Stramigioli, A. Van der Schaft, B. Maschke, and C. Melchiorri, "Geometric scattering in robotic telemanipulation," *IEEE Transactions on Robotics and Automation*, vol. 18, no. 4, pp. 588–596, 2002.
- [73] G. Niemeyer and J.-J. Slotine, "Stable adaptive teleoperation," *IEEE Journal of Oceanic Engineering*, vol. 16, no. 1, pp. 152–162, 1991.
- [74] R. Anderson and M. Spong, "Asymptotic stability for force reflecting teleoperators with time delay," *The International Journal of Robotics Research*, vol. 11, no. 2, pp. 135–142, 1992.
- [75] G. Niemeyer and J.-J. Slotine, "Towards force-reflecting teleoperation over the internet," in *Proceedings of IEEE International Conference on Robotics and Automation*, pp. 1909–1915, 1998.
- [76] J. Ueda and T. Yoshikawa, "Force-reflecting teleoperation with time delay by signal filtering," *IEEE Transactions on Robotics and Automation*, vol. 20, no. 3, pp. 613–619, 2004.
- [77] G. Niemeyer and J. Slotine, "Telemanipulation with time delays," *The International Journal of Robotics Research*, vol. 11, no. 2, pp. 873–890, 2004.
- [78] Y. Yokokohji, T. Imaida, and T. Yoshikawa, "Bilateral control with energy balance monitoring under time-varying communication delay," in *Proceedings of IEEE International Conference on Robotics and Automation*, pp. 2684–2689, 2000.
- [79] Y. Yokokohji, T. Imaida, and T. Yoshikawa, "Bilateral teleoperation under time-varying communication delay," in *Proceedings of IEEE/RSJ International Conference on Intelligent Robots and Systems*, pp. 1854 – 1859, 1999.

- [80] C. Benedetti, M. Franchini, and P. Fiorini, "Stable tracking in variable time-delay teleoperation," in *Proceedings of IEEE/RSJ International Conference on Intelligent Robots and Systems*, pp. 2252 – 2257, 2001.
- [81] T. Mirfakhrai and S. Payandeh, "A delay prediction approach for teleoperation over the internet," in *Proceedings of IEEE International Conference on Robotics and Automation*, pp. 2178 – 2183, 2002.
- [82] H. Baier, "Transparency and stability of bilateral kinesthetic teleoperation with time-delayed communication," *Journal of Intelligent and Robotic Systems: Theory and Applications*, vol. 40, no. 1, pp. 1–22, 2004.
- [83] S. Munir and W. Book, "Internet-based teleoperation using wave variables with prediction," *IEEE/ASME Transactions on Mechatronics*, vol. 7, no. 2, pp. 124–133, 2002.
- [84] D. Lee and M. W. Spong, "Passive bilateral teleoperation with constant time delay," *IEEE Transactions on Robotics*, vol. 22, no. 2, pp. 269–281, 2006.
- [85] N. Chopra and M. W. Spong, "Adaptive coordination control of bilateral teleoperators with time delay," in *Proceedings of IEEE Conference on Decision and Control*, pp. 4540–4547, 2004.
- [86] N. A. Tanner and G. Niemeyer, "Improving perception in time-delayed telerobotics," *The International Journal of Robotics Research*, vol. 24, pp. 631–644, 2005.

- [87] H. Ching and W. J. Book, "Internet-based bilateral teleoperation based on wave variable with adaptive predictor and direct drift control," *Journal of Dynamic Systems, Measurement, and Control*, vol. 128, pp. 86–93, 2006.
- [88] A. Bejczy, W. Kim, and S. Venema, "The phantom robot: predictive displays for teleoperation with time-delay," in *Proceedings of IEEE International Conference on Robotics and Automation*, pp. 546–551, 1990.
- [89] J. Kikuchi, K. Takeo, and K. Kosuge, "Teleoperation system via computer network for dynamic environment," in *Proceedings of IEEE International Conference on Robotics and Automation*, pp. 3534–3539, 1998.
- [90] Z. Ping, K. Tanaka, E. Shimizu, and M. Ito, "A teleoperating system for underwater manipulator with virtual model aid," in *Proceedings of IEEE International Conference on Robotics and Automation*, pp. 882–886, 2003.
- [91] T. Kotoku, "A predictive display with force feedback and its application to remote manipulation system with transmission time delay," in *Proceedings of IEEE/RSJ International Conference on Intelligent Robots and Systems*, vol. 1, pp. 239 – 246, 1992.
- [92] G. Hirzinger, J. Heindl, and K. Landzettel, "Predictive and knowledge-based telerobotic control concepts," in *Proceedings of IEEE International Conference on Robotics and Automation*, pp. 1768–1777, 1989.
- [93] L. Conway, R. Volz, and M. Walker, "Teleautonomous systems: projecting and coordinating intelligent action at a distance," *IEEE Transactions on Robotics and Automation*, vol. 6, no. 2, pp. 146–158, 1990.

- [101] J. Richard, "Time-delay systems: an overview of some recent advances and open problems," *Automatica*, vol. 39, pp. 1667–1694, 2003.
- [102] K. Watanabe, E. Nobuyama, and A. Kojima, "Recent advances in control of time delay systems - a tutorial review," in *Proceedings of IEEE Conference on Decision and Control*, pp. 2083 – 2089, 1996.
- [103] V. Kharitonov, "Robust stability analysis of time delay systems: a survey," *Annual Reviews in Control*, vol. 23, pp. 185–196, 1999.
- [104] A. Olbrot, "Robustness of time-delay systems: a survey," in *Proceedings of IEEE Conference on Decision and Control*, pp. 508 – 514, 1988.
- [105] W. Kwon and A. Pearson, "Feedback stabilization of linear systems with delayed control," *IEEE Transactions on Automatic Control*, vol. 25, no. 2, pp. 266–269, 1980.
- [106] Z. Artstein, "Linear systems with delayed controls: a reduction," *IEEE Transactions on Automatic Control*, vol. 27, no. 4, pp. 869–879, 1982.
- [107] C. Foias, H. Ozbay, and A. Tannenbaum, *Robust control of infinite dimensional systems:(frequency domain methods)*. Springer, 1996.
- [108] L. Mirkin and G. Tadmor, " $H^\infty$  control of system with I/O delay: A review of some problem-oriented methods," *IMA Journal of Mathematical Control and Information*, vol. 19, pp. 185–199, 2002.
- [109] L. Mirkin, "On the extraction of dead-time controllers and estimators from delay-free parametrizations," *IEEE Transactions on Automatic Control*, vol. 48, no. 4, pp. 543–553, 2003.

- [126] D. L. Mills, "Improved algorithms for synchronizing computer network clocks," *IEEE/ACM Transactions on Networking (TON)*, vol. 3, no. 3, pp. 245–254, 1995.
- [127] U. Mackenroth, *Robust Control Systems*. Springer-Verlag, 2004.
- [128] D. Bennett, "What are the advantages of variable stiffness control?," *IEEE Engineering in Medicine and Biology Magazine*, vol. 11, no. 4, pp. 86–87, 1992.
- [129] H. Kimura, *Chain-Scattering Approach to  $H^\infty$  Control*. Birkhauser, 1996.
- [130] C. Riviere, R. Rader, and P. Khosla, "Characteristic of hand motion of eye surgeons," in *Proceedings of Annual International Conference - IEEE/Engineering in Medicine and Biology Society*, pp. 1690–1693, 1997.
- [131] O. Hijab, *Introduction to Calculus and Classical Analysis*. Springer-Verlag, 1997.
- [132] F. Amato, *Robust control of linear systems subject to uncertain time-varying parameters*. Springer Verlag, 2006.
- [133] K. Zhou, J. Doyle, and K. Glover, *Robust and Optimal Control*. Prentice-Hall, 1995.